eman ta zabal zazu

Universidad del País Vasco

Euskal Herriko Unibertsitatea

Departamento de Física

Programa de doctorado: Física

PhD Thesis

Subcooling in Plastic Crystals: Characterization, understanding and mitigation

A dissertation presented by:

Sergio Santos Moreno

Supervisors:

Dra. Stefania Doppiu

Dr. Gabriel Alejandro López

Leioa, March 2023

Universidad del País Vasco
Euskal Herriko Unibertsitatea
ZIENTZIA ETA TEKNOLOGIA FAKULTATEA
FACULTAD DE CIENCIA Y TECNOLOGÍA

PhD Thesis

Subcooling in Plastic Crystals: Characterization, understanding and mitigation

A dissertation presented by:

Sergio Santos Moreno

In fulfillments of the requirements of the University of Basque Country for the degree of Doctor in Philosophy in Applied Physics

Supervisors:

Dra. Stefania Doppiu and Dr. Gabriel Alejandro López

Tutor:

Dr. Gabriel Alejandro López

Leioa, March 2023

CIC energiGUNE
MEMBER OF BASQUE RESEARCH & TECHNOLOGY ALLIANCE

tecnalia
MEMBER OF BASQUE RESEARCH & TECHNOLOGY ALLIANCE

"I am not afraid of storms
for I am learning how
to sail my ship"
– Louisa May Alcott

Acknowledgements

I cannot imagine other words to start this last part of the thesis than by referring to a famous song, but in this case, it would be the opposite: "*Time goes by… so quickly!*" It is quite impressive how fast 4 years can pass over a single person. Honestly, it has been a rollercoaster of emotions. Since the beginning, the fact of moving to a new city and starting from scratch was a very appealing idea to me. A mind reset is necessary from time to time to open new doors and even to know who you really are. Moreover, it was clear to me that my career was to be focused on research and Vitoria was offering me that.

I am so grateful to CIC energiGUNE. I find it a research center characterized by an extraordinary research philosophy, but also by an unbeatable human team. The youthfulness of the research groups makes the research even more exciting and motivates your working day in the sense of; "what will happen today and how will we solve it?" But after one year, we decided to change the initial topic of my thesis, something frustrating at first, but it also taught when research cannot go ahead to complete a four-year thesis. This is where my first acknowledgement stars, as it could not be otherwise. Stefania, my supervisor from the very first moment, with whom I had an incredible connection and good vibes who always gave me the freedom and confidence to take the research where I thought. With my victories, but also with my defeats. I will always be indebted to her, and I will always bring with me your comments regarding my English ("World is growing"). Elena, the big boss, it is quite difficult to explain by words how fruitful and rewarding a scientific discussion with her can be, and how it results enriching. Moreover, it would be unfair not to mention the good times spent outside work environment with her, Stefania and Jean Luc. I want also to thank Kerman and Juan Miguel, much of this thesis would not have been possible without your huge knowledge in NMR. Marie, Alex, AlexL and Mirek, thank you very much for trusted me in the different international internships. Even if the situation in Ukraine at that moment made me return from Poland, it was an experience I will never forget. Yarik, I will always be grateful for your help in arranging my internship in Katowice. Gabriel, thank you so much for your concern and help without any hesitation, you definitely more than meet the role of a tutor and supervisor.

My TES crew: Leticia, Yasmina, Yagmur, MikelD, Ángel, María. Undoubtedly my battle buddies, those who made my research not only more bearable, but also who made my free

time outside CIC the best thing that I bring with me from these 4 years. Not only they are true vocational scientists, but they are also magnificent people who make any second spent with them truly unforgettable. Of course, I can not forget my two “puretas”: La Eche y La Ampa. It all started as “fumaleku” colleagues, and today I can say that we have a true friendship which I will bring always with me. My time at CIC would not have been the same without them, and despite we are currently more far away, I am happy for the better position of Eche and for the maternity of Ampa. I do not want to forget all the people that not only somehow scientifically helped me, but also that have given me great moments: Francesco, Artem, Imanol, Jorge, Edu, Jaime, Luis, LuisB, MikelA, Estikitiki, Antonio, Nagore, Jauregui… Thank you all very much.

Tecnalia… Cuántas experiencias vividas contigo. Una tesis enmarcada en un proyecto de colaboración entre dos centros de investigación tiene dos vertientes: la pasión por conocer nuevas personas y una ciencia diferente, y el vértigo de trabajar en dos centros diferentes. Es increíble como un centro tecnológico puede ser tan multidisciplinar, y qué contento estoy de haber trabajado en las dos mejores sedes sin ninguna duda. Mikeletegi 2, ante todo, gracias por haberme dado la oportunidad de conocer Donosti tan de cerca. Mis compañeros, Aiala, Íñigo, Aitor, Nevena, Ana, Anastasia, Iñaki… No solo he aprendido mucho de vosotros, sino que además los momentos vividos fuera de Tecnalia, ya sean de cena de empresa, o incluso viajando a Lisboa. Mis agradecimientos infinitos por lo bien que me acogisteis todos. Elena Silveira… Si tuviera un ángel de la guarda, sería ella. Complicidad extrema, cafés en la terraza aunque lloviera a mares, apoyo científico, y si no sabía, se encargaba de encontrar a la persona adecuada. Ha confiado en mi desde el primer momento, y me ha dado la libertad para llevar la investigación donde más nos gustaba. De hecho, ella ha sido el artífice que me abrió las puertas de Tecnalia Miñano, lo que hoy en día es mi casa. Elena, nuestro esfuerzo y tu involucración por mi futuro ha dado sus frutos, sin ti no hubiera sido posible. Muchísimas gracias de corazón.

Tecnalia Miñano, antes de empezar esta nueva etapa con vosotros, ya erais una familia para mí. No solo hacéis una investigación de excelencia, los excelentes sois vosotros sin ninguna duda. Beñat, Leire, Ander, Olga, Marta, Pablo y Bea, sois unos compañeros increíbles, y nos esperan muchos debates científicos y proyectos que sacar adelante juntos, así que a darlo todo, que el nueva área depende de nosotros, y desde luego va a despuntar sin ninguna duda. Me siento realmente orgulloso de ser investigador en vuestro equipo.

Finalmente, lo más importante, los que siempre están ahí, los que han estado siempre y siempre van a estar. Mi familia. Mamá, desde siempre has puesto toda tu confianza en mí,

has sabido ponerme límites sin coartar en ningún momento mi libertad para tomar las decisiones oportunas sobre mi vida y su dirección. Tu apoyo incondicional siempre, en mis buenos y malos momentos, en mis éxitos y en mis tropiezos, es lo que siempre llevo conmigo. Te quiero muchísimo. Javi, Kike, junto a mamá formáis parte de esa familia que no se elige la cual no podría haber sido mejor, aunque seáis mis hermanos pequeños, más de una lección me habéis dado, y estoy realmente orgulloso de vosotros. Papá, aunque al principio un poco más reticente en que hiciera la tesis, también has mirado siempre por mi bienestar y por mi buen hacer, y espero que todos os sintáis orgullosos de este trabajo que he llevado a cabo. Cati, sin duda esta es la parte que más me cuesta escribir. No sabes lo que supuso para mí al principio separarme de ti, después de 6 años juntos 24/7, y mis otros 18 años siendo tu ojito derecho. Pero lo más importante, es que tú siempre has sido el mío también. Nada es igual sin vivir contigo, y me encanta la vida que estoy formando ahora, pero te echo de menos todos los días. Muchas gracias por ser como has sido siempre conmigo, mi guardiana y protectora, y de la que espero separarme lo más tarde posible. Por supuesto, Geli, Maite, Miguel, tres pilares super importantes para mí, ejemplos a seguir por su capacidad de resiliencia, perseverancia, y honestidad, no podría dejarlos atrás de ninguna de las maneras. Iker… La última persona en llegar a mi familia, y la que se ha convertido en el pilar de mi día a día. Has tenido que aguantarme diariamente en todas las etapas de mi tesis; éxitos, fracasos, enfados, frustraciones, viajes a congresos, estancias, comidas de empresa, y una lista interminable de cosas que desde luego solo tú has podido vivir. Quiero darte las gracias. No eres la persona con más paciencia del mundo (yo tampoco), y aun así, has sabido llevar todos mis diferentes estados de ánimo que una persona puede experimentar durante una tesis doctoral. Sé que no ha sido fácil, pero mira, aquí está, ya la hemos acabado, juntos.

People who leave, new people who comes in, doors continuously opening and closing. It is not something that I am unrevealing, it is how the life goes on itself. Life is not only about learning to say goodbye, it is also about learning to say “welcome”, “here I am”, and “go for it”. These four years made me grow not only as a professional, but also as a person, and I am very grateful for that. Thank you all, this thesis is a work of all of us, and here it is, finally it comes to an end. I hope that you feel proud of it and always carry me in your good memories.

Abstract

Energy management is nowadays a crucial concern for all the humanity, since our future strongly depends on it and on the replacement of the fossil fuels by renewable energies. However, their intermittency, caused by the unpredictability of the energy source, is the main drawback for their implementation. To this end, Thermal Energy Storage (TES) arises as a technology that manages the energy in order to be used furtherly for heating and cooling applications as well as power generation, hence covering the gap between the supply and the demand of energy. Here is where Phase Change Materials (PCMs) comes to play, as materials that store energy during a phase transition. Taking the melting/solidification phase transitions as examples, the performance of a PCM is as simple as the energy absorption during melting, and the further release during solidification. PCMs are already used in a wide range of applications such as building isolation or industrial heat recovery, but they are usually based on solid-liquid transitions, and dealing with liquid phases in some applications can imply big challenging designs and hence higher costs. Therefore, PCMs based on solid-solid transitions are proposed in this thesis as a potential alternative for TES applications.

Plastic Crystals (PCs), are pointed out as energetic solid-solid PCMs with a huge potential due to the wide variety of functional groups they can have, and therefore the large temperature ranges that their transitions can cover. However, most of these PCs show an undesired phenomenon for being considered PCMs, the thermal hysteresis in the temperatures, usually known as subcooling. This well-known drawback attracted great interest in the last years because its suppression opens to the use of many compounds for TES applications, but it is still not an evident phenomenon in solid-solid phase transitions since there is just a few studies about it so far. The early stage in which the understanding of the subcooling in solid-solid transitions is located, motivates this thesis focused on the understanding of the mechanism behind such a phenomenon in order to mitigate it.

A first selection of five PCs was carried out regarding different and potentially energetic functional groups such as alcohol and amines. All the candidates, neopentylglycol (NPG), 2-amino-2-methyl-1,3-propanediol (AMP), pentaglycerin (PG), tris(hydroxymethyl)aminomethane (TRIS), and pentaerythritol (PE), are polyalcohols which show medium-large subcooling in their solid-solid phase transitions. Therefore, after a

complete characterization of important thermophysical parameters such as the transition temperatures and enthalpies, temperatures of melting and degradation, specific heats, thermal conductivities, densities, and thermal expansions; a deep insight on the subcooling phenomenon was carried out.

Subcooling present in the solid-solid transitions of PCs does not depend on different operational parameters such as the sample mass, the heating/cooling rates, and the thermal cycling, pointing out that it does not follow a nucleation-crystal growth mechanism like solid-liquid transitions. Since the solid-solid transitions of these PCs are based on structural changes in the hydrogen bonds disposition, hydroxyl groups suffer the biggest change from the low temperature (crystalline) solid phase to the high temperature (plastic) solid phase. They are the first part of the molecules to start the phase transition upon heating, and the last ones to undergo the reverse transition upon cooling. The big differences in molecular motions between both solid phases are mainly due to the breaking of the hydrogen bonds during the crystalline-plastic phase transition, added to the weakening of the remaining hydrogen bonds in the plastic phase. This promotes an orientational disorder caused by a high rotational freedom of the molecules located at fixed positions in the unit cell. In addition, a clear difference can be found between NPG and PG on one side, and AMP, TRIS and PE on the other side. The rigidness of all the crystalline phases is higher increasing the hydroxyl and/or amine groups in the molecules due to the hydrogen bonds interactions. However, despite of the rigidness of the plastic phase of NPG and PG follows this simple rule, the plastic phases of AMP, TRIS and PE show an unexpected lower rigidness. This is due to a concerted motion of protons in a “water-like cloud” due to a crystal lattice whose cohesion forces are mainly based on hydrogen bonds. This phenomenon is even more evident for AMP and TRIS, due to the higher ionic character of the protons linked by hydrogen bonds between alcohol and amine groups. In addition, the plastic to crystalline phase transition upon cooling starts with the loss of the skeletal motion of the core of the molecules. However, the alcohol/amine protons keep the fast dynamics characteristic of the plastic phase, hence hindering the needed reorganization of hydrogen bonds to undergo the transition to the crystalline phase. This is the reason why molecules located at grain boundaries or surfaces are the first to start the solid-solid phase transition, since they are not involved in the “proton cloud” and can be easily rearranged. Therefore, the lack of reorganization of the molecules in the plastic phase becomes the main cause for the subcooling present in these plastic crystals, even larger for AMP and TRIS due to the huge difference in the molecular motion between both solid phases.

Considering the beforehand mentioned insights about the subcooling causes in PCs, several approaches were tested in order to mitigate it as much as possible. Since superficial molecules seem to firstly start the phase transition, a physical treatment by ball milling of the PCs was carried out in order to reduce the particle size and hence increase the specific surface area. The reduction of particles sizes was directly related to the decrease of the subcooling degree up to the 69 % in the case of PG, hence supporting the hypothesis of the superficial molecules as the first ones to start the phase transition.

Another approach followed was to try to anchor the hydroxyl and amine protons which are fast moving in the plastic phase by the dispersion of dopants such as expanded graphite and graphene particles. In this case, a subcooling reduction up to the 62 % was achieved for PG. Even though most of cases the enthalpy of the transition for the final composite was decreased due to the addition of an inert material, the composite NPG-oxidized graphene particles showed and unexpected increase of enthalpy of around 22 %. The increase of the solid-solid transition enthalpy was probably due to the creation of new hydrogen bonds between the PC and the oxidized groups of the graphene particles, hence reinforcing the active hydrogen bonds and increasing the enthalpy of the solid-solid transitions.

Finally, the application of an external pressure was also tested in order to try to modify the equilibrium of the phase transition. Since these materials were reported to undergo huge barocaloric effects, pressures up to 350 MPa were applied achieving temperature`s displacements up to almost 40 ºC of the phase transition. However, the subcooling was not modified substantially, resulting in a similar value of subcooling for both the materials prepared by casting method (with an initial large subcooling) and for materials prepared by ball milling with a lower subcooling. Therefore, despite pressure variations do not lead to big subcooling improvements, the sum of different approaches such as the processing of materials and the dispersion of oxidized particles, points out the PCs as potential candidates for next generation of solid-state heat pumps, in which the application of pressure can lead to big temperatures changes in energetic materials whose subcooling has been previously reduced.

Resumen

La gestión energética es hoy en día una preocupación crucial para toda la humanidad, ya que nuestro futuro depende en gran medida de ella y de la sustitución de los combustibles fósiles por energías renovables. Sin embargo, la intermitencia de estos vectores energéticos causada por la imprevisibilidad de la correspondiente fuente de energía es el principal inconveniente para su implantación actual a gran escala. Para ello, el Almacenamiento de Energía Térmica (TES, por sus siglas en inglés) surge como una tecnología capaz de gestionar la energía con el fin de ser utilizada posteriormente para aplicaciones como la calefacción y refrigeración, así como para la generación de energía, cubriendo así la brecha entre la oferta y la demanda de energía. Es aquí donde entran en juego los Materiales de Cambio de Fase (PCM) como materiales que almacenan energía durante una transición de fase. Tomando como ejemplo las transiciones de fusión y solidificación, el funcionamiento de un PCM viene dado por la energía absorbida durante la fusión, y su posterior liberación durante la solidificación. Los PCMs ya se utilizan en una amplia gama de aplicaciones, como el aislamiento de edificios o la recuperación del calor industrial. Sin embargo, los PCMs suelen estar basados en transiciones sólido-líquido, y el hecho de tener que lidiar con fases líquidas implica grandes retos en cuanto a diseño de la instalación, y por tanto costes más elevados. Por lo tanto, en esta tesis se proponen PCMs basados en transiciones sólido-sólido como una potencial solución a este inconveniente.

Los Cristales Plásticos (PCs) destacan por ser PCMs con energéticas transiciones sólido-sólido con un enorme potencial debido a la gran variedad de grupos funcionales que pueden poseer, y por tanto el amplio rango de temperaturas que pueden cubrir sus transiciones. Sin embargo, la mayoría de los PCs muestran un fenómeno indeseable para ser considerados buenos PCMs; la no reversibilidad completa de su transición de fase, es decir; la histéresis térmica en cuanto a las temperaturas de transición, ampliamente conocido como el fenómeno de subenfriamiento. Este inconveniente es la principal causa de pérdidas energéticas y desplazamientos de las temperaturas de transición, por lo que su estudio ha venido despertando gran interés durante los últimos años. Sin embargo, aún no es un fenómeno evidente en las transiciones de fase sólido-sólido. Por lo tanto, el estado de inmadurez en el que se encuentra la comprensión de dicho fenómeno en estas transiciones

motiva esta tesis centrada en la comprensión del mecanismo subyacente con el fin de mitigarlo lo máximo posible.

Para ello, se llevó a cabo una primera selección de cinco PCs con diferentes grupos funcionales potencialmente energéticos como alcoholes y aminas. Todos los candidatos, neopentilglicol (NPG), 2-amino-2-metil-1,3-propanodiol (AMP), pentaglicerina (PG), tris(hidroximetil)aminometano (TRIS), y pentaeritritol (PE), son polialcoholes que muestran un subenfriamiento medio-elevado en sus transiciones de fase sólido-sólido. Por lo tanto, tras una completa caracterización de importantes parámetros termofísicos tales como las temperaturas y entalpías de transición, las temperaturas de fusión y degradación, los calores específicos, las conductividades térmicas, densidades y expansiones térmicas; se llevó a cabo un estudio en profundidad del fenómeno del subenfriamiento.

A diferencia del subenfriamiento presente en las transiciones sólido-líquido, el fenómeno en las transiciones bajo estudio no es dependiente de diferentes parámetros operativos como pueden ser la masa de la muestra, la velocidad de calentamiento y enfriamiento ni el ciclado térmico, lo que indicaría que no sigue un mecanismo de nucleación-crecimiento cristalino como las transiciones sólido-líquido. Dado que las transiciones en estado sólido de los PCs se basan en cambios estructurales en la disposición de los puentes de hidrógeno, los grupos hidroxilo son aquellos que sufren el mayor cambio desde la fase sólida de baja temperatura (fase cristalina) a la fase sólida de alta temperatura (fase plástica). Además, es el primer grupo de las moléculas en iniciar la transición de fase al calentarse, y las últimas en iniciar la transición inversa al enfriarse. Las grandes diferencias en los movimientos moleculares entre ambas fases se deben principalmente a la ruptura de ciertos puentes de hidrógeno en la transición cristalina-plástica, así como el debilitamiento de aquellos que aún siguen en la fase plástica. Esta característica confiere a las moléculas de la fase plástica un desorden orientacional promovido por una elevada libertad de rotación de las moléculas que se encuentran en posiciones fijas dentro de la celdilla unidad. Además, se encuentra una clara diferencia entre NPG y PG, por un lado, y AMP, RIS y PE, por el otro. La rigidez de todas las fases cristalinas es mayor a mayor número de grupos hidroxilo y/o amina en las moléculas, debido a una mayor interacción por puentes de hidrógeno. Sin embargo, a pesar de que la rigidez de la fase plástica de NPG y PG sigue esta simple regla, las fases plásticas de AMP, TRIS y PE muestran una inesperada menor rigidez. Ello es debido a un movimiento concertado de los protones dentro de una “nube de protones” debido a que son redes principalmente basadas en interacciones por puentes de hidrógeno. Este fenómeno es aún más evidente en el caso de AMP y TRIS, debido al mayor carácter iónico de los enlaces

de hidrógeno entre los grupos alcohol y amina. Además, la transición desde la fase plástica a la cristalina comienza con la pérdida de la rápida movilidad del núcleo molecular, mientras que los protones tanto de los grupos alcohol como de amina continúan con la rápida dinámica de la fase plástica, dificultando así la reorganización necesaria de los puentes de hidrógeno para formar de nuevo la fase cristalina. Esta es la principal razón por la que las moléculas situadas en los límites de granos cristalinos o en las superficies son las primeras en iniciar la transición de fase, ya que no están enteramente implicadas en la "nube de protones" y pueden reorganizarse de forma más sencilla. Por lo tanto, esta falta de reorganización se convierte en la principal causa del subenfriamiento presente en estos cristales plásticos, aún más evidente par AMP y TRIS debido a la enorme diferencia de movimiento entre ambas fases sólidas.

Teniendo en cuenta las anteriores conclusiones, diferentes estrategias fueron probadas para mitigar el subenfriamiento en los PCs lo máximo posible. Dado que las moléculas superficiales parecen ser las primeras en iniciar la transición de fase, se llevó a cabo un tratamiento morfológico de los PCs con el fin de reducir el tamaño de las partículas y aumentar así la relación superficie/masa. Para ello, un tratamiento de molienda por bolas fue llevado a cabo en lugar de preparar las muestras por un método de fusión/solidificación. La reducción del tamaño de partícula está directamente relacionada con la disminución del subenfriamiento hasta en un 69 % para el caso de PG, apoyando así la hipótesis de que las moléculas superficiales son las primeras en iniciar la transición de fase.

Otro intento de mejora del subenfriamiento para anclar los protones de grupos hidroxilo y amina y que por tanto cesen el rápido movimiento característico de la fase plástica, fue la dispersión de agentes dopantes, como partículas de grafito expandido y grafeno. En este caso, se consiguió una reducción del subenfriamiento de hasta el 62% para el PG. Sin embargo, en la mayoría de los casos, la entalpía de transición del composite final disminuyó debido a la adición de un material inerte. Por otro lado, la dispersión de partículas con grupos oxidados, como el óxido de grafeno, provocó un aumento de la entalpía de hasta un 22 % para el caso de NPG. Este sorprendente resultado se debe al refuerzo de la red de puentes de hidrógeno promovido por la formación de nuevos puentes de hidrógeno entre el PC y los grupos oxidados del grafeno, reforzando así los puentes de hidrogeno activos en la transición de fase, y por tanto la entalpía de transición

Por último, también se testeó la aplicación de presión externa durante la transición de fase para modificar el equilibrio. Dado que diferentes estudios reportan que estos materiales sufren enormes efectos barocalóricos, se aplicaron presiones de hasta 350 MPa,

consiguiendo desplazamientos de la temperatura de transición de hasta casi 40 ºC. Sin embargo, el subenfriamiento no fue modificado sustancialmente con el aumento de presión, resultando en un valor común ya sea para los materiales preparados mediante el método de molienda por bolas, como aquel preparado por el método de fusión/solidificación. Por tanto, a pesar de que las variaciones de presión no conducen a grandes mejoras del subenfriamiento, la suma de diferentes estrategias como lo son el procesado de los materiales y la dispersión de partículas para aumentar la entalpía, convierten a los PCs como potenciales candidatos para la siguiente generación de bombas de calor en estado sólido, en las que la aplicación de presión puede conducir a grandes cambios de temperaturas de transición en materiales muy energéticos cuyo subenfriamiento ha sido reducido previamente.

Nomenclature

Acronyms:

AEO	Annual Energy Outlook
AMP	2-amino-2-methyl-1,3-propanediol
BCC	Body Centered Cubic
BHPA	2,2-bis(hydroxymethyl)propionic acid
BNP	2-bromo-2-nitro-1,3-propanediol
CDA	Cellulose diacetate
CEL	Cellulose
CNT	Carbon nanotube
CSP	Concentrated solar power
DAPE	Diaminopentaerythritol
DMPA	2,2-dimethylpropionic acid
DSC	Differential Scanning Calorimetry
EES	Electrochemical Energy Storage
EG	Expanded graphite
FCC	Face Centered Cubic
FTIR	Fourier-transform Infrared
GHG	Greenhouse gases
GO	Graphene oxide
HNP	2-hydroxymethyl-2-nitro-1,3-propanediol
IR	Infrared
LHS	Latent heat storage
MAPE	Monoaminopentaerythritol
MNP	2-methyl-2-nitro-1,3-propanol
MNPD	2-methyl-2-nitro-1,3-propanediol
NMR	Nuclear Magnetic Resonance

NP	Neopentane
NPA	Neopentylalcohol
NPG	Neopentylglycol
NPG-d_2	Deuterated neopentylglycol
PC	Plastic Crystal
PCM	Phase Change Material
PE	Pentaerythritol
PEG	Polyethylene glycol
PEO	Polyethylene oxide
PG	Pentaglycerin
PG_AR	PG as received from the supplier
PG_BM	PG powder after a ball milling treatment
PG_C	PG processed by casting
PG_P	PG compacted by uniaxial pressure after a ball milling treatment
PG-d_3	Deuterated pentaglycerin
PTFE	Polytetrafluoroethylene (Teflon)
PU	Polyurethane
SHS	Sensible heat storage
ssNMR	Solid-state nuclear magnetic resonance
TcHS	Thermochemical heat storage
TES	Thermal Energy Storage
THA	Tris(hydroxymethyl)acetic acid
TMP	Trimethylolpropane
TMS	Tetramethylsilane
TNB	*t*-nitrobutane
TRIS	Tris(hydroxymethyl)aminomethane
TRIS-d_5	Deuterated tris(hydroxymethyl)aminomethane

Symbols:

α	Conversion rate
ρ	Density
δ	Chemical shift
μ	Reduced mass
ν_0	Frequency of an external magnetic field
ν_r	Frequency emitted by a reference
ν_s	Frequency emitted by the sample
$\tilde{\nu}$	Wavenumber
ΔG	Gibbs free energy
ΔH_c	Enthalpy of solid-solid phase transition upon cooling
ΔH_h	Enthalpy of solid-solid phase transition upon heating
ΔH_r	Enthalpy of reaction
ΔS	Entropy variation during the phase transition
B_0	External magnetic field
C_p	Specific heat
k	Strength bond constant
k_T	Thermal conductivity
T_1	Relaxation time
T_c	Onset temperature of solid-solid transition upon cooling
T_f	Final temperature within a range
T_h	Onset temperature of solid-solid transition upon heating
T_i	Initial temperature within a range
T_m	Melting point
T_r	Temperature of the reference
T_s	Temperature of the sample

Table of contents

Chapter 1

Introduction

1.1. Global energy scenario.

The production of energy has been a topic of interest since lot of decades ago, even more noticeable after the industrial revolution of the XVIII century. Energy is indispensable for social and economic development all over the world, and it becomes the driving force for new advances in science and technology and hence for an improvement of the live quality [1,2]. However, are we managing correctly the production, use and storage of it?

Historically, energy systems heavily rely on fossil fuels, such as petroleum, coal, or natural gas. These energy sources have marked the development of certain countries in spite of others, mainly due to the places where a huge exploitability is available, or where there is a high demand of such sources. For instance, petroleum is the major source of energy in the United Sates. In the 1970s, it reached the maximum demand up to 45%, but after the energy crisis of that decade the use declined to about 40%, being practically constant from then to nowadays. Natural gas and coal also followed the same trend. The former consumption was almost four times great in 2007 than in 1950. Coal consumption, on the other hand, was 35% of the total in 1950, but it declined to about 20%, again, after the energy crisis, and this

proportion has remained since then. However, coal is currently the most important fuel for electricity generation [3]. Some projections giving by the Annual Energy Outlook (AEO) in 2014 predicted a more or less constant demand for the next years until 2040 (Table 1.1). Even though some restraints have been taken in order to decrease the energy consumption, the economic growth in the developed and developing countries is causing a rapid increase in this consumption [4,5].

Table 1.1. Comparison of projections in the AEO2014 and AEO2013 reference cases from 2011 to 2040. Source: ref. [5].

Year	Reference cases	Energy consumption by fuel (quadrillion Btu)		
		Petroleum and other liquid fuels	Natural gas	Coal
2011		36.56	24.91	19.62
2012		35.87	26.20	17.34
2025	AEO2014	36.28	28.97	19.03
	AEO2013	36.87	27.28	19.35
2040	AEO2014	35.35	32.32	18.75
	AEO2013	36.07	29.83	20.35

The use of this huge amount of energy is linked to the diversity of applications for which the fossil fuels have been widely used. These are classified in three big groups: Buildings, transportation and industrial. The buildings sector represents the energy use for both residential and commercial purposes (Figure 1.1), and it is considered as the biggest single contributor to world energy consumption [6]. In 2010, this sector accounted for more than 20% of total worldwide consumption of delivered energy in a variety of applications such as isolation, heating, and cooling systems [7,8]. The energy delivered to the industrial sector is quite important since the development leads to a socio-economic progress in the society. Indeed, the worldwide demand in this sector is expected to increase from 200 quadrillion Btu to 307 quadrillion Btu from 2010 to 2040, (a 1.4% of growing per year). Something similar occurs in the transportation sector, where the petroleum is the master fuel. About 71% of the total petroleum demand was devoted to this sector in 1950, and it has been reduced in recent years to 65% [3]. Moreover, it is worth noting that within these sectors, a big part of the consumed energy is devoted for the generation of electricity (Figure 1.1), mostly in the building sector. Taking all these values into account, we can expect raising prices/costs of different ambits of the usual life by modifying the energy supply or demand. This is one of the

reasons why we have to carefully manage the way to reduce the consumption of the fossil fuels. However, the main reason for putting these fossil fuels aside is not the differences in prices of fuel sources and other economic issues, but the main reason is much more important and well-known for every one of us: The emission of greenhouse gases.

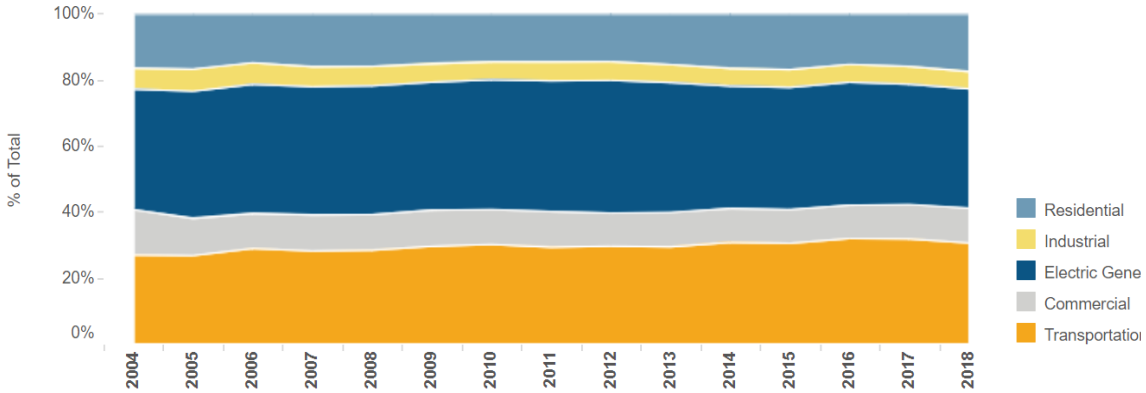

Figure 1.1. Primary consumption of energy by sectors in the U.S. in 2018.

The greenhouse gases (GHGs) are those compounds in gas state that trap a huge amount of heat in the atmosphere. Among them, the most abundant ones are the combustion gases, such carbon dioxide, or nitrogen and sulfur oxides, as well as methane and the fluorinated gases. In 2020, 5981 million metric tons of CO_2 equivalent were released to the atmosphere in the U.S. Actually, carbon dioxide is the primary greenhouse gas emitted through human activities such as the burning of hydrocarbons, the decomposition of biomass, and so on (Figure 1.2), and despite of being present in the natural Earth's carbon cycle, its concentration is increasing due to the combustion of fossil fuels for the different applications beforehand commented [9]. Therefore, the high amount of these gases in the atmosphere is causing the global warming on the Earth, and hence the well-known climate change, which is becoming more noticeable with the passing of time.

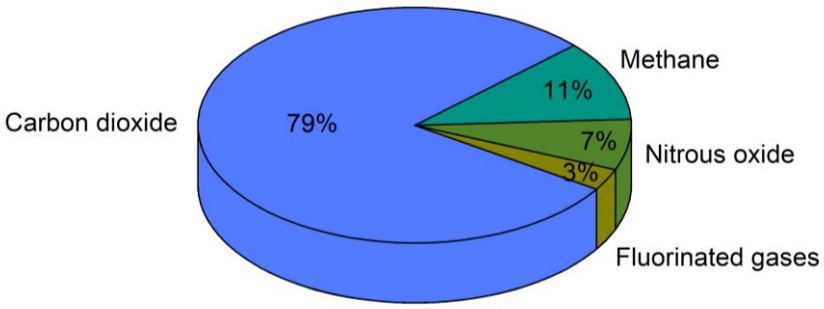

Figure 1.2. Main greenhouse gases emitted to the atmosphere in 2020 in the U.S.

Considering the excessive emissions of greenhouse effects, our focus as a society must be trying to reduce them as soon as possible [10]. To this end, and since their main source is the use of fossil fuels, the best path is to replace these traditional fuels with new renewable vectors (Figure 1.3). Renewable energies are defined as those which comes from renewable resources that are naturally replenished on a human timescale, such as the wind, the solar radiation, the water, and so on. [11]. Therefore, and since the global energy demand increased by 30% between 2006 and 2021, the boost of renewable energies is an urgent matter [12].

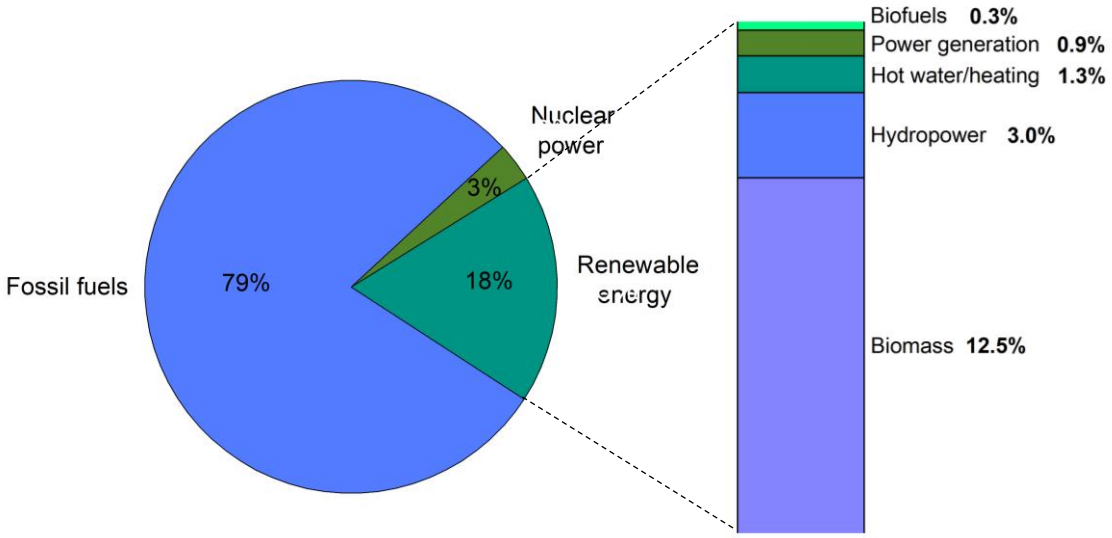

Figure 1.3. Global energy demand by type of source in 2010.

The global renewable energy demand is growing by a 5.62% per year, so that it is growing three times faster than the annual growth rate of fossil fuels demand. Among them, the hydropower is the major energy source for electricity production, however, it is the less

applicable for the common use, e.g., for building isolation, transportation, etc. This is why the growth rate of the hydropower was just 0.56% per year. However, such a grow of other renewable energies reached 16.64%, this is, about 11 times higher than the annual growth rate of fossil energy consumption. In summary, in the last decade the consumption of renewable energies has increased 41.59% [13,14]. Figure 1.4 shows the global steady growth rate that the renewable energy generation has reached for more than a decade, and this is the path we must follow in order to decrease the greenhouse gases emission and hence to contribute to a climate recovery.

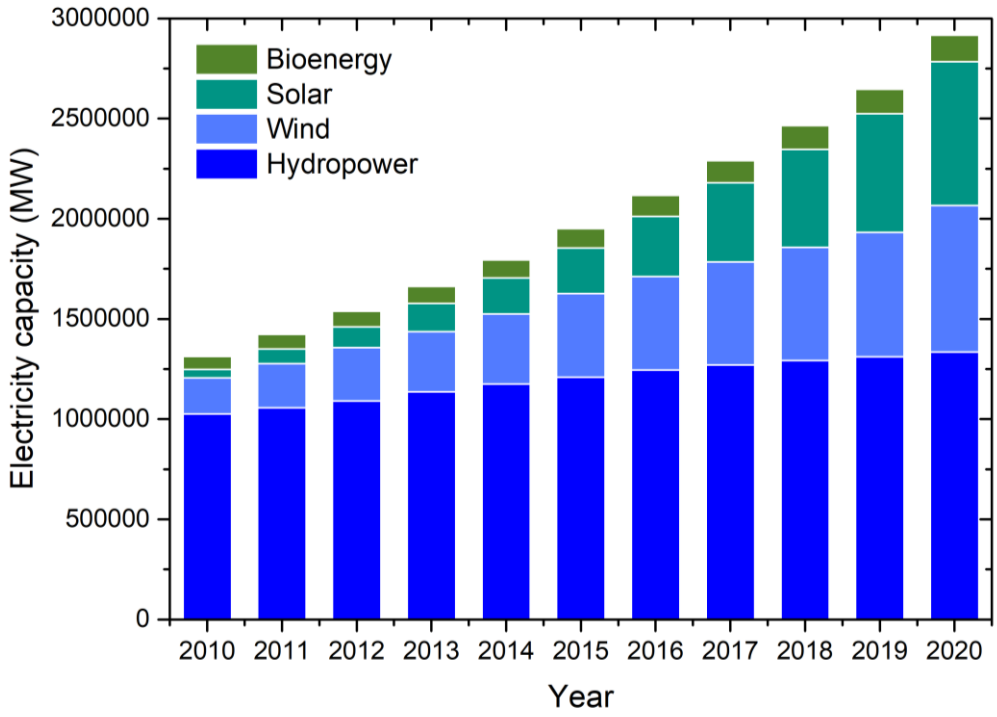

Figure 1.4. Global electricity capacity in MW classified by type of main technology. Source: ref. [15].

However, some approaches have still to be implemented in the renewable energy world in order to go on applying them in our daily lives. In spite of the numerous advantages, such as the running out of the fossil fuels due to the depletion of mineral deposits in the next years, as well as the huge reduction of greenhouse gases emissions (from 1-2 kg CO_2/kWh of fossil fuels based power plants, to 0.01-0.1 kg CO_2/kWh of renewable energies based power plants), some limitations have to be firstly solved [16], such as, for example, the improvement of the efficiency and the intermittency [17] and the dependency on geographical location and weather conditions. This is usually known as volatility and unpredictability of most

of the renewable energies. Therefore, there must always be a sufficient reserve in the system in the form of available power which can eliminate the deficiency that occurs when such a renewable energy source is not available. In order to solve this problem, we can turn into the hot trend field of the energy storage.

1.2. Thermal Energy Storage.

The main aim of the energy storage is the capability to give humans the power of managing the energy with security, efficiency and at any desired moment. This goal can be achieved by using different forms of energy storage, such as the Electrochemical Energy Storage (EES), in which batteries are in the spotlight, and also the Thermal Energy Storage (TES). The latter one has become nowadays a key technology in the energetic transition since it allows to stock thermal energy that can be furtherly used for heating/cooling applications and power generation [18]. This is one of the main reasons why TES has been gaining more and more interest in recent times, since it can overcome the intermittence and fluctuation of renewable energies by solving the gap between supply and demand of energy [19,20]. In order to easily understand how a TES system works, an analogy regarding the solar energy harvesting can be done (Figure 1.5). During the day, the energy generation peak occurs when the sun is in its maximum point but, in general terms, the demand is not too high at those hours. On the other hand, the highest energy demand occurs at night and in the morning when there is a lack of available energy to be used directly. In this situation, an efficient TES system comes into play: The system will be able to collect the energy during the generation peak, and store it until the desired demand.

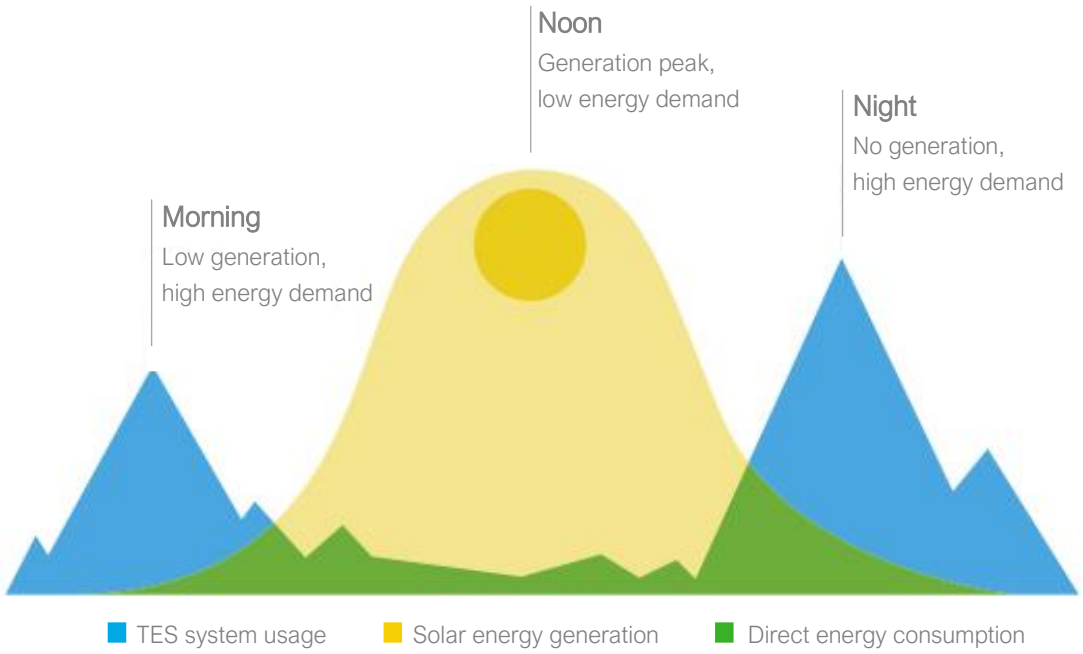

Figure 1.5. Solar energy generation, storage, and consumption scheme during the day.

An appropriate description for the suitability of an energy storage system can be done in terms of the following characteristics [21]:

- ◊ **Capacity**: Amount of energy stored in the system, which depends on the storage process, the size of the system, and the medium used to transfer the energy.
- ◊ **Power**: Rate at which the energy stored in the system can be discharged or charged.
- ◊ **Efficiency**: Ratio between the energy provided by the system to the energy needed to charge it. It considers the thermal losses during the storage period and/or the charging/discharging cycles.
- ◊ **Storage period**: Useful life of the energy when it is stored. It can last from hours (short-term energy storage) to months (long-term or seasonal storage).
- ◊ **Cost**: Value per capacity (€/kWh) or per power (€/kW) of the storage system, and it considers the benefits, the invested capital, and the operation costs of such a system during its lifetime.

These characteristics will clearly depend on how the storage of energy is carried out. Nowadays, there are three main ways to store thermal energy: Thermochemical Heat Storage, Sensible Heat Storage and Latent Heat Storage (Figure 1.6) [22].

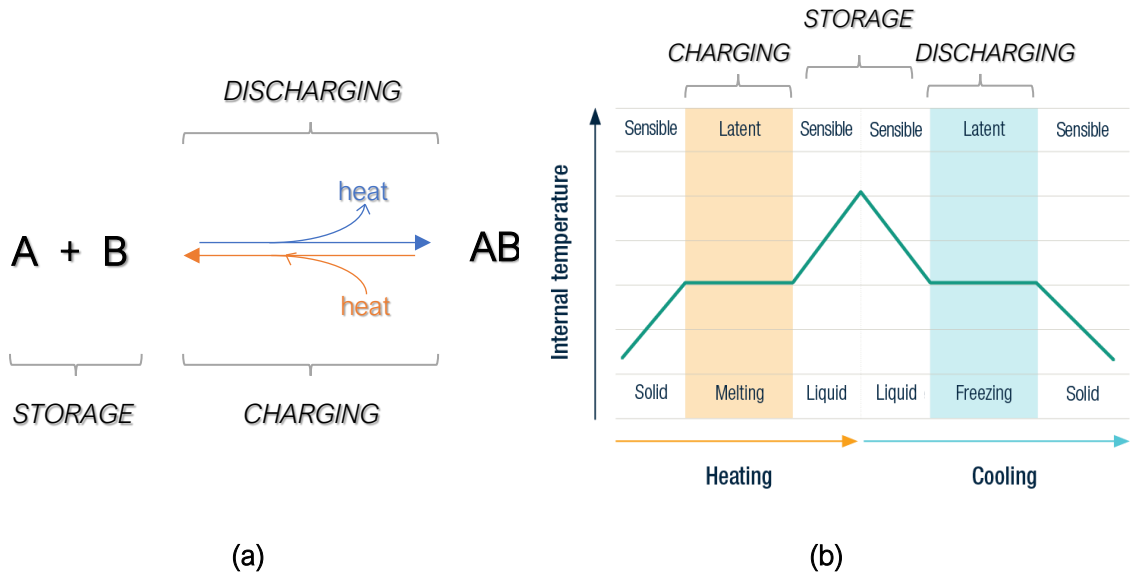

Figure 1.6. Scheme of the different thermal energy storage methods: (a) thermochemical heat storage, (b) latent heat storage and sensible heat storage.

Thermochemical heat storage (TcHS) is based in the absorption or release of energy during a reversible chemical reaction. In it, the endothermic reaction will absorb the energy known as enthalpy of reaction, and it will be released during the reverse process (Figure 1.6a). This approach allows to work in a wide range of temperatures in which the common chemical reactions take place. Therefore, the storage capacity of these systems will be a direct consequence of the enthalpy of reaction, and it will be proportional to the amount of the active material (m), the enthalpy of reaction (ΔH_r) and the extent of the conversion (α_r), as showed in Equation 1.1 [23–26].

$$\boldsymbol{Q = m \cdot \Delta H_r \cdot \alpha_r} \qquad (1.1)$$

In TcHS systems, many different reversible and energetic chemical reactions can be considered to be used as TcHS candidates. For example:

◊ **Hydration/dehydration**: Reversible hydration from a metal oxide to a metal hydroxide, e.g. $CaO/Ca(OH)_2$ at 440 ºC (ΔH_r = 1400 J/g) [27,28].

◊ **Absorption/desorption**: Reversible transformation between a metal and its hydride, e.g. Mg/MgH_2 at 279 ºC under atmospheric pressure (ΔH_r = 2800 J/g) [29,30].

◊ **Carbonation/decarbonation**: Reversible reaction from a metal oxide and carbon dioxide to form carbonates, e.g. $CaO/CaCO_3$ at 890 ºC under atmospheric pressure (ΔH_r = 1800 J/g) [31,32].

◊ **Oxidation/reduction**: Reversible redox reactions in metal oxides, e.g. CoO/Co_3O_4 at 905 ºC under atmospheric pressure (ΔH_r = 800 J/g) [33–35].

The high energy density involved in these reactions is due to the breaking and formation of chemical bonds instead of just physical interactions as occurs in both sensible and latent heat storage. However, TcHS has a low maturity in the sector, mainly because they heavily rely on the nature of each chemical reaction, as well as the complexity of the design of the final TES system [36]. Therefore, the other two options to store thermal energy are nowadays more developed and are attracting more interest: the sensible and the latent heat storage.

Sensible heat storage (SHS) is the simplest method to store thermal energy, being based on the physical interactions of a material at different temperatures. In this case, the material stores energy when heated up, and releases it when cooling down (Figure 1.6.b). The SHS capacity of a material is given by Equation 1.2:

$$\boldsymbol{Q = m \cdot C_p \cdot \Delta T} \tag{1.2}$$

where m is the mass of the sample, C_p is the specific heat and ΔT is the temperature difference between the starting and the end point of the storage [37]. The limiting condition for this type of storage is the selection of materials with a high C_p. Traditionally and still nowadays, the two most used materials in this case are water or wood, with specific heats of 4.18 J/g/K and 2.39 J/g/K, respectively. Usually, a liquid material is expected to have a higher C_p than a solid one, and it is usually even higher for gases. Therefore, despite of the use of solid SHS systems avoids leakages or evaporations, usually SHS liquids have higher specific heats, and they are plentiful and economically competitive [38]. However, the required amount of material in some cases can be quite large, becoming a problem with solids with low C_p or low density liquids requiring higher volumes [22]. In Table 1.2, the most used SHS materials are showed together with their properties [39,40].

Table 1.2. Common solid and liquid state SHS materials.

Storage material	Type	Working temperatures (ºC)	Density (g/cm³)	Specific heat (J/g/K)
Ethanol	Organic liquid	≤ 78	0.79	2.40
Propane	Organic liquid	≤ 97	0.80	2.50
Butane	Organic liquid	≤ 118	0.81	2.40
Octane	Organic liquid	≤ 126	0.70	2.40

Isobutanol	Organic liquid	≤ 100	0.81	3.00
Isopentanol	Organic liquid	≤ 148	0.83	2.20
Engine oil	Oil mixture	≤ 160	0.89	1.88
Calorie HT43	Oil mixture	≤ 260	0.87	2.20
NaKMgCl	Molten salt	≤ 700	1.90	1.02
KMgCl	Molten salt	≤ 700	2.13	1.01
LiNaKF	Molten salt	≤ 700	2.53	0.98
Reinforced concrete	Solid SHS	≤ 400	2.20	0.85
Cast steel	Solid SHS	≤ 700	7.80	0.60
Silica fire bricks	Solid SHS	≤ 700	1.82	1.00
Magnesia fire bricks	Solid SHS	≤ 1200	3.00	1.15

In addition, SHS systems can suffer from thermal losses when transferring the heat (directly proportional to the temperature difference between the charger and the discharger) [41]. For example, there are several applications in which SHS systems are currently applied such as concentrated solar power (CSP), which store the heat in solar salts; metallic nitrates with high C_p in liquid state [42,43].

Latent heat storage (LHS) is the TES method that has raised more interest in the last decades, what is evidenced by the growing number of scientific publications that was multiplied by 20 in the last twenty years [18]. LHS systems are based on the absorption and release of energy during the phase change of a material (Figure 1.6.b), e.g., solid to liquid, liquid to gas or solid to solid. Phase transitions happens at a determined temperature which depends on the material and remains constant until the end of the transition [26]. The capacity of storing energy is directly proportional to the enthalpy (latent heat) involved in the phase change, which is related to the entropy differences between the two involved phases by the Gibbs equation (Equation 1.3):

$$\Delta \boldsymbol{G} = \Delta \boldsymbol{H} - \boldsymbol{T} \cdot \Delta \boldsymbol{S} \xrightarrow{\Delta G = 0} \Delta \boldsymbol{H} = \boldsymbol{T} \cdot \Delta \boldsymbol{S} \tag{1.3}$$

where ΔG if the Gibbs free energy change, ΔH is the enthalpy change of the phase transition, T is the temperature of transition and ΔS the entropy variation during the transition. Regarding the most common phase changes, classified as first order transitions, the Gibbs free energy is continuous, in other words, the difference of Gibbs energy between the two phases is equal to zero [44,45]. Consequently, the enthalpy of transition will be directly proportional to the entropy differences between the two phases involved, so the higher the entropy differences between the two phases, the higher the enthalpy absorbed or released during the transition.

This is the reason behind the high enthalpies associated to sublimations, due to the high entropy difference between the solid and the gas phase.

LHS materials typically have higher energy densities (from 80 kWh/m^3 to 200 kWh/m^3), than SHS materials, for which it usually ranges from 30 to 70 kWh/m^3. In Table 1.3 there are some general examples and their properties of interest in order to compare both SHS and LHS systems [46,47]. Since there are a lot of different useful transitions (solid-solid, solid-liquid, solid-gas, liquid-gas) among organic, inorganic or metallic compounds that cover a wide range of temperatures of transitions, there is an increasingly number of studies dedicated to these LHS based materials, which are widely known as Phase Change Materials.

Table 1.3. Overall comparison of properties for some heat storage media. Mass for storing 10^6 kJ for SHS materials is calculated considering ΔT = 15 ºC.

	TES method			
	SHS		LHS	
Property	Rock	Water	Organic	Inorganic
Latent heat of melting (kJ/kg)	*	334	190	230
Specific heat (kJ/kg/ºC)	1.0	4.2	2.0	2.0
Density (kg/m^3)	2240	1000	800	1600
Mass for storing 10^6 kJ (kg)	67000	16000	5300	4350
Volume for storing 10^6 kJ (m^3)	30	16	6.6	2.7

* Melting temperature is too high.

1.3. Phase Change Materials.

Phase Change Materials (PCMs) can be used in a wide range of applications on thermal energy storage such solar energy storage, building isolation and heating/cooling, as well as new textiles, industrial heat recovery or the recent thermal management for batteries [36,48]. A series of desired properties for PCMs, listed in Table 1.4, were given by Lane in 1983 and are still valid nowadays in order to validate a PCM for a selected application [26,49–51].

Table 1.4. Desirable properties for a PCM.

Properties	Characteristics
Thermal properties	Phase change temperature suitable for the application. High latent heat. High thermal conductivity and specific heat.
Physical properties	Favorable phase equilibrium. Low vapor pressure. High density. Small volume change during the phase transition.
Chemical properties	Long term chemical stability. Compatibility with container's materials. Safe material (nontoxic and nonflammable).
Kinetic properties	No thermal hysteresis (subcooling) in the phase change.
Economics	Abundant. Widely available. Cost-effective.
Sustainability	Embodied energy. Recyclability.

A material fulfilling all these properties is not easy to find. Usually, the selected PCM must undergo the phase transition 5-10 ºC below the system operation temperature in order to ensure a good performance of the required application. A large selection of materials can match the phase change temperature with the operation one, so other properties have to be taken into account. The enthalpy of transition must be high not only in mass terms, but also from a volumetric point of view, so that a high density is also required. Both involved phases in the phase transition have to be stable and not to degrade (oxidations, hydrolysis, volatilize, etc.) or segregate in different phases (as occurs for some salt hydrates). When thinking about the application, other additional parameters have also to be considered such as a good thermal conductivity, or the compatibility with the container. Moreover, a good reversibility of the phase change is also required, i.e., the endothermic and the opposite exothermic transitions must occur at the same temperature for each heating/cooling cycle, otherwise, the

so-called subcooling phenomenon is going to prevent the heat extraction from the PCM at the operating temperature of the system. These are the reasons why the material selection is a first important step in order to design and optimize the LHS system.

1.3.1. Solid-liquid PCMs.

Usually, the vast majority of PCMs reported in literature are based in solid-liquid transitions, this is, melting and crystallizations [26,52–55]. The reason behind this is that almost all the materials undergo stable and congruent melting transitions, so that historically LHS systems have been based in solid-liquid transitions. In general terms, PCMs have been classified into three major categories regarding the nature of the compound itself: Metals, inorganic salts and organic molecules. In most of the cases, a nice correlation can be found between the nature of the PCM (metallic, inorganic or organic) and the range of temperatures at which is going to operate: High temperatures (T > 300 ºC), medium temperatures (100 ºC < T < 300 ºC) and low temperatures (T < 100 ºC) (Figure 1.7). In any case, this is a general rule and each family of materials involves a large difference among them, so it is possible to find materials within the same family of compounds which cover different temperatures of operation. In addition, the classification regarding the nature of the compound is also interesting since some properties besides the melting temperature can be correlated with the nature of the substance, such as enthalpies, corrosiveness, volatility, etc. [53].

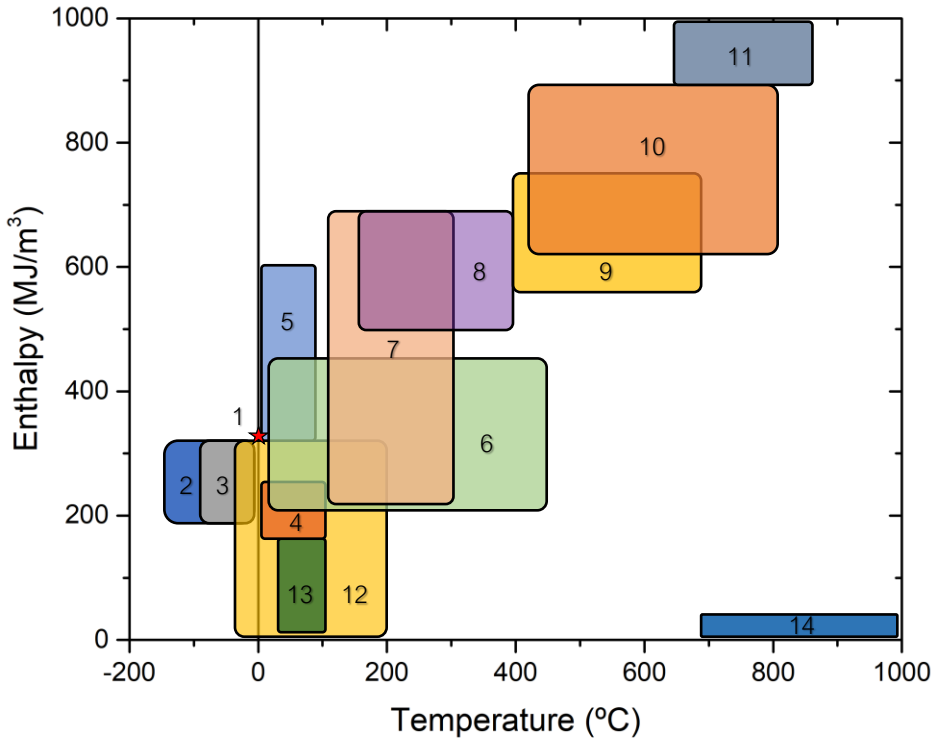

Figure 1.7. Overall enthalpies and temperatures ranges for different families of solid-liquid PCMs: (1) Water, (2) water-salt solutions, (3) clathrates, (4) paraffins, (5) salt hydrates, (6) sugar alcohols, (7) nitrates, (8) hydroxides, (9) chlorides, (10) carbonates, (11) fluorides, (12) organics, (13) organometallics, and (14) metallics.

Metallic compounds

Pure metals and alloys usually are selected as high temperature PCMs. Historically, the first proposed metallic PCMs were Al-based alloys with different elements such as Cu, Mg, Si or Zn, since alloys rich in Al or Si had large heat storage density (around 1600 kJ/L) [56,57]. Moreover, a fine tuning of the temperature of operation can be done by studying the eutectic composition of some binary mixtures. Due to the inherent high density of metals (commonly higher than 3 g/mL), metallic PCMs have high energy densities, and usually they show a small volume change during the solid-liquid transition, which is a major asset from the technical point of view. Moreover, they are characterized by high thermal conductivities (higher than 100 W/m/K) and low vapor pressures [58]. On the other hand, the two main drawbacks of metallic PCMs are reported to be the high cost and the high corrosivity under specific media that usually they suffer at high temperatures [59,60]. Consequently, metallic PCMs are scarcely considered in LHS applications, although they are more common in large capacity power plants applications. Some pure metals and alloys previously proposed as

PCMs are collected in Table 1.5 regarding the temperature and enthalpies of melting [61–63].

Table 1.5. Melting temperatures and enthalpies of transition of selected metallic PCMs.

Material	Melting temperature (ºC)	Latent heat (J/g)
Ga	30	80
Bi(22%) - In(78%)	72	25
Li	179	663
Mg(71%) - Zn(29%)	343	138
Zn	420	112
Al(62.5%) - Mg(37.5%)	451	310
Al(82.5%) - Cu(17.5%)	548	351
Al(80%) - Si(20%)	585	460
Al	661	400
Mg(41.1%) - Si(52.9%)	946	774
Cu	1084	209
Mn	1244	266
Be	1287	1754
Si	1412	1414

Inorganic compounds

Inorganic PCMs are mainly based in ionic salts usually composed by a metal cation (such as sodium, potassium, lithium, and sometimes calcium) and an inorganic anion such a nitrate, sulfate, carbonate or halides, although sometimes small organic anions are also possible. In Table 1.6, some common pure inorganic salts and other salt hydrates with potential use as PCM are collected [47,64–71]. The inherent characteristic of these materials of being a crystal with a strong ionic interaction, leads to usually high melting points and, for the same reason, medium-high enthalpies of melting. Nowadays they are widely used as pure materials or as eutectic mixtures, [72]. The fact of synthetizing an eutectic mixture promotes a decrease of the transition temperature with just a slight effect on the enthalpies of transition, so it is possible to tune the operation temperature of such materials by covering the gaps in temperature existents when considering only pure salts [73,74]. However, both single and eutectic mixtures of molten salts have common issues like leakages, corrosivity of the medium and medium-low thermal conductivities, so usually they need to be modified (by encapsulation or by dispersing different classes of particles) to improve their performances [75,76].

Salt hydrates are other inorganic PCMs widely found in large quantities in nature or as by-products of industrial and chemical processes, such as the production of soda ash [77–80]. Usually, some thermophysical properties of these salts are milder than metallic PCMs, like the lower density ranging around 1.5-1.8 g/cm^3, negligible volume changes during the melting (around the 1%), and thermal conductivities within the order of 0.6-0.9 W/m/K [81–84]. However, they show high enthalpies of melting up to 300 J/g in some cases [77]. Moreover, the common range of temperatures in which these materials operate falls within room temperature and 50 ºC (Table 1.6), However, they show some drawbacks as incongruent and poor-reversible melting transitions in which the material segregates in two or more phases [68,85]. Despite this problem is currently partially solved by mechanical stirring or by adding excess water to prevent forming a supersaturated solution, they can also promote some corrosion to metals, so the selection of the container must be carefully done.

Table 1.6. Melting temperatures and enthalpies of transition of selected inorganic PCMs [86–89].

Family of compounds	Compound	Melting temperature (ºC)	Enthalpy of melting (J/g)
Salt hydrates	$KF{\cdot}4H_2O$	18	231
	$Mn(NO_3)_2{\cdot}6H_2O$	25	126
	$CaCl_2{\cdot}6H_2O$	28	195
	$Na_2CO_3{\cdot}10H_2O$	33	247
	$Na_2HPO_4{\cdot}12H_2O$	40	280
	$Zn(NO_3)_2{\cdot}6H_2O$	36	147
	$Na_2S_2O_3{\cdot}5H_2O$	50	201
	$Na(CH_3COO){\cdot}3H_2O$	56	240
	$Ba(OH)_2{\cdot}8H_2O$	78	266
	$(NH_4)Al(SO_4)_2{\cdot}12H_2O$	95	269
Pure salts	$AlCl_3$	192	280
	$LiNO_3$	250	370
	KNO_3	333	266
	KOH	380	150
	$KClO_4$	527	1253
	LiH	699	2678
	$MgCl_2$	714	452
	Na_2CO_3	854	276
	NaF	993	750
	MgF_2	1271	936

Organic compounds

Organic PCMs are likely the most versatile and advantageous LHS family of materials, since there are a lot of different functional groups which lead to different molecules and behaviors. Due to its mainly covalent character regarding intermolecular interactions, the phase transitions are usually at medium-low temperatures (< 300 ºC), so that they can be devoted to applications such as buildings isolation, district hot water, industrial heat recovery, and so on [26,55,90,91]. They can cover a wide range of temperatures of transition following a nice trend regarding the main functional group, giving useful hint for the search of suitable compounds for a certain application (Table 1.7). In addition, organic PCMs usually undergo congruent melting and solidification with no phase segregation, so that there is no a decrease of the enthalpy upon thermal cycling. Moreover, most of these materials do not show any corrosiveness [26].

Table 1.7. Melting temperatures and enthalpies of transition of selected organic PCMs.

Family of compounds	Compound	Melting temperature (ºC)	Enthalpy of melting (J/g)
Paraffins	n-Tetradecane	6	228
	n-Hexadecane	19	216–236
	n-Octadecane	28	200–244
	n-Eicosane	37	247
	n-Tetracosane	51	255
Fatty esters	Methyl palmitate	29	215
	Methyl stearate	39	222
	Ethyl palmitate	23	182
	Ethyl stearate	34	202
	Vinyl stearate	27	122
Fatty acids	Caprylic acid	17	148
	Lauric acid	43	191
	Myristic acid	53	194
	Palmitic acid	62	204
	Stearic acid	69	214
Fatty alcohols	Tetradecanol	38	231
	Pentadecanol	44	141
	Hexadecanol	49	238
	Octadecanol	58	148
	Docosanol	70	263
Sugar alcohols	Xylitol	93	232

	Erythritol	118	319
	D-Mannitol	166	308
	Dulcitol	187	357
	Inositol	224	266
Organic carbonates	Dodecyl carbonate	19	200
	Tetradecyl carbonate	34	227
	Hexadecyl carbonate	45	219
Halides	1-Iodehexadecane	22	131
	Bromobenzene	31	65
	Tribromobenzene	122	67
Sulfides	Dilauryl thiopropionate	39	159
Ketones	Phorone	27	124
Amides	Acetamide	82	241

Paraffin waxes is the traditional name to refer the n-alkanes, linear chain hydrocarbons with no functional groups. Therefore, being the only intermolecular interactions in these molecules weak Van Der Waals forces, the temperatures of transition are expected to be low. As a consequence, the higher the size of the molecules (or the number of carbon atoms), the higher the number of Van der Waals forces to be broken, the higher the temperature and enthalpy of transition expected. The reported temperatures of transition can range from values below 0 ºC for paraffins with number of carbon atoms lower than 14, up to almost 100 ºC for the linear paraffin with 40 carbon atoms [50]. The densities of the solid phases of these materials are usually low, rounding 0.7 g/cm^3, also due to the weak intermolecular forces leading to a poor packaged crystal system [92]. These are good PCMs for low temperature applications due to the lack of corrosiveness, the safety, and cheapness. Moreover, due to the low density of the solid phase, they show small volume change during the melting/solidification. However, the main drawback is the high vapor pressure, again, due to the weak Van der Waals interactions, causing mass losses during the phase transition. In addition, other drawbacks to be considered are the low thermal conductivity and the flammability [53,65].

Following the increasing melting temperatures of organic PCMs, **esters derived from fatty acids** are the next family of compounds. They are usually used for low temperature applications as insulators in building applications by impregnating them in gypsum and bricks, as well as for cosmetics or textiles [93]. They are attractive PCMs due to the large availability, the high energy storage per unit mass, no odors, and no corrosiveness [94–99]. The precursors of these esters, the **fatty acids**, are a well-known family of organic PCMs whose

solid-liquid transition involves large enthalpies compared to paraffins and fatty esters, reproducible melting/solidification and no subcooling [26,100]. When the molecule has less than 7 carbon atoms, the melting temperature is below 0 ºC, except for formic and acetic acids, with a melting point of 8 ºC and 17 ºC and a latent heat of 266 J/g and 186 J/g, respectively [101–105]. However, apart from the low thermal conductivity typical of the organic PCMs, there is an added mild corrosivity due to the acid character of the carboxylic group. Moreover, they are not cheap; commonly 2-2.5 times more expensive than paraffin waxes [50,106].

For alcohol-based molecules, there is a general differentiation: fatty-alcohols (or n-alcohols) and sugar alcohols. **Fatty-alcohols** are the reduced form of fatty acids, so they can be named fatty alcohols as well. They usually have similar temperatures and enthalpies of melting than fatty acids and fatty esters, with the advantage of the non-corrosiveness [55,107,108]. On the other hand, **sugar alcohols** are also linear molecules (despite inositol, which is a cyclic hexose) with more than one hydroxyl group, and they are usually classified by having 4, 5 and 6 atoms of carbon, and hence 4,5 or 6 hydroxyl groups. Therefore, despite of being similar molecules with the same number of hydroxyl groups, the differences in the chirality of their hydroxyl groups confer different enthalpies to these materials. The higher the number of hydroxyl groups, the higher the enthalpy, reaching more than 350 J/g for the melting of dulcitol [109–112]. These molecules are promising solid-liquid PCMs due to the high energetic density, the suitable range of temperatures that they possess, as well as the lack of corrosiveness [113]. Other organic PCMs are widely reported, such as polyethylene glycol polymers (PEG), as well as organic carbonates, halides, sulfides, and amides. However, as reported in literature, these materials are less studied and applied as PCMs since they show other drawbacks such poor thermal stability, as well as low melting temperatures and enthalpies (Table 1.7) [96,114,115].

Summarizing, organic PCMs provide great possibilities in terms of ranges of temperatures and enthalpies, chemical stability, and mild characteristic for the compatibility with the medium or container. However, not only organic PCMs, but in general solid-liquid PCMs have disadvantages both related with the liquid phase involved in these transitions:

◊ **Volume changes**: Despite some PCMs have low volume changes, the difference of density between a solid and a liquid phase is always needed to be considered for the application.

◊ **Leakages**: The phase transition is characterized by the loss of the initial shape of the PCM, with the possibility to leak out of the container. These problems increase the complexity of the TES system design and cost.

Different approaches have been considered to solve these aspects such as the encapsulation of the PCMs or the confinement in porous materials [116–120]. However, the addition of an inert material to the PCM decreases the amount of active material and therefore the final effective energy. This is the reason why scientists started to look for new solutions avoiding the addition of inert materials. Accordingly, this work takes advantage of solid-solid transitions based PCMs instead of solid-liquid based PCMs in order to overcome at least some of the beforehand mentioned drawbacks.

1.3.2. Solid-solid PCMs.

There is a growing interest in the search for new PCMs based on solid-solid transitions characterized by solid-solid transitions from a solid ordered phase to a disordered solid phase. Usually, these high-temperature stable solid phases are based in molecules and/or ions which are translationally fixed, but shows a high rotational freedom. It is worth being careful not to confuse the disordered solid phase with an amorphous phase where there is no long-range order. In such a case, the transition would be a glass transition without a substantial energy involved in it. On the other hand, an orientationally disordered solid phase is a structure with a greater motion of the atoms, but still within a crystalline lattice. Generally, solid-solid transitions have been reported to have smaller latent heat than that for the melting transitions, since there are higher differences of entropy between a solid and a liquid phase than between two solid phases (Eq. 1.3). However, there is an existing search for energetic solid-solid PCMs due to the major advantages they provide such as no leakages and the small volume changes during the phase transition (Table 1.8) [121,122].

Table 1.8. Comparison of properties of solid-solid and solid-liquid PCMs.

Property	Solid-solid PCMs	Solid-liquid PCMs
Storage density	Medium	High
Volume changes	Small	Moderate
Containment	Little stringent	More stringent
Encapsulation	Not needed	Needed
Design	Flexible	Moderate
Cost	Medium	Low
Availability	Available	Available

These transitions are common in the field of polymers. For example, whereas polyethylene oxide (PEO) and cellulose diacetate (CDA) suffer from solid-liquid transitions, the chemically linked material made from PEO and CDA undergoes a solid-solid transition as well [123]. The same occurs in polymers blends synthetized using different solvents, such as PEO and cellulose (CEL) blends, whose synthesis from dimethylsulfoxide/paraformaldehyde originated a blend with a solid-solid transition, whereas the synthesis using N,N-dimethylacetamide/lithium chloride does not [124]. Other examples of polymers as potential solid-solid PCMs are some copolymers made from a polyurethane (PU) and a branched polyester as a chain extender. This is the case of the copolymer PEO/PU, in which the soft PEO segments undergo a solid-solid transitions whilst the PU skeleton restricts the free movement of the molecular chains of PEO, so that the material is able to change its solid phase before reaching the melting [125].

Another family of organic compounds are the metal organic salts complexes of general formula $(n\text{-}C_nH_{2n+a}NH_2)_2CuCl_2$ which transforms from a low temperature stable polymorph to another one at medium-high temperatures depending on the alkyl chain length [126,127]. From a conformational point of view, in the low temperature structure the alkyl chains are ordered with the carbon-carbon bonds in trans states, while in the high temperature polymorph the hydrocarbon chains are partially disordered, but still without reaching the liquid state (Figure 1.8). Moreover, similar inorganic salts without transition metal are reported to have solid-solid transitions, such as some alkylammonium salts derivatives [128,129], which show solid-solid transitions below 100 ºC with attractive enthalpies of around 150-200 J/g. However, in these cases, the melting is really close to the solid-solid transition, so lot of precautions must be taken in order to avoid reaching the melting point. Therefore, in the search for versatile organic molecules which undergo energetic and stable solid-solid transitions, an attractive, cheap and widely available option arises for solid-state thermal energy storage at low-medium temperatures; the Plastic Crystals.

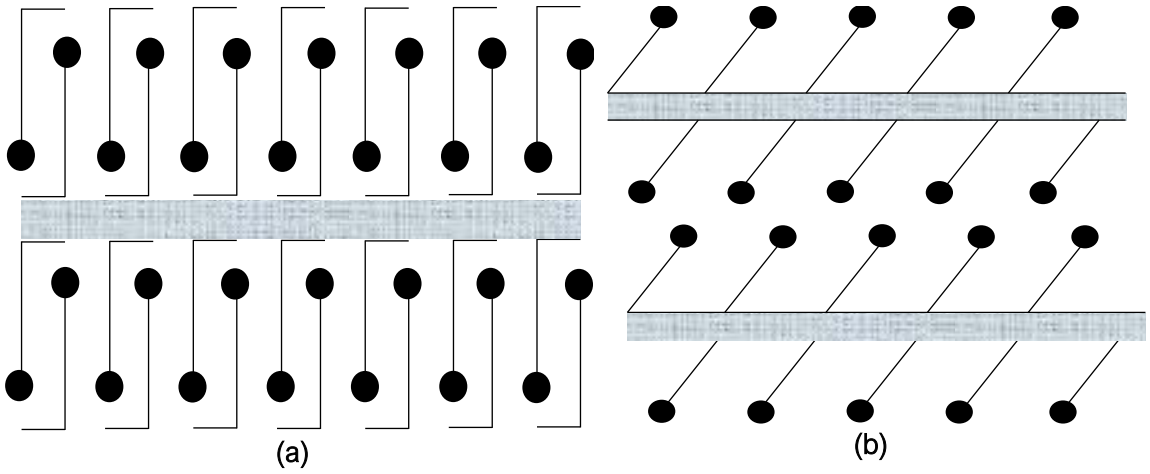

Figure 1.8. (a) Low temperature stable and (b) high temperature stable solid phases of metal organic salt complexes. Shaded zones reflect the ionic interactions, the solid lines the alkyl chain and solid circles the methyl end of such alkyl chains.

1.4. Plastic Crystals.

Plastic crystals (PCs) are organic molecules with low molecular weight, usually below 200 g/mol, which undergo energetic and stable solid-solid phase transitions [130]. The high energy involved in the transition is mainly due to the big entropy difference between both solid phases. Therefore, the entropy differences between the high temperature solid phase and the liquid phase are not as high as expected, and hence the enthalpy of melting is lower than that of other common solid-liquid PCMs (see Eq. 1.3). Historically, Timmermans reported a first definition of PCs referring to some compounds which have a very low entropy of melting, and with the peculiarity that they possess a globular shape, this is, they have a symmetrical point in their centers, such as methane or carbon tetrachloride, giving a sphere by rotation around an axis, such as cyclohexane or camphor (Figure 1.9) [131]. Therefore, this symmetry afforded these materials to freely rotate and to fix pretty well in highly symmetrical crystal systems such the cubic lattices, so that they are able to transform from an ordered crystalline phase to an orientationally disordered cubic phase upon heating. As pointed out beforehand, the biggest entropy changes occur during the solid-solid transition due to the similarity of the plastic phase and the liquid phase. In addition, the plastic tendence of such a phase was mainly the responsible for the designation “plastic crystal” [132,133].

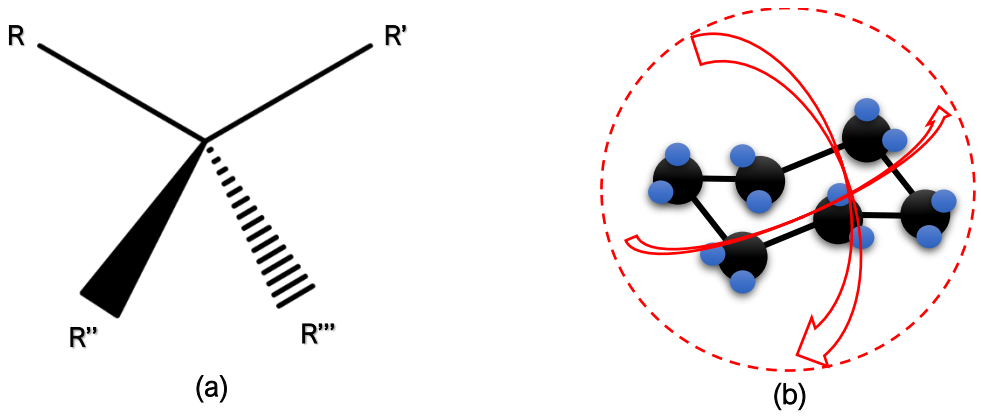

Figure 1.9. Scheme of globular molecules (a) with a symmetrical center and (b) with a rotational axis. In Figure 1.9a, methane (for R, R', R'', R''' = H), carbon tetrachloride (for R, R', R'', R''' = Cl), and neopentane (for R, R', R'', R''' = CH_3).

This first definition fitted quite well to most of the studied molecules of that time, but years later, it was expanded to other compounds showing reversible solid-solid transitions, such as the dialkylammonium salts, or even some paraffins and polymers, which were a priori out of the definition of Plastic Crystals [128,129]. In general terms, the weak intermolecular interactions would allow the rapid movements of neighboring molecules, and in the opposite scenario, the strong interlocking forces would prevent the plastic phase formation. Therefore, some years later, Postel et al. set a new structural criterion for predicting a plastic behavior in some molecules in which they related the globularity of a determined molecule and the molecular packing in a crystal lattice, through a parameter *R*, defined in Equation 1.4 as follows,

$$\boldsymbol{R = \frac{d_m}{D_m}} \tag{1.4}$$

where d_m is the minimum distance between two molecular centers inside the crystal lattice, and D_m is the maximum diameter of the sphere that one freely rotating molecule can circumscribe [134]. The calculation of this parameters for some already known materials with or without plasticity, leaded to set *R* values higher than 0.80 for molecules which have plastic phases. Figure 1.10 shows how the calculations fit quite well with the experimental results of some organic compounds and it gives hints for the search of new potential PCs.

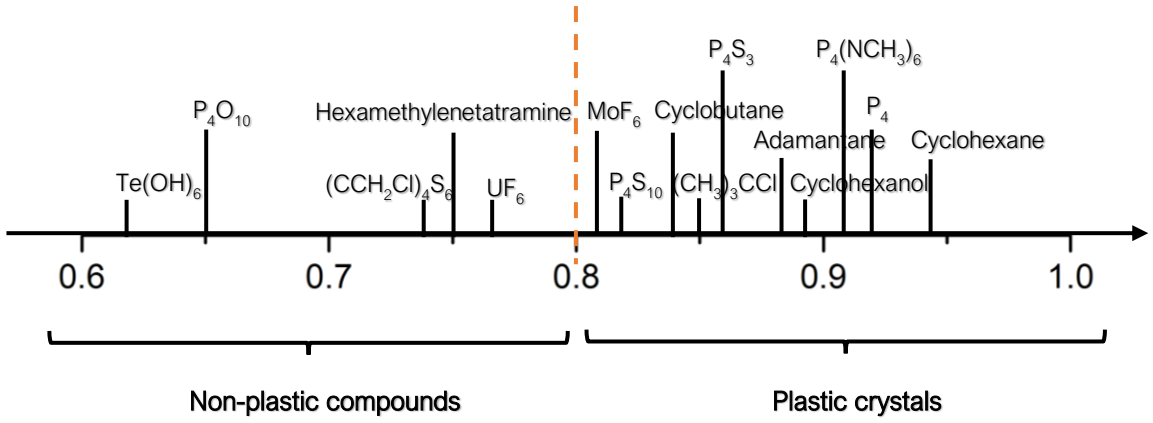

Figure 1.10. R-scale for different compounds.

In this context, a special focus has been done on interesting and energetic materials which are neopentane derivatives (Figure 1.9.a). Neopentane is a molecule that fits perfectly in the definition of globular molecule due to the symmetrical center in its quaternary carbon. Therefore, by the substitution of some functional groups in the structure, such as hydroxyl, amines, carboxylic acids, etc., it is possible to get a large family of globular compounds which undergo solid-solid transitions with big differences in the thermophysical properties. All these PCs undergo a transition from a low temperature stable crystalline phase to a high temperature orientationally disordered plastic phase which usually is a cubic lattice (Figure 1.11). Recently, these PCs are pointed out as potential PCMs for applications such as building isolation, district hot water or even industrial heat recovery, depending on the solid-solid transition temperature [135].

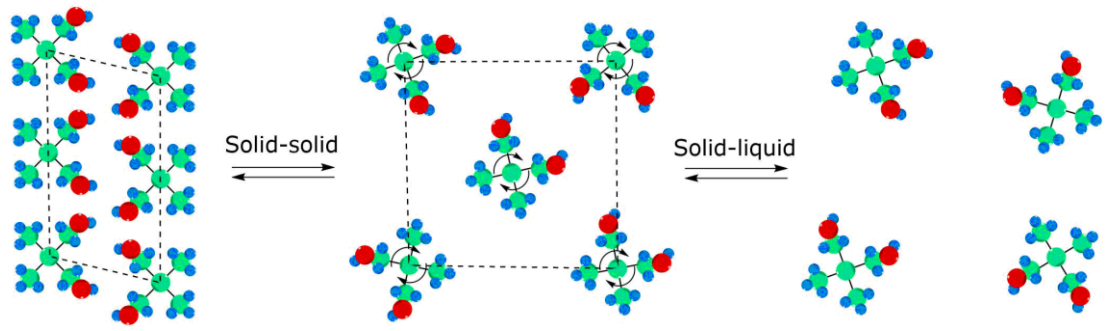

Figure 1.11. Scheme of solid-solid and solid-liquid transitions in neopentylglycol.

In literature, we can find a lot of PCs derived from neopentane with different functional groups and hence different temperatures and enthalpies of transition (Table 1.9) [136,137]. The molecules containing a larger proportion of non-polar functional groups, such as neopentane (NP), neopentylalcohol (NPA) and *t*-nitrobutane (TNB) have the lowest temperatures and enthalpies of transition, below 0 ºC and 100 J/g, respectively. On the other hand, the stronger the hydrogen bonds the PCs are able to form, the higher the temperatures and enthalpies of transition are. This is the reason why the carboxylic acids, alcohols and amines with acid hydrogens show the most energetic transitions. Moreover, molecules that combine alcohol and amine functional groups show the highest enthalpies of transition, due to the presence of stronger hydrogen bonds due to an ionic character between the amine and alcohol groups, promoted by an acid-base behavior, such as the cases of 2-amino-2-methyl-1,3-propanediol (AMP) and tris(hydroxymethyl)aminomethane (TRIS) [138]. In summary, there are a lot of possibilities regarding neopentane derivatives with different functionality, with transitions ranging from -33 ºC to 190 ºC, and with enthalpies as attractive as 300 J/g. All these molecules are chemically stables and are cheap and widely found. Moreover, they undergo solid-solid transitions fulfilling several of the desirable properties of a PCM listed in Table 1.4, regarding the low volume change during the phase transition, as well as avoiding of a liquid phase. Unfortunately, these PCs have a common drawback: the subcooling.

Table 1.9. Plastic Crystals derived from neopentane. Acronyms comes from traditional names listed in Annex A.2.

Functional group	Acronym	Molecular formula	Temperature of transition (ºC)	Enthalpy of transition (J/g)	Melting temperature (ºC)	Melting enthalpy (J/g)	Refs.
Alkane	NP	C_5H_{12}	- 133	35.9	- 16.54	45.2	[139]
Alcohol	NPA	$C_5H_{12}O$	- 31	51	51 – 54	46	[140]
			- 37.8	31.6	56.6	28.4	[141]
			- 31	50.6 – 53.3	51 – 55	46.1	[139]
	NPG	$C_5H_{12}O_2$	40 – 43	131	125 – 126	45	[140]
			40	135.4	125	38.4	[142]
			41.2	119.3	126.6	41.7	[141]
			40 – 48	110.4 – 131	125 – 126	45.3	[139]
	PG	$C_5H_{12}O_3$	81	193	197	45	[140]
			80.3	179.8	186	34.1	[142]
			83.5	174.3	201.2	39.3	[141]
			81 – 89	139 – 193	197 – 198	44.6	[139]

	TMP	$C_6H_{14}O_3$	54.6	121.9	59.5	6.7	[143]
	PE	$C_5H_{12}O_4$	182 – 183	301	258	37	[144]
			187.5	293.8	266	38.2	[141]
			182 – 188	269 – 303.3	258 – 260	37.2	[139]
			187.5	301.1	261.3	38.2	[142]
Amine	AMP	$C_4H_{11}NO_2$	78 – 80	239	110 – 112	28	[140]
			79.4	221.6	109.2	26.8	[145]
			78 – 80	223.9 – 264	110 – 112	28	[139]
	TRIS	$C_4H_{11}NO_3$	131 – 134	283	166 – 169	25	[140]
			133.6	280.7	169.5	26.4	[145]
			133.6	280.7	169.5	30.5	[141]
			131 – 135	285.3	166 – 172	27.6	[146]
	MAPE*	$C_5H_{13}NO_3$	86	192			[92]
	DAPE*	$C_5H_{14}N_2O_2$	68	184			[92]
Nitro	TNB	$C_4H_9NO_2$	- 13.2	45	25.3	24.8	[141]
	MNP	$C_4H_9NO_3$	38.3	122.8	90.7	26.6	[141]
			35 – 39	144	88 – 89	31	[140]
	MNPD	$C_4H_9NO_4$	79 – 80	190	149 – 153	28	[140]
			79 – 80	190 – 201	149 – 153	28 – 32	[139]
	HNP*	$C_4H_9NO_5$	80 – 82	148			[140]
			80 – 82	149			[139]
Carboxylic acid	DMPA	$C_5H_{10}O_2$	135	288	194 – 197	27	[140]
			152 – 155	287 – 289	194 – 197	26.8	[139]
	BHPA	$C_5H_{10}O_4$	7 – 9	86	32 – 36	24	[140]
	THA*	$C_5H_{10}O_5$	124	205			[92]
Halide	BNP	$C_3H_6BrNO_4$	94	110.56	128	13.38	[147]

* Thermal degradation before melting.

1.5. Subcooling phenomenon.

The thermal hysteresis in phase transitions, also known as subcooling, is a kinetic phenomenon in which the high temperature phase (liquid or plastic) remains below the transition temperature, and hence it is defined as a range of temperatures equal to the difference between the onset temperatures of transition upon heating and cooling (Figure 1.12) [20,148,149]. Due to this undesirable displacement in the temperature of transition, upon cooling, two main correlated problems can arise from the application point of view: the temperature may not be suitable for the application, and the energy will not be recovered [150,151]. Big unexpected density changes during the phase transition can also occur, since

the PCM is far away the equilibrium temperature, so it may cause the rupture or deformation of the PCM container.

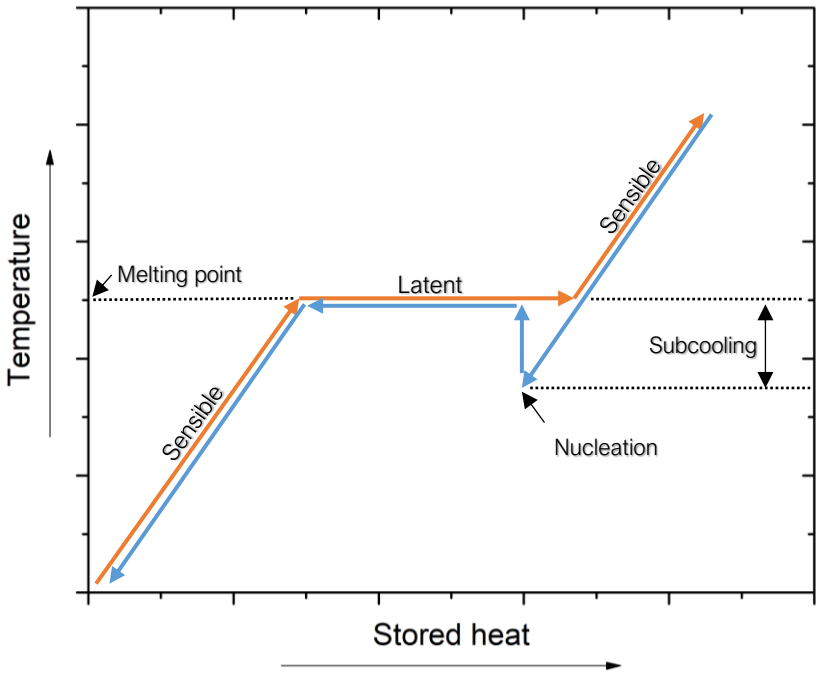

Figure 1.12. Effect on heat storage due to the subcooling phenomenon and subsequent nucleation.

Therefore, a deep understanding of the fundamentals of the subcooling phenomenon is required and it is still a big challenge in the research on PCMs. From the literature, subcooling seems to be affected by many different parameters such as the nature of the material, the amount, the geometry, the microstructure, the purity, the heating/cooling rate, etc.

For liquid-solid transitions, subcooling is a random phenomenon in nature, since crystallization follows a two-step mechanism in which a nucleation is involved. This stochasticity added to the many affecting variables to consider, explains why different schemes of subcooling can be found in literature (Figure 1.13) [20]. For example, Figure 1.13.a and 1.13.b depict a subcooling behavior due to poor nucleation, so that once this step occurs the temperature rises to the melting point in order to finalize the crystallization. The main differences between both are that in Figure 1.13.b the thermal diffusivity of the sample is higher than that of Figure 1.13.a, so the melting temperature is reached very quickly compared to the case of Figure 1.13.a. On the other hand, in Figure 1.13.c, the subcooling is due to a poor rate of crystal growth, this is, once the nucleation occurs and the

crystallization begins, the delivery of the latent heat occurs at the same rate as the heat dissipation in the system, so that the temperature stabilizes under the transition temperature due to poor crystallization kinetics. The last possible case is depicted in Figure 1.13.d, where the subcooling is not a matter of poor nucleation or crystal growth, but it is a matter of a low thermal diffusivity of the sample and/or a very high rate of heat dissipation of the sample. In all the cases, the latent heat is not released at the right temperature, and there is a loss of storage capacity in form of sensible heat for that range of temperatures, hence causing a phase transition less energetic than expected.

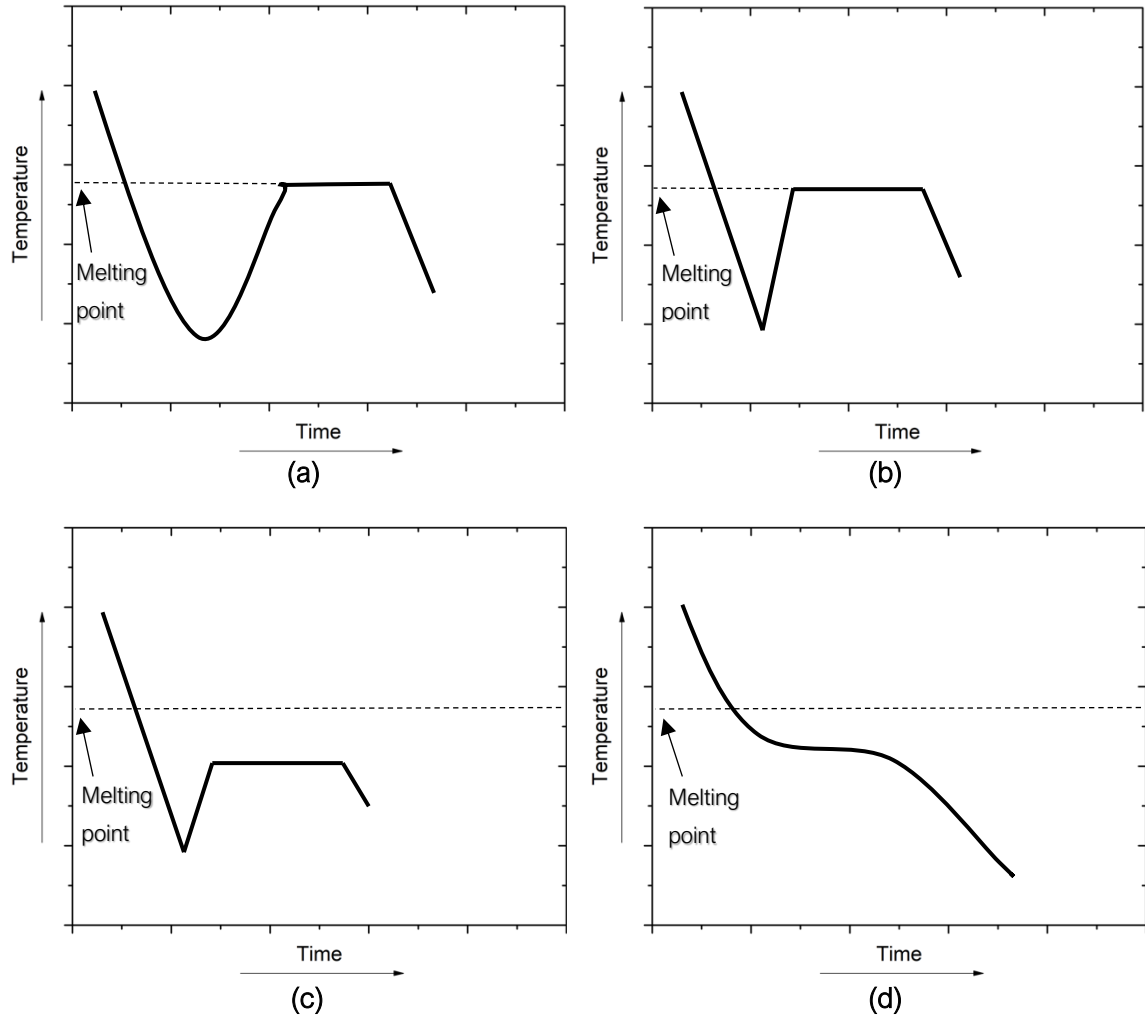

Figure 1.13. Different types of supercooling curves.

Erythritol is a well-known solid-liquid PCM within the family of sugar alcohols with quite attractive thermal properties such as mid-temperature phase change (around 120 ºC) involving a high latent heat of about 300-340 J/g [152–154]. However, for this material the

subcooling can reach 75 ºC, and it is not acceptable for practical applications. As mentioned before, and from the traditional crystallization theory, the subcooling can be mainly caused by a poor nucleation performance, but also it can be worsened by a low crystal growth rate [152,155], so that several approaches have been developed in order to mitigate the subcooling in erythritol. For example, the addition of some particles which act as nucleating agents, such as expanded graphite (EG), graphene oxide (GO) or carbon nanotubes (CNT) have been able to reduce the subcooling up to c.a. 45 ºC, as well as the confinement of erythritol in porous materials such as polyurethane foams [156–159]. On the other hand, since solid-liquid transitions are equilibrium phase changes, it is possible to support one direction of the equilibrium by varying some of the parameters involved, such as the pressure. In this same example of erythritol, the application of an increasing pressure does not lead to an improvement in the subcooling, but a worsening of it by c.a. 15 ºC [160]. This result was attributed to the confinement of erythritol in nano-Alumina, and the pores and the contact angles were modified by applying that pressure. Therefore, the decrease of the pore diameters and surface areas leads to an amorphous state in the liquid phase of erythritol, so the transition to the solid phase was hindered. Other two parameters to be considered are the mass of the sample and the heating and cooling rates applied to the PCM [161]. Firstly, the influence of the sample mass on subcooling is mostly a stochastic phenomenon, since the first step for a crystallization is the nucleation, statistics set that the higher the amount of material, the higher the possibility of appearance of the first point of solid material. However, the effect of heating and cooling rates on subcooling has a deeper explanation: In general terms, the higher the cooling rate, the higher the subcooling degree. The peaks of the phase transitions recorded by Differential Scanning Calorimetry (DSC) are wider when the heating rate is also higher, and this means that the material is overheated before all the sample is completely in the liquid state [148,162]. However, the onset temperature of the transition does not change. On the other hand, when the cooling rate is higher, not only the signal of the transition is wider, but also the onset temperature of the transition is also displaced to lower temperature, i.e., the subcooling is higher. This effect can be sometimes neglected since some materials have quite low thermal conductivities, so that the material is not able to follow as fast as the equipment the cooling ramp, and hence the subcooling seems to be higher. Therefore, this subcooling is not a matter of the material itself, but it is enlarged due to an instrumental artefact. Consequently, for large differences on subcooling regarding different cooling rates, or highly conductive materials, the subcooling differences do have to be considered, but the report of results must clarify all the possible affecting parameters such as the sample mass, the atmosphere, the heating and cooling rate, and so on.

It is worth noting that most of the reported information about approaches to mitigate the subcooling are referred to liquid-solid transitions, and even in these cases which are deeply studied, an effective method to overcome subcooling is still not found. However, what does really happen in solid-solid transitions? Do they follow the same mechanism than liquid-solid transitions? Is it possible to find an approach to mitigate subcooling in these interesting phase transitions? It is clear that deeper studies are still needed to understand the subcooling phenomenon in solid-solid transitions, looking for right approaches to reduce it in order to use potentially promising PCMs which are a priori discarded due to this problem.

1.6. Concluding remarks and scope of the thesis.

As a matter of fact, society needs to skip the use of fossil fuels and has to implement new renewable energies that must become the main source for the global energy consumption since traditional sources such as coal, crude oil and natural gas are not only harmful to the environment, but also are finite in the long term. Climate change, growing energy demand and limited resources will urge people to adjust their energy landscapes and address future energy needs. To this end, thermal energy storage is an efficient way to achieve it. In particular, PCMs based on latent heat storage systems are gaining more and more attraction due to the multiple benefits they show, not only due to the capacity of storing energy and hence covering the gap between the energy generation and consumption, but also due to all the advantages for being materials which can be adapted to different applications.

Despite PCMs are mostly reported to be based on solid-liquid transitions, the limitation of dealing with a liquid phase is present. To avoid all the drawbacks of wettability, leakages, and substantial changes in density, solid-solid based PCMs are gaining more interest due to the possibility of working with a solid phase with no needs of containers or pipes. However, despite all the advantages of solid-solid transitions in Plastic Crystals, there is still a common drawback to improve: the subcooling, a phenomenon that is not fully understood so far in order to implement solid-solid PCMs as a solution for many applications. Therefore, the main objective of the research in this thesis relies on the understanding of the subcooling as a phenomenon that hinders the direct application of some interesting potential solid-solid PCMs such as the Plastic Crystals. In addition, once knowing the basis and the reason why this phenomenon is occurring in these materials, it will become the perfect starting point to think about how to mitigate or minimize it.

To this end, this thesis is structured in 6 chapters, three of them are the main body of all the research carried out (Chapters 3, 4 and 5). Chapter 1 has provided a general introduction of the general framework in which this thesis is encompassed, presenting the currently energy scenario and how thermal energy storage can be an approach to solve some of the issues which we are facing nowadays. Moreover, the state-of-the-art of the research carried out about PCMs and the subcooling phenomenon are collected in this chapter.

Chapter 2 briefly describes the state-of-the-art methods and experimental techniques used for the synthesis and characterization of the materials studied during this work, and also the ones that have been used to understand the subcooling phenomenon in solid-solid transitions.

Chapter 3 presents a full characterization of all the interesting thermophysical properties of the Plastic Crystals selected and comparing them to the values reported in literature, and integrating with not available new data. Information about temperatures and enthalpies of the solid-solid transition of the PCs are collected under different experimental conditions. The characterization is completed by measuring the specific heats of both crystalline and plastic phases, as well as the decomposition temperatures. Other properties more focused on the final application as PCMs are also reported in this chapter, such as the thermal conductivities and densities of both solid phases, as well as the volume changes during the transitions.

Chapter 4 is devoted to the understanding of the molecular mechanism involved during the phase transition, both upon heating and upon cooling in order to find the cause of the subcooling in the solid-solid transition of PCs. To this end, two main techniques were used: I) Temperature-variable Infrared Spectroscopy, which was carried out in order to obtain all the bonding information of these hydrogen-bonded based materials. In particular, the study at different temperatures allowed to follow the evolution of the hydrogen bond network during the phase transition. II) Temperature-variable solid-state NMR spectroscopy, which was carried out in order to obtain information about atomic motions and surrounding changes during the phase transition, since it is a local technique highly sensitive to changes in dynamics and coordination of atoms, so it can give a lot of information about hydrogen bond configurations in both the crystalline and the plastic phases.

Chapter 5 reports the approaches explored to mitigate the subcooling. This includes, I) different processing methods of the materials to modify their microstructure and to look for a relationship between morphology and subcooling, as well as II) the dispersion of different

types of particles acting as heterogeneous points inducing the phase transitions similar to the strategy followed in liquid-solid transitions, and III) the application of a determined pressure during the phase transition as external stimuli. All these approaches have been tested according to the information included on this chapter on how to minimize the subcooling in solid-liquid transitions, as well as taking into account the conclusions obtained in Chapter 4 about the understanding of the phenomenon.

Chapter 6 summarizes the most important findings and overall conclusions from the whole research work, as well as the future perspectives to use Plastic Crystals as the next generation solid-state PCMs.

References in Chapter 1

[1] B. Selcuk, Calculation and Interpretation of the Standard Chemical Exergies of Elements Using the Chemical Reference Species, Acta Physico-Chimica Sinica. 25 (n.d.) 1645–1649.

[2] T. Kousksou, P. Bruel, A. Jamil, T. El Rhafiki, Y. Zeraouli, Energy storage: Applications and challenges, Solar Energy Materials and Solar Cells. 120 (2014) 59–80.

[3] G.E.C.N.-H.U. Peake, U.S. energy :overview of the trends, statistics, supply and consumption, (n.d.).

[4] K. Kaygusuz, S. Bilgen, Energy Related Environmental Policies in Turkey, Energy Sources, Part B: Economics, Planning, and Policy. 3 (2008) 396–410.

[5] E.I.A. Annual Energy Outlook, U.S. Energy Information Administration, DOE/EIA-0383, April (2014).

[6] A. Allouhi, Y. El Fouih, T. Kousksou, A. Jamil, Y. Zeraouli, Y. Mourad, Energy consumption and efficiency in buildings: current status and future trends, J Clean Prod. 109 (2015) 118–130.

[7] A.E. Outlook, with Projections to 2050, US Energy Information Administration. (2007).

[8] S. Bilgen, Structure and environmental impact of global energy consumption, Renewable and Sustainable Energy Reviews. 38 (2014) 890–902.

[9] T.F. Stocker, D. Qin, G.-K. Plattner, M.M.B. Tignor, S.K. Allen, J. Boschung, A. Nauels, Y. Xia, V. Bex, P.M. Midgley, Climate Change 2013: The physical science basis. Contribution of working group I to the fifth assessment report of IPCC the intergovernmental panel on climate change, (2014).

[10] H.Ö. Paksoy, Thermal energy storage for sustainable energy consumption: fundamentals, case studies and design, Springer Science & Business Media, 2007.

[11] A. Kumar, K. Kumar, N. Kaushik, S. Sharma, S. Mishra, Renewable energy in India: current status and future potentials, Renewable and Sustainable Energy Reviews. 14 (2010) 2434–2442.

[12] T. Ahmad, D. Zhang, A critical review of comparative global historical energy consumption and future demand: The story told so far, Energy Reports. 6 (2020) 1973–1991.

[13] L. Li, J. Lin, N. Wu, S. Xie, C. Meng, Y. Zheng, X. Wang, Y. Zhao, Review and outlook on the international renewable energy development, Energy and Built Environment. (2020).

[14] BP, Statistical review of world energy-All data 1965–2019, (n.d.).

[15] IRENA, Query Tool, Renewable Electricity Capacity and Generation Statistics, July, 2022, (n.d.). https://www.irena.org/Statistics/View-Data-by-Topic/Capacity-and-Generation/Statistics-Time-Series.

[16] R. Dones, T. Heck, S. Hirschberg, Greenhouse gas emissions from energy systems: comparison and overview, 2004.

[17] D. Maradin, Advantages and disadvantages of renewable energy sources utilization, 670216917. (2021).

[18] A.I. Calderón, A., Barreneche, C., Hernández-Valle, K., Galindo, E., Segarra, M., & Fernández, Where is Thermal Energy Storage (TES) research going–A bibliometric analysis., Solar Energy. (2019).

[19] S.A. Mohamed, F.A. Al-Sulaiman, N.I. Ibrahim, Md.H. Zahir, A. Al-Ahmed, R. Saidur, B.S. Yilbas, A.Z. Sahin, A review on current status and challenges of inorganic phase change materials for thermal energy storage systems, Renewable & Sustainable Energy Reviews. 70 (2017) 1072–1089.

[20] A. Safari, R. Saidur, F.A. Sulaiman, Y. Xu, J. Dong, A review on supercooling of Phase Change Materials in thermal energy storage systems, Renewable & Sustainable Energy Reviews. 70 (2017) 905–919.

[21] S. Nikolina, International Renewable Energy Agency (IRENA), (2016).

[22] S.S. Chandel, T. Agarwal, Review of current state of research on energy storage, toxicity, health hazards and commercialization of phase changing materials, Renewable and Sustainable Energy Reviews. 67 (2017) 581–596.

[23] P. Pinel, C.A. Cruickshank, I. Beausoleil-Morrison, A. Wills, A review of available methods for seasonal storage of solar thermal energy in residential applications, Renewable and Sustainable Energy Reviews. 15 (2011) 3341–3359.

[24] B. Mette, H. Kerskes, H. Drück, H. Müller-Steinhagen, New highly efficient regeneration process for thermochemical energy storage, Appl Energy. 109 (2013) 352–359.

[25] Z.N. Meng, P. Zhang, Experimental and numerical investigation of a tube-in-tank latent thermal energy storage unit using composite PCM, Appl Energy. 190 (2017) 524–539.

[26] D. Sharma, A., Tyagi, V. V., Chen, C. R., & Buddhi, Review on thermal energy storage with phase change materials and applications., Renewable and Sustainable Energy Reviews. (2009) 318–3.

[27] F. Schaube, L. Koch, A. Wörner, H. Müller-Steinhagen, A thermodynamic and kinetic study of the de- and rehydration of Ca(OH)2 at high H2O partial pressures for thermo-chemical heat storage, Thermochim Acta. 538 (2012) 9–20.

[28] Y.A. Criado, M. Alonso, J.C. Abanades, Kinetics of the CaO/Ca(OH)2 Hydration/Dehydration Reaction for Thermochemical Energy Storage Applications, Ind Eng Chem Res. 53 (2014) 12594–12601.

[29] B. Bogdanović, A. Ritter, B. Spliethoff, Active MgH2 Mg Systems for Reversible Chemical Energy Storage, Angewandte Chemie International Edition in English. 29 (1990) 223–234.

[30] A. Chaise, P. de Rango, Ph. Marty, D. Fruchart, Experimental and numerical study of a magnesium hydride tank, Int J Hydrogen Energy. 35 (2010) 6311–6322.

[31] Y. Kato, D. Saku, N. Harada, Y. Yoshizawa, Utilization of High Temperature Heat Using a Calcium Oxide/Lead Oxide/Carbon Dioxide Chemical Heat Pump, JOURNAL OF CHEMICAL ENGINEERING OF JAPAN. 30 (1997) 1013–1019.

[32] M.S. Murthy, P. Raghavendrachar, S. V Sriram, Thermal decomposition of doped calcium hydroxide for chemical energy storage, Solar Energy. 36 (1986) 53–62.

[33] C. Agrafiotis, M. Roeb, M. Schmücker, C. Sattler, Exploitation of thermochemical cycles based on solid oxide redox systems for thermochemical storage of solar heat. Part 1: Testing of cobalt oxide-based powders, Solar Energy. 102 (2014) 189–211.

[34] S. Tescari, C. Agrafiotis, S. Breuer, L. de Oliveira, M.N. Puttkamer, M. Roeb, C. Sattler, Thermochemical Solar Energy Storage Via Redox Oxides: Materials and Reactor/Heat Exchanger Concepts, Energy Procedia. 49 (2014) 1034–1043.

[35] Y. Portilla-Nieto, A. Zaki, K. Vidal, M. Hernaiz, E. Aranzabe, S. Doppiu, A. Faik, Development of Co3-xNixO4 materials for thermochemical energy storage at lower red-ox temperature, Solar Energy Materials and Solar Cells. 230 (2021) 111194.

[36] Y. Zhao, C.Y. Zhao, C.N. Markides, H. Wang, W. Li, Medium- and high-temperature latent and thermochemical heat storage using metals and metallic compounds as heat storage media: A technical review, Appl Energy. 280 (2020) 115950.

[37] A. Kumar, S.K. Shukla, A Review on Thermal Energy Storage Unit for Solar Thermal Power Plant Application, Energy Procedia. 74 (2015) 462–469.

[38] S.M. Hasnain, M. Smiai, Y. Al-Saedi, M. Al-Khaldi, Energy Research Institute-Internal Report, Riyadh, Saudi Arabia: KACST. (1996).

[39] Y. Tian, C.Y. Zhao, A review of solar collectors and thermal energy storage in solar thermal applications, Appl Energy. 104 (2013) 538–553.

[40] S. Ayyappan, K. Mayilsamy, V. V Sreenarayanan, Performance improvement studies in a solar greenhouse drier using sensible heat storage materials, Heat and Mass Transfer. 52 (2016) 459–467.

[41] F. Kuznik, K. Johannes, D. David, 13 - Integrating phase change materials (PCMs) in thermal energy storage systems for buildings, in: L.F.B.T.-A. in T.E.S.S. Cabeza (Ed.), Woodhead Publishing Series in Energy, Woodhead Publishing, 2015: pp. 325–353.

[42] T. Wang, D. Mantha, R.G. Reddy, Thermal stability of the eutectic composition in LiNO3–NaNO3–KNO3 ternary system used for thermal energy storage, Solar Energy Materials and Solar Cells. 100 (2012) 162–168.

[43] U. Nithiyanantham, Shape effect of Al2O3 nanoparticles on the thermophysical properties and viscosity of molten salt nanofluids for TES application at CSP plants., Appl Therm Eng. 169 (2020) 114942.

[44] G.N. Lewis, M. Randall, Thermodynamics: By Gilbert Newton Lewis and Merle Randall. Rev. by Kenneth S. Pitzer and Leo Brewer, McGraw-Hill, 1961.

[45] L. Pauling, General chemistry, Courier Corporation, 1988.

[46] D.N. Nkwetta, F. Haghighat, Thermal energy storage with phase change material—A state-of-the art review, Sustain Cities Soc. 10 (2014) 87–100.

[47] S.M. Hasnain, REVIEW ON SUSTAINABLE THERMAL ENERGY STORAGE TECHNOLOGIES, PART I: HEAT STORAGE MATERIALS AND TECHNIQUES Solar energy applications Thermal energy storage Sensible heat storage Phase change material Extended surfaces Heat pipe, (n.d.).

[48] Y. Konuklu, N. Şahan, H. Paksoy, Latent Heat Storage Systems, 2018.

[49] G.A. Lane, G.A. Lane, Solar heat storage: latent heat materials, CRC press Boca Raton, FL, USA:, 1983.

[50] A. Abhat, Low temperature latent heat thermal energy storage: Heat storage materials, Solar Energy. 30 (1983) 313–332.

[51] N. Soares, J.J. Costa, A.R. Gaspar, P. Santos, Review of passive PCM latent heat thermal energy storage systems towards buildings' energy efficiency, Energy Build. 59 (2013) 82–103.

[52] R. Sharma, P. Ganesan, V. Tyagi, H. Metselaar, S. Sandaran, Developments in organic solid–liquid phase change materials and their applications in thermal energy storage, Energy Convers Manag. 95 (2015) 193–228.

[53] K. Pielichowska, K. Pielichowski, Phase change materials for thermal energy storage, Prog Mater Sci. 65 (2014) 67–123.

[54] I. Sarbu, C. Sebarchievici, A comprehensive review of thermal energy storage, Sustainability (Switzerland). 10 (2018).

[55] M.M. Kenisarin, Thermophysical properties of some organic phase change materials for latent heat storage. A review, Solar Energy. 107 (2014) 553–575.

[56] L.I. Cherneeva, E.K. Rodionova, N.M. Martynova, Use of alloys for heat storage, Izv Vyssh Uchebn Energy. 7 (1982) 52–55.

[57] G. Wei, P. Huang, C. Xu, D. Liu, X. Ju, X. Du, L. Xing, Y. Yang, Thermophysical property measurements and thermal energy storage capacity analysis of aluminum alloys, Solar Energy. 137 (2016) 66–72.

[58] A.I. Fernández, C. Barreneche, M. Belusko, M. Segarra, F. Bruno, L.F. Cabeza, Considerations for the use of metal alloys as phase change materials for high temperature applications, Solar Energy Materials and Solar Cells. 171 (2017) 275–281.

[59] M. Liu, W. Saman, F. Bruno, Review on storage materials and thermal performance enhancement techniques for high temperature phase change thermal storage systems, Renewable and Sustainable Energy Reviews. 16 (2012) 2118–2132.

[60] J.Q. Sun, R.Y. Zhang, Review of thermal energy storage with metal phase change materials, Mater Rev. 19 (2005) 99–101.

[61] C.E. Birchenall, A.F. Riechman, Heat storage in eutectic alloys, Metallurgical Transactions A. 11 (1980) 1415–1420.

[62] N. Maruoka, T. Akiyama, Exergy recovery from steelmaking off-gas by latent heat storage for methanol production, Energy. 31 (2006) 1632–1642.

[63] X. Wang, J. Liu, Y. Zhang, H. Di, Y. Jiang, Experimental research on a kind of novel high temperature phase change storage heater, Energy Convers Manag. 47 (2006) 2211–2222.

[64] R. Naumann, H.-H. Emons, Results of thermal analysis for investigation of salt hydrates as latent heat-storage materials, Journal of Thermal Analysis. 35 (1989) 1009–1031.

[65] J. PARIS, M. FALARDEAU, C. VILLENEUVE, Thermal Storage by Latent Heat: A Viable Option for Energy Conservation in Buildings, Energy Sources. 15 (1993) 85–93.

[66] K. Nagano, T. Mochida, S. Takeda, R. Domański, M. Rebow, Thermal characteristics of manganese (II) nitrate hexahydrate as a phase change material for cooling systems, Appl Therm Eng. 23 (2003) 229–241.

[67] K. Bilen, F. Takgil, K. Kaygusuz, Thermal energy storage behavior of CaCl2.6H2O during melting and solidification, Energy Sources, Part A: Recovery, Utilization and Environmental Effects. 30 (2008) 775–787.

[68] V. V Tyagi, D. Buddhi, Thermal cycle testing of calcium chloride hexahydrate as a possible PCM for latent heat storage, Solar Energy Materials and Solar Cells. 92 (2008) 891–899.

[69] L.F. Cabeza, G. Svensson, S. Hiebler, H. Mehling, Thermal performance of sodium acetate trihydrate thickened with different materials as phase change energy storage material, Appl Therm Eng. 23 (2003) 1697–1704.

[70] G. Belton, F. Ajami, Thermochemistry of salt hydrates, Pennsylvania Univ., Philadelphia (USA). Towne School of Civil and Mechanical, 1973.

[71] J. Heckenkamp, H. Baumann, Latentwärmespeicher, Sonderdruck Aus Nachrichten. 11 (1997) 1075–1081.

[72] T. Bauer, D. Laing, R. Tamme, Recent Progress in Alkali Nitrate/Nitrite Developments for Solar Thermal Power Applications, in: Molten Salts Chemistry and Technology, 2014: pp. 543–553.

[73] B.D. Iverson, S.T. Broome, A.M. Kruizenga, J.G. Cordaro, Thermal and mechanical properties of nitrate thermal storage salts in the solid-phase, Solar Energy. 86 (2012) 2897–2911.

[74] F. Roget, C. Favotto, J. Rogez, Study of the KNO3–LiNO3 and KNO3–NaNO3–LiNO3 eutectics as phase change materials for thermal storage in a low-temperature solar power plant, Solar Energy. 95 (2013) 155–169.

[75] P.D. Myers, D.Y. Goswami, Thermal energy storage using chloride salts and their eutectics, Appl Therm Eng. 109 (2016) 889–900.

[76] L. Du, J. Ding, H. Tian, W. Wang, X. Wei, M. Song, Thermal properties and thermal stability of the ternary eutectic salt NaCl-CaCl2-MgCl2 used in high-temperature thermal energy storage process, Appl Energy. 204 (2017) 1225–1230.

[77] F. Berroug, E.K. Lakhal, M. El Omari, M. Faraji, H. El Qarnia, Thermal performance of a greenhouse with a phase change material north wall, Energy Build. 43 (2011) 3027–3035.

[78] D. Buddhi, S.D. Sharma, A. Sharma, Thermal performance evaluation of a latent heat storage unit for late evening cooking in a solar cooker having three reflectors, Energy Convers Manag. 44 (2003) 809–817.

[79] M.S. Gruszkiewicz, J.M. Simonson, Vapor pressures and isopiestic molalities of concentrated CaCl2(aq), CaBr2(aq), and NaCl(aq) to T=523 K, J Chem Thermodyn. 37 (2005) 906–930.

[80] M. Kenisarin, K. Mahkamov, Salt hydrates as latent heat storage materials:Thermophysical properties and costs, Solar Energy Materials and Solar Cells. 145 (2016) 255–286.

[81] V.D. Bhatt, K. Gohil, A. Mishra, Thermal energy storage capacity of some phase changing materials and ionic liquids, Int J Chemtech Res. 2 (2010) 1771–1779.

[82] B. Norton, Storage of Solar Heat, in: Harnessing Solar Heat, Springer, 2014: pp. 75–90.

[83] M. Veerappan, S. Kalaiselvam, S. Iniyan, R. Goic, Phase change characteristic study of spherical PCMs in solar energy storage, Solar Energy. 83 (2009) 1245–1252..

[84] D. Zhou, C.Y. Zhao, Experimental investigations on heat transfer in phase change materials (PCMs) embedded in porous materials, Applied Thermal Engineering. 31 (2011) 970–977.

[85] G.A. Lane, G. Warner, P. Hartwick, H. Rossow, Macro-encapsulation of PCM, Report No. Oro/5117-8, Dow Chemical Company, Midland, Michigan. 152 (1978).

[86] K. Kaygusuz, Experimental and theoretical investigation of latent heat storage for water based solar heating systems, Energy Convers Manag. 36 (1995) 315–323.

[87] L.F. Cabeza, J. Illa, J. Roca, F. Badia, H. Mehling, S. Hiebler, F. Ziegler, Middle term immersion corrosion tests on metal-salt hydrate pairs used for latent heat storage in the 32 to 36° C temperature range, Materials and Corrosion. 52 (2001) 748–754.

[88] D.R. Biswas, Thermal energy storage using sodium sulfate decahydrate and water, Solar Energy. 19 (1977) 99–100.

[89] B. Carlsson, H. Stymne, G. Wettermark, An incongruent heat-of-fusion system—CaCl2· 6H2O—Made congruent through modification of the chemical composition of the system, Solar Energy. 23 (1979) 343–350.

[90] B. Zalba, J. Marín, L.F. Cabeza, H. Mehling, Review on Thermal Energy Storage with Phase Change: Materials, Heat Transfer Analysis and Applications, Appl Therm Eng. 23 (2003) 251–283.

[91] M. Kenisarin, K. Mahkamov, Solar energy storage using phase change materials, Renewable and Sustainable Energy Reviews. 11 (2007) 1913–1965.

[92] D. V Hale, M.J. Hoover, M.J. Oneill, Phase change materials handbook, 1971.

[93] S. Scalat, D. Banu, D. Hawes, J. Parish, F. Haghighata, D. Feldman, Full scale thermal testing of latent heat storage in wallboard, Solar Energy Materials and Solar Cells. 44 (1996) 49–61.

[94] R. Nikolić, M. Marinović-Cincović, S. Gadžurić, I.J. Zsigrai, New materials for solar thermal storage—solid/liquid transitions in fatty acid esters, Solar Energy Materials and Solar Cells. 79 (2003) 285–292.

[95] A.A. Aydın, Fatty acid ester-based commercial products as potential new phase change materials (PCMs) for thermal energy storage, Solar Energy Materials and Solar Cells. 108 (2013) 98–104.

[96] D. Feldman, M.M. Shapiro, D. Banu, Organic phase change materials for thermal energy storage, Solar Energy Materials. 13 (1986) 1–10.

[97] A.M. Khudhair, M.M. Farid, A review on energy conservation in building applications with thermal storage by latent heat using phase change materials, Energy Convers Manag. 45 (2004) 263–275.

[98] M.J. Van Bommel, H.A.J. Oonk, J.C. Van Miltenburg, Heat capacity measurements of 13 methyl esters of n-carboxylic acids from methyl octanoate to methyl eicosanoate between 5 K and 350 K, J Chem Eng Data. 49 (2004) 1036–1042.

[99] M.C. Costa, L.A.D. Boros, M.L.S. Batista, J.A.P. Coutinho, M.A. Krähenbühl, A.J.A. Meirelles, Phase diagrams of mixtures of ethyl palmitate with fatty acid ethyl esters, Fuel. 91 (2012) 177–181.

[100] M. Duquesne, C. Mailhé, S. Doppiu, J.-L. Dauvergne, S. Santos Moreno, A. Godin, G. Fleury, F. Rouault, E. Palomo del Barrio, Characterization of Fatty Acids as Biobased Organic Materials for Latent Heat Storage, Materials. 14 (2021) 4707.

[101] K. Pielichowski, K. Flejtuch, Differential scanning calorimetry study of blends of poly(ethylene glycol) with selected fatty acids, Macromol Mater Eng. 288 (2003) 259–264.

[102] K. Pielichowski, K. Flejtuch, Binary blends of polyethers with fatty acids: A thermal characterization of the phase transitions, J Appl Polym Sci. 90 (2003) 861–870.

[103] N. Adriaanse, H. Dekker, J. Coops, Some physical constants of normal saturated fatty acids and their methyl esters, Recueil Des Travaux Chimiques Des Pays-Bas. 83 (1964) 557–572.

[104] R.C.F. Schaake, J.C. van Miltenburg, C.G. de Kruif, Thermodynamic properties of the normal alkanoic acids II. Molar heat capacities of seven even-numbered normal alkanoic acids, J Chem Thermodyn. 14 (1982) 771–778.

[105] R.C.F. Schaake, J.C. van Miltenburg, C.G. de Kruif, Thermodynamic properties of the normal alkanoic acids I. Molar heat capacities of seven odd-numbered normal alkanoic acids, J Chem Thermodyn. 14 (1982) 763–769.

[106] D. Buddhi, R.L. Sawhney, Proc: Thermal energy storage and energy conversion, School of Energy and Environmental Studies, Devi Ahilya University, Indore, India. (1994).

[107] J.C. Van Miltenburg, H.A.J. Oonk, L. Ventola, Heat capacities and derived thermodynamic functions of 1-octadecanol, 1-nonadecanol, 1-eicosanol, and 1-docosanol between 10 K and 370 K, J Chem Eng Data. 46 (2001) 90–97.

[108] J.C. van Miltenburg, G.J.K. Van den Berg, M. Ramirez, Heat Capacities and Derived Thermodynamic Functions of 1-Dodecanol and 1-Tridecanol between 10 K and 370 K and Heat Capacities of 1-Pentadecanol and 1-Heptadecanol between 300 K and 380 K and Correlations for the Heat Capacity and the Entropy of Liquid n-, J Chem Eng Data. 48 (2003) 36–43.

[109] B. Tong, Z.-C. Tan, Q. Shi, Y.-S. Li, D.-T. Yue, S.-X. Wang, Thermodynamic investigation of several natural polyols (I): Heat capacities and thermodynamic properties of xylitol, Thermochim Acta. 457 (2007) 20–26.

[110] B. Tong, Z.C. Tan, Q. Shi, Y.S. Li, S.X. Wang, Thermodynamic investigation of several natural polyols (II), J Therm Anal Calorim. 91 (2008) 463–469.

[111] B. Tong, Z.C. Tan, J.N. Zhang, S.X. Wang, Thermodynamic investigation of several natural polyols, J Therm Anal Calorim. 95 (2009) 469–475.

[112] B. Tong, Y. Yu, Z.-C. Tan, C.-G. Meng, L.-J. Cui, G. Xiao, R.-B. Liu, Thermodynamic investigation of several natural polyols (IV): Heat capacities and thermodynamic properties of adonitol, Thermochim Acta. 499 (2010) 117–122.

[113] A. Kaizawa, N. Maruoka, A. Kawai, H. Kamano, T. Jozuka, T. Senda, T. Akiyama, Thermophysical and heat transfer properties of phase change material candidate for waste heat transportation system, Heat and Mass Transfer. 44 (2008) 763–769.

[114] M.W. Babich, S.W. Hwang, R.D. Mounts, The search for novel energy storage materials using differential scanning calorimetry, Thermochim Acta. 210 (1992) 83–88.

[115] F. Michaud, D. Mondieig, V. Soubzmaigne, P. Negrier, Y. Haget, E. Tauler, A system with a less than 2 degree melting window in the range within −31 °C and −45 °C: chlorobenzene-bromobenzene, Mater Res Bull. 31 (1996) 943–950.

[116] J. Tang, M. Yang, F. Yu, X. Chen, L. Tan, G. Wang, 1-Octadecanol@hierarchical porous polymer composite as a novel shape-stability phase change material for latent heat thermal energy storage, Appl Energy. 187 (2017) 514–522.

[117] Y. Lan, X.-Q. Zhu, L.-M. Chen, F.-G. Wang, Y. Bie, J.-H. Chang, Preparation and investigation of composite phase change materials with porous matrixes, 115 (2017) 186–196.

[118] X. Huang, C. Zhu, Y. Lin, G. Fang, Thermal properties and applications of microencapsulated PCM for thermal energy storage: A review, Appl Therm Eng. 147 (2019) 841–855.

[119] H.M. Shih, Y.-P. Lin, L.P. Lin, C.-M. Lai, Thermal characterization of a heat management module containing microencapsulated phase change material, Energies (Basel). 12 (2019) 2164.

[120] M.M. Umair, Y. Zhang, K. Iqbal, S. Zhang, B. Tang, Novel strategies and supporting materials applied to shape-stabilize organic phase change materials for thermal energy storage–A review, Appl Energy. 235 (2019) 846–873.

[121] X. Wang, E. Lu, W. Lin, T. Liu, Z. Shi, R. Tang, C. Wang, Heat storage performance of the binary systems neopentyl glycol/pentaerythritol and neopentyl glycol/trihydroxy methyl-aminomethane as solid–solid phase change materials, Energy Convers Manag. 41 (2000) 129–134.

[122] . K.A.T., Review on Latent Heat Storage and Problems Associated With Phase Change Materials, Int J Res Eng Technol. 04 (2015) 176–182.

[123] E.-Y. Ding, Y. Jiang, G.-K. Li, Comparative studies of the structures and transition characteristics of cellulose diacetate modified with polyethylene glycol prepared by chemical bonding and physical blending methods, Journal of Macromolecular Science, Part B. 40 (2001) 1053–1068.

[124] Y.-Q. Guo, X.-H.L. Lclc, The miscibility of cellulose-polyethylene glycol blends, Journal of Macromolecular Science, Part B: Physics. 38 (1999) 439–447.

[125] Q. Cao, P. Liu, Crystalline-amorphous phase transition of hyperbranched polyurethane phase change materials for energy storage, J Mater Sci. 42 (2007) 5661–5665.

[126] V. Busico, C. Carfagna, V. Salerno, M. Vacatello, Thermal behavior of complexes of general formula (n-CnH2n+1NH2)2CuCl2, Thermochim Acta. 39 (1980) 1–5.

[127] W. Li, D. Zhang, T. Zhang, T. Wang, D. Ruan, for Thermal Energy Storage, 326 (1999) 8–11.

[128] M.J.M. Van Oort, M.A. White, Polymorphism in Dialkylammonium Chlorides. an Adiabatic Calorimetry Study., Berichte Der Bunsengesellschaft/Physical Chemistry Chemical Physics. 92 (1988) 168–176.

[129] S. Steinert, W. Voigt, R. Glausch, M. Neuschütz, Thermal characteristics of solid-solid phase transitions in long-chain dialkyl ammonium salts, Thermochim Acta. 435 (2005) 28–33.

[130] J. Timmermans, Un nouvel état mésomorphe les cristaux organiques plastiques, Journal de Chimie Physique. 35 (1938) 331–344.

[131] J. Timmermans, Plastic crystals: a historical overview, J. Phys. Chem. Solids. 18 (1961) 1–8.

[132] R.C. Miller, C.P. Smyth, Molecular Shape and Rotational Freedom in the Tetrahalogenated Methanes in the Solid State1, J Am Chem Soc. 79 (1957) 20–24.

[133] P.A. Winsor, G.W. Gray, Liquid Crystals & Plastic Crystals, New York, NY, 1974.

[134] M. Postel, J.G. Riess, Plastic phases in globular phosphorus compounds. A new structural criterion for plastic behavior, J Phys Chem. 81 (1977) 2634–2637.

[135] H. Singh, A. Talekar, W.M. Chien, R. Shi, D. Chandra, A. Mishra, M. Tirumala, D.J. Nelson, Continuous solid-state phase transitions in energy storage materials with orientational disorder - Computational and experimental approach, Energy. 91 (2015) 334–349.

[136] M.M. Kenisarin, K.M. Kenisarina, Form-stable phase change materials for thermal energy storage, Renewable and Sustainable Energy Reviews. 16 (2012) 1999–2040.

[137] N.R. Jankowski, F.P. McCluskey, A review of phase change materials for vehicle component thermal buffering, Appl Energy. 113 (2014) 1525–1561.

[138] M. Barrio, J. Font, D.O. López, J. Muntasell, J.L. Tamarit, F. Cossio, Polymorphism in 2-Amino-2-Methyl-l, 3 propanediol plastic crystal, Journal of Phase Equilibria. 12 (1991) 409–415.

[139] D. Benson, J. Webb, R. Burrows, J. McFadden, C. Christensen, Materials research for passive solar systems: Solid-state phase-change materials, NASA STI/Recon Technical Report N. (1985).

[140] E. Murrill, L. Breed, Solid-solid phase transitions determined by differential scanning calorimetry. Part I. Tetrahedral substances, Thermochim Acta. 1 (1970) 239–246.

[141] J. Salud, D.O. López, M. Barrio, J.L. Tamarit, Two-component systems of isomorphous orientationally disordered crystals. Part 1: Packing of the mixed crystals, J Mater Chem. 9 (1999) 909–916.

[142] M. Barrio, J. Font, J. Muntasell, J. Navarro, J.L. Tamarit, Applicability for heat storage of binary systems of neopentylglycol, pentaglycerine and pentaerythritol: A comparative analysis, Solar Energy Materials. 18 (1988) 109–115.

[143] D. Chandra, H. Mandalia, W.-M. Chien, D.W. Lindle, R. Rudman, Solid-solid phase transition in trimethylolpropane (TRMP), (2002).

[144] E. Murrill, L. Breed, Solid—solid phase transitions determination by differential scanning calorimetryPart II. Octahedral substances, Thermochimica Acta - THERMOCHIM ACTA. 1 (1970) 409–414.

[145] M. Barrio, J. Font, D.O. Lopez, J. Muntasell, J.L.I. Tamarit, Y. Haget, Plastic molecular alloys: the binary system tris (hydroximethyl) aminomethane/2-amino-2-methyl-1, 3-propanediol, Journal de Chimie Physique. 91 (1994) 189–202.

[146] Q. Yan, C. Liang, The thermal storage performance of monobasic, binary and triatomic polyalcohols systems, Solar Energy. 82 (2008) 656–662.

[147] D.S. Sake Gowda, R. Rudman, Polymorphism of crystalline poly(hydroxymethyl) compounds. V. X-ray diffraction investigation of crystalline and plastic 2-bromo-2-nitro-1,3-propanediol, J Chem Phys. 77 (1982) 4666–4670.

[148] D. Lilley, J. Lau, C. Dames, S. Kaur, R. Prasher, Impact of size and thermal gradient on supercooling of phase change materials for thermal energy storage, Appl Energy. 290 (2021) 116635.

[149] K.G. Rao, P. Rasoor, G. Anjaneya, J.R. Nataraj, M.R. Srinivas, A review on methods of preventing super cooling in phase change materials (PCMs), in: AIP Conf Proc, AIP Publishing LLC, 2021: p. 20003.

[150] M.H. Zahir, S.A. Mohamed, R. Saidur, F.A. Al-Sulaiman, Supercooling of phase-change materials and the techniques used to mitigate the phenomenon, Appl Energy. 240 (2019) 793–817.

[151] R. Gotoh, T. Totani, M. Wakita, H. Nagata, Controlling heat release of crystallization from supercooling state of a solid-solid PCM, 2-amino-2-methyl-1,3-propanediol, Int J Heat Mass Transf. 137 (2019) 1132–1140.

[152] A.J. Lopes Jesus, S.C.C. Nunes, M. Ramos Silva, A. Matos Beja, J.S. Redinha, Erythritol: Crystal growth from the melt, Int J Pharm. 388 (2010) 129–135.

[153] H. Ji, D.P. Sellan, M.T. Pettes, X. Kong, J. Ji, L. Shi, R.S. Ruoff, Enhanced thermal conductivity of phase change materials with ultrathin-graphite foams for thermal energy storage, Energy Environ Sci. 7 (2014) 1185–1192.

[154] Y. Wang, Z. Zhang, T. Zhang, Z. Qin, D. Zhang, H. Ji, Preparation and Characterization of Erythritol/Graphene Oxide Shape-Stable Composites with Improved Thermal-Physical Property, ChemistrySelect. 4 (2019) 1149–1157.

[155] Y. Wang, S. Li, T. Zhang, D. Zhang, H. Ji, Supercooling suppression and thermal behavior improvement of erythritol as phase change material for thermal energy storage, Solar Energy Materials and Solar Cells. 171 (2017) 60–71.

[156] S. Guo, Q. Liu, J. Zhao, G. Jin, X. Wang, Z. Lang, W. He, Z. Gong, Evaluation and comparison of erythritol-based composites with addition of expanded graphite and carbon nanotubes, Appl Energy. 205 (2017) 703–709.

[157] J.-L. Zeng, Y.-H. Chen, L. Shu, L.-P. Yu, L. Zhu, L.-B. Song, Z. Cao, L.-X. Sun, Preparation and thermal properties of exfoliated graphite/erythritol/mannitol eutectic composite as form-stable phase change material for thermal energy storage, Solar Energy Materials and Solar Cells. 178 (2018) 84–90.

[158] M. Inagaki, T. Morishita, A. Kuno, T. Kito, M. Hirano, T. Suwa, K. Kusakawa, Carbon foams prepared from polyimide using urethane foam template, Carbon N Y. 42 (2004) 497–502.

[159] L. Jiang, Y. Chen, L. Shu, Y. Zhang, T. Xie, N. Tan, Y. Fang, S. Wang, L. Zhang, J. Zeng, Preparation and characterization of erythritol/polyaniline form-stable phase change materials containing silver nanowires, Int J Energy Res. 43 (2019) 8385–8397.

[160] M. Yuan, C. Xu, T. Wang, T. Zhang, X. Pan, F. Ye, Supercooling suppression and crystallization behaviour of erythritol/expanded graphite as form-stable phase change material, Chemical Engineering Journal. 413 (2021) 127394.

[161] Z. Zhang, Y.-N. Chen, J. Qi, Z. Zhang, K. Ohara, O. Sakata, Z.-D. Zhang, B. Li, High-energy x-ray diffraction study on phase transition asymmetry of plastic crystal neopentylglycol, Chinese Physics B. 31 (2022) 36802.

[162] S.R. Aubuchon, T.A. Instruments, Interpretation of the Crystallization Peak of Supercooled Liquids Using Tzero® DSC, TA344. (2007).

Chapter 2

Experimental techniques

2.1. Materials and processing.

All the Plastic Crystals; 2,2-dimethyl-1,3-propanediol (Neopentylglycol, NPG), 2-amino-2-methyl-1,3-propanediol (AMP), 1,1,1-tris(hydroxymethyl)ethane (pentaglycerol, PG), tris/hydroxymethyl)aminomethane (TRIS), and 2,2-bis(hydroxymethyl)-1,3-propanediol (pentaerythritol, PE) were purchased from Sigma-Aldrich®, (see Table 2.1). To avoid eventual degradation or hydration, all the PCs were stored in closed glass recipients inside a glove box with a controlled argon atmosphere and levels of oxygen and humidity below 0.1 ppm. Unless specified for some cases, all the PCs were used as received without any prior purification.

Table 2.1. Commercial data of NPG, AMP, PG, TRIS and PE provided by Sigma-Aldrich®.

Acronym	NPG	AMP	PG	TRIS	PE
CAS number	126-30-7	115-69-5	77-85-0	77-86-1	115-77-5
Molecular formula	$C_5H_{12}O_2$	$C_4H_{11}NO_2$	$C_5H_{12}O_3$	$C_4H_{11}NO_3$	$C_5H_{12}O_4$
Molecular weight (g/mol)	104,15	105,14	120,15	121,14	136,15
Purity (%wt.)	99	> 99	> 98	> 99.8	99

For the carbon-based composites synthesis, two types of particles were dispersed in the PCs. Highly conductive expanded graphite (EG) powder of different particles sizes (EG75 and EG600) was purchased from SGL Carbon SE, and highly conductive graphene microparticles with different oxygen contents (70i, rGO and GO) were purchased from Avanzare®. The commercially available data together with some properties determined in this work are listed in Table 5.2 in Chapter 5.

A Microbalance XP2U (Figure 2.1a), purchased from Mettler Toledo, was used for weighing the materials. The uncertainty of the weight was provided from the manufacturer to be ± 1 µg, but the monthly calibration reports a slightly higher uncertainty of ± 2 µg.

The materials were grounded by hand in a mortar and/or by mechanochemical treatment using a Sampleprep mixer ball milling from Spex (Figure 2.1b), with stainless steel vials and three stainless-steel balls of 3 mm of diameter using a ball-to-powder ratio of 1.

A hydraulic manual uniaxial press from Specac Ltd. (Figure 2.1c) was used to compact and prepare cylindrical pellets by applying different pressures up to 5 Tn using Specac Pellet Die of 13 mm diameter (Figure 2.1d).

For selected cases, the material was melted in order to synthetize the carbon-based composites. To this end, a chamber furnace NAT 30/85 from Nabertherm® (Figure 2.1e) was used with a temperature accuracy of ± 3.5 ºC. For fast heating/cooling cycles, a TS1500 Linkam Microfurnace (Figure 2.1f) purchased from Linkam was used to apply different heating and cooling ramps to the samples.

Figure 2.1. (a) Microbalance XP2U from Mettler Toledo, (b) SamplePrep 8000D vibratory mill from SPEX, (c) hydraulic manual uniaxial press from Specac, (d) Stainless-steel pellet die of 13mm diameter from Specac, (e) chamber furnace NAT 30/85 from Nabertherm, and (f) Linkam TS1500 microfurnace from Linkam.

2.2. Differential Scanning Calorimetry.

Differential Scanning Calorimetry (DSC) is a thermal analysis technique which measures the temperatures and heat flows of materials as a function of time. Therefore, this technique provides quantitative information about physical and chemical changes that involve endothermic or exothermic processes, such phase transitions or heat capacity changes. The

technique is based in the difference in heat flows between a sample and an inert reference which are both subjected to the same conditions, i.e., temperature, pressures, times, atmosphere, etc [1]. Such a difference will provide a thermogram in which every time that an exothermic or endothermic event happens, the equipment registers a peak (Figure 2.2a).

A Q2500 Calorimeter manufactured by TA Instruments® was used to carry out the measurements (Figure 2.2b). Heat flows were measured in the sample and the reference by two metallic disks connected to thermocouples arranged in series, so that trough the Ohm's law, it is possible to measure heat flow as a function of time and temperature variations. The obtained thermograms (compensation heat flux vs. temperature) were used to determine phase transition temperatures, enthalpies, and specific heats [2].

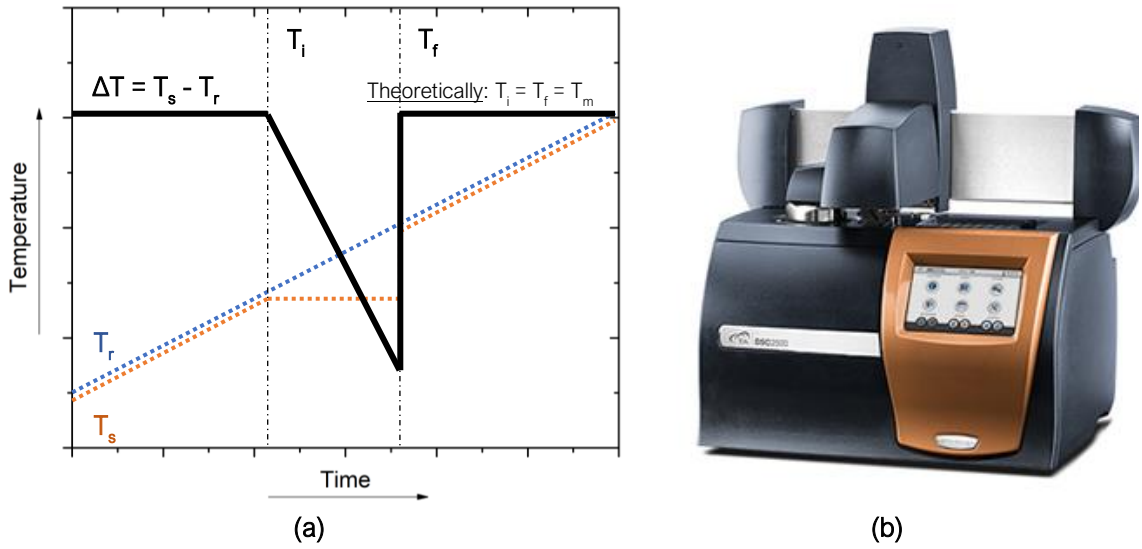

Figure 2.2. (a) Scheme of the recorded DSC signal: ΔT (signal recorded by DSC); T_r (temperature of the reference); T_s (temperature of the sample), T_i (initial temperature); T_f (final temperature). (b) DSC Q2500 from TA Instruments.

In this work, in which the materials undergo isothermal phase transitions, the transition temperature is given by the onset temperature [3]. Calibration of heat flow and temperatures was carried out monthly by using high purity (< 99.99 %) indium standard, and the accuracy in the determination of transitions temperatures is about ± 0.9 ºC. The enthalpies of phase transition are calculated by integration of the endothermic peaks assuming a linear baseline according to the guidelines stated in ref. [4]. The accuracy given by the integral is about ± 5% of error. The specific heat of the samples was measured over different range of

temperatures by a direct measurement and a determination of the error using a high purity sapphire (> 99.99 %) as standard material, also given an accuracy about ± 5% of error.

All the samples, with masses from 2.5 to 25.0 mg, were measured inside T-zero closed aluminium crucibles. Depending of the desired experiment, from three to ten heating/cooling runs were performed at different heating/cooling rates varying from 1 ºC/min to 20 ºC/min. All experiments were performed with argon (50 mL/min) as purge gas to provide a uniform and stable thermal environment which ensure a flat baseline and a good signal-to-noise ratio, and nitrogen to cool below room temperature when desired. Prior to the measurements, a first rapid heating/cooling cycle is completed to ensure an adequate sample/crucible contact. The temperature ranges varied depending on the sample, in order to record completely the solid-solid phase transition without reaching the melting temperature. Therefore, the temperature ranges were 20 ºC – 60 ºC for NPG, 60 ºC – 100 ºC for PG, 160 ºC – 200 ºC for PE, -40 ºC – 100 ºC for AMP and 60 ºC – 150 ºC for TRIS.

2.3. Thermogravimetric analysis.

Thermogravimetric analysis (TGA) is a thermal analysis in which the amount and rate of change of the weight of a sample is measured in a controlled environment. Consequently, the equipment is able to determine mass changes, rate of such a change, and the temperature, in order to determine oxidations, decompositions, reactions, dehydrations, and so on [1]. A strong magnet is placed above or below the weight balance in order to calibrate weight and temperature by giving an initial weight gain or loss at room temperature [5]. In this work, a vertical temperature calibration configuration was set up in the equipment, so the magnet is placed under the sample pan (Figure 2.3a).

Thermogravimetric measurements were performed on a TF 209 F1 Libra instrument, manufactured by NETZSCH (Figure 2.3b), in order to determinate the degradation temperature of the materials and the mass losses during heating. The temperatures were calculated based on the onset in the slope of the thermogravimetric curve. The equipment is calibrated for temperatures using nickel (purity > 99.99%) as a reference.

The samples, of around 40-50 mg, are placed in open alumina crucibles and are submitted to heating ramps of 10 ºC/min from room temperature up to 700 ºC. Two different atmospheres, air and pure nitrogen, were used in order to study the degradation behaviour

of the samples, at 60 mL/min of flow rate. The experimental error supplied by NETZSCH is ± 2% for both the temperature determination and the weight.

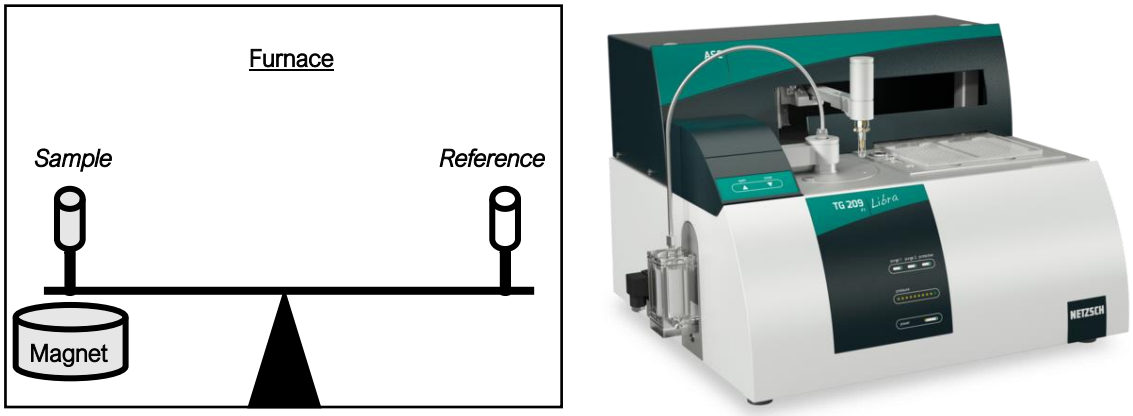

(a) (b)

Figure 2.3. (a) Scheme of a thermogravimetric equipment with a temperature calibration configuration, and (b) TF 209 F1 Libra instrument.

2.4. Hot Disk.

Hot disk is a technique to determine the thermal conductivities of materials by using the transient plane source method. It is based on the use of a disk-shaped sensor placed in the middle of the material of interest that, when heated, it is possible to know the heat flow exchange between the sensor and the sample. Therefore, according to the theory of thermal conductivity by Fourier, which states that the local heat flow is proportional to the negative local temperature gradient, it is possible to calculate the thermal conductivity using Equation 2.1,

$$Q = -k \cdot dT/dx \tag{2.1}$$

where Q is the heat flow, k is the thermal conductivity of the material and dT/dx is the temperature variation across the surface [6,7]. This equation comes from the definition of thermal conductivity as the rate at which the heat is transferred by conduction through a given surface of a material.

The thermal conductivity determination was carried out by means of a Hot Disk TPS 2500S from Hot Disk AB (Figure 2.4a). The apparatus is coupled to a Kapton sensor of 4 mm diameter (type 7577 F1, Figure 2.4b), which transfer and receive the heat flow from and to the sample. By carefully following the guidelines from the Hot Disk norm (ISO 22007-2:2015), the power applied to the sensor ranges from 20 to 50 mW during 20 to 4 s, respectively. The accuracy given by the apparatus was ca. ± 5 %, whereas the reproducibility of the measurements is within ± 2 %.

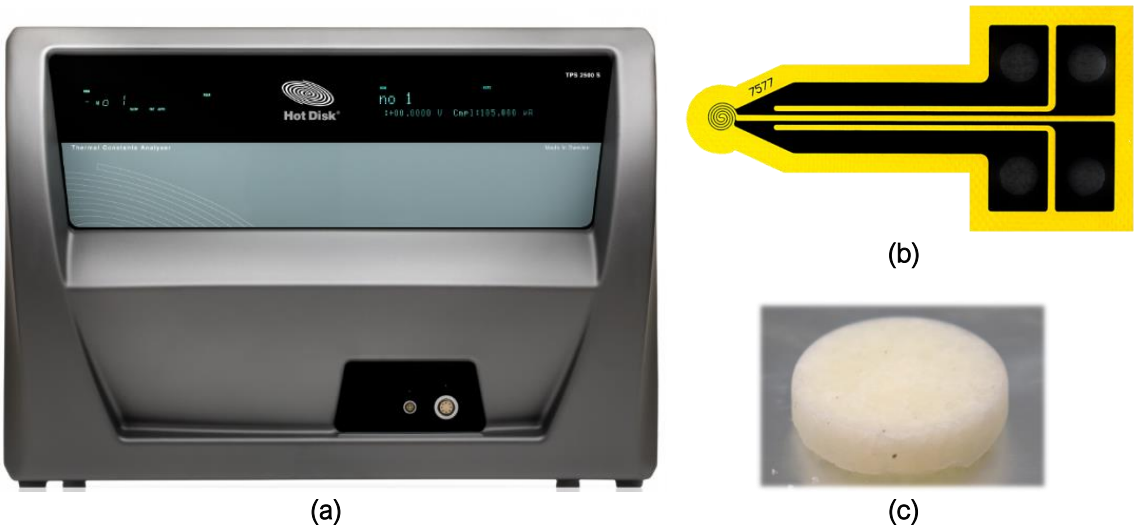

Figure 2.4. (a) Hot Disk TPS 2500S, (b) Kapton sensor type 7577 F1, and (c) sample of PG processed by casting.

Since the technique needs a good contact between the samples and the sensor, two identical samples were prepared for each experiment in order to attach the sensor between them. The samples must to be plane to ensure a good contact with the sensor avoiding discontinuity (e.g., air bubbles). Therefore, samples of all the materials were prepared twice by a first melting inside an aluminium pan of 20 mm diameter and subsequent slow solidification in order to prevent the formation of metastable phases. Subsequently, the samples were polished using a fine sandpaper in order to ensure a flat surface of about 8 mm thickness (Figure 2.4c). For the thermal conductivities' measurements of the plastic phases of the PCs, a Dynamic Climate Chamber MKFT 115 from BINDER® was needed to heat up the sample above the solid-solid transition. In all the cases, the measurements were repeated four times.

2.5. Helium pycnometry.

Helium pycnometry is a technique widely used to determine densities in solid materials. The fundamental behind this technique is as simple as the direct relationship between pressure and volume of a gas. In this sense, helium is used due to its inertness to any kind of material. Therefore, the differences of the volume of helium at two different pressures is used to do a prior calibration of the volume of the empty chamber. Then, the same operation is carried out once the sample is introduced in order to determine the free volume, so that the differences between both operations gives the volume of the sample [8,9]. By a prior determination of the mass sample, the calculation of the density is obtained straightforwardly.

The equipment used to determine the true density of the studied materials is an Accupyc II 1340 pycnometer purchased from Micromeritics. The measurement procedure follows several steps (Figure 2.5):

1) Helium is inserted in the sample chamber.
2) Pressure equilibrium is reached inside the sample chamber.
3) Helium reaches a secondary chamber for the volume determination.
4) Pressure reaches the equilibrium again.
5) By knowing the sample mass, the reported value of volume leads to the density calculation.
6) Helium is released to comes back the equipment to atmospheric pressure.

Reproducibility of the results is ± 0.2 %, whereas the accuracy of each measurement is ± 0.3 %, both values provided by the manufacturer.

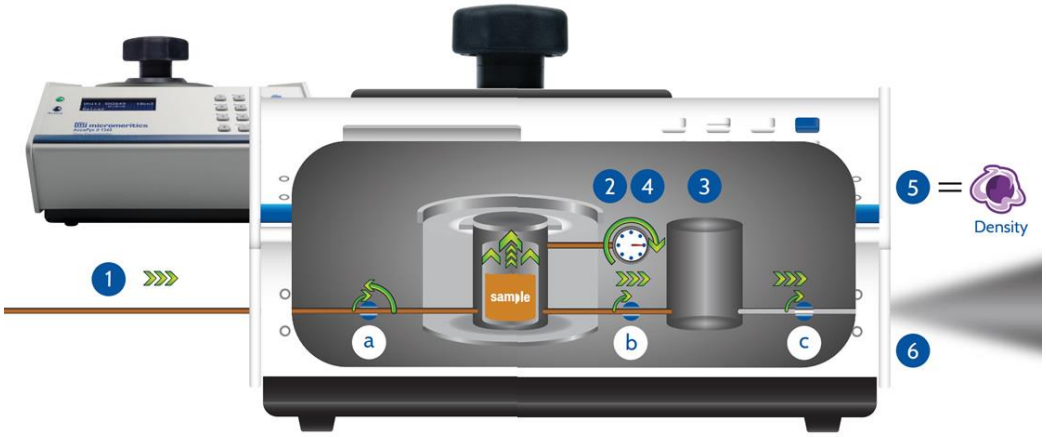

Figure 2.5. Scheme of functioning of the Accupyc II 1349 pycnometer from Micromeritics.

All the plastic crystals were measured in powder without any prior treatment. After the accurate weighing of the sample in the Microbalance XP2U from Mettler Toledo, the powders were placed inside the chamber (1 mL volume) and covered with a microporous lid in order to prevent the leak of sample enabling the insertion of helium.

2.6. Dilatometry.

Thermal dilatation of the samples was measured upon heating and cooling and during the solid-solid phase transition. The equipment registers the expansions and contractions of the material by a one-direction push rod to determine the volume variation (Figure 2.6a).

The equipment used was a push-rod dilatometer 402 C from NETZSCH (Figure 2.6b). The studied temperatures ranged from room temperature to 220 ºC using heating and cooling rates of 2 ºC/min under controlled nitrogen atmosphere (100 mL/min). A calibration correction was used in order to measure the temperature with a calibrated S-thermocouple placed close to the sample. For the length determination, a calibration was carried out by applying the same thermal program of the sample to an alumina standard whose length and thermal expansion is well known.

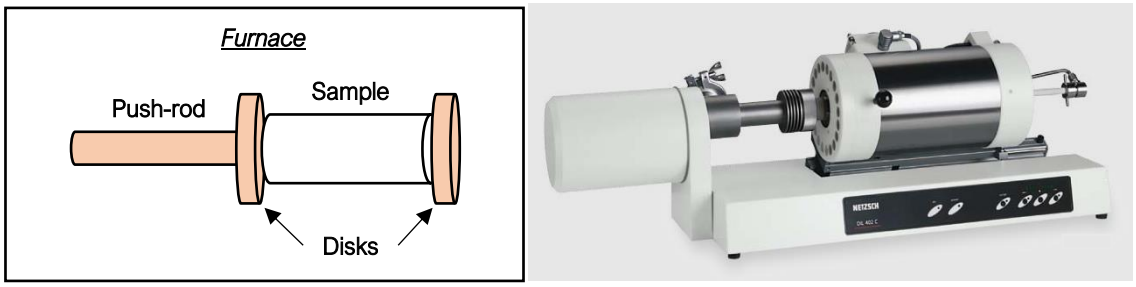

Figure 2.6. (a) Scheme of the measurement of the dilatometry and (b) Push-rod dilatometer 402C from NETZSCH.

Cylindrical shaped samples of 15-25 mm length and 6 mm in diameter were prepared using a 6 mm diameter pellet die. The samples were compacted in a uniaxial Press by applying 5 tons of pressure 1 min and placed in the equipment between two alumina disks to avoid any undesired vibration or displacement during the measurement (Figure 2.6a).

2.7. Infrared spectroscopy.

The fundamentals of this technique are based on the absorption of an infrared (IR) radiation by the sample, whose energy is on the same energy level than the differences on the vibration levels of a molecule (Figure 2.7) [10]. The material of interest must have an electric dipole moment that changes upon the vibration caused by the irradiation. Therefore, to observe such an effect, the molecule must possess heteronuclear diatomic bonds. Once the radiation is absorbed, the bonds expands and contract, or even change the spatial configuration, hence resulting in a change in the polarity [11,12]. Therefore, since each single bond would have different energy levels of vibration depending on many parameters such as the atomic nuclei involved, the geometry, the strength of the bond, and so on, it is possible to record an IR spectrum that affords the identification of different bonds inside a molecule.

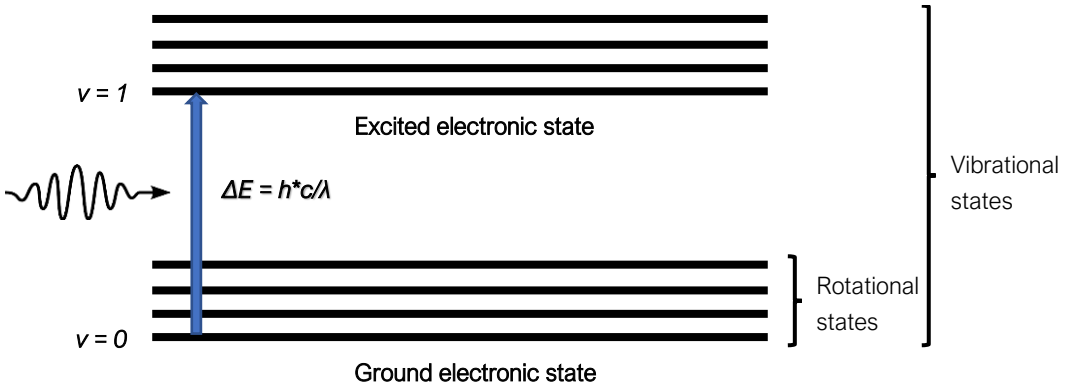

Figure 2.7. Vibrational energy levels for IR radiation absorption.

The infrared spectrum can be divided into three main regions: the far-IR (100-400 cm^{-1}), the mid-IR (400-4000 cm^{-1}) and the near-IR (4000-13000 cm^{-1}), but the vast majority of the measurements are performed in the mid-IR since it is possible to obtain a lot of information about the typical chemical bonds, such as C-O, C=O, O-H, N-H, C-H, and so on [13]. In particular, for the plastic crystals, it is of special interest to study of the O-H bonds, because the formation of hydrogen bonds within a crystal lattice influences the strength of these O-H bonds, modifying the frequency of vibration. In general, the O-H stretching vibration in alcohols is observed in the 3600-3700 cm^{-1} range.

Temperature variable FTIR measurements were carried out in an ALPHA FT-IR Spectrometer purchased from Bruker (Figure 2.8). The equipment is based in a simultaneous irradiation and detection window in which the sample is easily placed for the measurement. A prior correction of the atmosphere was carried out in order to ensure a flat baseline without interfering to the measurements. The temperatures reached were the maximum afforded by the equipment, 120 ºC, and the minimum was room temperature (20 ºC).

Figure 2.8. ALPHA FT-IR Spectrometer from Bruker.

2.8. Solid-state Nuclear Magnetic Resonance.

Nuclear Magnetic Resonance (NMR) is a spectroscopic technique based on the interaction of a magnetic field with a specific atomic nucleus. The principle behind this technique is that some nuclei have non zero spin. Therefore, by applying an external magnetic field is possible to give energy enough to the atoms to promote an electronic transition between the base energy level to an excited energy level of spin (Figure 2.9). The energy transferred between both energetic levels has an associated wavelength in the order of radiofrequencies. After the excitation, the spin returns to the base level and releases energy at the same frequency, so that it is possible to construct a NMR spectrum relating different atomic nuclei or even same atomic nuclei in different surroundings [14–16]. The so-called resonant frequency of the energy transition will be dependent on the effective magnetic field at the nucleus, which depends on the strength of the applied external magnetic field, and on the chemical environment of each nucleus due to different electron shielding.

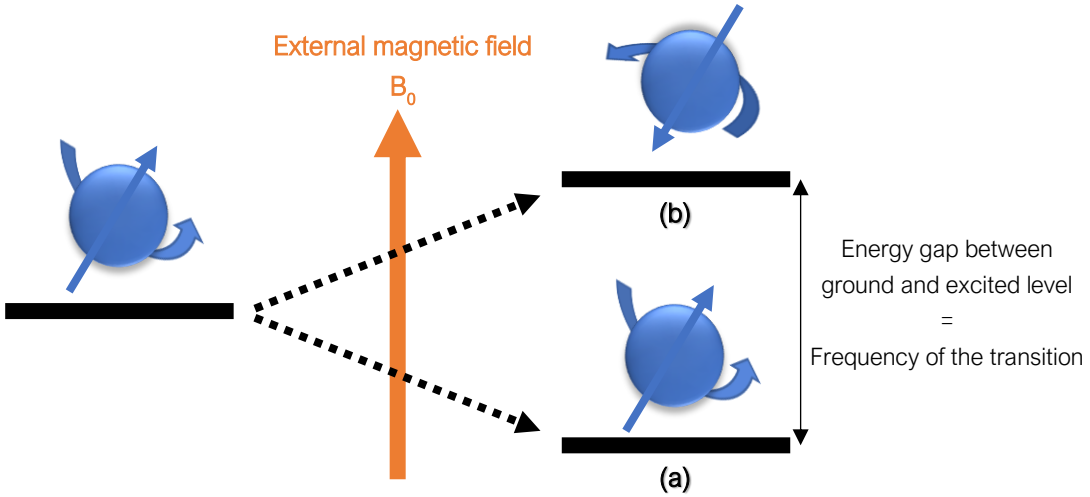

Figure 2.9. Energy diagram for a spin-1/2 nucleus in which (a) the applied magnetic field is aligned to the atomic magnetic field and results in a low energy level, and (b) the applied magnetic field is in the opposite direction to the atomic magnetic field and results in a high energy level.

Traditionally, solution-base NMR was performed in order to obtain information about the chemical distribution in a certain sample, so that any possible intermolecular interaction is discarded. As a result, the recorded NMR spectra of a sample consists of a series of very sharp peaks, and each one is the results of the time-averaging effect of the fast motions of the different molecules. However, the increasing interest to study the solid matter has led to constantly improve the solid-state Nuclear Magnetic Resonance (ssNMR) in order to obtain atomic information of solid samples. This technique allows to determine local molecular environments by an atomic response, and it does not require crystalline samples [17]. Comparing to solution NMR, solid-state NMR spectra consist of a series of very broad peaks, since in this case, the effects of anisotropic or orientation-dependent interactions are also present (Figure 2.10a). This orientation dependence is due to the inner location of molecular orbitals and crystallographic symmetry which sometimes are able to induce local magnetic fields. Therefore, the interaction with the applied magnetic field from the spectrometer will be preferred over others. The presence of this broadening, provides information about chemistry, structure and dynamics in the solid state [18,19].

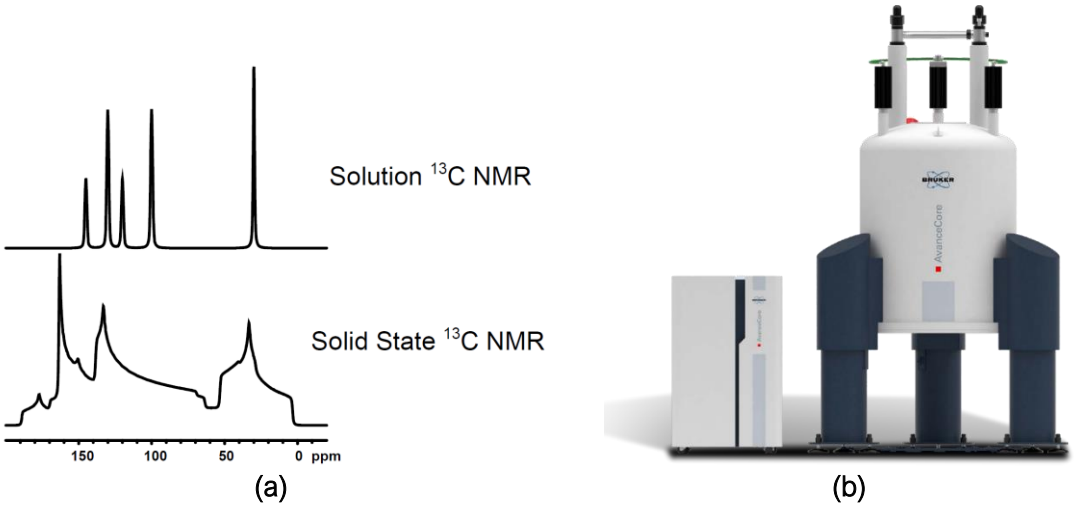

Figure 2.10. (a) Differences between ^{13}C NMR in solution or in solid state, and (b) Bruker WB 500Hz spectrometer.

Temperature variable ssNMR experiments were performed in a WB 500Hz spectrometer purchased from Bruker from room temperature to 150 ºC (Figure 2.10b). All the experiments were carried out in a static mode using a 5 mm static probe. ^{1}H NMR spectra were acquired by using single pulse experiments in order to ensure a full spin relaxation between experiments, with excitation pulses of 2.5 µs. ^{2}H solid-state NMR spectra were acquired using rotor synchronized echo experiments and a recycling delay of 15 s. The values of chemical shifts (δ) in ppm were referred to bulk water resonating at 4.7 ppm.

All the samples were measured as received in powder, unless indicated for each singular case. The PCs were finely powdered by using a mortar in order to fill the glass probe of 5 mm diameter closed with a PTFE cap. ^{2}H NMR experiments were performed in samples in which the hydroxylic and/or amine positions were previously deuterated. The deuteration was performed by hydrogen/deuterium exchange dissolving the sample in D_2O (1:100 in volume) and sonicating the solution in an ultrasound bath for 15 min. The solvent was evaporated at reduced pressure in a rotary evaporator in order to obtain the deuterated PC. This procedure was repeated twice in order to ensure the maximum deuteration degree.

2.9. Transitiometry.

As pointed out in Section 2.2, calorimetry is a powerful thermal technique in which it is possible to obtain a lot of information regarding phase transitions. In them, the most common are the known as first order transitions, in which the variations of volume and enthalpies are

discontinuous during the phase change. Therefore, such a phase transition can be described by the Clapeyron equation (Eq. 2.2),

$$\frac{dT}{dP} = \frac{T \cdot \Delta V}{\Delta H} \tag{2.2}$$

where ΔV and ΔH are the discontinuous changes in volume and enthalpy, respectively, upon the phase change, and dT and dP are the temperature and pressure variations, respectively. Transitiometry offers the possibility to control also a dynamic pressure in the calorimetric measurements [20,21]. Therefore, it is possible to simultaneously measure both thermal and mechanical contributions to the phase transitions.

To this end, a Scanning Transitiometer 400 MPa designed by Randzio et al. (Figure 2.11a) was used in this research. Simultaneous determination of temperature, heat flow, volume, and pressure during a phase transition was carried out by keeping constant one variable and programming another one as a function of time. Consequently, other two variables, one thermal (heat flow) and another mechanical (volume or pressure) can be obtained as output values of the measurements. This is a technique that combines calorimetric and volumetric techniques in order to obtain a complete thermodynamic description of a phase transition in a single measurement [22].

The equipment (Figure 2.11b) consists of two symmetrical calorimetric detectors similar to those of differential scanning calorimetry. The reference vessel contains the pressure transmitting fluid and the measuring vessel the sample to measure. Both vessels are surrounded by a calorimetric block and a heating/cooling shield. The measuring vessel is connected to a PV line from the bottom part. Therefore, pressure can be applied to the sample by the mercury as the pressure transmitting fluid or any other liquid whose compressibility is well-know. In this study, fluorinated fluid Fluorinert™ FC-40 was purchased from 3M and was used as pressure transmitting fluid. Solubility tests of the PCs were carried out at high temperatures and pressures in order to ensure that there is no solubility of the investigated materials in it. The equipment can work up to 400 MPa and 250 ºC.

(a)

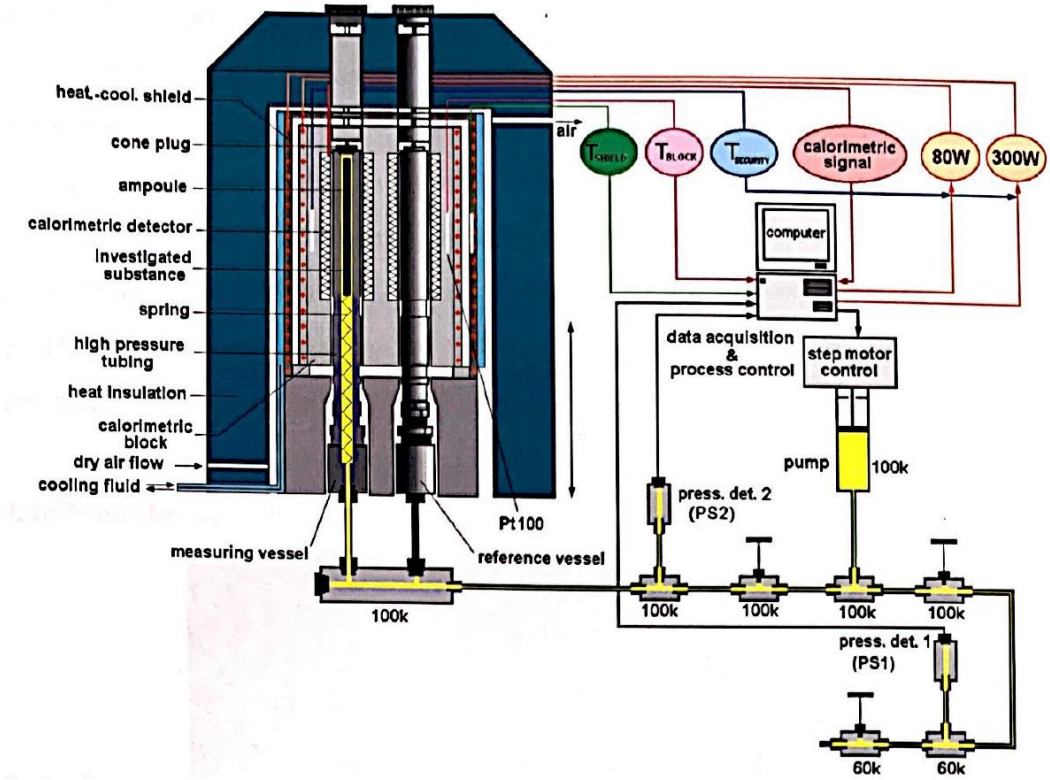

(b)

Figure 2.11. (a) Scanning transitiometer 400 MPa and (b) scheme of its different calorimetric and PV system parts.

The samples were prepared following the requirements of the equipment. A small stainless-steel open container was used in order to maintain the sample at the top part of the measuring vessel, guaranteeing the contact with the pressure transmitting fluid. To this end, a 7 cm length and 3.5 mm in diameter stainless-steel tube was closed by the bottom part with PTFE and the top part was remained open to enable the fluid to transmit the pressure. The tubes were filled with the powdered sample by compacting it manually, whereas the bulk sample was molten and afterwards solidified inside the tube. The samples were weighed before and after the measurement to ensure that there were no mass losses during the measurement. Controlled isobaric experiments were carried out applying different heating and cooling ramps in order to obtain two output signals: the heat flow and the volumetric changes. This allowed to obtain all the thermal and mechanical information about the solid-solid phase transition of the PCs subjected to different pressures.

References in Chapter 2

[1] G.W.H. Höhne, S.M. Sarge, W. Hemminger, Calorimetry: fundamentals, instrumentation and applications, John Wiley & Sons, 2014.

[2] C. Barreneche, A. Solé, L. Miró, I. Martorell, A.I. Fernández, L.F. Cabeza, Study on differential scanning calorimetry analysis with two operation modes and organic and inorganic phase change material (PCM), Thermochimica Acta. 553 (2013) 23–26.

[3] M. Teisseire, N.B. Chanh, M.A. Cuevas-Diarte, J. Guion, Y. Haget, D. Lopez, J. Muntasell, Calorimetry and X-ray diffraction investigations of the binary system neopentylglycol-pentaerythritol, Thermochimica Acta. 181 (1991) 1–11.

[4] W.J. Boettinger, U.R. Kattner, K.-W. Moon, J.H. Perepezko, DTA and heat-flux DSC measurements of alloy melting and freezing, in: Methods Phase Diagram Determination, Elsevier, 2007: pp. 151–221.

[5] W. Xu, S. Li, N. Whitely, W.-P. Pan, Fundamentals of TGA and SDT, (2005).

[6] W.J. Parker, R.J. Jenkins, C.P. Butler, G.L. Abbott, Flash method of determining thermal diffusivity, heat capacity, and thermal conductivity, Journal of Applied Physics 32 (1961) 1679–1684.

[7] R.D. Cowan, Pulse method of measuring thermal diffusivity at high temperatures, Journal of Applied Physics. 34 (1963) 926–927.

[8] W.C. Schumb, E.S. Rittner, A helium densitometer for use with powdered materials, Journal of American Chemistry Society. 65 (1943) 1692–1695.

[9] E.Y.H. Keng, Air and belium pycnometer, Powder Technology. 3 (1969) 179–180.

[10] H. Günzler, H.-U. Gremlich, IR spectroscopy. An introduction, (2002).

[11] P. Atkins, J. de Paula, J. Friedman, Chemical equilibrium, Atkins' Phys. Chem. 7th Edn. Oxford Univ. Press. Oxford, UK. (2002) 222–251.

[12] A. Vincent, Molecular symmetry and group theory: a programmed introduction to chemical applications, John Wiley & Sons, 2013.

[13] G. Keresztury, J.M. Chalmers, P.R. Griffith, Raman Spectroscopy: Theory in Handbook of Vibrational Spectroscopy, vol. 1, John Wiley & Sons Ltd. (2002).

[14] J.A. Koutcher, C.T. Burt, Principles of nuclear magnetic resonance, Journal of Nuclear Medicine. 25 (1984) 101–111.

[15] B. Diehl, Principles in NMR spectroscopy, in: NMR Spectrosc. Pharm. Anal., Elsevier, 2008: pp. 1–41.

[16] J.C. Edwards, Principles of NMR, Process NMR Assoc. LLC, 87A Sand Pit Rd, Danbury CT. 6810 (2009).

[17] M.J. Duer, Solid state NMR spectroscopy: principles and applications, John Wiley & Sons, 2008.

[18] F. Taulelle, Fundamental principles of NMR crystallography, NMR Crystallography. 4 (2009) 245.

[19] V.I. Bakhmutov, Solid-state NMR in materials science: Principles and applications, CRC press, 2011.

[20] S.L. Randzio, Scanning transitiometry, Chemical Society Rev. 25 (1996) 383–392.

[21] S.L. Randzio, Transitiometric analysis of pressure effects on various phase transitions, Journal of Thermal Analysis. Calorim. 57 (1999) 165–170.

[22] S.L. Randzio, A. Kutner, Metastability and instability of organic crystalline substances, Journal of Physical Chemistry B. 112 (2008) 1435–1444.

Chapter 3

Selection and characterization of Plastic Crystals

3.1. Antecedents.

In this chapter, the selection and characterization of the Plastic Crystals are discussed. Many PCs are reported in literature, but only some of them can be suitable for the application in thermal energy storage. As for common organic PCMs, the solid-solid transitions of PCs occur up to 200 ºC, so they are mostly devoted to medium-low temperature applications such as heating and cooling living spaces, isolating buildings, district hot water, or even industrial heat recovery. Moreover, as pointed out in Chapter 1, PCMs which undergoes phase transitions with high enthalpies are also preferred due to the potential high storage capacity. Having this in mind, and regarding the neopentane derivatives collected in Table 1.9, some functionalities will be preferred to others. Since latent heat storage is based in intermolecular forces, strong hydrogen bonds will provide more energetic transitions than materials whose intermolecular forces are based only on Van der Waals forces. Therefore, neopentane-based alkanes and halides can be directly discarded as subject of study. On the other hand, nitro compounds, although energetic, are not usually as stable as other neopentane derivatives due to the inherent character of this functional group, for this reason

they are also discarded. Taking that into account, the functionalities of interest are basically those forming strong hydrogen bonds: alcohols, amines, and carboxylic acids. However, carboxylic acid based PCs usually suffer from thermal degradations at medium temperatures, so despite they could seem an interesting option in terms of enthalpy, they were discarded in this study [1–3].

Therefore, alcohol and amine-based PCs are considered the most interesting as potential PCMs. Pure polyols range from one hydroxyl group (neopentylalcohol, NPA), to two (Neopentylglycol, NPG), three (pentaglycerin, PG, and trimethylolpropane, TMP) or four (pentaerythritol, PE) groups. NPA and TMP were discarded because their solid-solid transition occur below 0 ºC in the first case, and in the proximity to the melting point in the latter case. [4,5]. Amine-based PCs are also an interesting class of materials due to the acid-base character of the hydrogen bonds between alcohol and amine groups. However, some molecules as monoaminopentaerythritol (MAPE) and diaminopentaerythritol (DAPE), are not thermally stable and degrade at medium temperatures before melting, so they were not considered in this study [1].

Taking into consideration the reasons mentioned above, this research has been focused on three pure polyols (NPG, PG and PE) and on two aminopolyols (AMP and TRIS) (Figure 3.1). Whereas pure polyols have a moderated subcooling, AMP and TRIS have a severe subcooling of more than 60 ºC. Consequently, it is important to reach a fundamental understanding of the influence of different functional groups on the subcooling degree. This requires a preliminary deep characterization of the different materials with the determination of key thermophysical parameters.

3.2. Results and discussion.

After the selection of the five PCs of interest, a prior thermophysical characterization is required in order to know the suitability of the materials for potential applications. As PCMs, the determination of temperatures of the solid-solid phase transition upon heating and cooling is crucial. This study is carried out regarding different parameters such as the mass of the PC and the different heating/cooling rates applied. Moreover, 50 heating/cooling ramps were measured in order to determine the durability and repeatability upon thermal cycling. The melting and degradation temperatures were also determined in order to stablish the useful range of temperatures for each PC. The enthalpies of the solid-solid transitions as well as the specific heats of both crystalline and plastic phases are also pointed out since energetic

materials are required to be useful as PCMs. Finally, some parameters useful from the technical point of view are also of interest: Thermal conductivity, density, and thermal expansion during the phase transition, in order to do a correct design of the future set up required for applying these materials in upcoming applications.

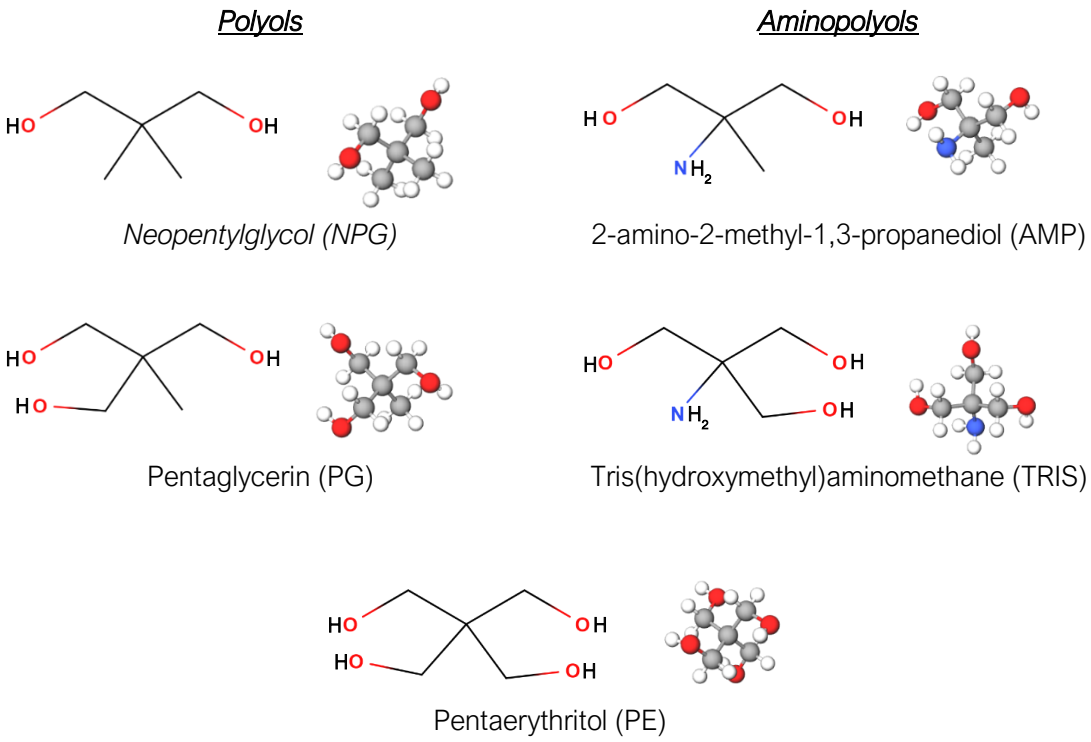

Figure 3.1. 2D and 3D molecular structures of NPG, AMP, PG, TRIS and PE.

3.2.1. Temperatures of solid-solid transition, melting and degradation.

All the solid-solid phase transitions of the PCs selected were studied by DSC. Taking inspiration from the work reported in literature in case of solid-liquid transitions, a deep study was carried out both applying different heating/cooling rates and different sample masses in order to determine any influence on the subcooling in this class of materials. To this end, samples with masses ranging from 2.5 to 25.0 mg were submitted to 10 cycles of heating and cooling using heating rates ranging from 1.0 to 20.0 ºC/min. The results of these measurements are all collected in Annex 1 from Table A.1.1 to Table A.1.5.

For pure polyalcohols (NPG, PG, PE), the standard deviations of the measured temperatures in each cycle never exceeded 3 ºC (Table A.1.1, Table A.1.3, Table A.1.5,

respectively). This means that, considering the DSC accuracy for temperatures (± 1 ºC), some deviations of the averaged temperatures can be due to an intrinsic behavior of the sample, since no trend was found regarding the number of cycles applied to the sample. Moreover, the standard deviation in the onset temperatures upon cooling were, in all the cases, higher than those upon heating, hence supporting the behavior beforehand commented in which the thermal hysteresis seems to be a matter of the transition from the plastic to the crystalline phase. Nevertheless, the small variation of the transition temperatures can be seen in Figure 3.2, where the 10 heating/cooling cycles applied to NPG, PG and PE are depicted.

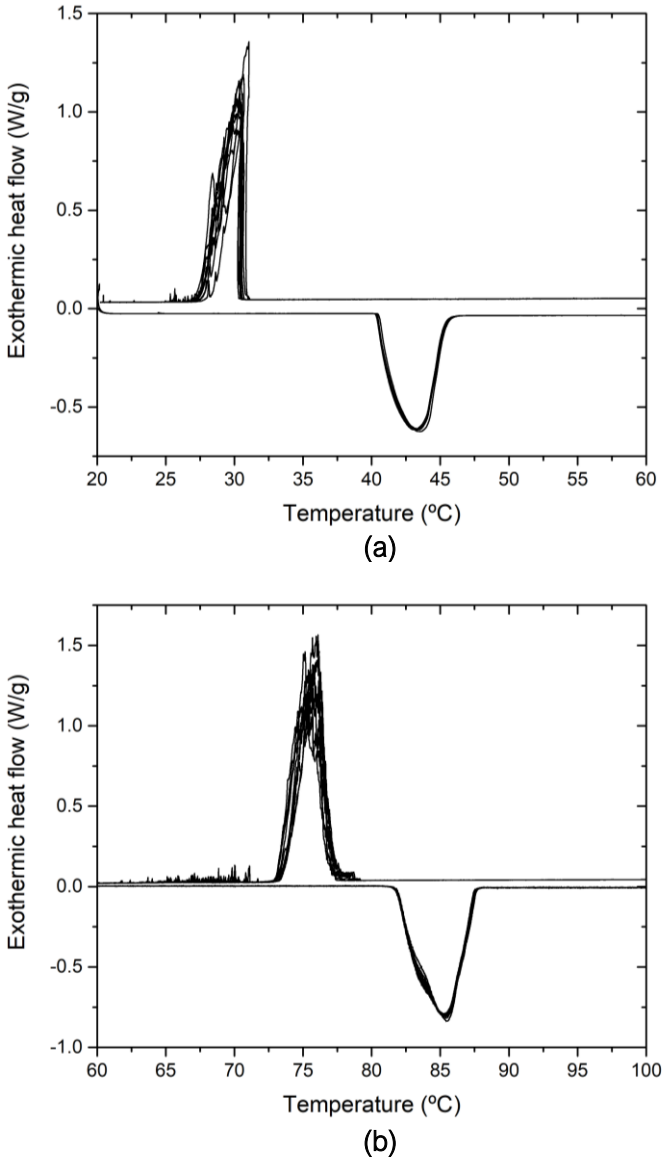

Figure 3.2. DSC thermograms of the 10 heating/cooling scans of (a) NPG, (b) PG and (c) PE at 1 ºC/min.

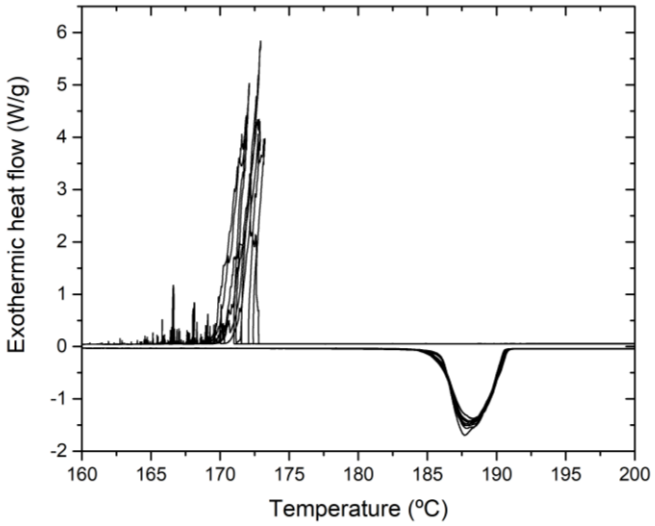

(c)

Figure 3.2. (Continued).

For TRIS, the standard deviations of the temperatures upon cooling were found to be higher than those of pure polyalcohols NPG, PG and PE (Table A.1.4), probably due to the instability and unpredictability promoted by the big difference between the onset temperatures upon heating and upon cooling. Another consequence of this big gap is the looping-shaped signal of the transition upon cooling (Figure 3.3a), due to the energetic transition and the rate at which such an energy is released. This phenomenon is even worse in the case of AMP (Table A.1.2), where the subcooling is so high that in some DSC scans the transition upon cooling does not occur, happening during the subsequent heating ramp (Figure 3.3b); a phenomenon usually named as cold crystallization [6,7]. As a consequence, only the data obtained from sample masses of 2.5 and 25.0 mg, and heating/cooling ramps of 1.0 and 20.0 ºC/min were considered. It is also important to control properly the operation temperature for AMP and TRIS, since the melting temperatures are close to the solid-solid transitions and a liquid phase could form.

Considering the huge number of data obtained from DSC regarding the 10 thermal cycles with no substantial variation, the results from Table A.1.1 to Table A.1.5 are averaged in Table 3.1 and Table 3.2. Regarding Table 3.1, the standard deviation values are calculated based on different heating/cooling ramps for the same sample mass. In this case, the small deviations for all the tested sample masses are similar among them, concluding that the difference of them in the studied range do not affect the subcooling. On the other hand, regarding Table 3.2, the standard deviation values were calculated based on different sample

masses for the same heating and cooling rate, and it is shown how both the average and the standard deviation are higher than those in Table 3.1 for the same compound. Therefore, subcooling seems to be affected by different heating and cooling rates, and the same conclusion can be drawn by checking Figure 3.4, in which, whereas the difference on sample masses just leads to small differences in the shape of the signals, different heating and cooling rates affect also to the onset temperatures, specially upon cooling.

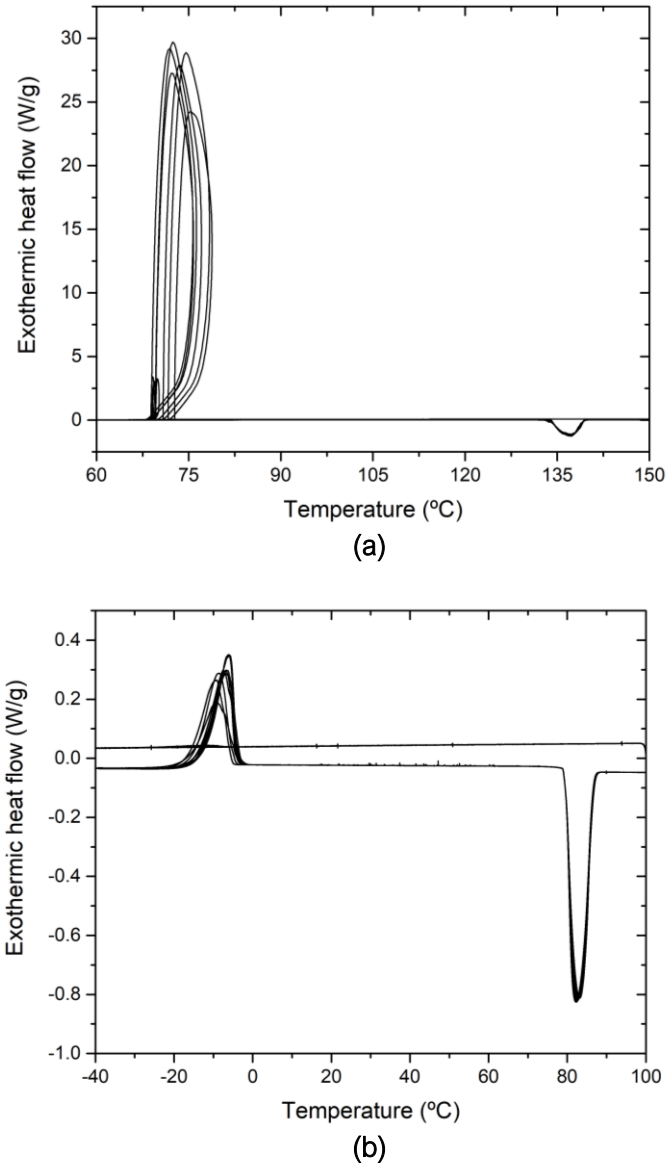

Figure 3.3. DSC thermograms of the 10 heating/cooling scans of (a) TRIS and (b) AMP at 1 ºC/min.

Table 3.1. Averaged onset temperatures and standard deviations of solid-solid transitions upon heating (T_h) and cooling (T_c) from the values obtained at different heating/cooling rates.

Compound		Sample mass (mg)			
		2.5	5.0	10.0	25.0
NPG	T_h (ºC)	40.7 ± 0.5	40.9 ± 0.5	41.0 ± 0.6	40.4 ± 0.6
	T_c (ºC)	28.7 ± 1.5	28.6 ± 1.6	28.5 ± 1.5	28.9 ± 1.8
AMP	T_h (ºC)	80.4 ± 0.9	n.m.	n.m.	79.9 ± 0.4
	T_c (ºC)	12.8 ± 27.8	n.m.	n.m.	1.2 ± 21.1
PG	T_h (ºC)	81.3 ± 0.6	81.5 ± 0.8	81.8 ± 0.5	82.0 ± 0.2
	T_c (ºC)	70.4 ± 2.3	72.4 ± 4.1	71.5 ± 4.5	74.1 ± 3.8
TRIS	T_h (ºC)	133.8 ± 0.4	133.9 ± 0.5	133.5 ± 0.2	133.2 ± 0.4
	T_c (ºC)	67.7 ± 2.1	67.5 ± 4.5	66.2 ± 4.0	67.4 ± 1.2
PE	T_h (ºC)	185.7 ± 0.1	185.9 ± 1.3	185.5 ± 0.2	185.6 ± 0.4
	T_c (ºC)	169.4 ± 1.4	169.7 ± 3.2	171.2 ± 0.9	172.2 ± 1.0

*n.m.: not measured

Table 3.2. Averaged onset temperatures and standard deviations of solid-solid transitions upon heating (T_h) and cooling (T_c) from the values obtained of different sample masses.

Compound		Rates (ºC/min)			
		1.0	5.0	10.0	20.0
NPG	T_h (ºC)	40.3 ± 0.1	40.5 ± 0.6	40.7 ± 0.5	41.4 ± 0.3
	T_c (ºC)	30.7 ± 0.4	28.8 ± 0.2	28.0 ± 0.3	27.1 ± 0.1
AMP	T_h (ºC)	79.7 ± 0.1	n.m.	n.m.	80.6 ± 0.7
	T_c (ºC)	-10.3 ± 4.8	n.m.	n.m.	24.3 ± 11.5
PG	T_h (ºC)	82.0 ± 0.23	81.4 ± 0.4	81.1 ± 0.7	82.1 ± 0.4
	T_c (ºC)	75.63 ± 2.18	73.8 ± 1.7	71.9 ± 1.6	67.1 ± 1.6
TRIS	T_h (ºC)	133.5 ± 0.3	133.4 ± 0.2	133.4 ± 0.5	134.0 ± 0.4
	T_c (ºC)	67.6 ± 2.6	69.4 ± 2.3	66.7 ± 3.3	65.2 ± 2.9
PE	T_h (ºC)	185.8 ± 0.3	185.5 ± 0.2	185.0 ± 1.0	186.0 ± 0.4
	T_c (ºC)	172.7 ± 1.6	171.0 ± 1.7	169.9 ± 2.6	169.4 ± 1.9

*n.m.: not measured

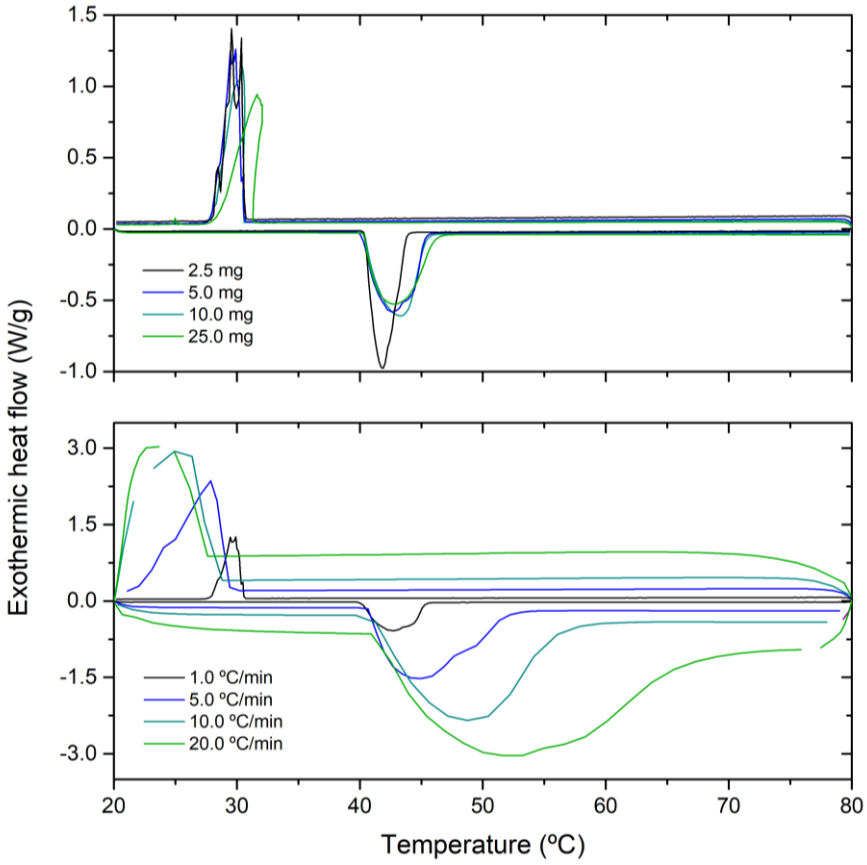

Figure 3.4. DSC thermograms for (a) different sample masses of NPG at 1 °C/min and (b) 5.0 mg of NPG at different heating and cooling rates.

Nevertheless, these results must be considered carefully. When applying fast heating and cooling rates in DSC, the sample may not be able to follow the velocity of the applied heating or cooling ramp, being this effect even more pronounced in the case of samples with poor thermal conductivity. Consequently, the differences in the subcooling are not attributable to the different heating/cooling rates, but to a thermal phenomenon at fast rates. Therefore, the three parameters considered in DSC measurements; thermal cycling, sample mass, and velocity of the scans, do not affect the subcooling, so it is possible to report the values for the onset temperatures of the solid-solid transitions of the five PCs and to compare to the ones already reported in literature (Table 3.3). The results in this study are in good agreement with the ones available in literature. It is worth mentioning that for the PCs considered in this study, a full characterization of solid-solid transition is not reported, especially in the case of the aminopolyols AMP and TRIS.

Table 3.3. Averaged transition temperatures upon heating (T_h) and cooling (T_c) and melting points (T_m) compared to those reported on references.

Compound	Crystalline phase	Plastic phase	T_h (ºC)	T_c (ºC)	T_m (ºC)	References
NPG	Monoclinic	FCC	41.9	27.9	125.1	[8–10]
			42.4	30.0	125.9	[8,11,12]
			40.1	32.0	129.3	[9,13,14]
			40.7	28.7	127.4	This work
AMP	Monoclinic	BCC	80.0	-5.5[a]	112.0	[15,16]
			79.0	n.r.	108.0	[17]
			80.6	n.r.	110.9	[18]
			80.1	7.0[a]	110.2	This work
PG	Tetragonal	FCC	83.4	77.4	200.9	[19,20]
			83.5	76.6	200.6	[21,22]
			83.6	76.6	201.3	[4,23]
			81.6	72.1	197.4	This work
TRIS	Orthorhombic	BCC	132.4	70.9	171.9	[8,11,24]
			134.9	58.1	172.9	[8,20,25]
			134.2	n.r.	172.3	[13,25]
			133.6	70.9	165.8	This work
PE	Tetragonal	FCC	185.4	168.5	255.0	[9,11,15]
			187.6	167.2	261.4	[9,26]
			187.9	174.9	259.9	[27,28]
			185.6	170.8	262.2	This work

[a] Transition appears in the following heating ramp of the sample; n.r.: not reported

From the results of Table 3.3, it is possible to determine with precision the subcooling values for each PC (Table 3.4). Despite the most reliable values of onset temperatures are those registered at 1.0 ºC/min and 2.5 mg of sample mass, because thermal gradients inside the material and thermal lags due to the measurement itself are avoided, the effect of both parameters on the subcooling is negligible, and are considered in the standard deviations. Moreover, the values reported in literature have been determined using different sample masses and heating/cooling rates, so a more realistic comparison can be done to the results of this study. Table 3.4 points out a subcooling degree of c.a. 10-15 ºC for pure polyalcohols, and it is even higher for the case of aminoalcohols, being around 65 ºC for TRIS.

Table 3.4. Subcooling values for the studied plastic crystals.

Compound	Subcooling degree (ºC)
NPG	12.1 ± 1.9
AMP	90.0 ± 4.8
PG	9.5 ± 3.7
TRIS	66.6 ± 3.2
PE	14.8 ± 2.1

The cyclability of these materials was also tested in order to determine their behavior upon multiple cycles. Despite 10 heating and cooling scans are reported from Table A.1.1 to Table A.1.5, 40 additional cycles were carried out in a Linkam microfurnace. After the 50 total cycles, the sample was measured in the DSC, and the values obtained were compared to the ones of the first cycle (see Figure 3.5). It is noticeable how both temperatures of transition upon heating and cooling are practically the same after 50 scans, showing the good reversibility of these materials.

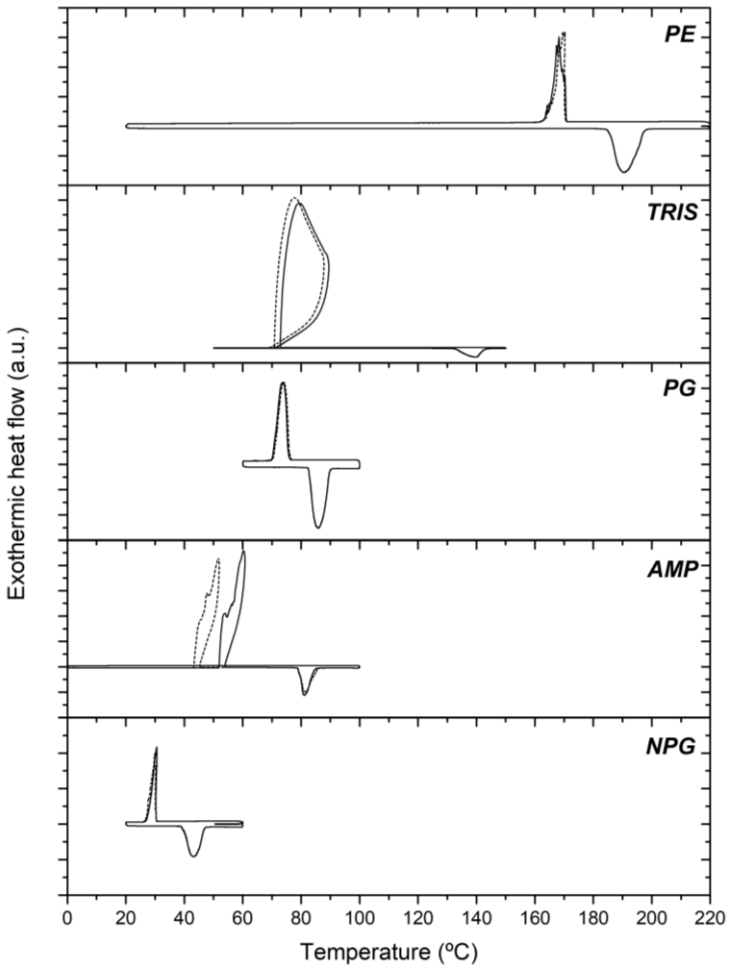

Figure 3.5. Comparison of the first (solid lines) and fifth (dotted lines) scans of the plastic crystals by means of DSC.

Thermogravimetric analysis was carried out up to 700 ºC in order to determine the stability at high temperature of these materials (Figure 3.6). The determined decomposition temperatures range from 150 ºC to 300 ºC, showing a nice trend as a function of the number of hydroxyl groups: the higher the number of hydroxyl and/or amine groups, the higher the decomposition temperature, due to an increasing number of hydrogen bonds.

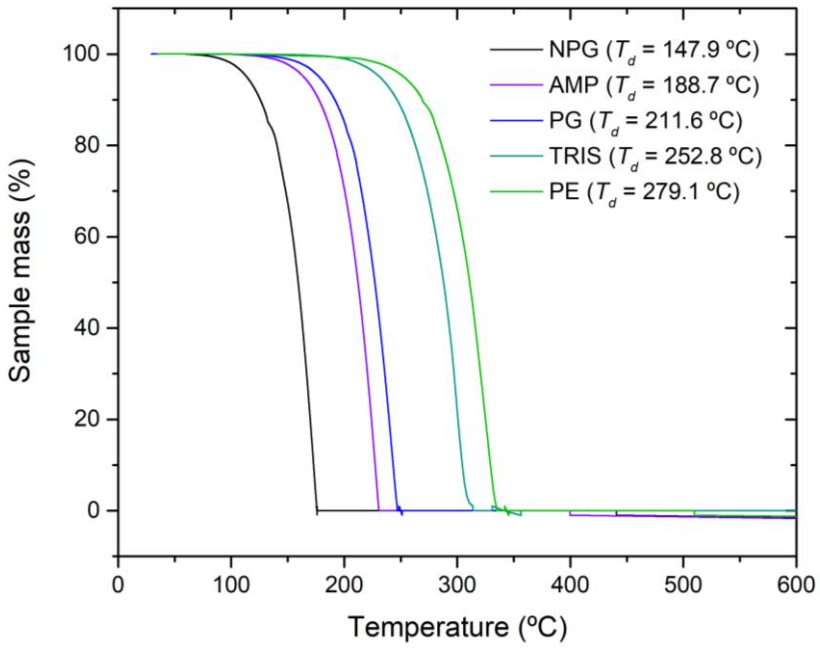

Figure 3.6. Thermogravimetric curves for the five studied plastic crystals.

3.2.2. Enthalpy of transition and specific heat.

The same DSC experiments carried out to analyze the subcooling of the PCs reported in Section 3.2.1 were used to determine the enthalpies of the solid-solid transitions upon heating and cooling. The results confirm that the higher the number of hydroxyl and/or amine groups, the higher the enthalpy of transition, due to the higher number of hydrogen bonds that can be formed, leading to stronger intermolecular forces [30]. This is confirmed by plotting the enthalpies of transition as a function of the number of hydroxyl groups, showing the expected linear trend (Figure 3.7). In case of AMP and TRIS, the enthalpies of transition are higher in comparison with the polyols with the same number of hydroxyl groups. This is due to the presence of the amine group able to form stronger hydrogen bonds due to the

higher ionic nature promoted by certain acid-base character. Additionally, these molecules show one extra hydrogen than the pure polyols that probably is also taking part of the hydrogen bond network. However, analyzing the thermogram of TRIS in Figure 3.8, some endothermic events can be observed during the transition from the plastic to the crystalline phase. Therefore, in order to avoid misunderstandings, the averaged values of the enthalpy upon cooling in Table 3.5 and 3.6 was done considering only the measurements carried out at cooling rates of 1.0 and 5.0 ºC/min. For this reason, the corresponding rows in the table appears as "not calculated".

Table 3.5. Averaged enthalpies of transition and standard deviations of solid-solid transitions upon heating (ΔH_h) and cooling (ΔH_c) from the values at different heating/cooling rates.

Compound		Sample mass (mg)			
		2.5	5.0	10.0	25.0
NPG	ΔH_h (J/g)	122.4 ± 1.1	123.6 ± 1.6	123.8 ± 2.5	120.2 ± 7.0
	ΔH_c (J/g)	110.0 ± 2.3	110.8 ± 3.7	107.1 ± 6.8	111.5 ± 5.1
AMP	ΔH_h (J/g)	219.5 ± 23.4	n.m.	n.m.	217.6 ± 9.9
	ΔH_c (J/g)	128.2 ± 20.9	n.m.	n.m.	127.8 ± 17.3
PG	ΔH_h (J/g)	179.6 ± 7.6	177.9 ± 5.6	176.5 ± 4.4	174.0 ± 10.7
	ΔH_c (J/g)	162.4 ± 2.4	163.7 ± 0.2	156.1 ± 8.4	157.0 ± 1.6
TRIS	ΔH_h (J/g)	281.1 ± 6.8	271.5 ± 14.0	276.5 ± 8.0	277.6 ± 6.6
	ΔH_c (J/g)	n.c.	n.c.	n.c.	n.c.
PE	ΔH_h (J/g)	265.3 ± 8.9	281.2 ± 2.3	273.5 ± 18.6	282.9 ± 7.1
	ΔH_c (J/g)	251.3 ± 0.5	275.1 ± 0.3	274.5 ± 3.3	172.8 ± 3.4

*n.m.: not measured; n.c.: not calculated

Table 3.6. Averaged enthalpies of transition and standard deviations of solid-solid transitions upon heating (ΔH_h) and cooling (ΔH_c) from the values at different sample masses.

Compound		Rates (ºC/min)			
		1.0	5.0	10.0	20.0
NPG	ΔH_h (J/g)	121.5 ± 0.8	123.4 ± 0.8	125.3 ± 1.5	123.2 ± 0.9
	ΔH_c (J/g)	112.5 ± 0.8	106.3 ± 3.5	104.6 ± 1.8	110.3 ± 2.2
AMP	ΔH_h (J/g)	213.7 ± 15.3	n.m.	n.m.	223.3 ± 18.0
	ΔH_c (J/g)	114.5 ± 1.6	n.m.	n.m.	141.5 ± 2.0
PG	ΔH_h (J/g)	171.0 ± 4.7	170.2 ± 4.0	179.9 ± 5.4	184.1 ± 3.9
	ΔH_c (J/g)	162.4 ± 3.8	158.8 ± 3.8	158.0 ± 4.0	153.6 ± 5.1
TRIS	ΔH_h (J/g)	270.4 ± 3.5	285.5 ± 2.8	280.0 ± 8.3	276.7 ± 4.8
	ΔH_c (J/g)	181.4 ± 3.0	194.7 ± 6.2	n.c.	n.c.
PE	ΔH_h (J/g)	282.5 ± 4.2	285.1 ± 1.4	275.6 ± 7.5	278.1 ± 2.5
	ΔH_c (J/g)	276.5 ± 5.5	276.5 ± 1.0	269.6 ± 7.8	274.1 ± 4.8

*n.m.: not measured; n.c.: not calculated

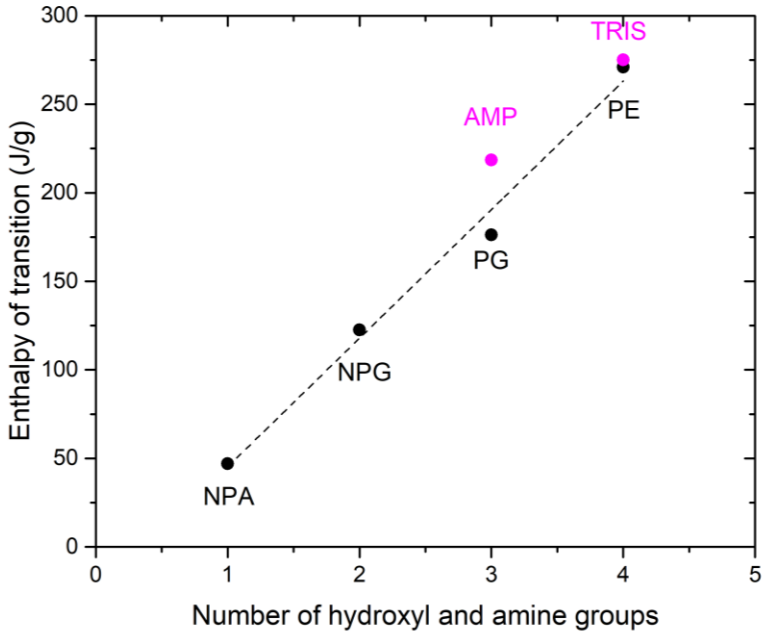

Figure 3.7. Linear trend found between the enthalpy of the solid-solid transition and the number of groups of NPA, NPG, PG and PE which are able to link by hydrogen bonds. Linear fit equation: ΔH (J/g) = 72.62·(#OH) – 27.36 (r^2 = 0.9891).

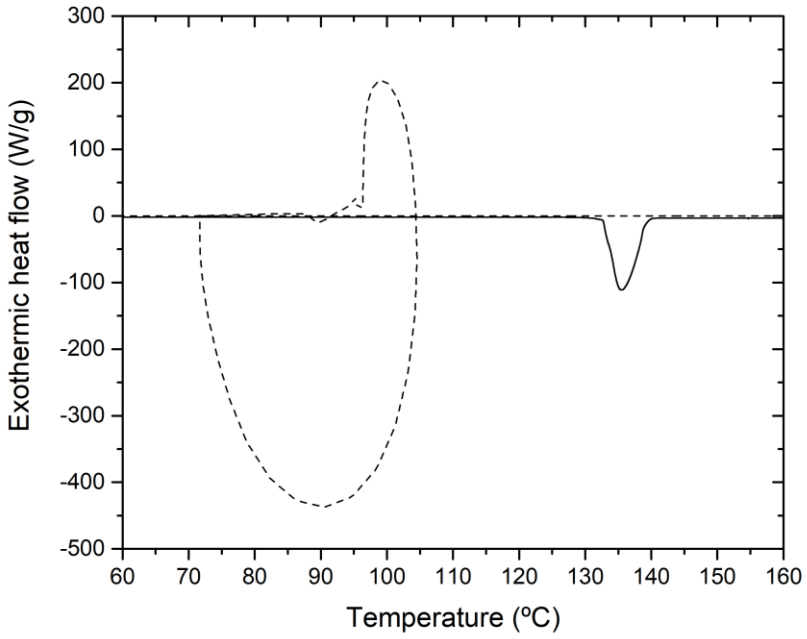

Figure 3.8. Heating (solid line) and cooling (dotted line) ramps of 10.0 mg of TRIS at 10 ºC/min.

The experimental results are in more than acceptable agreement with the ones reported in literature, considering the typical scattering of data observed in the values of enthalpies for this type of transitions (Table 3.7). Again, the aminopolyols AMP and TRIS are not fully characterized upon cooling and there is a lack of information about these transitions.

Table 3.7. Averaged enthalpies of transition upon heating (ΔH_h) and cooling (ΔH_c) compared to those reported in literature.

Compound	Crystalline phase	Plastic phase	ΔH_h (J/g)	ΔH_c (J/g)	References
NPG	Monoclinic	FCC	130.6	110.1	[8,31]
			135.4	114.0	[9,12]
			119.1	n.r.	[11]
			122.5	109.8	This work
AMP	Monoclinic	BCC	239.5	139.4	[3,16]
			226.1	n.r.	[17]
			223.1	n.r.	[18]
			218.5	128.00	This work
PG	Tetragonal	FCC	182.8	164.0	[19,20]
			158.6	159.1	[21,22]

			174.3	162.9	[4,23]
			176.3	158.2	This work
TRIS	Orthorhombic	BCC	269.9	203.0	[8,20]
			295.6	n.r.	[11]
			271.6	n.r.	[25]
			275.1	188.0[a]	This work
PE	Tetragonal	FCC	339.6	238.9	[11,32]
			301.1	225.6	[9,26]
			303.1	280.9	[27,28]
			271.1	267.3	This work

[a] Averaged values only from the measurements performed at 1 ºC/min and 5 ºC/min.; n.r.: not reported

Despite one of the most interesting parameters for PCMs is the enthalpy of transition, specific heats have also been measured by DSC. PCs show unusual high specific heats compared to other organic molecules such fatty acids or polymers, in the order of 1.00-1.80 J/g/ºC for the solid state [33]. The values obtained for the plastic phase are higher than those of the crystalline phase, probably due to the structural configuration of the plastic phase. In this study, the results obtained are generally lower than those reported in literature [27] (Table 3.8). These differences, also noticeable in the equations of the fitted values of *Cp* (see Table A.1.6 in Appendix A.1), can be ascribed to the different way of measuring the specific heat. Whereas in our case a direct measurement is carried out in which the error is given by the measurement of the sapphire as standard, Chandra et al. [27] determined the specific heats by calculations considering also the specific heat of the sapphire.

Table 3.8. Specific heat values (C_p) of the crystalline and plastic phases of plastic crystals from determined temperature ranges compared to those reported on references.

Compound	Phase	Temperature range (ºC)	C_p (J/g/ºC)	
			This work	Ref. [27]
NPG	Monoclinic	30 - 40	1.7 - 1.8	1.9 – 2.0
	FCC	55 - 120	2.5 - 2.8	2.6 - 2.9
AMP	Monoclinic	30 - 75	1.3 - 1.6	1.6 - 2.3
	BCC	100 - 105	2.8 – 3.0	3.4 - 3.7

PG	Tetragonal	30 - 80	1.6 - 1.8	1.6 – 2.0
	FCC	100 - 175	2.6 - 2.8	2.6 – 3.0
TRIS	Orthorhombic	30 - 130	1.6 - 2.2	1.6 - 2.3
	BCC	155 - 165	3.1 - 3.2	3.4 - 3.5
PE	Tetragonal	30 - 175	1.4 - 2.4	1.5 - 3.4
	FCC	200 - 210	2.9 - 3.1	3.4 - 3.5

3.2.3. Thermal conductivity.

Another important parameter when considering the application of these materials in thermal energy storage is the thermal conductivity (k_T), because it is crucial to control the heat release or dissipation in the material. Usually, organic materials are poor thermal conductors. The thermal conductivity of fatty acids, sugar alcohols and polymers in the solid state ranges from 0.28 to 0.51 W/m/K [34], from 0.77 to 1.31 W/m/K [35], and from 0.09 to 0.20 W/m/K [33], respectively. Thermal conductivities of the crystalline and plastic phases of PCs are reported in Table 3.9. For all the PCs, the plastic phases have a thermal conductivity lower than the crystalline phase, due to the different packaging of the molecules in the crystal lattice. These differences are more pronounced in the case of the aminopolyols, probably, because the BCC structure is less dense than the FCC, and hence there is a bigger difference between both phases.

Table 3.9. Thermal conductivities (k_T) of plastic crystals in the crystalline and plastic phases at different temperatures compared to those from references.

Compound	Phases	Temperature (ºC)	k_T (W/m/ºC)	References
NPG	Monoclinic	27	0.25	[36]
		25	0.36	[12]
		25	0.25	This work
	FCC	60	0.21	[36]
		100	0.18	This work
AMP	Monoclinic	20	0.33	[37]
		50	0.57	[38]
		25	0.59	This work
	BCC	100	0.24	This work

PG	Tetragonal	65	0.36	[36]
		25	0.23	[22]
		25	0.37	This work
	FCC	95	0.34	[36]
		100	0.25	This work
TRIS	Orthorhombic	25	0.21	[39]
		20	0.33	[37]
		25	0.44	This work
	BCC	100	0.10	This work
		150	0.07	This work
PE	Tetragonal	170	1.07	[36]
		25	0.51	This work
	FCC	205	0.51	[36]
		180	0.36	This work
		200	0.26	This work

3.2.4. Density and thermal expansion.

Density measurements form helium pycnometry, together with those reported in literature, are reported in Table 3.10. In general terms, organic materials cover a wide range of densities regarding the different functional groups and crystalline structures, from less than 1.0 g/cm^3 for paraffins [41], passing through around 1.0 g/cm^3 for fatty acids [42], to 1.5 g/cm^3 for sugar alcohols [43]. In the case of PCs, the measured densities are in agreement with those reported on literature considering the ± 0.3 % of accuracy of the equipment (Table 3.10). There is a nice trend between the increasing number of functional groups able to form hydrogen bonds (hydroxyl and amine groups) in the PCs and the density. This behavior is related to the stronger lattice networks formed for those with a higher number of hydrogen bonds, promoting a more compacted structure.

Table 3.10. True densities of plastic crystals in the crystalline phase at room temperature compared to those reported in literature.

Compound	Density (g/cm^3)	References
NPG	1.07	[44]
	1.06	[27]
	1.06	This work
AMP	1.21	[45]
	1.20	This work
PG	1.15	[46]
	1.19	[36]
	1.21	This work
TRIS	1.33	[47]
	1.33	This work
PE	1.44	[48]
	1.40	[36]
	1.40	This work

Another important property is the thermal expansion that the PCM suffers before, after, and during the phase transition. Usually, liquid-solid transitions have large volume changes during the phase transition in the order of 12-15 % for fatty acids or wax paraffins, for instance [49]. Solid-solid phase transitions are expected to show lower volume changes during the phase change as well as the shape stability of the material. The results of thermal expansions upon heating and cooling are provided in Figure 3.9 for each one of the PCs excluding AMP, due to the lack of reversibility of the solid-solid transition and the capabilities of the equipment that cannot cool below room temperature.

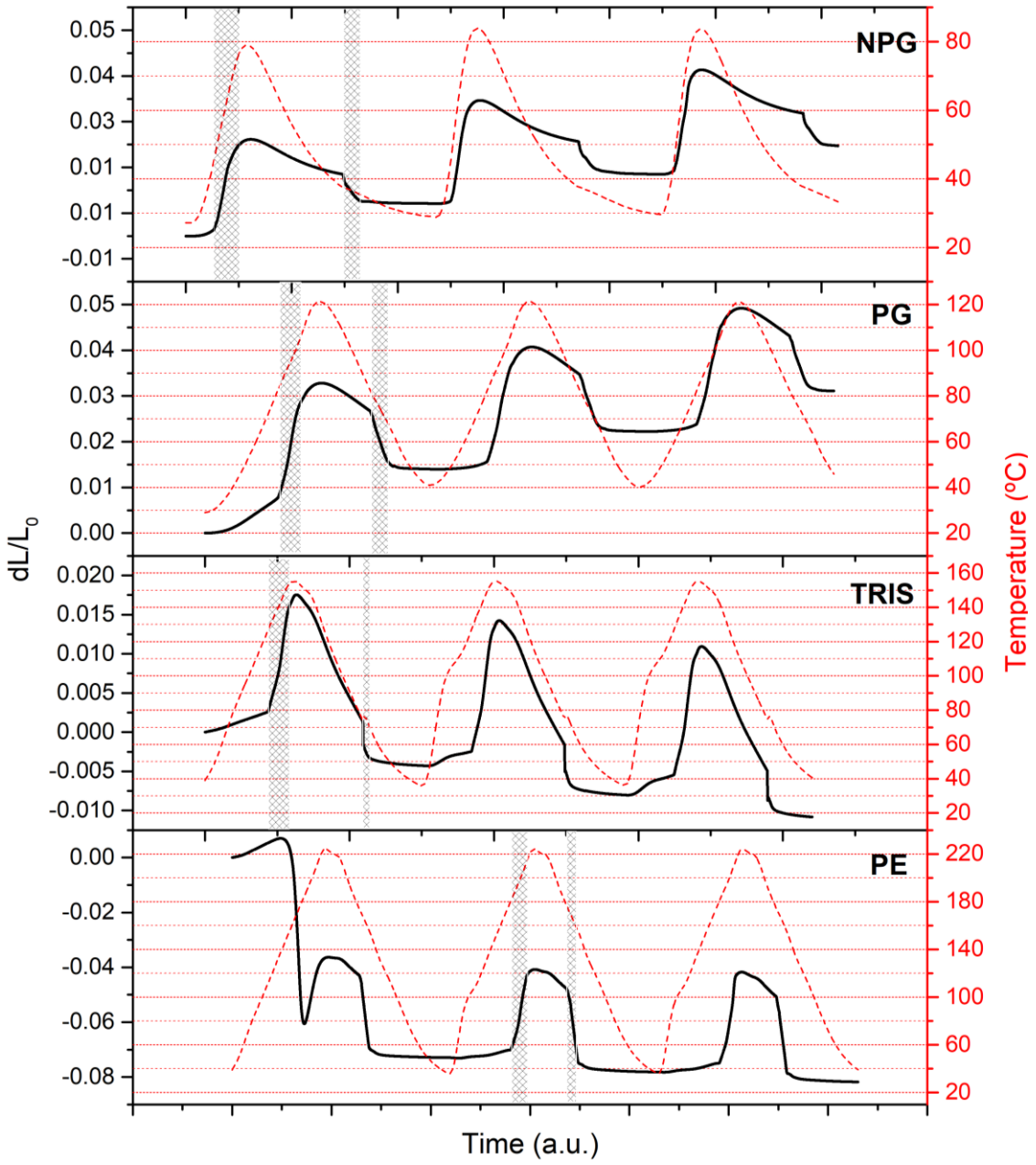

Figure 3.9. Three cycles of thermal expansion/contraction during the solid-solid phase change of NPG, PG, TRIS, and PE. Shaded marks reflect the expansion and contraction of the first cycle of dilatometry

The results show a reproducibility of the volume expansion/contraction upon the thermal cycling, despite the first cycle which is discarded for all the measurements. The sample preparation can be responsible of this result. As pointed out in Section 2.6, the samples finely hand grinded were compacted in a pellet die using 5 tons of pressure. This means that in the first cycles the sample is not only expanding and contracting due to the

solid-solid transition, but also there is a consolidation of the pellet upon the consecutive cycles in which the pellets have reached the equilibrium in form and the expansions and contractions are going to be symmetrical. Nonetheless, despite of being reproducible, the cycling is not symmetrical. During the phase transition from the crystalline to the plastic phase an expansion of all the samples can be observed (shaded marks in each PC), due to the transition to a less dense crystal lattice with consequent increasing of the distance between the molecules. Upon cooling, the sample does not return to the initial length. This phenomenon is clearly shown in the shadow marks in Figure 3.9, where the sample does not recover the initial length upon cycling showing that a plastic deformation occurred. As collected in Table 3.11, the ΔV of the phase transition upon heating is always higher than upon cooling.

Analyzing the total volumetric change in Table 3.11, the volume variations for NPG and PG are bigger upon heating than upon cooling. This larger volumetric change upon heating is expected, because the volume difference during the transition is also higher. However, the behavior is exactly the opposite for TRIS and PE: the material shrinks upon thermal cycling. This fact can be due to the subcooling phenomenon commented in Section 3.1. Whereas for NPG and PG the volume changes as a function of the temperature in the plastic phases are higher than for the crystalline phases, likely due to a high molecular motion in the former phase, the large subcooling in TRIS added to the fact just explained, promotes a bigger thermal contraction during the plastic phase upon cooling than the thermal expansion upon heating, contributing to a total shrinking of the material. The ranges of temperatures studied for each sample as well as the densities from which all this data are obtained are summarized in Table A.1.7 in the Annex A.1.

In any case, the results of Figure 3.9 must be analyzed carefully. Apparently, we are in front of an “infinite” elongation for NPG and PG and an “infinite” contraction for TRIS and PE. However, 10 additional cycles of expansion/contraction were applied to PG, (Figure 3.10) demonstrating how a stabilization of the elongation of the sample after the fifth cycle occurs. As beforehand explained, this behavior is likely due to the consolidation of the compacted pellet upon thermal cycling, so that it is expected to also occur also in the rest of PCs since all of them were prepared following the same protocol.

Table 3.11. Thermal volumetric expansion (%) of the plastic crystals upon heating and cooling of both solid phases and during the solid-solid transition.

		ΔV (%)			
Dynamic ramp	Phase	NPG	PG	TRIS	PE
Heating	Crystalline	0.19	0.16	0.57	0.91
	Transition	5.8	7.68	4.96	9.11
	Plastic	0.76	2.32	0.01	0.30
	Total	**6.75**	**10.16**	**5.54**	**10.32**
Cooling	Crystalline	0.04	0.13	0.46	1.27
	Transition	2.16	1.52	1.57	8.86
	Plastic	2.55	3.58	4.61	1.91
	Total	**4.75**	**5.23**	**6.64**	**12.04**

n.d.: not determined

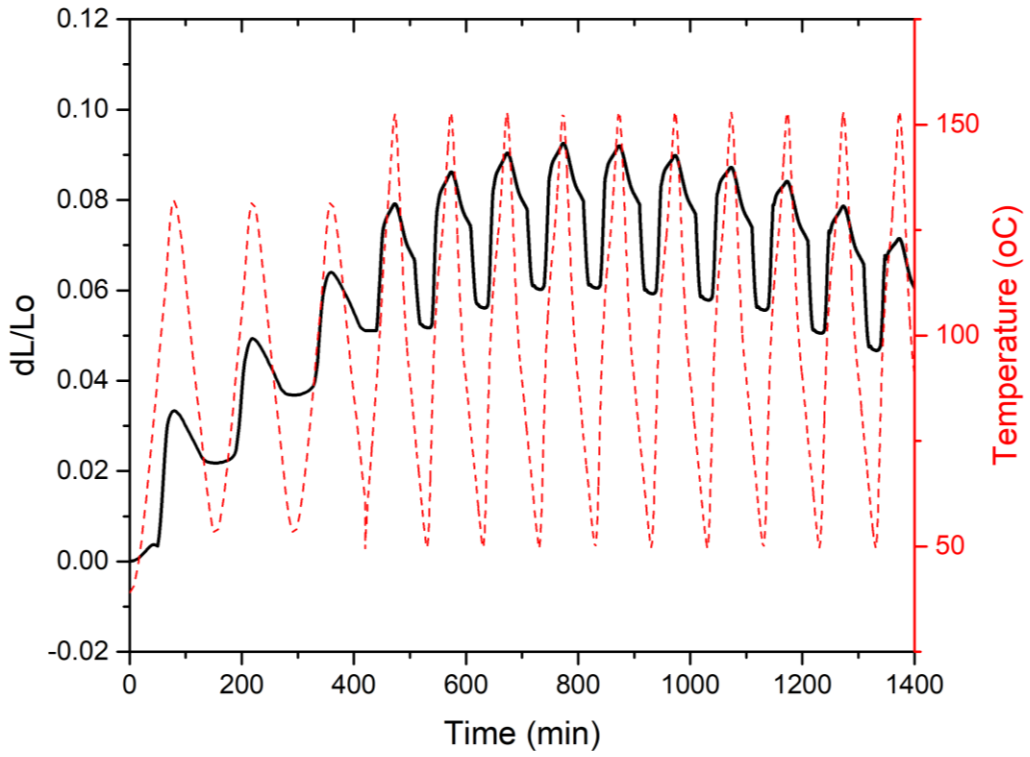

Figure 3.10. Expansion/contraction profile of PG upon 13 cycles of dilatometry around the solid-solid phase transition.

Apart from the behavior found in the first cycles of thermal expansion/contraction, the velocity of both volume changes is not the same. Regarding the shaded marks on Figure 3.9,

which highlights the start and the final point of the expansion, the expansion is slower than the contraction covering a wider range of temperatures. This behavior is confirmed by calculating the coefficient of linear expansion (α), defined as the volume change as a function of the temperature (Table 3.12). The higher velocity of the plastic-crystalline transition is probably another consequence of the subcooling phenomenon, due to the high degree of metastability of the materials so far from equilibrium conditions. Therefore, as shown in Table 3.12, whereas the calculated α coefficients are similar for the crystalline and plastic phases, the α coefficients during the phase transitions show more different values among the different PCs, especially higher for the plastic-crystalline transition.

Table 3.12. Linear thermal expansion coefficient (α) of the plastic crystals upon heating and cooling of both solid phases and during the transition between them.

		$\alpha \cdot 10^4$ (ºC^{-1})			
Dynamic ramp	Phase	NPG	PG	TRIS	PE
Heating	Crystalline	1.30	0.51	0.66	0.64
	Transition	1.77	33.36	17.79	24.75
	Plastic	1.31	5.33	0.26	3.96
Cooling	Crystalline	0.90	1.33	1.27	1.08
	Transition	50.96	6.31	56.01	41.87
	Plastic	5.65	5.23	5.54	4.04

3.3. Concluding remarks.

Subcooling phenomenon is present in all the solid-solid transitions of plastic crystals, and it is even more pronounced for the aminoalcohols AMP and TRIS. This thermal hysteresis is not affected by the heating and cooling rates, as well as by different sample masses. Moreover, cycling the sample up to 50 times, the temperatures and enthalpies remain constant, so the materials show a good preliminary thermal stability.

The solid-solid transitions of plastic crystals are energetic, more than 100 J/g in all the cases and up to 290 J/g for TRIS. Due to the subcooling phenomenon, the transitions from the plastic to the crystalline phase usually occur faster than that from the crystalline to the plastic phase, because of being so far from the equilibrium temperature of the transition. The

specific heats of the plastic phases are higher than those of the crystalline phases and, in general, both are unusually high compared to other organic compounds.

Thermal conductivities are in the order of other organic compounds, as well as the densities. Such parameters are lower for the plastic phase than for the crystalline phase, which is a logical trend considering the packaging of the molecules within the different crystal lattices. In addition, the volume changes of the materials during the transitions are in all the cases lower than 10%.

Some characteristics of the plastic crystals such as the transition temperatures, melting points, enthalpies, degradation temperatures and densities follow a nice trend regarding the number of functional groups with hydroxyl and amine groups: the higher the number of groups able to form hydrogen bonds, the higher the values of the parameters abovementioned. Moreover, all the studied parameters are in good agreement with the already reported in literature. However, there is missing information of some properties of plastic crystals, such the transition upon cooling of these materials and hence the subcooling degree. This is true especially for AMP and TRIS, but this lack of information has been covered in this chapter.

References in Chapter 3

[1] D. V Hale, M.J. Hoover, M.J. Oneill, Phase change materials handbook, 1971.

[2] D. Benson, J. Webb, R. Burrows, J. McFadden, C. Christensen, Materials research for passive solar systems: Solid-state phase-change materials, NASA STI/Recon Tech. Rep. N. (1985). https://doi.org/10.2172/5923397.

[3] E. Murrill, L. Breed, Solid-solid phase transitions determined by differential scanning calorimetry. Part I. Tetrahedral substances, Thermochim. Acta. 1 (1970) 239–246. https://doi.org/10.1016/0040-6031(70)80027-2.

[4] J. Salud, D.O. López, M. Barrio, J.L. Tamarit, Two-component systems of isomorphous orientationally disordered crystals. Part 1: Packing of the mixed crystals, J. Mater. Chem. 9 (1999) 909–916. https://doi.org/10.1039/a808258h.

[5] D. Chandra, H. Mandalia, W.-M. Chien, D.W. Lindle, R. Rudman, Solid-solid phase transition in trimethylolpropane (TRMP), (2002).

[6] G.R. Saad, A.A. Mansour, A.H. Hamed, Dielectric investigation of cold crystallization of poly(3-hydroxybutyrate), Polymer (Guildf). 38 (1997) 4091–4096. https://doi.org/10.1016/S0032-3861(96)00979-2.

[7] M. Tanaka, T. Motomura, N. Ishii, K. Shimura, M. Onishi, A. Mochizuki, T. Hatakeyama, Cold crystallization of water in hydrated poly(2-methoxyethyl acrylate) (PMEA), Polym. Int. 49 (2000) 1709–1713. https://doi.org/10.1002/1097-0126(200012)49:12<1709::AID-PI601>3.0.CO;2-L.

[8] D. Chandra, R. Chellappa, W.M. Chien, Thermodynamic assessment of binary solid-state thermal storage materials, J. Phys. Chem. Solids. 66 (2005) 235–240. https://doi.org/10.1016/j.jpcs.2004.08.047.

[9] M. Barrio, J. Font, D.O. López, J. Muntasell, J.L. Tamarit, N.B. Chanh, Y. Haget, M. Teisseire, J. Guion, X. Alcobé, Binary system neopentylglycol/pentaerythritol, J. Chim. Phys. 89 (1992) 695–705. https://doi.org/10.1051/jcp/1992890695.

[10] B. Li, Y. Kawakita, S. Ohira-Kawamura, T. Sugahara, H. Wang, J. Wang, Y. Chen, S.I. Kawaguchi, S. Kawaguchi, K. Ohara, K. Li, D. Yu, R. Mole, T. Hattori, T. Kikuchi, S. ichiro Yano, Z. Zhang, Z. Zhang, W. Ren, S. Lin, O. Sakata, K. Nakajima, Z. Zhang, Colossal barocaloric effects in plastic crystals, Nature. 567 (2019) 506–510. https://doi.org/10.1038/s41586-019-1042-5.

[11] X. Wang, E. Lu, W. Lin, C. Wang, Micromechanism of heat storage in a binary system of two

kinds of polyalcohols as a solid-solid phase change material, Energy Convers. Manag. 41 (2000) 135–144. https://doi.org/10.1016/S0196-8904(99)00096-5.

[12] A. Serrano, M. Duran, J.-L. Dauvergne, S. Doppiu, E.P. Del Barrio, Tailored transition temperature plastic crystals with enhanced thermal energy storage capacity, Sol. Energy Mater. Sol. Cells. 220 (2021) 110848. https://doi.org/https://doi.org/10.1016/j.solmat.2020.110848.

[13] R. Shi, D. Chandra, A. Mishra, A. Talekar, M. Tirumala, D.J. Nelson, Thermodynamic reassessment of the novel solid-state thermal energy storage materials: Ternary polyalcohol and amine system pentaglycerine-tris(hydroxymethyl)-amino-methane-neopentylglycol (PG-TRIS-NPG), Calphad Comput. Coupling Phase Diagrams Thermochem. 59 (2017) 61–75. https://doi.org/10.1016/j.calphad.2017.08.003.

[14] D. Lilley, J. Lau, C. Dames, S. Kaur, R. Prasher, Impact of size and thermal gradient on supercooling of phase change materials for thermal energy storage, Appl. Energy. 290 (2021) 116635. https://doi.org/https://doi.org/10.1016/j.apenergy.2021.116635.

[15] E. Murrill, L. Breed, Solid—solid phase transitions determination by differential scanning calorimetryPart II. Octahedral substances, Thermochim. Acta - THERMOCHIM ACTA. 1 (1970) 409–414. https://doi.org/10.1016/0040-6031(70)80022-3.

[16] R. Gotoh, T. Totani, M. Wakita, H. Nagata, Controlling heat release of crystallization from supercooling state of a solid-solid PCM, 2-amino-2-methyl-1,3-propanediol, Int. J. Heat Mass Transf. 137 (2019) 1132–1140. https://doi.org/10.1016/j.ijheatmasstransfer.2019.03.151.

[17] P. Mekala, V. Kamisetty, W.-M. Chien, R. Shi, D. Chandra, J. Sangwai, A. Talekar, A. Mishra, Thermodynamic modeling of binary phase diagram of 2-amino-2-methyl-1, 3-propanediol and TRIS(hydroxymethyl)aminomethane system with experimental verification, Calphad. 50 (2015). https://doi.org/10.1016/j.calphad.2015.05.003.

[18] Z.Y. Zhang, M.L. Yang, Heat capacity and phase transition of 2-amino-2-methyl-1,3-propanediol from 280 K to the melting point, Thermochim. Acta. 169 (1990) 263–269. https://doi.org/10.1016/0040-6031(90)80153-P.

[19] R. Shi, D. Chandra, A. Mishra, A. Talekar, M. Tirumala, D.J. Nelson, Thermodynamic reassessment of the novel solid-state thermal energy storage materials: Ternary polyalcohol and amine system pentaglycerine-tris(hydroxymethyl)-amino-methane-neopentylglycol (PG-TRIS-NPG), Calphad Comput. Coupling Phase Diagrams Thermochem. 59 (2017) 61–75. https://doi.org/10.1016/j.calphad.2017.08.003.

[20] A. Aznar, P. Lloveras, M. Barrio, P. Negrier, A. Planes, L. Mañosa, N.D. Mathur, X. Moya, J.L. Tamarit, Reversible and irreversible colossal barocaloric effects in plastic crystals, J. Mater.

Chem. A. 8 (2020) 639–647. https://doi.org/10.1039/c9ta10947a.

[21] J. Salud, D.O. López, M. Barrio, J.L. Tamarit, H.A.J. Oonk, P. Negrier, Y. Haget, On the Crystallography and Thermodynamics in Orientationally Disordered Phases in Two-Component Systems, J. Solid State Chem. 133 (1997) 536–544. https://doi.org/10.1006/jssc.1997.7530.

[22] N. Zhang, Y. Song, Y. Du, Y. Yuan, G. Xiao, Y. Gui, A Novel Solid–Solid Phase Change Material: Pentaglycerine/Expanded Graphite Composite PCMs, Adv. Eng. Mater. 20 (2018) 1800237. https://doi.org/https://doi.org/10.1002/adem.201800237.

[23] N. Zhang, Y. Jing, Y. Song, Y. Du, Y. Yuan, Thermal properties and crystallization kinetics of pentaglycerine/graphene nanoplatelets composite phase change material for thermal energy storage, Int. J. Energy Res. 44 (2020) 448–459. https://doi.org/https://doi.org/10.1002/er.4946.

[24] M. Zhai, S. Zhang, J. Sui, F. Tian, X.Z. Lan, Solid–solid phase transition of tris(hydroxymethyl)aminomethane in nanopores of silica gel and porous glass for thermal energy storage, J. Therm. Anal. Calorim. 129 (2017) 957–964. https://doi.org/10.1007/s10973-017-6223-6.

[25] N. Doshi, M. Furman, R. Rudman, The formation of the plastic crystal phase in several pentaerythritol derivatives, Acta Crystallogr. Sect. B Struct. Crystallogr. Cryst. Chem. 29 (1973) 143–144. https://doi.org/10.1107/s0567740873002104.

[26] P. Hu, P.P. Zhao, Y. Jin, Z.S. Chen, Experimental study on solid-solid phase change properties of pentaerythritol (PE)/nano-AlN composite for thermal storage, Sol. Energy. 102 (2014) 91–97. https://doi.org/10.1016/j.solener.2014.01.018.

[27] D. Chandra, W.M. Chien, V. Gandikotta, D.W. Lindle, Heat Capacities of “Plastic Crystal” Solid State Thermal Energy Storage Materials, Zeitschrift Fur Phys. Chemie. 216 (2002) 1433. https://doi.org/10.1524/zpch.2002.216.12.1433.

[28] D. Mani, M.K. Saranprabhu, K.S. Rajan, Intensification of thermal energy storage using copper-pentaerythritol nanocomposites for renewable energy utilization, Renew. Energy. 163 (2021) 625–634. https://doi.org/10.1016/j.renene.2020.08.119.

[29] J. Font, J. Muntasell, Comparative study on solid crystalline-plastic-vapour equilibrium in plastic crystals from pentaerythritol series, J. Mater. Chem. 5 (1995) 1137–1140. https://doi.org/10.1039/JM9950501137.

[30] D.K. Benson, R.W. Burrows, J.D. Webb, Solid state phase transitions in pentaerythritol and related polyhydric alcohols, Sol. Energy Mater. 13 (1986) 133–152. https://doi.org/10.1016/0165-1633(86)90040-7.

[31] P. Lloveras, A. Aznar, M. Barrio, P. Negrier, C. Popescu, A. Planes, L. Mañosa, E. Stern-Taulats, A. Avramenko, N.D. Mathur, X. Moya, J.L. Tamarit, Colossal barocaloric effects near room temperature in plastic crystals of neopentylglycol, Nat. Commun. 10 (2019) 1–7. https://doi.org/10.1038/s41467-019-09730-9.

[32] K.P. Venkitaraj, S. Suresh, Effects of Al2O3, CuO and TiO2 nanoparticles son thermal, phase transition and crystallization properties of solid-solid phase change material, Mech. Mater. 128 (2019) 64–88. https://doi.org/10.1016/j.mechmat.2018.10.004.

[33] M.M. Kenisarin, Thermophysical properties of some organic phase change materials for latent heat storage. A review, Sol. Energy. 107 (2014) 553–575. https://doi.org/10.1016/j.solener.2014.05.001.

[34] Ü. Bayram, S. Aksöz, N. Maraşlı, Temperature dependency of thermal conductivity of solid phases for fatty acids: Lauric acid, myristic acid, pivalic acid and stearic acid, J. Therm. Anal. Calorim. 118 (2014) 311–321. https://doi.org/10.1007/s10973-014-3968-z.

[35] E.P. del Barrio, A. Godin, M. Duquesne, J. Daranlot, J. Jolly, W. Alshaer, T. Kouadio, A. Sommier, Characterization of different sugar alcohols as phase change materials for thermal energy storage applications, Sol. Energy Mater. Sol. Cells. 159 (2017) 560–569. https://doi.org/https://doi.org/10.1016/j.solmat.2016.10.009.

[36] D.K. Benson, C. Christensen, Solid state phase change materials for thermal energy storage in passive solar heated buildings, United States, 1983. https://www.osti.gov/biblio/6378193.

[37] Z.-Y. Zhang, Y.-P. Xu, Measurement of the thermal conductivities of 2-amino-2-methyl-1,3-propanediol (AMP), 2-amino-2-hydroxymethyl-1,3-propanediol (TRIS) and the mixture (AMP+TRIS, mole ratio 50:50) in the temperature range from 20°C to their supermelting temperatures, Sol. Energy. 71 (2001) 299–303. https://doi.org/https://doi.org/10.1016/S0038-092X(01)00057-3.

[38] S. Akbulut, Y. Ocak, K. Keşlioğlu, N. Maraşlı, Thermal conductivities of solid and liquid phases for neopentylglycol, aminomethylpropanediol and their binary alloy, J. Phys. Chem. Solids. 70 (2009) 72–78. https://doi.org/10.1016/j.jpcs.2008.09.001.

[39] C.-B. Wu, G. Wu, X. Yang, Y.-J. Liu, T. Liang, W.-F. Fu, M. Wang, H.-Z. Chen, Preparation of microencapsulated medium temperature phase change material of Tris(hydroxymethyl)methyl aminomethane@SiO2 with excellent cycling performance, Appl. Energy. 154 (2015). https://doi.org/10.1016/j.apenergy.2015.05.029.

[40] Y. Xia, F. Jin, Z. Mao, Y. Guan, A. Zheng, Effects of Ammonium Polyphosphate to Pentaerythritol Ratio on Composition and Properties of Carbonaceous Foam deriving from Intumescent Flame-retardant Polypropylene, Polym. Degrad. Stab. 107 (2014).

https://doi.org/10.1016/j.polymdegradstab.2014.04.016.

[41] N. Ukrainczyk, S. Kurajica, J. Sipusic, Thermophysical Comparison of Five Commercial Paraffin Waxes as Latent Heat Storage Materials, Chem. Biochem. Eng. Q. 24 (2010). https://doi.org/10.15255/CABEQ.2014.240.

[42] K. Pielichowska, K. Pielichowski, Phase change materials for thermal energy storage, Prog. Mater. Sci. 65 (2014) 67–123. https://doi.org/10.1016/j.pmatsci.2014.03.005.

[43] E.P. del Barrio, A. Godin, M. Duquesne, J. Daranlot, J. Jolly, W. Alshaer, T. Kouadio, A. Sommier, Characterization of different sugar alcohols as phase change materials for thermal energy storage applications, Sol. Energy Mater. Sol. Cells. 159 (2017) 560–569. https://doi.org/10.1016/j.solmat.2016.10.009.

[44] D. Chandra, C.S. Day, C.S. Barrett, Low- and high-temperature structures of neopentylglycol plastic crystal, Powder Diffr. 8 (1993) 109–117. https://doi.org/10.1017/S0885715600017930.

[45] H. Rose, A. Camp, Crystallographic Data. 139. 2Amino2-methyl-1,3-propanediol, Anal. Chem. - ANAL CHEM. 28 (1956) 1790–1791. https://doi.org/10.1021/ac60119a048.

[46] D. Johnson, J. Ervin, M. Hanchak, S. Patnaik, X. Hu, Graphite Foam Infused with Pentaglycerine for Solid-State Thermal Energy Storage, J. Thermophys. Heat Transf. 29 (2015) 55–64. https://doi.org/10.2514/1.T4484.

[47] E. Kendi, Q.H. Abstract, Â. Pna, Molecular and crystal structure of tris (hydroxymethyl) aminomethane, 3 (1982). https://doi.org/10.1524/zkri.1982.160.14.139.

[48] V. Zhurov, E. Zhurova, Y.-S. Chen, A. Pinkerton, Accurate charge density data collection in under a day with a home X-ray source, J. Appl. Crystallogr. - J APPL CRYST. 38 (2005) 827–829. https://doi.org/10.1107/S002188980501856X.

[49] M. Duquesne, C. Mailhé, S. Doppiu, J.-L. Dauvergne, S. Santos Moreno, A. Godin, G. Fleury, F. Rouault, E. Palomo del Barrio, Characterization of Fatty Acids as Biobased Organic Materials for Latent Heat Storage, Materials (Basel). 14 (2021) 4707. https://doi.org/10.3390/ma14164707.

Chapter 4

Understanding of subcooling

4.1. Antecedents.

As explained in Chapter 1, subcooling in solid-solid transitions is a kinetic phenomenon whose cause still remains unknown because a direct extrapolation to the mechanism of solid-liquid transitions is not realistic since there is no liquid phase involved, and hence there is not a nucleation-based mechanism. Therefore, the first aim was to obtain as much information as possible regarding the molecular mechanism involved in the phase transition. To this end, a deep study of the phase transitions both upon heating and cooling was carried out using two different spectroscopic techniques: infrared and nuclear magnetic resonance spectroscopies.

There are already several studies about the molecular motion of the PCs during the solid-solid phase transition giving hints about the mechanism that plastic crystals undergo during the transition. The plastic phase of these neopentane derivatives is a solid phase where the molecules are arranged in a highly symmetrical way, but with a high degree of rotational freedom of the intermolecular bonds. This degree of disorder is hence related to the huge

number of possible conformations that the molecules can adopt within the lattice with no translational motion [1]. As a consequence, entropy differences become an important parameter to consider. Rao et al. found that both enthalpy and entropy of the solid-solid transition are higher when the stability of the plastic phase is lower [2]. For stability, they mean the range of temperatures in which the plastic phase is stable, i.e., between the solid-solid and solid-liquid transition temperatures. This finding fits quite well with the experimental data of the PCs under study; NPG, AMP, PG, TRIS and PE. AMP and TRIS show solid-solid transitions that are more energetic than the expected trend depicted in Figure 3.5 in Chapter 3. BCC lattices are the plastic phases with the lowest stability compared to all the studied PCs since the ranges of temperatures in which they are present are the narrowest (around 30 ºC between the crystalline and the liquid phase). Therefore, this means that the plastic phase in these cases is more similar to the liquid phase than for the other PCs, and that this disorder/instability can difficult the reorganization for the transition to the crystalline phase, leading to a substantial subcooling [2,3]. This hypothesis was also checked by the melting points, since they will be lower for AMP and TRIS since the BCC phase is more similar to the molten state. In fact, a melting enthalpy of 26 J/g for AMP and TRIS compared to a value of 40 J/g for NPG, PG and PE confirm this theory.

Since the PCs subject of this thesis are mainly characterized by strong hydrogen bond networks, some techniques can be more adequate than others for their study. In literature, there are few studies about the dynamics of hydrogen bonds in organic alcohols using techniques as, for example, the Infrared Spectroscopy [4]. The crystalline phases of PG and PE have been analysed in order to check the hydrogen bond structure through the differences in the O-H stretching vibration, demonstrating the existence of a strong hydrogen bond network both in PG and PE [5,6]. Moreover, temperature-variable IR spectroscopy of PE has been already carried out around the solid-solid transition [7]. The IR spectra of both crystalline and plastic phases show similar curves, as depicted in Figure 4.1, so no new chemical bonds are formed during the solid-solid phase transition. At room temperature, the strongest peak around 3367 cm^{-1} is assigned to the O-H stretching vibrations, ranging from 3000 cm^{-1} to 3700 cm-1. After the solid-solid phase transition, this peak is narrowed indicating that many hydrogen bonds have been destroyed, and the remaining are weaker than in the crystalline phase. Moreover, the spectra at the same temperature upon heating and upon cooling are not the same, this is, the signal upon heating is more intense than that upon cooling. This result indicates that the broken hydrogen bonds in the tetragonal-FCC transition cannot be fully recovered during the FCC-tetragonal transition upon the cooling process. In addition,

there are not meaningful differences regarding the peaks at 2955 cm^{-1} and 2886 cm^{-1} due to the vibrations of the methylene group during the phase transition, so it seems that the destruction and weakening of hydrogen bonds are the major structural change in these materials.

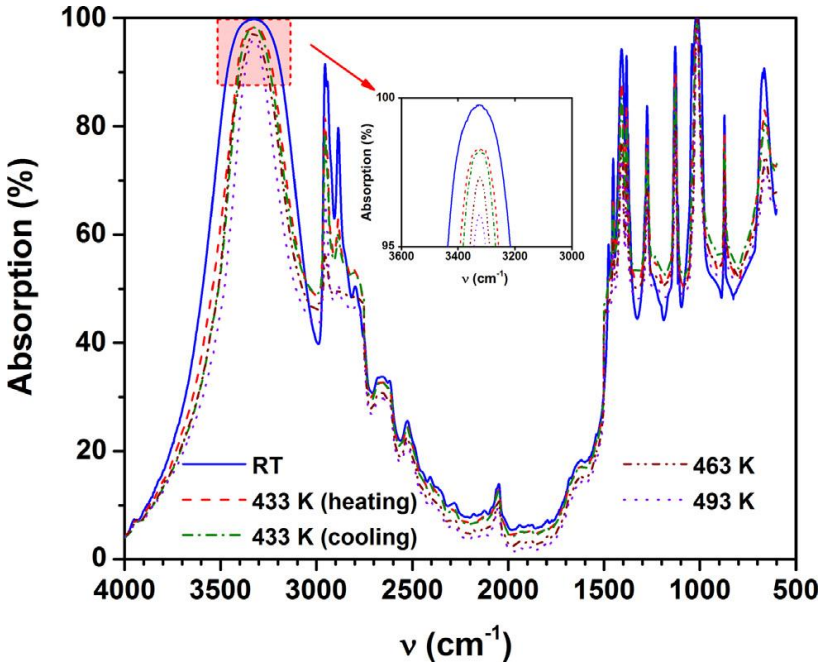

Figure 4.1. Absorption IR spectra of crystalline and plastic phases of PE upon heating and cooling. Adapted from ref. [7].

Another powerful spectroscopic technique to study these materials is the Nuclear Magnetic Resonance (NMR). In this case, recording the ^{1}H spectra allow to follow the motion of such atoms involved in the hydrogen bond network during the phase transition and, due to its sensitivity to local environment changes, it allows to obtain information about dynamics and coordination on molecules. Some research groups already implemented this technique for the study of hydrogen bond networks inside solid systems, such as geometries [8], kinetics [9,10] and proton transfer mechanisms [11,12]. Actually, there are already some scientific reports in which polymorphic transformations in PCs are studied [13]. Wilmet et al. used the NMR at different temperatures to study different solid-solid transitions in Plastic Crystals such as NPG and PG, hence allowing to determine structural differences between the crystalline and the plastic phases [14]. For both NPG and PG, the linewidths of the ^{13}C resonance signals abruptly narrow at the transition from the crystalline to the plastic phase, indicating the rapid inner molecular motion which averages the local magnetic interactions and hence promotes

a narrow signal similar to the liquid phase or even similar to solutions. In particular, the biggest change during the phase transition seems to occur in the hydroxymethyl groups that contribute to the hydrogen bond network of both crystalline and plastic phase (Figure 4.2). Moreover the signals corresponding to these groups are the first to narrow showing that the transition begins with the hydrogen bonds breaking [14]. Further studies on NPG and PG were carried out by measuring relaxation times T_1 of ^{13}C nuclei, obtaining similar conclusions: $-CH_2OH$ groups are the most rigid part in the crystalline phase since its relaxation times T_1 are bigger that those of the other ^{13}C atoms. Moreover, the activation energies are more important in the plastic phase due to the high reorientation speed, and also show the stronger effect of intermolecular hydrogen bonds in the case of PG compared to NPG [15]. However, these studies were more focused on the formation of blends between NPG and PG, not taking into account the behavior upon the cooling step of the pure compounds.

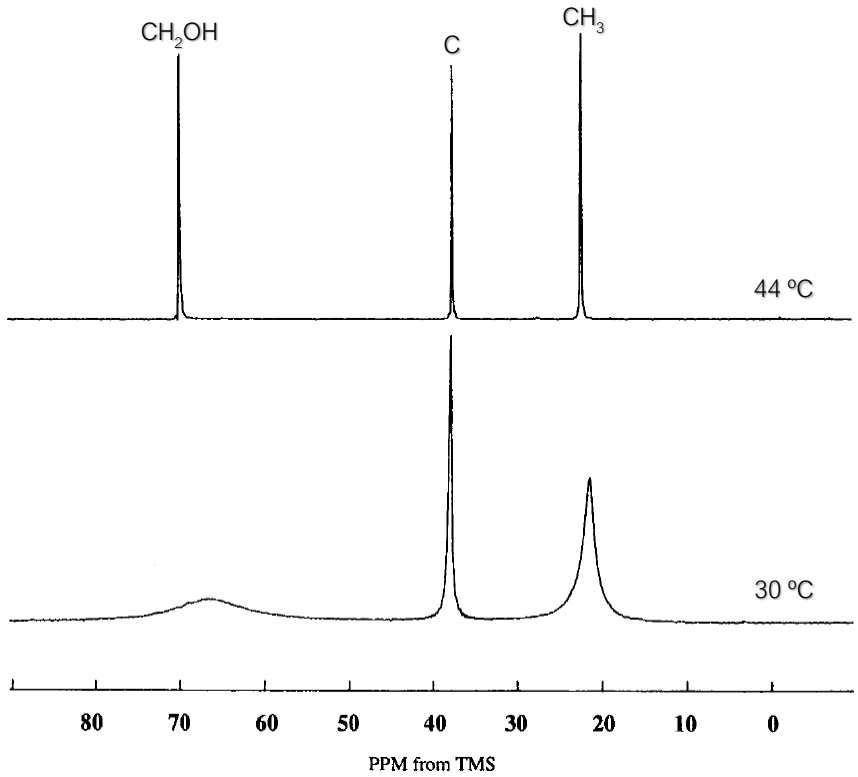

Figure 4.2. ^{13}C NMR spectra of the plastic phase at 44 ºC and crystalline phase at 30 ºC of NPG, adapted from ref. [14].

Therefore, in order to understand the subcooling in the solid-solid transitions of these PCs, the objective in this thesis was to perform a complete characterization of the solid-solid transition by using these two beforehand mentioned spectroscopic techniques, both upon

heating and cooling. Particular attention was paid to the plastic phase within the subcooling range in order to clarify the mechanism involved during the plastic-crystalline phase transition. To this end, temperature-driven IR spectroscopy was carried out in order to characterize the solid-solid phase transition and the main structural changes in the hydrogen bond network. This research was focused on NPG, PG and AMP, since the transition in TRIS and PE falls out the temperature range of the FTIR spectrometer. On the other hand, solid state NMR (ssNMR) is selected as the technique to understand the mechanism underlying the solid-solid phase transitions on PCs by a direct recording of the motion of hydrogen nuclei that are the involved entities on the formation and breaking of the different hydrogen bond networks. Therefore, this chapter focuses on the understanding of the subcooling phenomenon from the big scale of chemical bonds by FTIR spectroscopy (hydrogen bonds), to the small scale of atoms by ssNMR spectroscopy (hydrogen atoms).

4.2. Results and discussion.

Regarding FTIR measurements, a first characterization of the five PCs at room temperature was carried out. Figure 4.3 shows the absorbance spectra for the five PCs in the crystalline phase at room temperature. All PCs have two or more hydroxyl groups, even with amine groups in the case of AMP and TRIS, the huge signals at around 3000-3500 cm^{-1} are the results of the stretching vibration mode of both of O-H and N-H groups. In all the cases, the hydrogen bond network in the solid phases is confirmed by the broad and displaced to lower wavenumbers signal, hence confirming the weakening of the hydroxyl bond due to the hydrogen bond formation. For NPG, PG and PE, the signal is a typical symmetrical peak due to the distribution of the different hydrogen bonds inside the crystalline system. On the other hand, AMP and TRIS spectra show differentiated peaks in this zone of the spectrum, which are attributed to the N-H stretching vibrations. Moreover, and due to the presence of the amine groups, AMP and TRIS show a broader distribution of hydrogen bonds, with signals below 2800 cm^{-1} characteristic of the stretching vibrations of the methyl and methylene groups. The broad signal, covering the range from 2200 cm^{-1} to 2800 cm^{-1}, can be due to two possible hydrogen bond distributions: intramolecular hydrogen bonds between alcohol and amine groups, and/or certain ionic character from a protonated amine group due to the hydrogen bonds, so that it is possible to record the $-NH_2^+$ stretching vibration mode.

In case of AMP, only the structural transformation upon heating was studied due to the high subcooling taking into account the limitations of the FTIR spectrometer (see Figure

A.1.1 in Annex 1). The spectra at different temperatures show the disappearance of the broad signal located from 2200 cm^{-1} to 2800 cm^{-1} at higher temperatures. If it was due to certain ionic character promoted by the existence of NH_2^+ groups, this signal would be more intense since the protons would have a higher motion at higher temperatures. However, since the signal decreases at higher temperatures, this can be attributed to the breaking of the intramolecular hydrogen bonds upon heating. Another difference of the FTIR spectra of AMP and TRIS is the absorption peak at 1615 cm^{-1} and 1585 cm^{-1} for AMP and TRIS, respectively. This absorption is the result of the bending vibration of the -NH_2 group, widely known as the "scissor" movement. The remaining spectra is similar for the five PCs. The signals located between 1300-1500 cm^{-1} are the resulting absorption due to the bending vibration movements of the methyl and methylene groups, including the "scissor" vibration for the latter one. Moreover, it is possible to see the vibration modes of the C-O bond of the hydroxymethyl groups, usually centered at 1000 cm^{-1} and 650 cm^{-1} for the stretching and the bending vibrations, respectively.

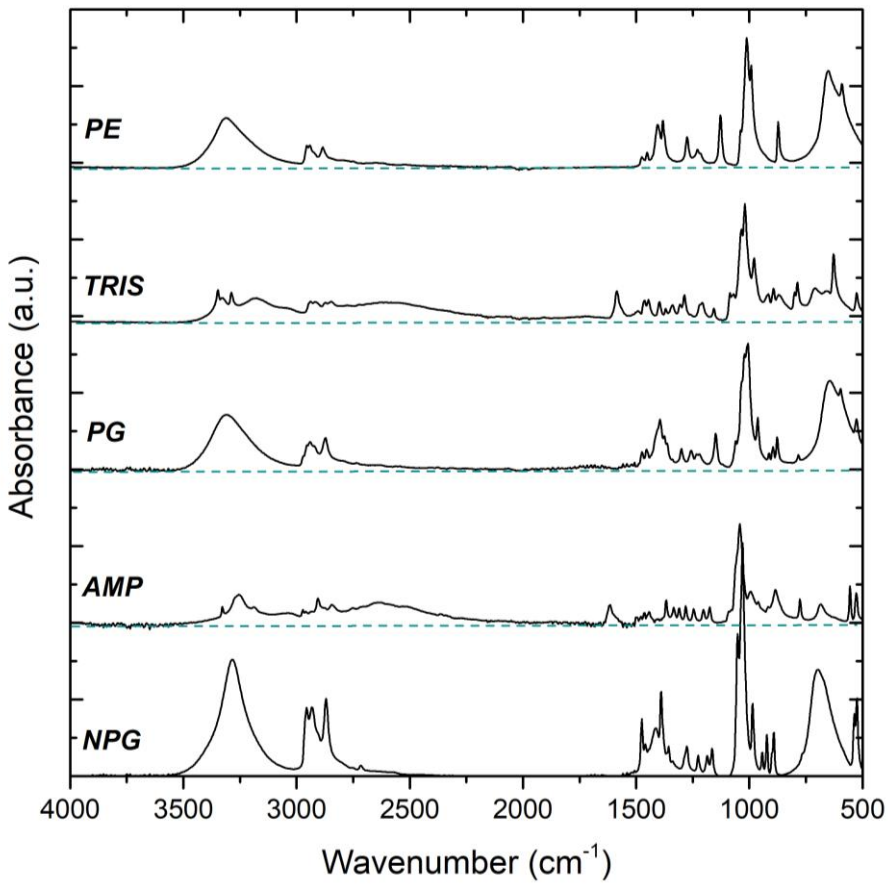

Figure 4.3. FTIR absorbance spectra of NPG, AMP, PG, TRIS and PE at room temperature.

Regarding NPG, a deeper study performed around the solid-solid transition at 40 ºC (Figure 4.4) shows that the higher is the temperature the less intense the signals are. This can be understood as a weakening of the hydroxyl bonds because of their increased motion. Moreover, there are some clear differences in the FTIR spectra before and after the solid-solid phase transition. This concerns the signals at around 3300 cm^{-1} and 700 cm^{-1} corresponding to the O-H stretching vibration and the C-O stretching vibration, respectively. These changes in the hydroxymethyl groups point out that the major difference between both solid phases is the distribution of the hydrogen bond network, so that only some hydrogen bonds are broken during the phase transition, and the remaining ones are weakened. This is also noticeable in the signals located in the 3100-3500 cm^{-1} range, which are displaced to higher wavenumbers due to the strengthening of the O-H bond. Figure 4.4b plots the shift in wavenumber of selected absorption FTIR peaks as a function of the temperature. The results show that the hydroxyl bonds are the first to suffer a substantial change in motion upon heating between 40 ºC and 42 ºC, followed by the methylene and the carboxy groups. This confirms that the transition starts with the breaking of some hydrogen bonds of the crystalline phase.

The behavior of the methyl and carboxy groups are totally reproducible upon cooling showing similar wavenumbers of the absorption peaks at certain temperatures. However, the changes in the hydroxyl and methylene groups show a slight hysteresis in temperatures, so that whereas the core of the molecule is the first part to lose the fast mobility typical of the plastic phase, the hydroxymethyl arms are still fast moving at temperatures between 40 and 42 ºC.

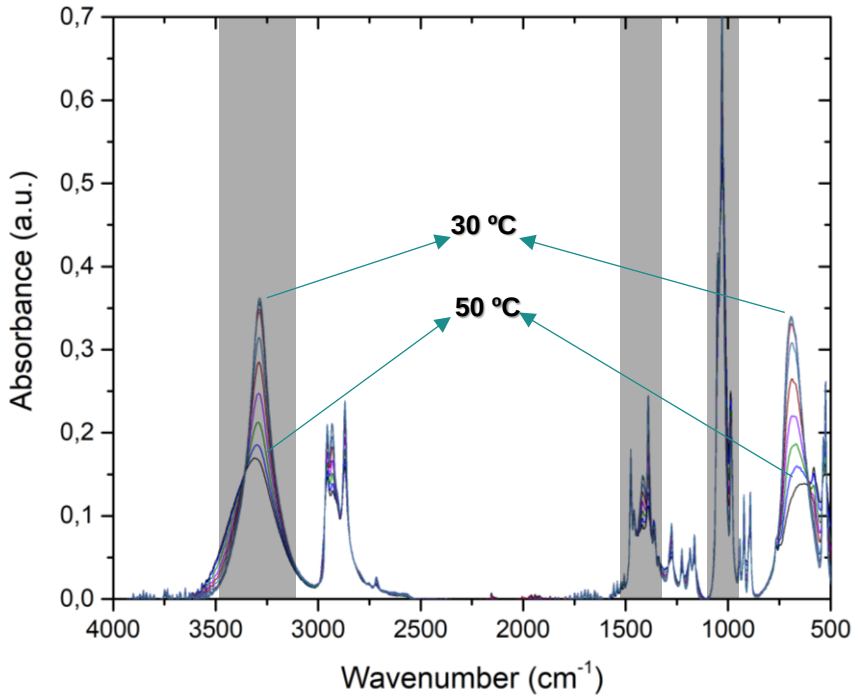

(a)

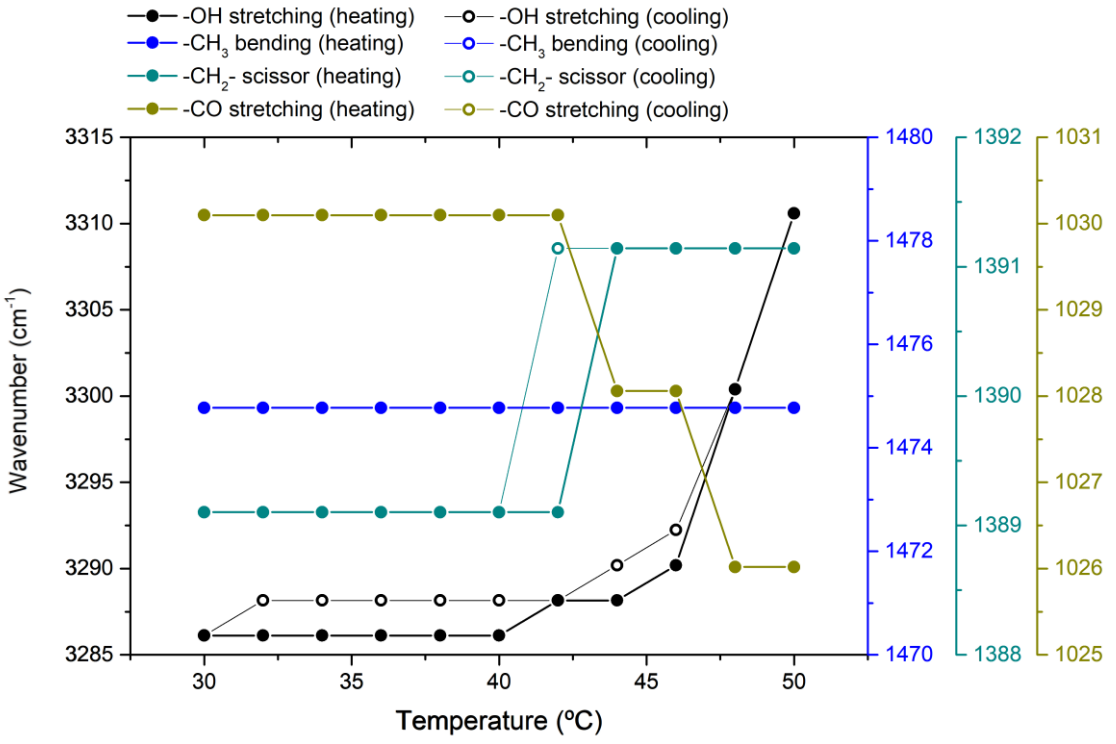

(b)

Figure 4.4. (a) FTIR absorbance spectra of NPG from 30 ºC to 50 ºC and (b) plots of the absorbance peaks as a function of temperature of the shadow regions of Figure 4.4a.

In the case of PG, the general behavior pointed out by FTIR spectroscopy is similar to that for NPG (Figure 4.5a): The O-H stretching band has lower intensity and it is displaced to higher wavenumbers in the tetragonal-FCC plastic phase due to the breaking of the hydrogen bonds and the weakening of the remaining ones. Moreover, as can be observed in the plot of Figure 4.5b, the changes of the O-H and the -CH_2 groups are more pronounced during the phase transition in comparison to those observed for NPG, confirming the biggest change in motion of the methylene groups of PG. Similar to NPG, the transition from the crystalline to the plastic phase starts in the hydroxyl groups since the O-H and the C-O bands are the first to change. In the solid-solid transition upon cooling, the fast motion of the hydroxyl groups characteristic of the plastic phase starts to decrease until ca. 80 ºC, in which this trend stops. From that moment, C-O bonds start the transition, and at a certain point, the hydroxyl groups come back to the typical distribution of the crystalline phase, at around 65 ºC. Therefore, it seems that for PG, there is a reorganization of the hydroxyl groups until the skeleton of PG (represented by the methylene and the carboxy groups) starts to stiff enabling the hydroxyl groups to reach the suitable configuration for the phase transition from the plastic to the crystalline phase.

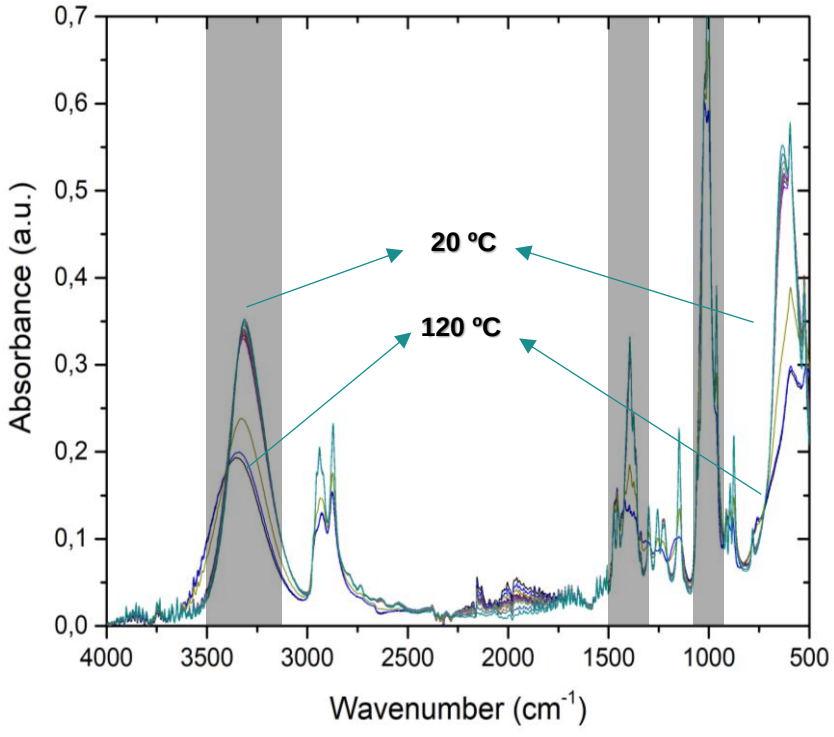

(a)

Figure 4.5. (a) FTIR absorbance spectra of PG from 20 ºC to 120 ºC and (b) plots of the absorbance peaks in function of temperature of the shadow regions of Figure 4.5a.

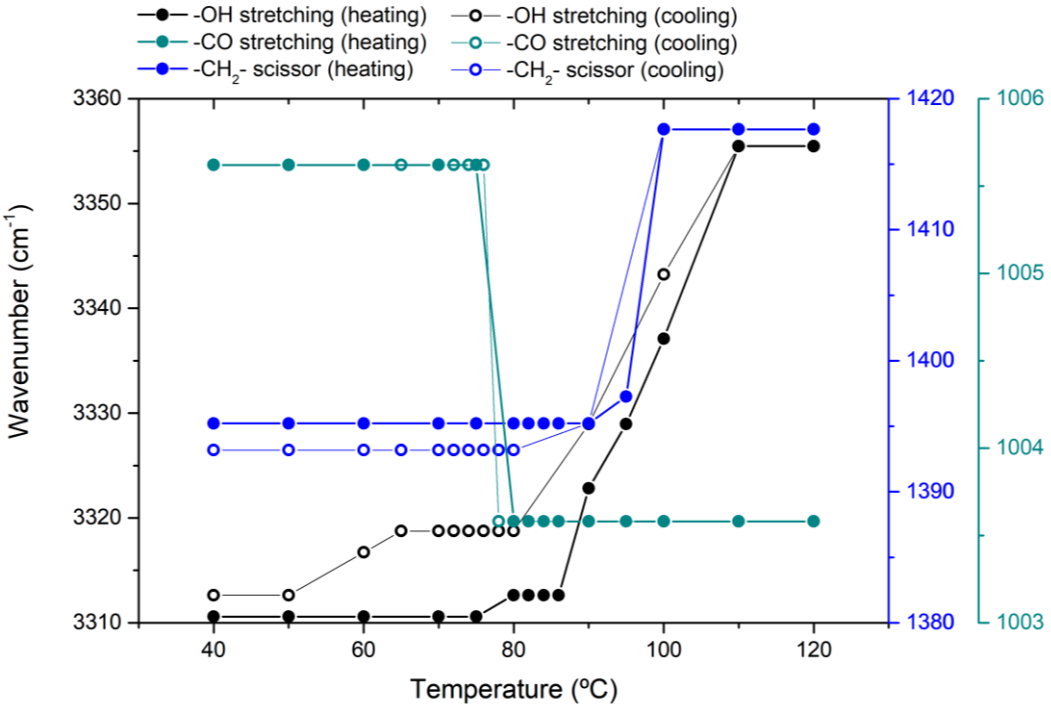

(b)

Figure 4.5. (Continued).

This study allowed to reach several interesting conclusions about the changes in the hydrogen bond structure of the PCs demonstrating, as expected, how the hydroxyl groups are the main responsible for the phase change. Summarizing, the phase transition from the crystalline to the plastic phase, upon heating, starts with the weakening and breaking of the hydrogen bonds, but upon cooling, the core of the molecule is the first part to stiff, and then the hydrogen bonds reorganize themselves once the molecule is quiet enough.

Against this background, and taking into account that ssNMR is a local technique, it is worth to track the behavior of the different atoms of the molecule during the phase transition and to analyze if it is affected by the near environment, in this case, by the hydrogen bond network. In other words, it is interesting to know how the motion of protons linked by hydrogen bonds evolves during the phase transition, and furthermore in the cooling step where the subcooling occurs. To this end, temperature-controlled NMR spectra were recorded around the solid-solid phase transition of NPG, PG, PE and TRIS in order to study the motion of the atoms and the reversibility of the phase transition. Again, AMP was not considered due to the lack of reversibility of the solid-solid phase transition within the range of temperatures afforded by the spectrometer.

A first ^{1}H spectra acquisition of NPG was carried out at two different temperatures, below and above the solid-solid phase transition at c.a. 40 ºC. Figure 4.6 shows the expected broad signal for the rigid crystalline phase in which the hydrogen bonds are fixed in determined positions leading to high anisotropic and orientation-dependent interactions as well as ^{1}H-^{1}H nuclear dipolar interactions. For the plastic phase, on the other hand, the ^{1}H spectrum is narrower than the corresponding to the crystalline phase, due to the time-averaging effect of the fast-tumbling motions and hence the anisotropic interactions.

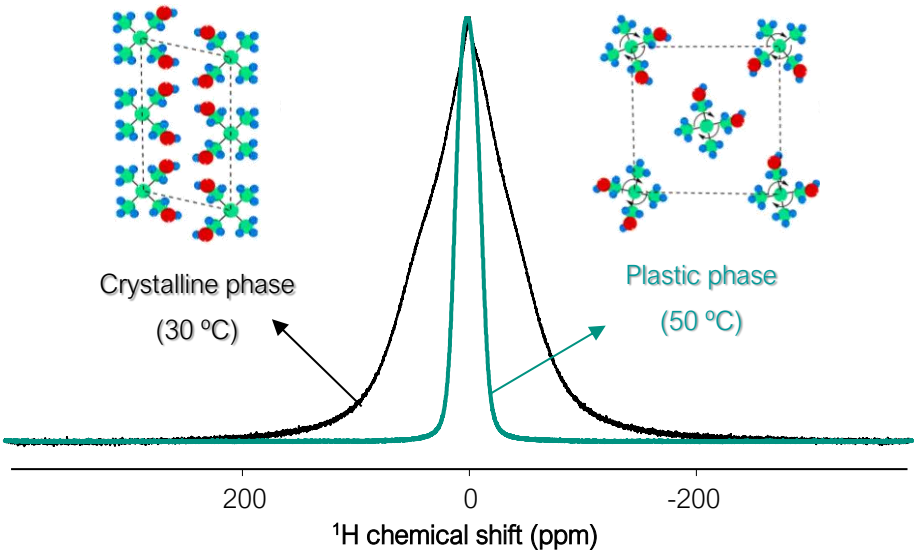

Figure 4.6. Comparison of ^{1}H NMR spectra of the crystalline and plastic phase of NPG at 30 ºC and 50 ºC, respectively.

The temperature-variable ^{1}H spectra of both crystalline and plastic phases of NPG are depicted in Figure 4.7. As expected, Figure 4.7a and Figure 4.7b show how the heating process led to a narrowing of the NPG signal independently on the structure of NPG. This behavior is expected due to the increase of the rotations or vibrations mode inside the crystal lattice at higher temperatures. On the contrary, upon cooling, the differences on linewidths in the subcooling range of temperatures (between c.a. 30 ºC and 40 ºC) are not so pronounced as in the rest of the cooling ramp (Figure 4.7c). This fact is in agreement with FTIR results: hydroxymethyl groups in the plastic phase start to lose the fast mobility until the subcooling range of temperatures. However, there are not more changes in motion until the molecule's skeleton is also stiffen.

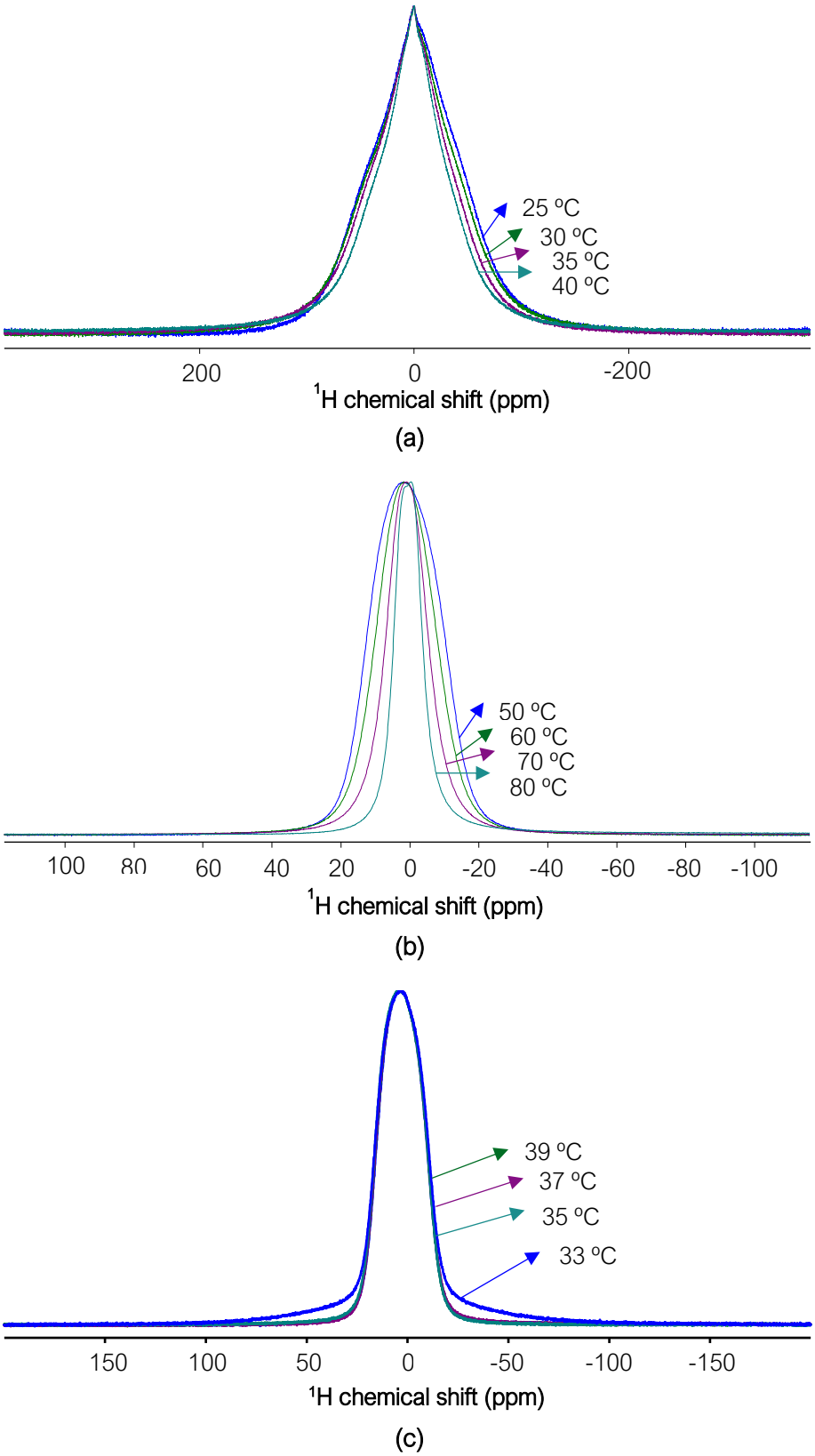

Figure 4.7. ^{1}H spectra at different temperatures of (a) the crystalline phase upon heating, (b) the plastic phase upon cooling and (c) the plastic phase upon cooling within the range of temperatures of subcooling.

For an easier understanding of the overall behavior of the solid-solid phase transition of NPG, Figure 4.8 shows the plot of the linewidths of the ^{1}H NMR spectra as a function of the temperature. As expected, the broad signals of the crystalline phase at low temperatures abruptly narrow upon heating at the phase change temperature, leading to thin signals characteristic of the plastic phase. This behavior is exactly the opposite upon cooling, but showing a thermal hysteresis between 33 ºC and 43 ºC. Therefore, it is possible to determine the temperatures of transition in 42 ºC for the monoclinic-FCC transition, and 33 ºC for the FCC-monoclinic one, which are in agreement with those found by DSC (Table 3.3).

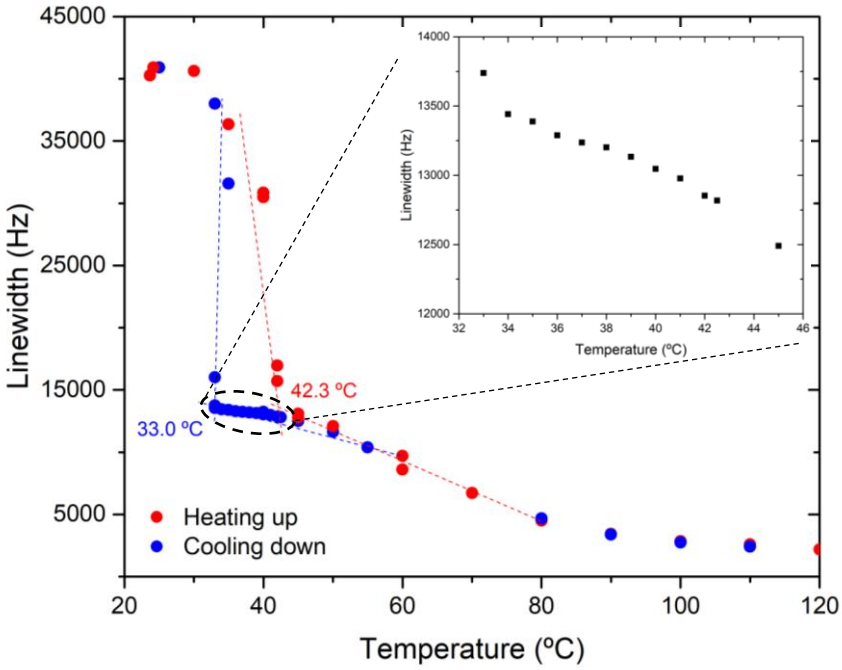

Figure 4.8. Plot of the linewidths of the ^{1}H spectra of NPG in function of temperature. The inset is a zoom of the region of temperatures at which subcooling occurs.

Another option to check the skeleton motion during the solid-solid phase transition is the acquisition of ^{13}C NMR. In Figure 4.9, the three non-equivalent carbon atoms (depicted as blue lines) in NPG can be well distinguished in the spectra of the plastic phase at 50 °C. The higher the chemical shift of a nucleus, the more deshielded it will be, i.e., it will be linked to a more electronegative atom; in this case, the oxygen of the hydroxyl group in the case of the nucleus resonating at 62.1 ppm. The quaternary carbon is the next one located at 32.4 ppm, and finally the methyl carbons are the ones resonating at 19.0 ppm. The linewidths of the three signals are similar, indicating that the motion of the carbon nuclei is also similar in the plastic phase. The crystalline phase (black line) is characterized by a broad signal (at 30

°C) covering the three carbon atoms in NPG. In this case, the signal corresponding to the quaternary and methyl carbon nuclei overlap. Therefore, these nuclei show the higher motion in the crystalline phase, whereas the hydroxymethyl carbon is firmly anchored to the hydrogen bond network and it gives a broad contribution to the NMR signal, making difficult to distinguish it from the baseline.

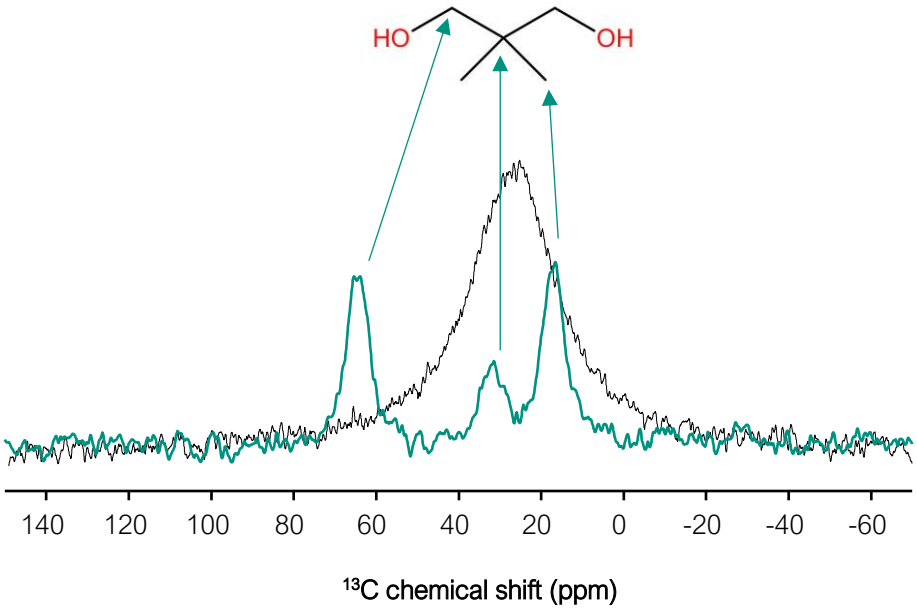

Figure 4.9. ^{13}C NMR spectra of the crystalline phase at 30 ºC (black line) and the plastic phase at 50 ºC (blue line) of NPG.

At this point, in order to clearly distinguish the behavior of the protons taking part in the hydrogen bonds network, a hydrogen/deuterium exchange of the hydroxylic positions was carried out. This treatment, explained in Chapter 2, allows to record both ^{1}H and ^{2}H spectra in order to check separately the behavior of the skeletal protons and the hydroxylic deuterium atoms, respectively. Figure 4.10 compares the ^{1}H spectra of NPG and NPG-d_2. In the crystalline phase (Figure 4.10a), the ^{1}H spectrum of NPG is broader than that of NPG-d_2. Therefore, taking into account that the only difference in the spectra is the presence of the hydroxyl group, it is clear that such groups are giving the broader signal, being the most rigid part in the crystalline phase of NPG. These results are in agreement with the results obtained from the ^{13}C NMR and FTIR measurements, also confirming the strong link of the hydrogen bond network. The ^{1}H spectra of the plastic phase of NPG and NPG-d^2 depicted in Figure 4.10b show a similar linewidth, reflecting a similar mobility of all the hydrogen atoms in the

structure. Consequently, the biggest change in motion during the solid-solid phase transition occurs in the hydroxyl groups, leading to big differences in the hydrogen bond network of both phases. This result is also in agreement with the FTIR results in which these bonds suffered the most pronounced change during the phase transition (Figures 4.4b and 4.5b).

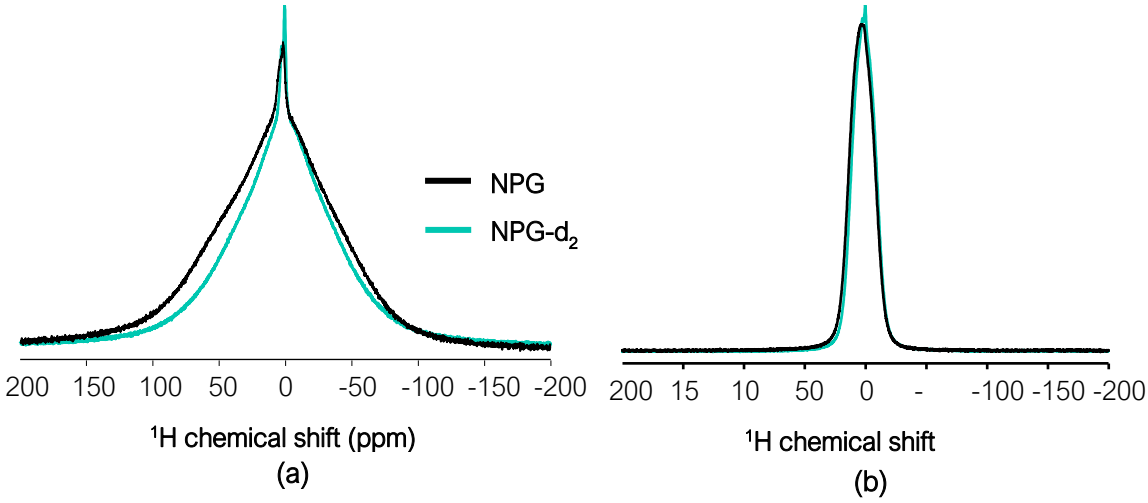

Figure 4.10. ^{1}H spectra comparison of NPG and NPG-d_2 (a) in the crystalline phase at 30 ºC and (b) the plastic phase at 50 ºC.

Moreover, thanks to the deuteration of NPG, an interesting behavior was highlighted. In the subcooling range (between 43 ºC and 32 ºC), whereas the ^{1}H spectra of NPG-d_2 broaden at lower temperatures, as expected due to the reduction of the inner molecular motion (Figure 4.11a), the ^{2}H spectra keep the same shape (Figure 4.11b). This confirms that, the hydrogen atoms participating in the hydrogen bonds network are still fast moving like in the plastic phase. This fast motion is likely hindering the reorganization of the structure to allow the transition to the crystalline phase and is the responsible of the subcooling phenomenon in NPG.

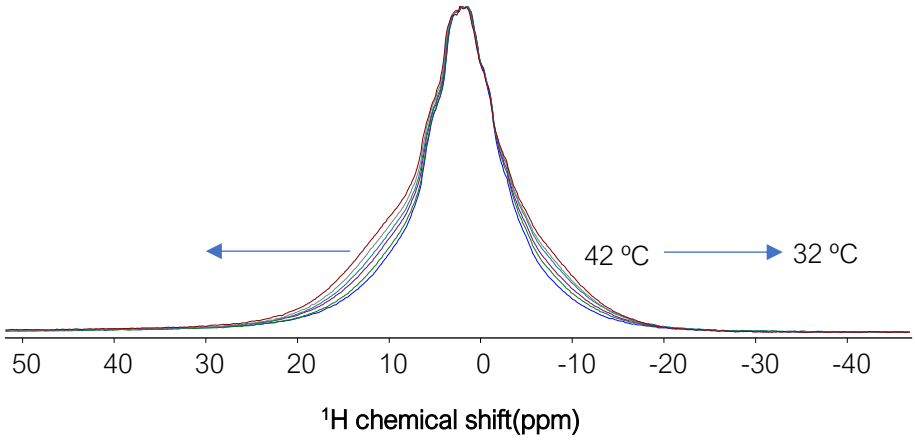

(a)

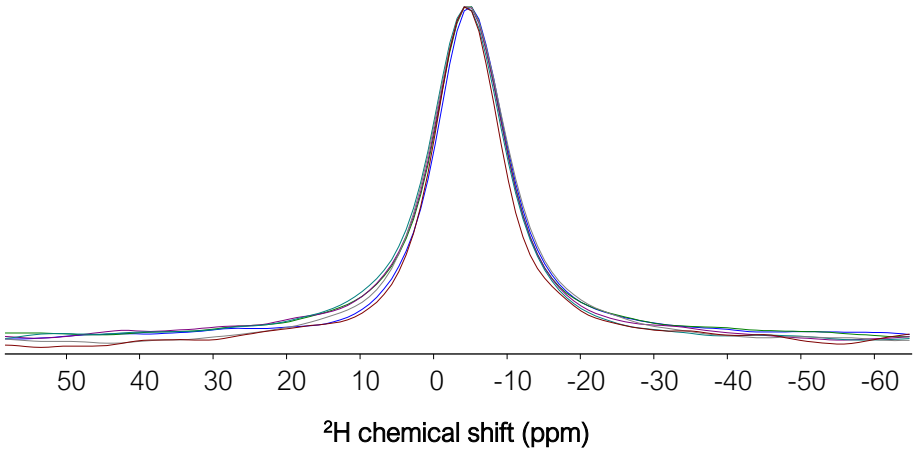

(b)

Figure 4.11. ^{1}H and ^{2}H spectra of NPG-d_2 upon cooling at 42 ºC, 40 ºC, 38 ºC, 36 ºC, 34 ºC and 32 ºC.

To further investigate this phenomenon, also PG was studied by ssNMR. A similar behavior as the one observed for NPG was found (Figure 4.12). Compared to NPG, the tetragonal crystalline phase of PG shows a broader signal than the monoclinic NPG, so the rigidness of the system is higher in the former case. This result agrees with FTIR measurements, since in PG there is one more hydroxyl group that participates in the hydrogen bond network. In the same line, the linewidth of the FCC plastic phase of PG is broader than the FCC of NPG at the same temperatures. One hypothesis to explain this result could be the more ionic character of the crystal lattice of PG, due to the higher number of hydroxyl groups and lower number of methyl groups. This fact could lead to a lattice whose interactions are mostly based on hydrogen bonds, instead of the "sandwich" character of NPG in which the

hydroxyl groups and methyl groups are arranged in parallel, hence distinguishing a more ionic and non-polar zone, respectively.

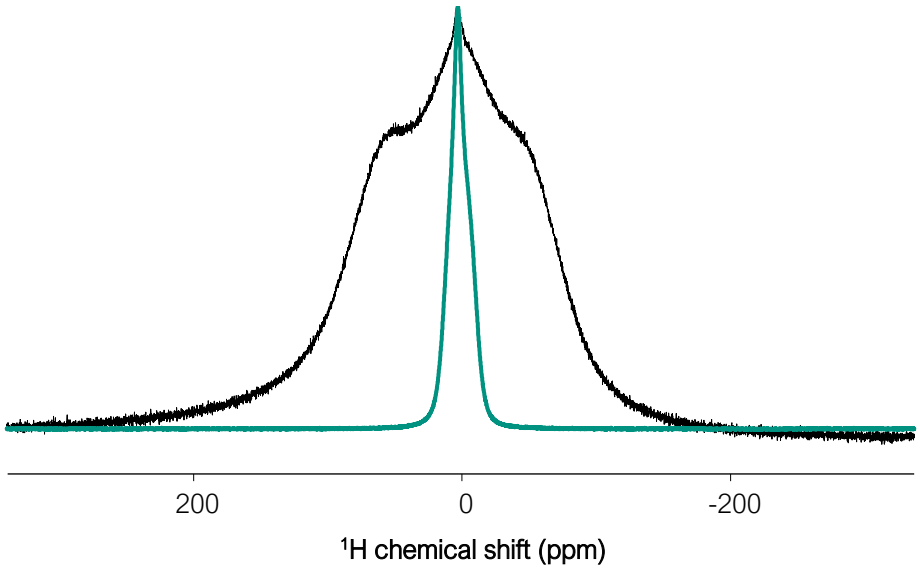

Figure 4.12. Comparison of ^{1}H NMR spectra of the crystalline (black line) and plastic phase (blue line) of PG.

In order to check the beforehand mentioned hypothesis, the same hydrogen/deuterium exchange of the hydroxylic positions was performed for PG to analyze separately the behavior of the hydrogen bonds and the protons of the molecular core. As shown in Figure 4.13a, the ^{1}H spectrum of the crystalline phase of PG-d_3 is narrower than that of PG for the same temperature, so as for NPG, hydroxyl groups are the most rigid part in the crystalline phase. On the other hand, for the plastic phase (Figure 4.13b), the linewidth for PG and PG-d_3 is similar, as occurs for the plastic phases of NPG and NPG-d_2. However, when comparing the ^{2}H spectra of the plastic phase of PG-d_3 and NPG-d_2 at the same temperature (Figure 4.14), it is possible to distinguish the behavior of the hydrogen bonds in the plastic phase of both molecules. The ^{2}H spectrum of PG-d_3 is slightly broader than that of NPG-d_2, so, besides the small difference noticed for the linewidths of the plastic phases of pure NPG and PG, the hypothesis of a more ionic plastic phase for PG compared to NPG is confirmed.

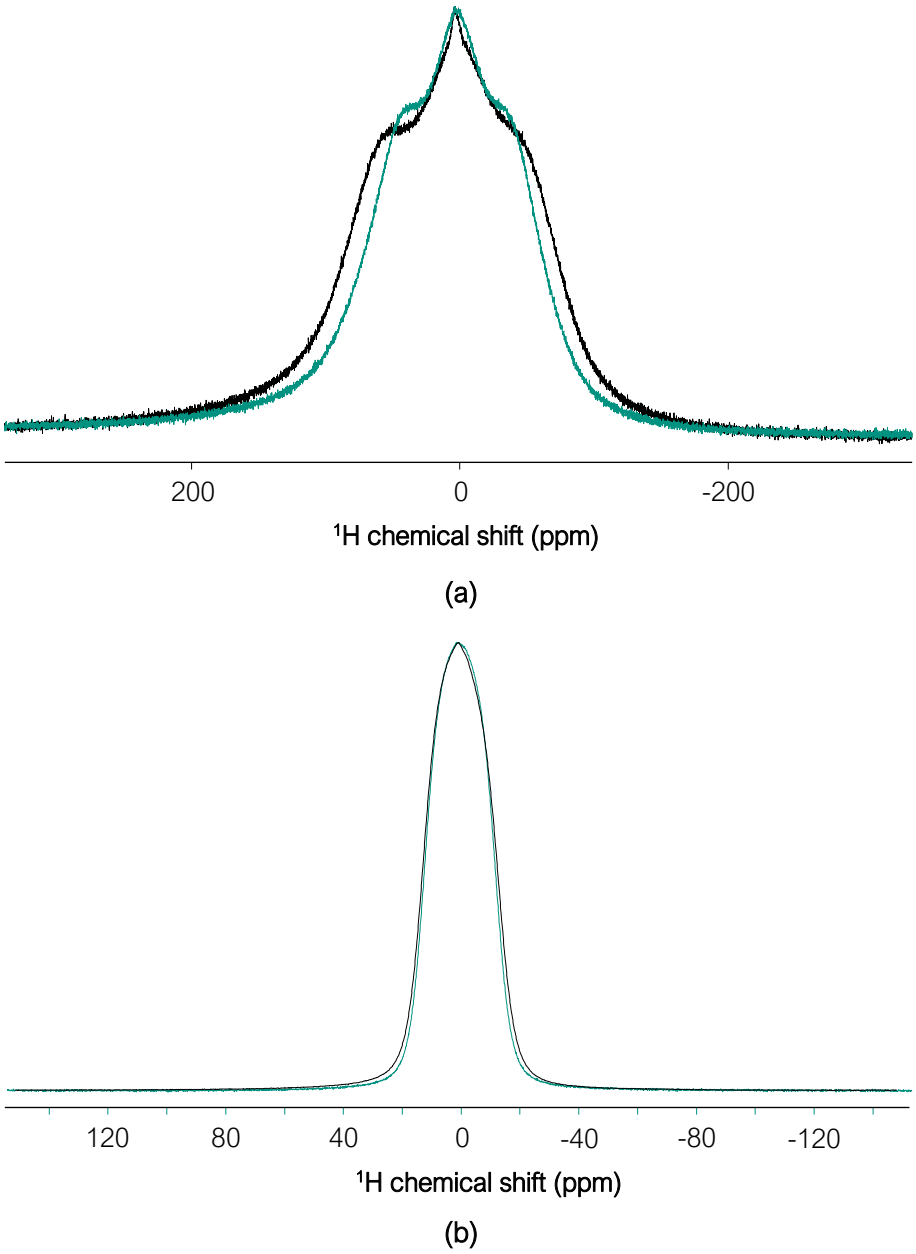

Figure 4.13. ^{1}H spectra comparison of PG (black lines) and PG-d_3 (blue lines) in (a) the crystalline phase at 30 ºC and (b) the plastic phase at 100 ºC.

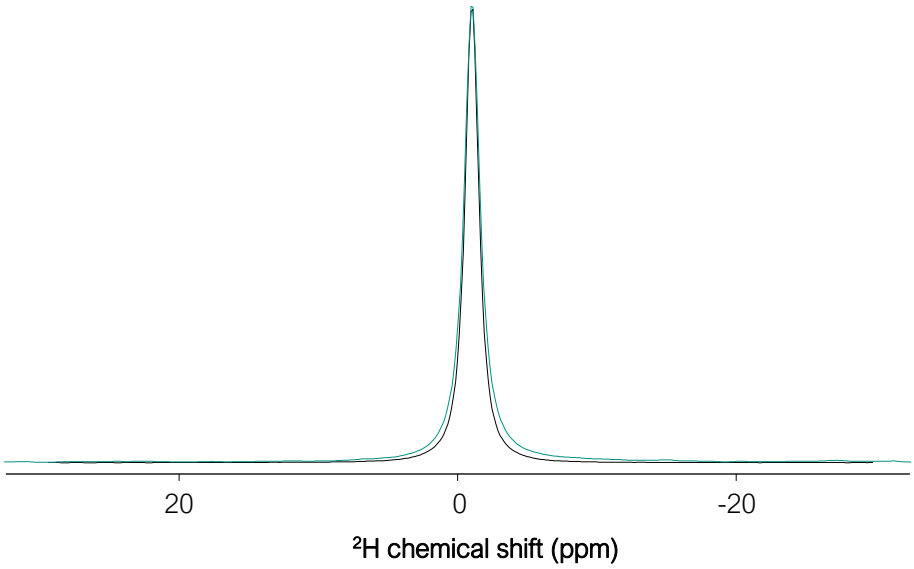

Figure 4.14. ^{2}H spectra of NPG-d_2 (black line) and PG-d_3 (blue line) at 100 ºC.

The solid-solid transition was also investigated for PE, evidencing a different behavior (Figure 4.15). Whereas, due to the higher number of hydroxylic groups with a more ionic character, the expected behavior for PE would be a higher linewidth of the crystalline phase signals in comparison to that of PG, the results show similar values for the two molecules (ranging from 50000 to 70000 Hz). Therefore, it is plausible to think that thanks to the four hydroxyl arms of PE, the interactions within the crystalline lattice will be mainly based on hydrogen bonds, so that the network will be characterized by a strong ionic contribution similarly to PG. Protons from the hydroxyl groups could be participating in a "concerted" motion in which they have higher mobility than expected, belonging to a certain molecule or to the neighboring one, hence showing a lower rigidness than for PG. This hypothesis is supported by the similarity of the signal's linewidths of the plastic phase compared to the plastic phase of NPG, despite of the bigger ionic character of PG and PE (Figure 4.15). Therefore, a concerted motion of protons in the plastic lattice is more probable for a higher number of hydrogen bonded groups, contrary to the expected behavior in which the higher the number of hydroxyl groups, the higher the rigidness of the system.

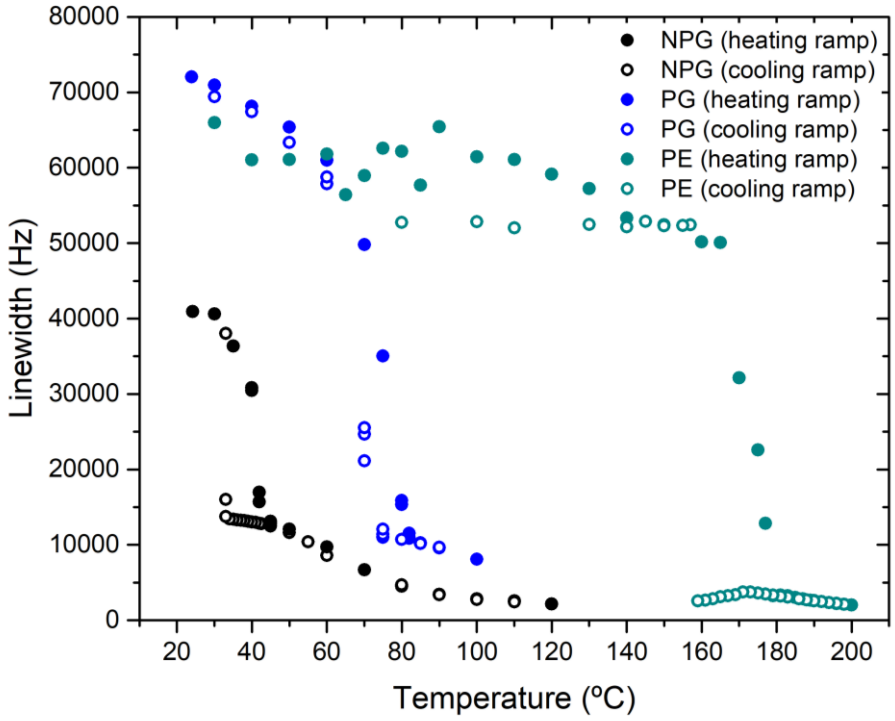

Figure 4.15. Plot of linewidth in function of temperatures of the ^{1}H spectra of NPG, PG and PE.

In order to prove the hypothesis of the concerted motion of protons, the study of TRIS compound could be very useful because it has a high number of hydrogen bonded protons with higher ionic character due to an eventual acid-base behavior between alcohol and amine groups. Therefore, variable temperature ^{1}H solid state NMR spectra around the orthorhombic-BCC phase transition of TRIS was recorded upon heating and cooling also under static conditions. Figure 4.16 shows the main differences between the spectra of the crystalline and the plastic phase of TRIS. The broad signals typical of the anisotropic interactions of the crystalline phases narrow at the transition temperature due to the disorder present in the plastic phase, in which the molecules are fixed within the unit cell, having a quasi-free rotation similar to the liquid state, as explained for NPG, PG and PE. Again, the impact of these fast local rotations in the spectra is explained by the averaging of the anisotropic interactions of the nuclear magnetic moments and it is evidenced by the narrowing of the signal in the spectrum of the plastic phase. Regarding the crystalline phase, as the temperature is increased, ^{1}H signals slightly narrow, as the solid structure is gaining in mobility at higher temperatures. The most noticeable change in the signals is found at 130 ºC, where the broad components observed at low temperatures disappears and the signal becomes much

narrower, in agreement with the solid-solid phase change temperature and the presence of a plastic phase (Figure 4.17).

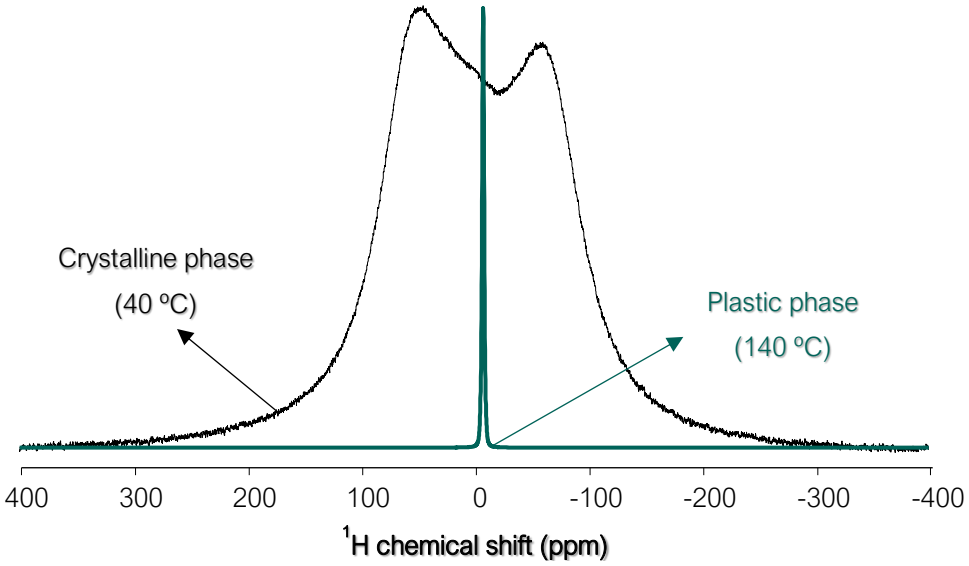

Figure 4.16. ^{1}H spectra of the orthorhombic crystalline and BCC plastic phases of TRIS at 40 ºC and 140 ºC, respectively.

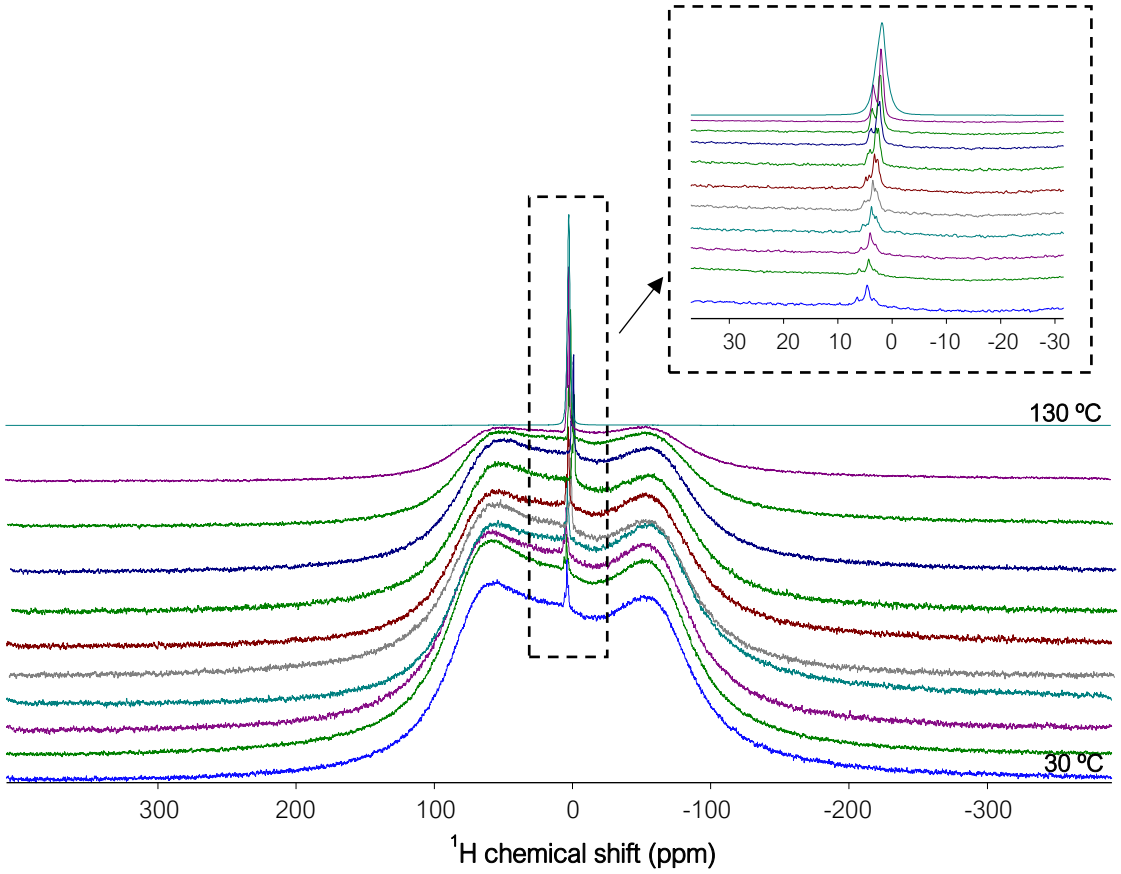

Figure 4.17. ^{1}H static NMR spectra of the first heating ramp to pristine TRIS from 30ºC to 130ºC by steps of 10 ºC, and inset with a zoom of the central region of the spectra.

In addition to the broad NMR signals present at low temperatures, a minor narrow contribution is present at all temperatures (inset of Figure 4.17). This component can be assigned to a minor portion of TRIS molecules that are subjected to fast motions even at room temperature. We can explain the presence of these molecules by two possible causes: the presence of reticular defects inside the crystal structure, or the presence of partial hydrated components at the surface of the crystals. It is well known that plastic crystals are hygroscopic due to their numerous hydroxyl groups, so this water content promotes a partial solubility of some molecules and hence increases their local mobility [16]. It should be taken into account that the signals shown in Figure 4.17 belong to the first heating process of the pristine sample. During the second heating ramp after cooling at room temperature back from 130 ºC (Figure 4.18), the narrow contribution at the centre of the signals is not present. Since the first heating was done over 100 ºC, we can easily assume that the sample was dehydrated. As for the case of reticular vacancies, we would expect the presence of narrow signals also after temperature cycling. In addition, the narrow component was observed to be bigger at higher temperatures (Figure 4.18), so, again, this effect is presumable due to an increasing solubility of molecules in the underlayer water around the particles.

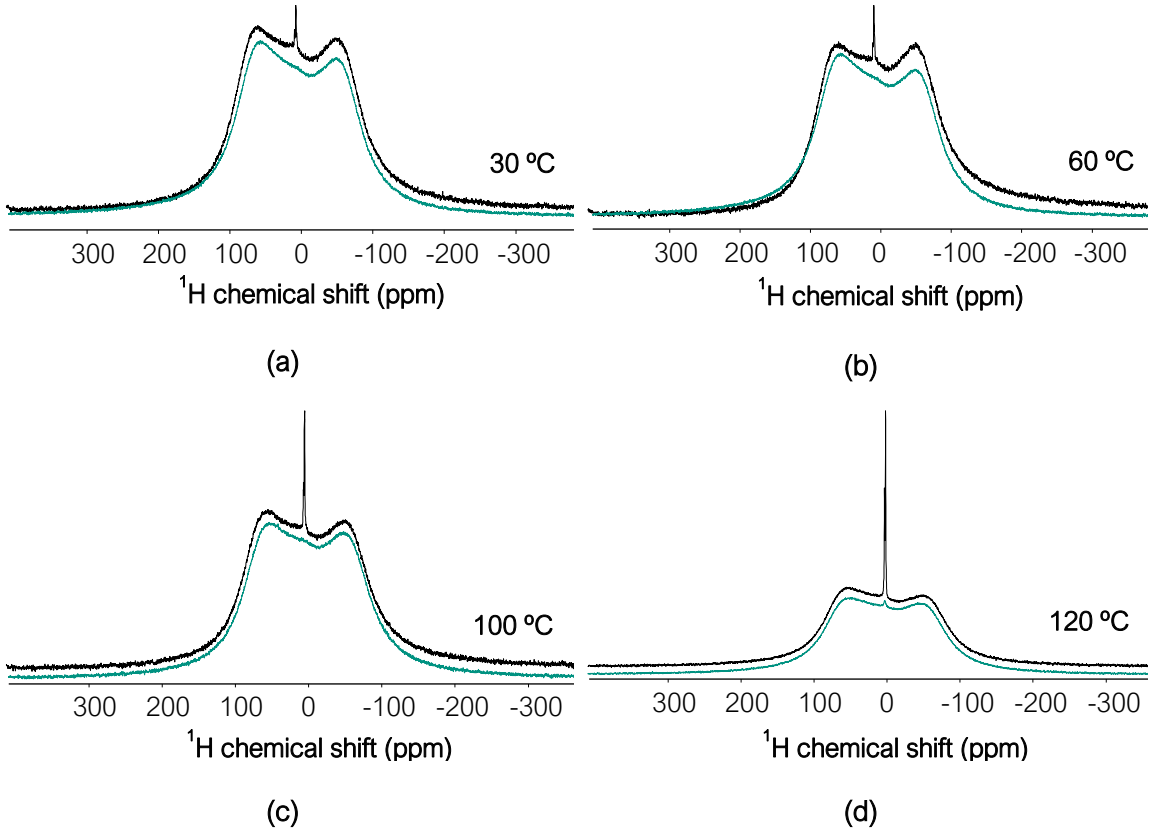

Figure 4.18. Comparison of the ^{1}H static NMR spectra of TRIS during the first heating ramp (black lines) and the second heating ramp (blue lines) of the same sample at (a) 30 ºC, (b) 60 ºC, (c) 100 ºC ad (d) 120 ºC.

Interestingly, the signal at 120 ºC during the second cycle of heating shows again a small narrow component (Figure 4.18d). In this case, this signal can be assignable to either structural defects or small temperature gradients in the body of the sample. This narrow component, observed in the second thermal cycle, is observed at temperatures close to the phase transition indicating that they are originated from molecules that already reached the necessary activation energy for the transition. The intensity of such signal in the second heating process at 120 ºC did not change after five minutes of annealing the sample (Figure 4.19a), supporting the hypothesis of local defects, as temperature gradients are expected to generate larger variations. At 125 ºC, when the transition is starting, the narrow contribution is observed to increase over time reaching a plateau at the first 15-20 min. (Figure 4.19b). This result indicates that at 125 ºC the transition is already undergoing for a fraction of the molecules. In Figure 4.19c, the plots of the intensity of the narrow components at 120 ºC and 125 ºC as a function of time are depicted. From this evolution we can clearly observe that this partial transition reaches a plateau at 15 min. Therefore, it is assumable that there is a gradient of activation energies in the sample and therefore a distribution of molecules that are changing from the crystalline to the plastic phase. We ascribe the molecules with a lower activation energy for the transition to molecules located at the surface of the particles or near to crystal defects. Consequently, the transition covers a range of temperatures from 120 ºC to 125 ºC, which is in agreement with the broad endothermic signals found by DSC (see Figure 3.3a in Chapter 3).

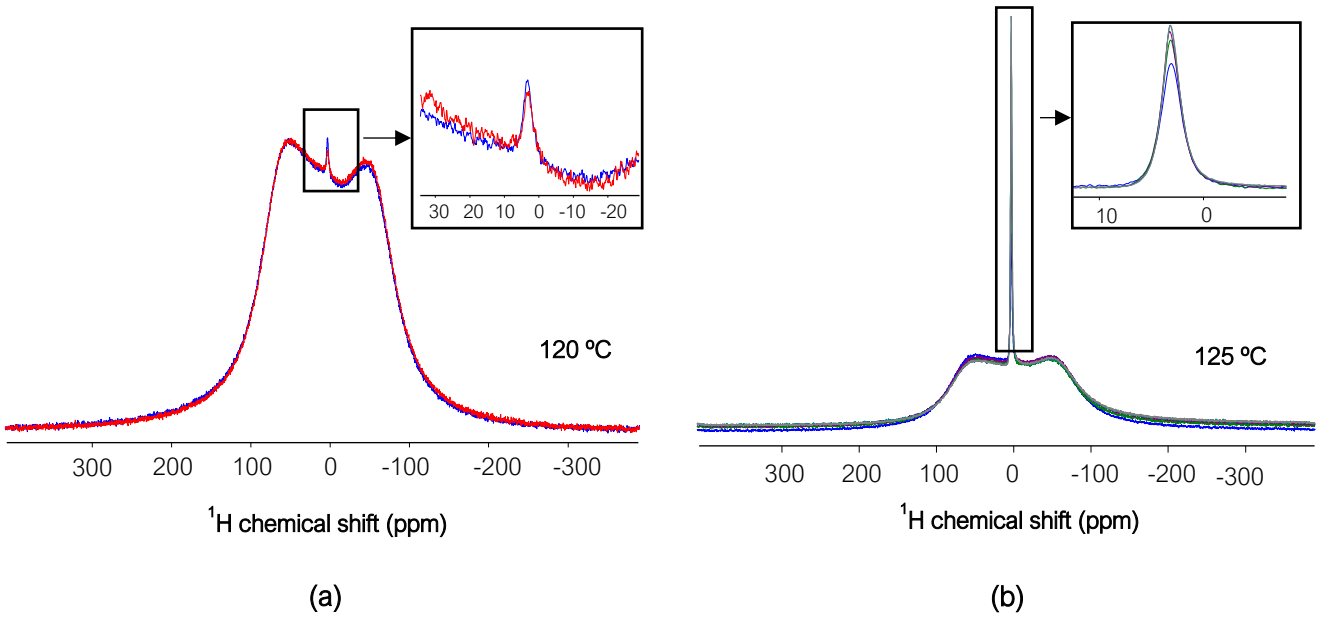

Figure 4.19. Comparison and inset of regions of the ^{1}H static NMR spectra of TRIS when annealing (a) 5 min at 120 ºC (fit to a linear function) and (b) 20 min at 125 ºC (fit to an exponential function). (c) Variation of intensity values versus time of both annealing.

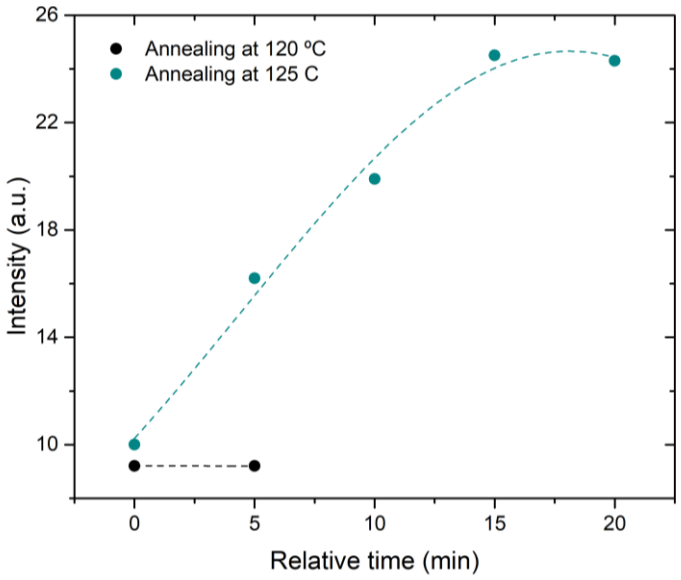

(c)

Figure 4.19. (Continued).

Once the solid-solid transition is completed, the signal typical of the plastic phase is narrowed compared to the one of the crystalline phases, so that we can now plot the different linewidths as a function of the temperature of the second heating cycle (Figure 4.20). The second heating cycle is considered for this representation as we can assume no influence of adsorbed water in this case. Since the differences in linewidths between the crystalline and the plastic phase are very large, a zoom of both crystalline and plastic phases is included for a clearer characterization of the temperature evolution within each phase. The trend observed upon heating is a decrease of the linewidth, due to an increase of the inner motion of the system due to thermal agitation, until the pronounced change in linewidths is observed when the phase transition occurs. Upon cooling, the trend is exactly the opposite; the lower the temperature, the broader the signal. By a careful inspection of the values of linewidth, it is observed that during the subcooling, the trend of increasing linewidths occurs more or less with the same slope, i.e., it seems that the molecules are losing the fast mobility with the same trend than they gain in mobility upon heating. Moreover, the differences in motion at different temperatures are more noticeable in the crystalline phase than in the plastic phase, since the differences in linewidths are higher in the former phase. It is worth mentioning that by the study of the linewidths, the orthorhombic crystalline phase of TRIS is the most rigid phase in all the studied PCs, whereas the BCC phase is the plastic phase which show the less rigidness of all the PCs. This fact supports the hypothesis drawn on the base of FTIR measurements

regarding the possible concerted motion of protons. When the hydroxyl groups are more than three, i.e., for PE and TRIS, the crystal lattice will be mainly based on ionic interactions by hydrogen bonds, so that these acid protons can be in a "proton could" in which the motion is higher than expected. This is the reason why probably PE and PG have similar crystalline phases. However, for TRIS the hydrogen bond network has a stronger character due to the more ionic behavior between hydroxyl and amine groups with some acid-base character. Concerning the plastic phase, it seems that the protons are moving even faster than for PE, and this is the consequence of a more ionic structure: The protons are freer in the TRIS molecule, so that the "hydrogen cloud" is even more possible in the case of TRIS, and this is translated into the narrower linewidths for the plastic phase.

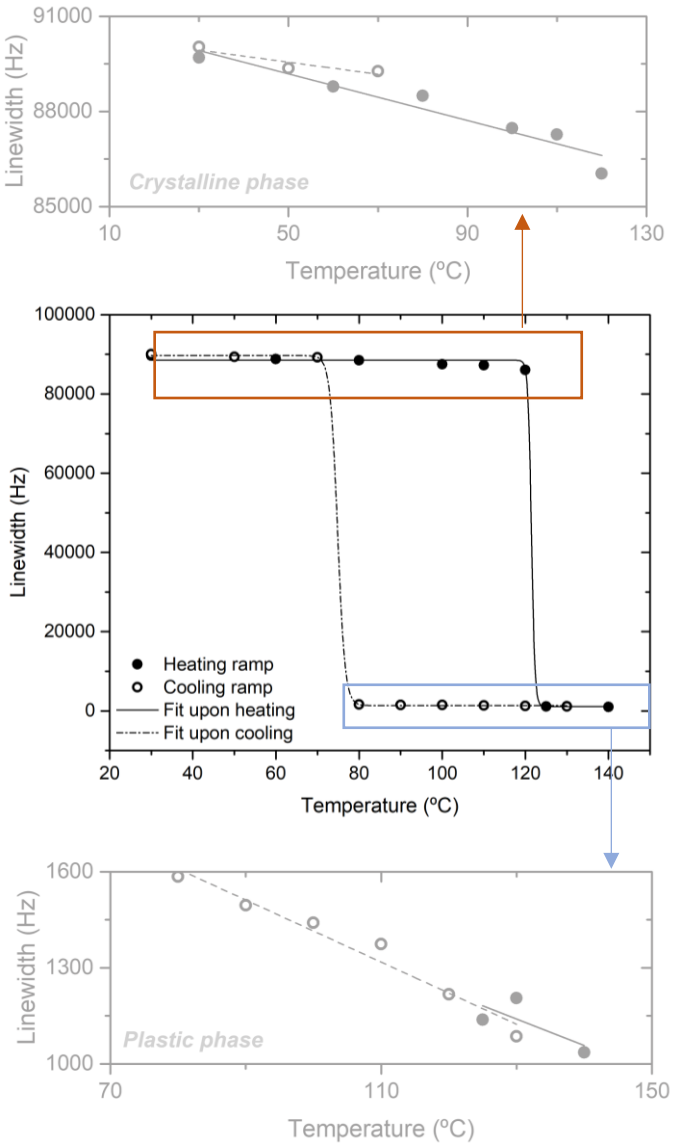

Figure 4.20. Plot of the ^{1}H NMR linewidths of TRIS at different temperatures upon heating and cooling and insets of the crystalline and the plastic phases.

In order to characterize the subcooling process after the second heating process of the plastic phase (140 ºC), the evolution of the ^{1}H NMR signals upon cooling are depicted in Figure 4.21a. From 140 ºC to 80 ºC, the ^{1}H NMR signals are characterized by the narrow linewidth of the plastic phase of TRIS, which are in agreement with the subcooling found by DSC in Figure 3.3a. In these spectra, a linear narrowing of the signals is observed during the subcooling in agreement with overall reduced dynamics. In addition, a chemical shift is also observed (Figure 4.21a). Variations in chemical shift are explained in this case by the reduction of the intermolecular distances in the crystal structure when temperature is reduced during the subcooling. From a careful inspection of the line shapes observed during the subcooling, different signal contributions with distinct linewidth are identified (Figure 4.21b). While at 140 ºC only one signal is apparent in the spectrum, a two-component deconvolution is clearly necessary to simulate the spectrum at 80 ºC obtained during the subcooling process. These results suggest that there are proton environments with very distinct local dynamics, and that these differences are more noticeable when the TRIS sample close to the transition temperature. From the deconvolution made at 80 ºC (Figure 4.21b), which is the closest temperature to the phase transition, two different contributions are present, with the integral ratio 55:45 for the broad and the narrow component, respectively. This ratio nicely fits with the proportion of methylene and alcohol/amine protons of the TRIS molecule (6:5), respectively. We can therefore clearly assign the narrow component to the hydrogens of the hydrogen bond network and the broader component to the methylene core. Thus, NMR experiments reveal that the first part of the molecule that is losing its fast mobility during the subcooling process are the methylene groups, instead of the alcohol/amine protons, which keep the dynamics of the plastic phase.

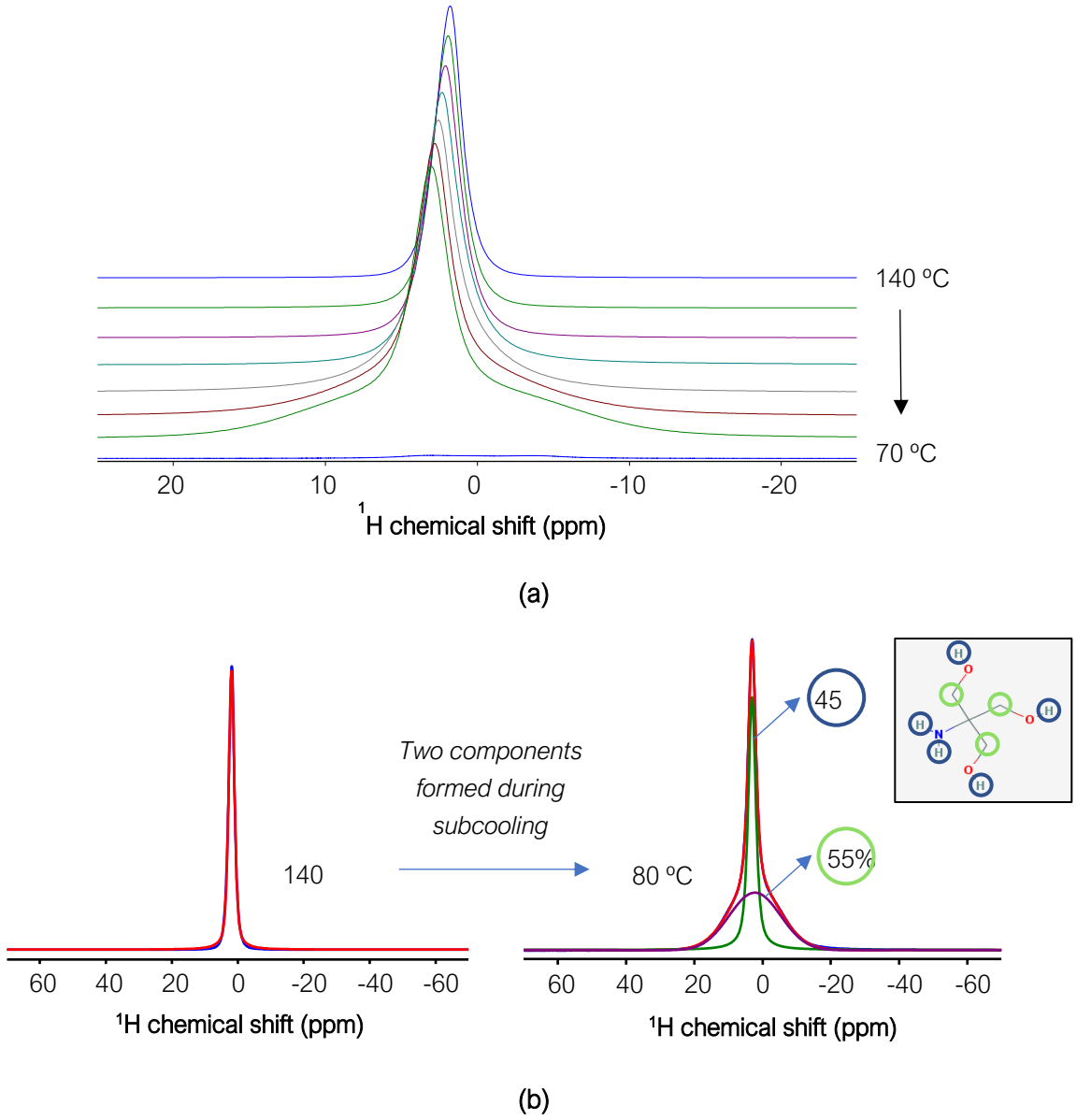

Figure 4.21. ^{1}H NMR spectra of a static sample of fully protonated TRIS (a) upon cooling from 140 ºC to 70 ºC by steps of 10 ºC, and (b) showing the deconvolution in two contributions of the signal at 80 ºC compared to the TRIS molecule.

In order to carefully follow the line shape evolution of each component in the proton spectra of figure 4.21a, the deconvolution of all the temperatures recorded during the subcooling were performed by fixing the ratio 55:45. The results, plotted in Figure 4.22b, show that while the methylene protons are becoming more static upon decreasing temperatures (higher linewidths), the alcohol/amine protons remain with approximately the same linewidths, i.e., they show a fast mobility characteristic of the plastic phase. Therefore, this proton mobility could hinder the needed reorganization of the hydrogen bonds to induce the phase transition

to the crystalline phase, and it could be the main cause for the subcooling phenomenon in this molecule.

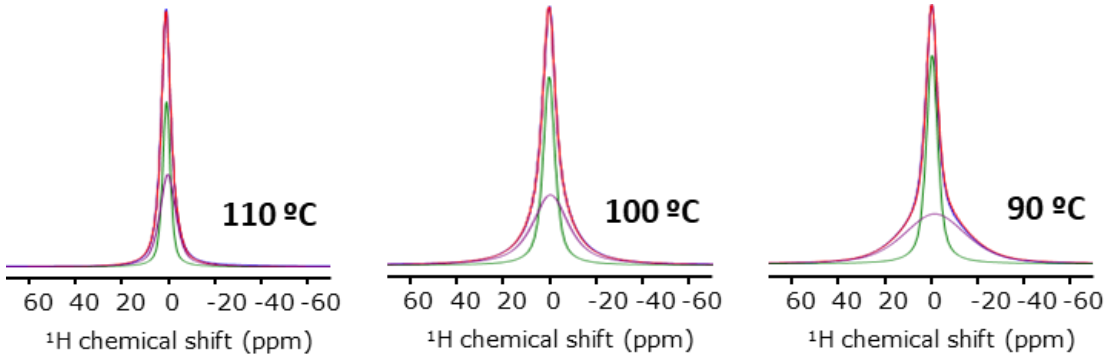

(a)

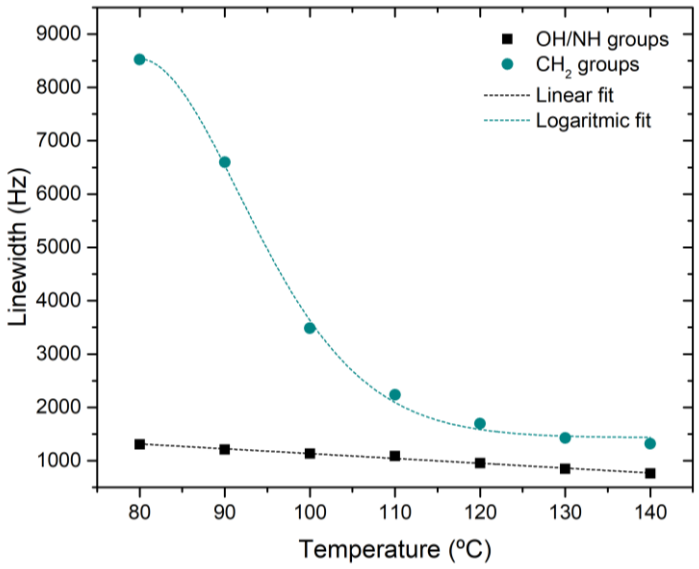

(b)

Figure 4.22. (a) Deconvolutions of three ^{1}H NMR spectra from Figure 4.21a, where the green lines show the OH/NH contributions and the purple ones show the CH_2 groups, and (b) linewidths of the deconvolution of the signals depicted in Figure 4.21a in two terms: OH/NH groups contribution fitting in a linear trend, and CH_2 groups contribution following a logarithmic trend.

In order to further investigate the different behaviour of the hydrogen bonding protons and the non-acidic protons of TRIS, a hydrogen/deuterium exchange was carried out in the alcohol/amine positions of TRIS. After deuteration, the TRIS-d_5 sample was also analysed by solid-state NMR at variable temperatures. As shown in Figure 4.23a, the signal of the ^{1}H NMR spectrum in the crystalline phase is broader for pure TRIS than that for TRIS-d_5. This is

explained by a reduced homonuclear dipolar broadening of the ^{1}H spectra when proton spins are partially diluted in the deuterated sample. This also indicates that protons at hydrogen bond positions are the most rigid groups in the crystalline phase. However, in the plastic phase (Figure 4.23b), the conclusions are the opposite: The broader signal corresponds to TRIS-d_5, confirming that in this plastic phase, the fastest motion is located on the protons which oversee the linking by hydrogen bond. The fast mobility of the hydrogen proton network can be explained by concerted intermolecular dynamics of these hydrogens, in which each proton does not belong to a specific molecule, but it is constantly moving in a proton cloud, and hence there are not located hydrogen bonds such as in the crystalline phase, but this concerted motion of protons in the plastic phase. On the other hand, the protons located in the methylene groups are also moving, but in their case, they are just rotating in fixed positions inside the unit cell. This result also agrees with the deconvoluted calculations shown in Figure 4.22b for the plastic phase of TRIS, in which the linewidths of the methylene protons are broader than that of the alcohol/amine protons.

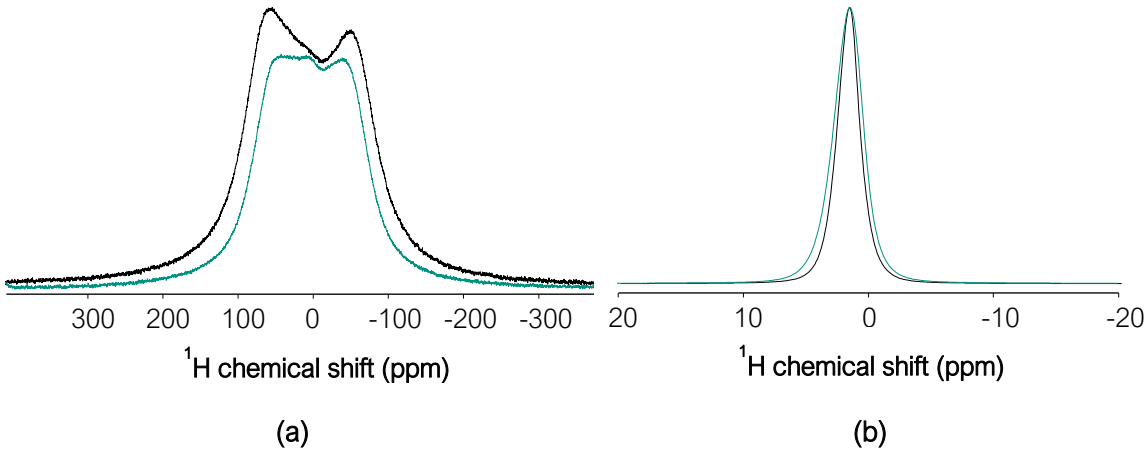

Figure 4.23. Comparison of the ^{1}H static NMR signals of TRIS (black lines) and TRIS-d_5 (blue lines) in (a) crystalline phase at 30 ºC and (b) plastic phase at 140 ºC.

Taking advantage of the deuteration of the molecules, ^{2}H NMR spectra were also recorded for TRIS-d_5 in order to specifically follow the mobility of the alcohol/amine protons (Figure 4.24a). The results are also in agreement with previous assumptions: the corresponding alcohol/amine protons (deuterium atoms in this case) do not show any variation in linewidth during the subcooling, indicating that these hydrogens remain fast moving as at high temperatures despite decreasing the temperatures. However, the ^{1}H NMR spectra in the same range of temperatures during the subcooling (Figure 4.24b), shows that

the signals are broadening upon cooling as expected for a situation where the methylene skeleton of the molecule is faster, hence restricting its dynamics upon decreasing temperatures. Hydroxyl and amine protons, which form the hydrogen bond network, are mostly unaffected during the subcooling, hence hindering the needed reorganization and the formation of the hydrogen bonds of the crystalline phase; and it becomes probably the main cause of the subcooling present in the solid-solid transition of TRIS.

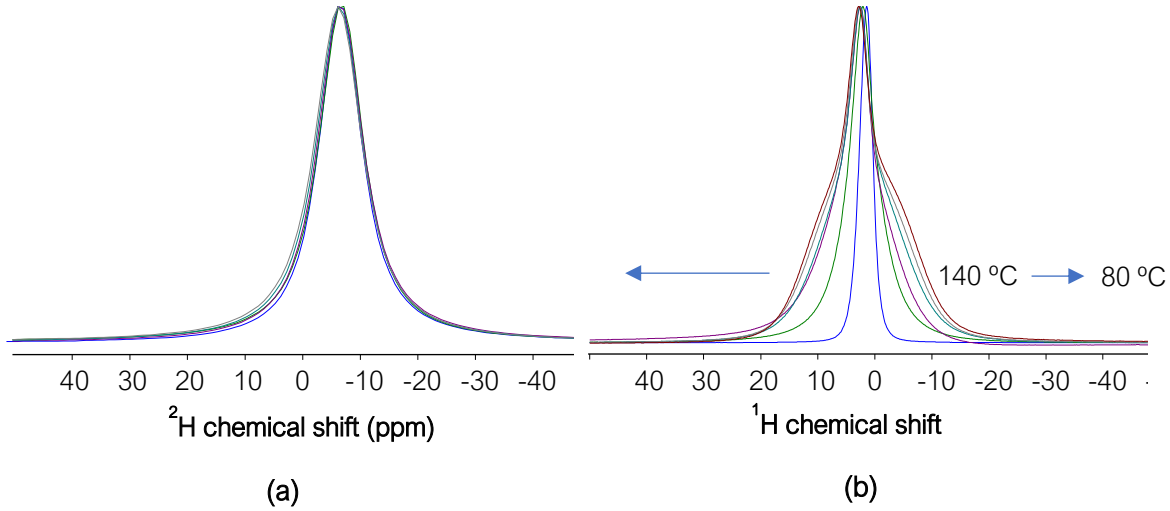

Figure 4.24. (a) ^{2}H static NMR spectra and (b) ^{1}H static NMR spectra upon cooling from 140 ºC to 80 ºC of TRIS-d_5.

4.3. Concluding remarks.

Crystalline phases of all the studied PCs are stiffer than the plastic phases, due to the stronger and higher number of hydrogen bonds in the former lattices, and the orientational disorder of the molecules within the latter ones. In addition, the higher the number of hydroxyl and/or amine groups, the more rigid and stronger is the crystalline phase. Tetragonal phase of PE shows a similar rigidness as PG, so it is lower than expected considering the number of hydroxyl groups. This is probably a consequence of a faster intermolecular dynamics of the hydrogens inside a crystal lattice mostly based on hydrogen bonds, in which each proton does not belong to a specific molecule, but it is constantly moving in a proton cloud. On the other hand, despite TRIS has a higher number of hydroxyl and amine protons than PE, the crystalline phase is more rigid than for PE, because the hydrogen bonds are more ionic creating a stronger network.

The behaviour for the plastic phases is similar for NPG and PG: the higher the number of hydroxyl and amine groups, the higher the rigidness of the system. Again, PE falls out this trend due to the "water-like cloud" of protons which the plastic phase shows, as well as TRIS, due to the higher number of hydroxyl and amine protons. Therefore, the trend found for the plastic phase is the opposite to the one observed for the crystalline phase: the higher the number of hydroxyl/amine groups, the less attachment of the protons to the "mother molecule" due to the higher freedom of such atoms.

Regarding the solid-solid phase transition, the biggest change during the phase transition occurs in the hydroxyl and amine groups for all the PCs, due to the hydrogen bond network arrangement. This is pointed out by the stretching and bending vibrations of the C-O and O-H bonds, respectively, as well as by the differences in linewidths of the PCs and their deuterated counterparts. Moreover, hydroxyl (as well as amine in TRIS) groups are the first to start the phase transition upon heating, followed by the core of the molecule. Upon cooling, there is a reversible behavior until the temperature reaches the subcooling zone. Within this range, methylene protons continue losing its fast mobility, but the alcohol/amine protons still keep the fast dynamics of the plastic phase. Therefore, this high proton mobility is probably hindering the needed reorganization of the hydrogen bonds to undergo the transition to the crystalline phase, and it could be the main cause for the subcooling phenomenon.

Therefore, the large subcooling present in TRIS is attributed to the lack of reorganization of the hydrogen bonds during the subcooling added to the huge difference in motion between both phases: a plastic phase characterized by a proton cloud, and a quite rigid crystalline phase in which the hydrogen bonds are firmly anchored by strongly ionic hydrogen bonds. Somehow, even though hydroxyl and amine groups are devoted to arrange the hydrogen bond network, the plastic-crystalline transition does not occur until the molecular core is quiet enough to promote a supportive environment for the needed reorganization. Therefore, a contraction of the crystal lattice, represented by the core of the molecule, is needed in order to reduce the number of molecular conformations and to facilitate the encounter of the hydroxylic positions of neighboring molecules, hence leading to the phase transition.

References in Chapter 4

[1] G.B. Guthrie, J.P. McCullough, Some observations on phase transformations in molecular crystals, J. Phys. Chem. Solids. 18 (1961) 53–61. https://doi.org/10.1016/0022-3697(61)90083-X.

[2] C.N.R. Rao, Molecular motion in plastic crystals, Proc. Indian Acad. Sci. - Chem. Sci. 94 (1985) 181–199. https://doi.org/10.1007/BF02841265.

[3] S. Ganguly, H.R. Swamy, C.N.R. Rao, A Raman spectroscopic study of the plastically crystalline state of organic compounds, J. Mol. Liq. 25 (1983) 139–147.

[4] A. Paul, L. Shi, C.W. Bielawski, A eutectic mixture of galactitol and mannitol as a phase change material for latent heat storage, Energy Convers. Manag. 103 (2015) 139–146. https://doi.org/10.1016/j.enconman.2015.06.013.

[5] P. Hu, P.P. Zhao, Y. Jin, Z.S. Chen, Experimental study on solid-solid phase change properties of pentaerythritol (PE)/nano-AlN composite for thermal storage, Sol. Energy. 102 (2014) 91–97. https://doi.org/10.1016/j.solener.2014.01.018.

[6] N. Zhang, Y. Song, Y. Du, Y. Yuan, G. Xiao, Y. Gui, A Novel Solid–Solid Phase Change Material: Pentaglycerine/Expanded Graphite Composite PCMs, Adv. Eng. Mater. 20 (2018) 1800237. https://doi.org/https://doi.org/10.1002/adem.201800237.

[7] 2019 FENG, Biao, et al. A molecular dynamics study of the effects of crystalline structure transition on the thermal conductivity of pentaerythrito.pdf, (n.d.).

[8] P.M. Tolstoy, J. Guo, B. Koeppe, N.S. Golubev, G.S. Denisov, S.N. Smirnov, H.-H. Limbach, Geometries and Tautomerism of OHN Hydrogen Bonds in Aprotic Solution Probed by H/D Isotope Effects on 13C NMR Chemical Shifts, J. Phys. Chem. A. 114 (2010) 10775–10782. https://doi.org/10.1021/jp1027146.

[9] J.M. Lopez, F. Männle, I. Wawer, G. Buntkowsky, H.-H. Limbach, NMR studies of double proton transfer in hydrogen bonded cyclic N,N′-diarylformamidine dimers: conformational control, kinetic HH/HD/DD isotope effects and tunneling, Phys. Chem. Chem. Phys. 9 (2007) 4498–4513. https://doi.org/10.1039/B704384H.

[10] J.M. Lopez del Amo, U. Langer, V. Torres, G. Buntkowsky, H.-M. Vieth, M. Pérez-Torralba, D. Sanz, R.M. Claramunt, J. Elguero, H.-H. Limbach, NMR Studies of Ultrafast Intramolecular Proton Tautomerism in Crystalline and Amorphous N,N′-Diphenyl-6-aminofulvene-1-aldimine: Solid-State, Kinetic Isotope, and Tunneling Effects, J. Am. Chem. Soc. 130 (2008) 8620–8632. https://doi.org/10.1021/ja801506n.

[11] O. Klein, F. Aguilar-Parrilla, J.M. Lopez, N. Jagerovic, J. Elguero, H.-H. Limbach, Dynamic NMR Study of the Mechanisms of Double, Triple, and Quadruple Proton and Deuteron Transfer in Cyclic Hydrogen Bonded Solids of Pyrazole Derivatives, J. Am. Chem. Soc. 126 (2004) 11718–11732. https://doi.org/10.1021/ja0493650.

[12] V. Torres, J.-M. Lopez, U. Langer, G. Buntkowsky, H.-M. Vieth, J. Elguero, H.-H. Limbach, Kinetics of Coupled Double Proton and Deuteron Transfer in Hydrogen-Bonded Ribbons of Crystalline Pyrazole-4-carboxylic Acid, Zeitschrift Für Phys. Chemie. 226 (2012) 1125–1148. https://doi.org/doi:10.1524/zpch.2012.0305.

[13] J.M. Lopez del Amo, U. Langer, V. Torres, M. Pietrzak, G. Buntkowsky, H.-M. Vieth, M.F. Shibl, O. Kühn, M. Bröring, H.-H. Limbach, Isotope and Phase Effects on the Proton Tautomerism in Polycrystalline Porphycene Revealed by NMR, J. Phys. Chem. A. 113 (2009) 2193–2206. https://doi.org/10.1021/jp8079414.

[14] F. Wilmet, M. Ribet, P. Bernier, Y. Girault, L. Elegant, 13C NMR investigation of the solid-plastic phase transition in polyols and their mixtures, Solid State Commun. 76 (1990) 621–626. https://doi.org/10.1016/0038-1098(90)90102-H.

[15] F. Wilmet, M. Ribet, P. Bernier, L. Elegant, T1 measurements by 13C NMR of the solid-plastic phase transition in polyols and their mixtures, Solid State Commun. 83 (1992) 961–964. https://doi.org/10.1016/0038-1098(92)90521-A.

[16] N. De La Pinta, S. Santos-Moreno, S. Doppiu, J.M. Igartua, E. Palomo Del Barrio, G.A. López, Npg–tris thermal storage system. Quantification of the limiting processes: Sublimation and water's adsorption, Crystals. 11 (2021). https://doi.org/10.3390/cryst11101200.

Chapter 5

Mitigation of subcooling

5.1. Processing of the materials.

5.1.1. Antecedents.

Different processing methods have been continuously assessed and improved in order to enhance the properties of the materials. As a consequence, not only differences in mechanical properties have been achieved, but also on some thermal properties such as the subcooling. As already reported on literature, processing of the materials can improve the hysteresis in liquid-solid transitions in the sense that in a continuous bulk of a material, the formation of the first stable nucleus of the solid phase will be more probable than in discreet microcapsules with small volumes of PCMs [1,2]. Following this approach, the effect of processing on the subcooling of solid-solid based PCs was studied in this chapter.

When discussing the understanding of the subcooling by solid state NMR in Chapter 4, it was pointed out that TRIS shows a gradient of activation energies in the solid-solid phase transition. Therefore, there should be a distribution of molecules that undergo the transformation crystalline-to-plastic before than the others. This is the case of the molecules located at unstable sites regarding the morphology, such as the surface of the particles or the

crystal defects which show lower activation energies of transition (Figure 5.1) [3]. Probably, the inverse transition will follow a similar trend. To this end, a processing method applied to a material which increases the specific surface area could be a good approach in order to promote the formation of "unstable points" located in particles surfaces or grain boundaries. Ball milling has been reported to be a technique that can achieve this goal [4,5].

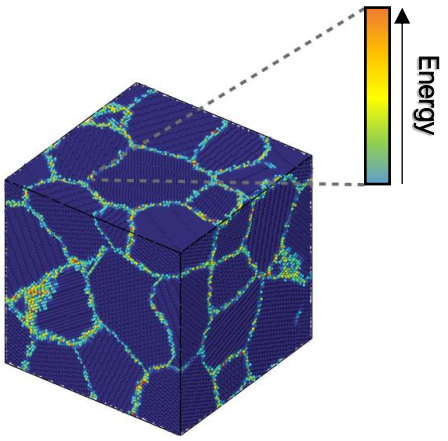

Figure 5.1. Scheme of grain boundaries of a solid as instability points inside the system.

Therefore, in this chapter, PG is selected as a proof-of-concept PCM since the solid-solid phase transition happening at 80 ºC is suitable for a high number of applications, such solar collectors, domestic hot water and low-temperature industrial heat recovery [6]. In this section, PG is studied in order to check how the microstructure of the material can affect the subcooling degree by testing different processing methods: The casting method and the uniaxial pressing of previously milled particles.

5.1.2. Results and discussion.

The two main processing methods tested for PG in this chapter are schemed in Figure 5.2. For the uniaxial pressing method, the powdered PG as received was grinded by ball milling at medium-low frequency in order to obtain a fine powder (Figure 5.2). Afterwards, it was compacted in a pellet die by applying a selected pressure in a single direction in order to obtain a solid pellet. This method has the advantages of being inexpensive and can increase the production rates compared to other methods, such as casting [7]. This latter processing method is based on the melting of PG inside a stainless-steel reactor placed inside an oven.

Afterwards, there is a solidification step at a slow rate (around 0.5 ºC/min) in order to get an homogeneous cooling of the sample.

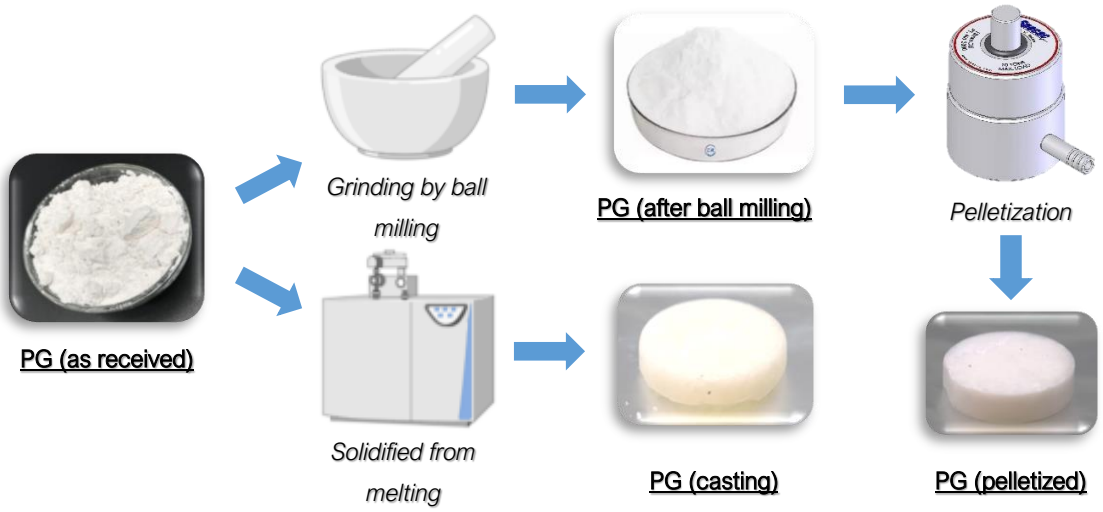

Figure 5.2. Scheme of the different processing methods applied to PG.

In order to analyze the microstructure of both samples, SEM was used to deeply check the morphologies of both materials. Two main regions can be identified in Figure 5.3a and 5.3b for PG processed by casting (hereinafter, PG_C): a chill zone and a columnar zone. The former is located at the edge of the bulk, where the solidification process starts, because heat is extracted firstly from the outer part and then from rest of the material. This chill zone is composed by a dense and fine grain structure due to a homogeneous cooling in all the edges of the sample (Figure 5.3a). The columnar zone, which is visible in both Figure 5.3a and 5.3b, is composed by several dendrites that grow along the radial axis from the edge to the center of the sample. These dendrites promote a substantial porosity due to the shrinkage produced during the solidification process, which is probably due to a local undercooling of PG before the nucleation. Figure 5.3b shows as the interdendritic distance ranges from 70 to 120 μm. The other processing method tested, the uniaxial pressed PG (hereinafter, PG_P) consists in a homogeneous structure in which there is no pores produced due to shrinkage, because there is not a solidification step from the melt (Figure 5.3c). However, there is a small porosity in the pellet typical of the compaction process. In any case, this processing method produces a sample of PG free of large defects with a distribution of small PG microcrystallites with an average grain size of 3.75 μm, probably due to effect of the milling process prior to the compaction process (Figure 5.3d).

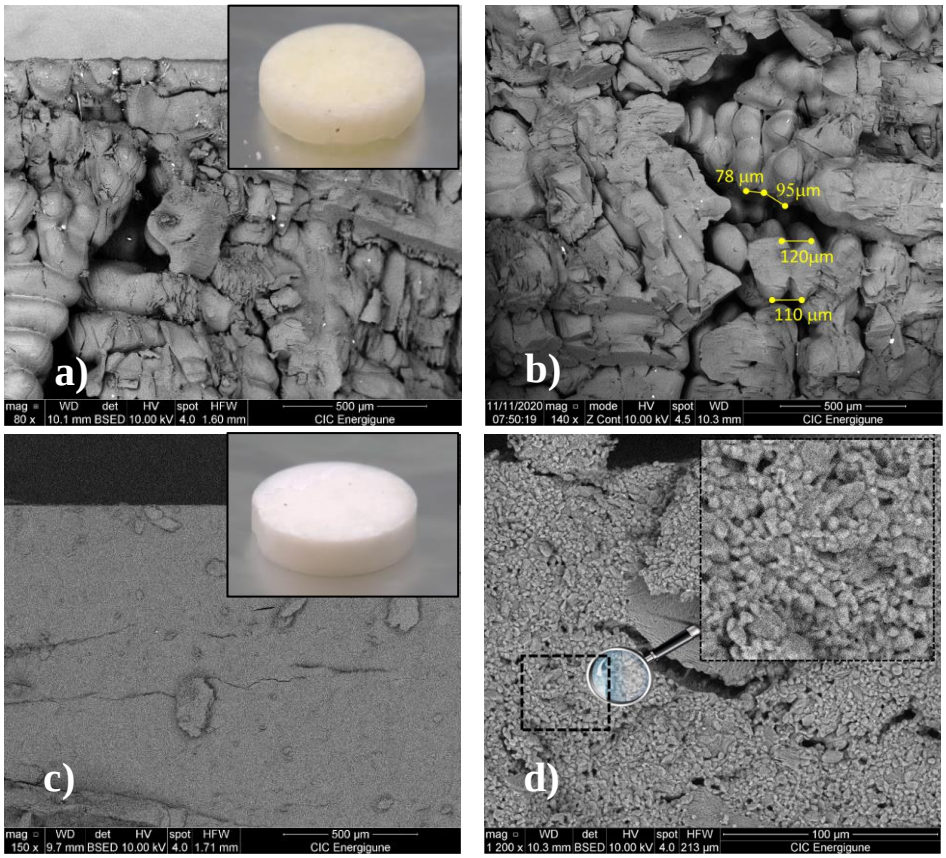

Figure 5.3. Pictures and SEM micrographs of (a) PG processed by casting (a. edge and b. center) and (c) PG processed by uniaxial pressing (c. low magnification and d. high magnification).

Once characterized the morphology by SEM, the subcooling was determined in order to find any relationship between it and the processing method used. Moreover, a comparison is also performed to the as received PG (hereinafter, PG_AR) and to the uniaxial processed samples at different pressures, in order to check the effect of pressure on the subcooling degree. In Table 5.1, it is possible to distinguish clearly two big differences regarding the subcooling degree. The as received and the casting processed PG samples show the typical subcooling degree of around 9-10 ºC. However, all the samples previously treated in the ball milling, no matter if they were compacted and at which pressure, show a lower subcooling. Therefore, the improvement of the subcooling is not a matter of the compaction process, but it seems due to the processing by ball milling. Therefore, powdered ball milled PG (hereinafter, PG_BM) without any compaction was selected to check why the subcooling is lower than that of the casting processed PG.

Table 5.1. Onset temperatures upon heating (T_h) and cooling (T_c), as well of the subcooling degree of the solid-solid transition of PG samples processed by different methods.

Sample treatment		T_h (ºC)	T_c (ºC)	Subcooling (ºC)
As received		81.6	72.1	9.5
Casting		81.3	71.6	9.7
Ball milling	Powder	82.0	77.1	4.9
	Pressed (1.0 ton)	82.0	76.4	5.5
	Pressed (2.5 ton)	81.9	76.0	5.8
	Pressed (5.0 ton)	82.2	76.9	5.3
	Pressed (7.0 ton)	81.9	76.4	5.5

Since ball milling gives rise to a high dispersion of different particles sizes of PG, a particle sieving was carried out in order to separate particles with different sizes. To this end, the particle sizes of the different groups determined by SEM were averaged by image treatment (ImageJ) [8,9]. The sieving afforded the separation of six different groups of particle sizes ranging from 3 μm to 250 μm. Samples of one were measured in the DSC in order to check the subcooling. Figure 5.4 shows the nice trend found: the smaller is the particles size of PG, the lower the subcooling is. In particular, particle sizes lower than 6 μm shows subcooling close to 3 ºC, whereas this value increases up to about 5.5 ºC for samples with particle sizes between 20 μm and 250 μm. This result is in agreement with Table 5.1 in which the subcooling for PG_BM is reported to be lower than for PG_AR and PG_C. This result could have been expected since the particles sizes obtained by ball milling are smaller than those of PG_C.

Taking into account these findings, it can be said that the preliminary hypothesis introduced by ssNMR analysis in Chapter 4 may be accurate: the lower the particle size, the higher is the ratio surface/bulk, so that there is a larger number of superficial molecules which are able to preferentially undergo a phase transition and hence decrease the subcooling degree. Indeed, for solid-solid transitions, usually suitable sites for starting the phase change are crystal defects such as vacancies, dislocations, grain boundaries, and so on. At the end, all kind of open surfaces are sites with a larger free energy in comparison to inner regions of a crystal. For example, the physical structure in grain boundaries is less dense than in other points of the material, as a consequence, the molecules can diffuse in an easier way [10,11]. Then, the molecules located at the grain boundaries will be the most unstable ones, and therefore they will be the preferred molecules to undergo the phase transition, since they are not strongly anchored to the lattice network as the ones located in the bulk of the material.

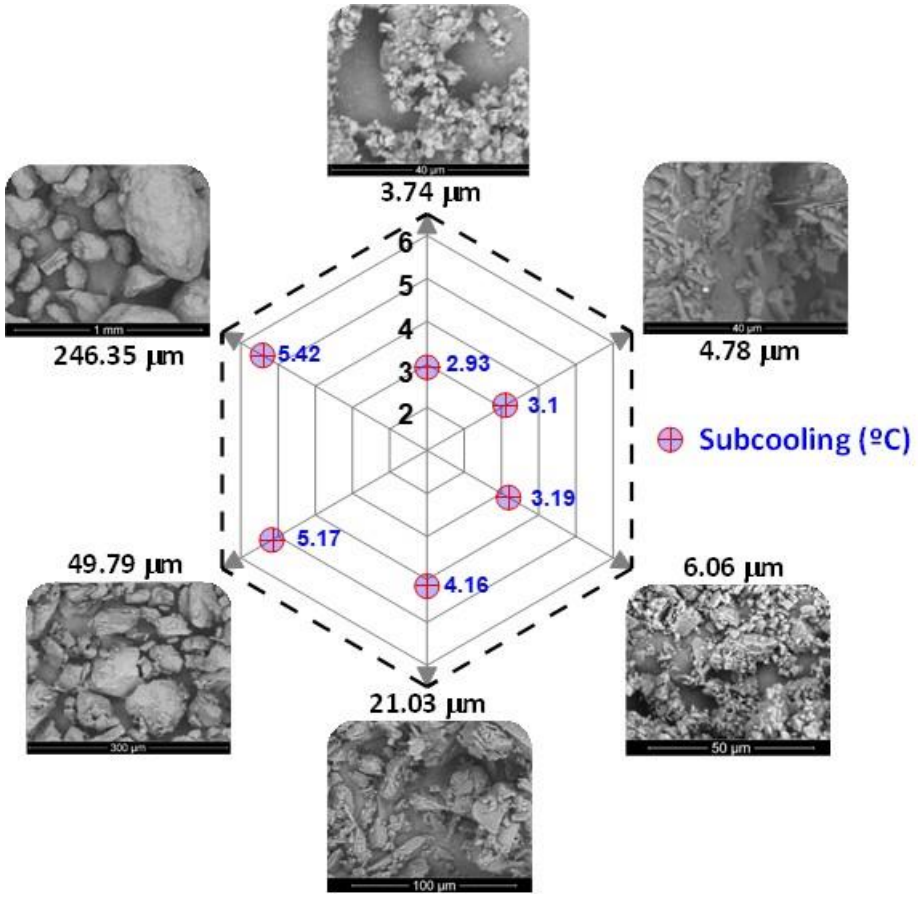

Figure 5.4. Averaged particles sizes of different sieved groups of PG_BM samples and the respective subcooling degree found for each of them.

To check the aforementioned hypothesis, ssNMR analysis was carried out to PG_C and PG_BM in order to determine the atomic motion in the crystal structures of both samples. Figure 5.5a shows the ^{1}H spectra of the crystalline phase of both samples. The narrowest zone located at the center of the signals for the PG_BM shows a higher intensity than that of PG_C. Therefore, as expected, there is a higher number of molecules with a higher local mobility in PG_BM, so they are presumably located at free surfaces. Moreover, the solid-solid transition upon heating and cooling of both samples were also followed by ssNMR (Figure 5.5b). Upon heating, PG_C transforms from the crystalline to the plastic at lower temperature than PG_BM does, since the narrow contribution of the signal characteristic of the plastic phase of the ^{1}H spectra is more pronounced for the former than for the latter sample. Upon cooling, the behavior is just the opposite: PG_BM undergoes the phase transition at higher temperatures than PG_C does, this is, the subcooling is lower for the former sample. Therefore, the transition from the crystalline to the plastic phase seems to start before in the

case of PG_C, because there is a continuous bulk where all the molecules have a direct interaction, so the propagation of the transition within the crystal lattice is easier than for the case of discreet particles. However, upon cooling, the presence of more defects or grain boundaries seems to promote the plastic-to-crystalline phase transition due to the higher number of superficial molecules. This behavior also points out the cascade effect of the solid-solid transition. One possibility would be that the transition occurring in the superficial molecules would not be transferred to the rest of the material due to the lack of interactions between particles. However, it is proven that once the transition has started, there is a propagation of the crystalline phase for all the material. Therefore, the subcooling is reduced due to the triggering of the transition temperature and it is not a matter of diffusivity problems within the crystal lattices involved.

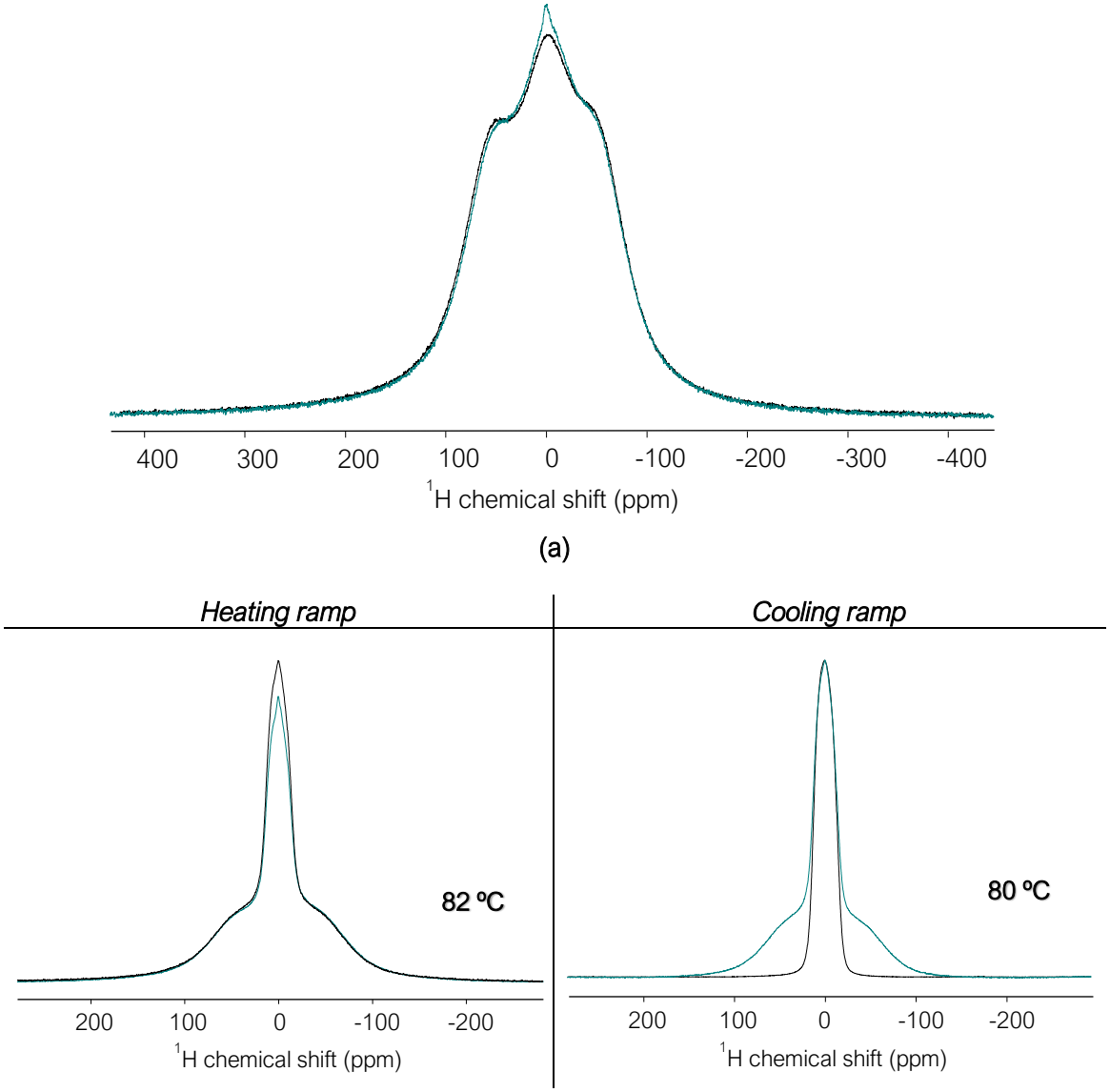

Figure 5.5. Comparison of ^{1}H NMR spectra of PG_C (black lines) and PG_BM (blue lines) at (a) 40 ºC and (b) during the solid-solid phase transition upon heating and cooling.

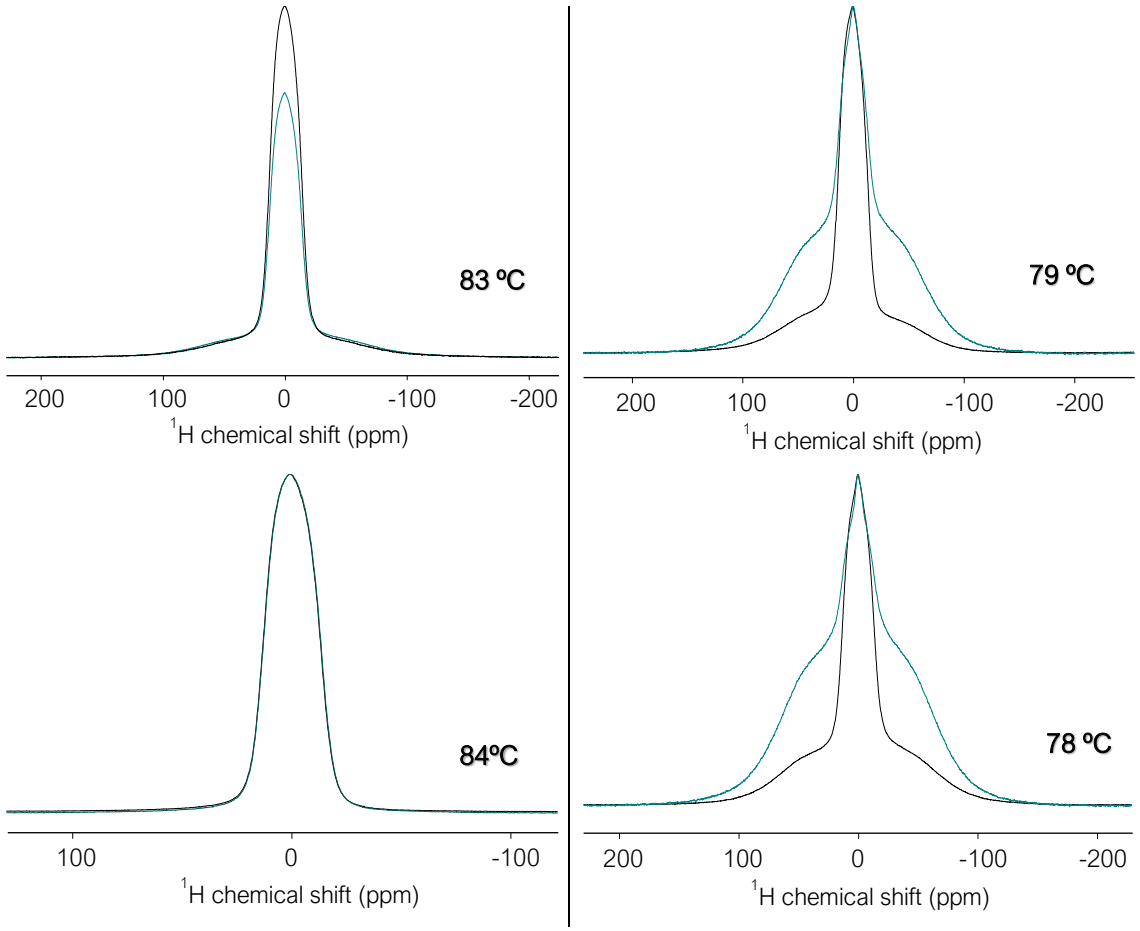

(b)

Figure 5.5. (Continued).

Hypothesizing about the preference of the molecules located at the surface or grain boundaries is not possible without talking about activation barriers. To this end, a kinetic study of the phase transition is required in order to analyze if the proposed mechanism is valid. To this end, the Friedman method was used for the calculation of the activation energy of the solid-solid transition [12,13]. The data obtained by DSC measurements of PG_C and PG_BM at different heating and cooling rates (1, 5, 10 and 20 ºC/min) afforded the determination of the apparent activation energy. For this purpose, the conversion ratio α was determined by different and consequent integrals of the hole DSC endothermic and exothermic signals of the transitions upon heating and cooling, respectively. Figure 5.6a shows how the conversion rate α of the crystalline-plastic phase transition is higher at higher temperatures, and as expected, this behavior is exactly the opposite for the plastic-crystalline transition, in which α is higher at lower temperatures. In addition, Figure 5.6a shows how, in agreement with the ssNMR results shown in Figure 5.5, the solid-solid transition upon heating starts before in

PG_C. Moreover, the reverse transition upon cooling starts before for PG_P, also agreeing with the ssNMR results.

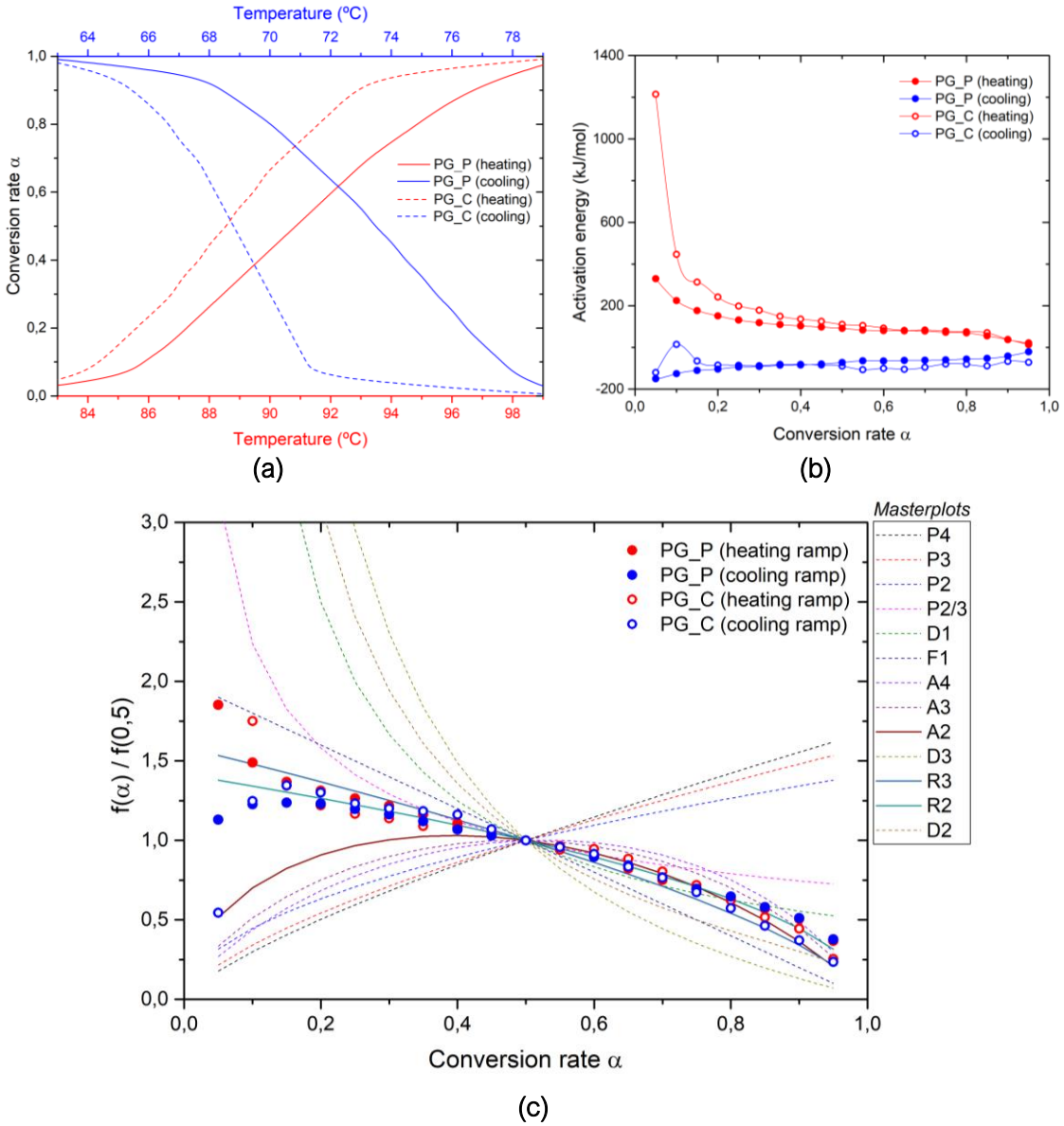

Figure 5.6. (a) Conversion rates of the solid-solid transitions upon heating and cooling of PG_C and PG_P in function of temperature, (b) Activation energies in function of such a conversion rates, and (c) comparison of the theoretical and the experimental masterplots for different transformation mechanisms.

In general terms, as shown in Figure 5.6b, the higher are the conversion rates, the lower are the activation energies (Figure 5.6b), and it makes sense since the transition has already started and there is some inertia with the progress of the transition. There is a slight

increase in activation energies for the plastic-crystalline transition at advanced conversion rates, but this is probably due to the higher resistance promoted by the crystalline phase that partially hinders the phase change advance. Afterwards, the plot of α in function of the inverse of the temperature gives the activation energy from the slope of the curves. The trends found for conversion ratios lower than 0.2 are discarded as their R^2 values were lower than 0.975. The values of activation energies were calculated to be 116.0 ± 49.7 kJ/mol and -81.3 ± 27.8 kJ/mol for the solid-solid transition of PG_BM upon heating and cooling, respectively. On the other hand, the activation energies for PG_C were determined to be 155.2 ± 63.1 kJ/mol and -82.0 ± 12.8 kJ/mol for the transitions upon heating and cooling, respectively. Considering such large errors of activation energies, it is not possible to conclude that there are significant differences between activation energies in the solid-solid transition of PG processed by different methods. However, considering these values it is possible to determine the mechanism of the solid-solid transition by using the masterplot method [14]. The experimental plot at different conversion ratios can be compared to theoretical models, plotted in Figure 5.6c and whose meaning is explained in Annex 1 in Table A.1.8. Figure 5.6c shows as the convergence between the masterplot of the transitions upon heating and cooling of both PG_C and PG_P follows a similar mechanism, usually called as R2 or R3: The mechanisms are based in a phase boundary control. This means that the beforehand hypothesis was right: The transition is promoted by the phase with a high surface/bulk ratio, since it is easily transmitted by the phase boundaries. Therefore, it makes sense that a material such PG_P in which the surface is higher than for PG_C, the transition starts before than in a bulk material.

5.1.3. Concluding remarks.

PG was processed in two different ways: ball milling followed by a uniaxial pressing, and casting method. Microstructures PG_C followed the typical and expected behavior for a casted material: i) a chill zone in the border where the solidification starts, and ii) a columnar zone where the phase transition is transmitted to the inner part of the material. On the other hand, PG_P shows an homogeneous structure in which there is no substantial porosity due to the shrinkage since there is not a solidification process, hence presenting a material without large inner defects in the solid structure.

The ball milling processing resulted in a decrease on the subcooling degree, no matter if the final material was pressed or not. Therefore, since this technique enables to reduce the particle size, a particles sieving was carried out in order to directly relate the particle size to

the subcooling. In such a comparison, as expected, the smaller the particle size, the lower the subcooling degree. This behavior is mainly due to a high surface/bulk ratio, where the particle on the surface undergoes the plastic-solid transition before than those in the bulk. This theory is supported by ssNMR measurements. The crystalline-plastic transition (heating step), on the other hand, seems to start before for PG_C than PG_P, because the propagation of the transition interface is not hindered due to a lack of intermolecular interactions. Therefore, there is a lower rotational freedom and once the molecules reached the required energy, they are able to undergo the phase transition.

Besides ssNMR, the hypothesis of a decreasing subcooling due to a smaller particle size was also checked by theoretical models. In them, the calculation of activation energies of the solid-solid phase transition of PG pointed out the mechanism as a phase boundary-controlled transformation, no matter the processing method used. Therefore, it is clear that the higher the number of phase boundaries within the material, the more promoted will be the phase transition, and this is the reason why the subcooling is lower in the case of PG_BM or PG_P in which the particles are smaller than for PG_C.

5.2. Particles dispersion.

5.2.1. Antecedents.

The dispersion of particles acting as nucleating agents has been a widely used approach to improve the subcooling in solid-liquid based PCMs. In these cases, heterogeneous crystallization happens when the nucleation starts on the surface of impurities or a different material than the PCM, i.e., the nucleation will start in the interface between such a material and the additive (Figure 5.7) [15,16]. The basis of this approach is the same explained in Chapter 5.1 about different surface/bulk ratio in the materials: Free surfaces, wall of the container, grain boundaries, and so on, are interfaces with relatively larger free energies. Therefore, the nucleation has to overcome a smaller activation barrier in order to undergo the phase transition. This approach has been widely used to improve subcooling up to a 17 % in solid-liquid based PCMs such as sugar alcohols by the dispersion of graphite particles or copper oxide nanoparticles [17,18]. The same approach can be found in literature for improving the subcooling in other substances such polymers or salt hydrates [19,20]. However, to the best of our knowledge, only a few studies have been reported about the mitigation of the subcooling in solid-solid based PCMs. These studies propose similar

approaches already investigated to mitigate the subcooling in liquid-solid transitions. For example, the dispersion of some metal nitrides [21,22] and oxides nanoparticles [23] in pentaerythritol, or expanded graphite in the eutectoid $NPG_{0.515}TRIS_{0.485}$ [24]. For all the cases, an improving of the subcooling degree of about the 10 % was achieved.

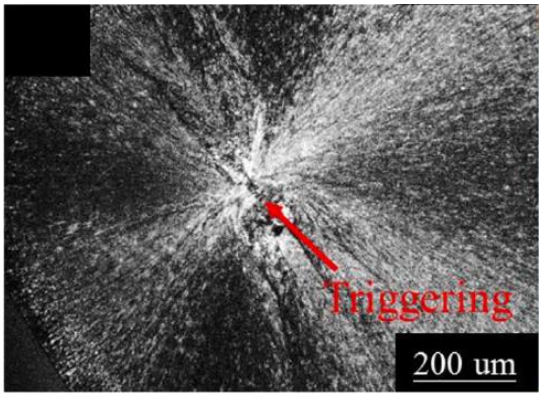

Figure 5.7. Triggering of the crystallization of erythritol due to expanded graphite (EG) as nucleating agent. Adapted from ref. [25]

Considering these references and the results shown in Chapter 4, where ssNMR results reveal that surface sites and grain boundaries within the PCMs seem to be preferred sites for starting the transition from the plastic to the crystalline phase, different carbon-based particles such as graphites or graphenes have been dispersed in NPG, PG and TRIS. The objective was to identify the proper additives for the best improvement of the subcooling degree. PG was selected in order to check if the processing of the composite affects the final subcooling degree as occurred for pure PCs. Then, the same particles were also dispersed in NPG and TRIS to study their influence on two materials with medium (NPG) and severe (TRIS) subcooling degree.

5.2.2. Results and discussion.

Being graphite and graphene particles widely used as nucleating agents, together with their compatibility with organic PCMs, they were preferentially selected to be dispersed in the PCs studied in this thesis (Table 5.2). Two different sizes of expanded graphite particles (EG75 and EG600) were chosen, as well as oxidized graphene particles with a progressively higher number of oxidized groups (70i, rGO and GO), such as hydroxyl or carboxylic groups.

Table 5.2. Nucleating agents and their properties used for dispersing in Plastic Crystals.

Particle	Composition		Geometry			
	% C	% O	Shape	Lateral size (LD_{50}, μm)	Surface (m^2/g)	Density (g/L)
GO	> 60.0	30.0	Layered	40	400	n.m.
rGO	> 90.0	8.0	Layered	70	280	n.m.
70i	> 95.0	2.5	Layered	70	416	125
EG75	> 95.0	< 2.0	Layered	75	25	120
EG600	> 95.0	< 2.0	Layered	600	25	100

n.m. Not measured, due to the limitations of the helium pycnometry

The graphene oxide-based and EG-based composites were synthetized by following the same routes used for pure PG: casting and uniaxial pressing (Figure 5.8). To this end, the plastic crystal was first treated in a ball milling at low frequency in order to obtain a fine powder. The casting method involved a first mixing of the PC with the selected additive in the desired ratio PC/particle. After a mild powder mixing in a mortar, the mixture is heated inside a furnace up to the melting temperature of the PC and then let slowly solidified by annealing at room temperature for at least 1 h in order to avoid vitrification of plastic phases. The uniaxial pressed composite was compacted with 5 tons in the uniaxial press after the mixing of the PC and the selected additive. Figure 5.9 shows the subcooling and the enthalpy obtained by DSC measurements of the PG based composites prepared by casting and uniaxial pressing. Comparing to pure PG (PG_AR), the addition of only 1 wt.% of EG600, following the two methods, led to a reduction of the subcooling degree up to 16 %. As for pure PG, the composite prepared by uniaxial pressure showed a lower subcooling degree than that prepared by the casting method (Table 5.1). Moreover, the influence of the additive concentration on the subcooling degree was also tested. For this purpose, different amount of EG600 from 1 wt.% to 10 wt.% were dispersed in PG. Figure 5.9 shows that for the composites prepared by uniaxial pressing, the increasing amount of additive does not have substantial effect on the subcooling. However, for the casting composite, there is even an increase of it. This phenomenon can be probably attributed to a non-homogeneous distribution of EG600 inside PG in the casting composite due to the high concentration (10 wt.%) and the preparation methods used.

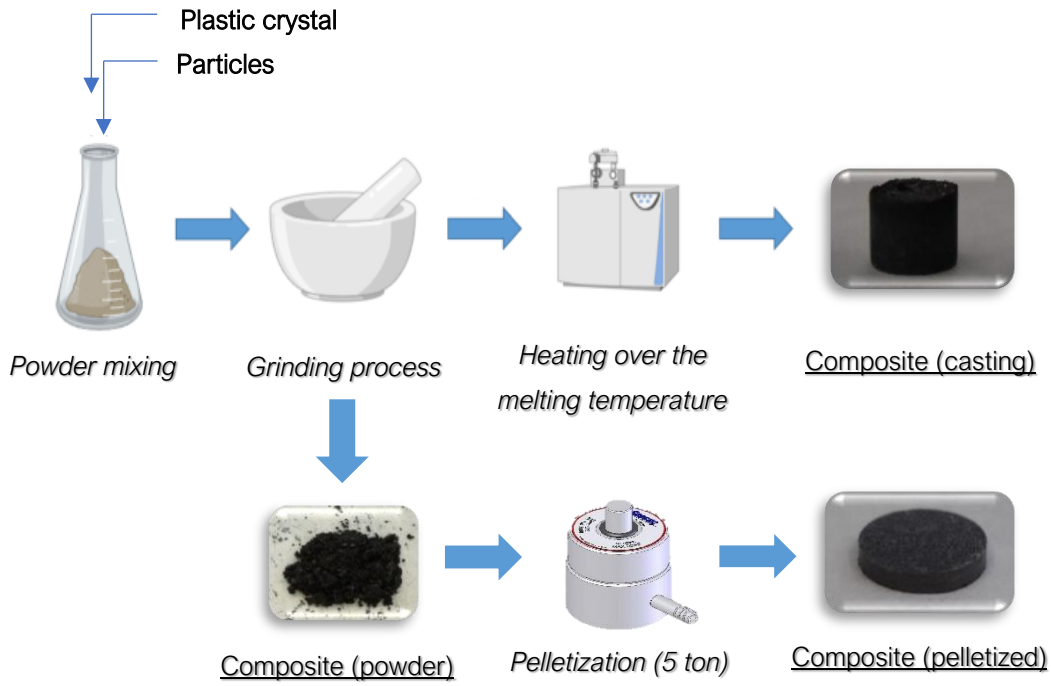

Figure 5.8 Two routes to synthetize the casting and pelletized particles-based composites of the PCs.

Concerning the phase transition enthalpies, again the composites prepared by casting have a negative effect on the enthalpy comparing to the pressed composites, being this effect even worst at higher particles concentration. This is a logical finding since in the casting composite there is likely a better distribution of PG in the EG600 surface, hence decreasing the number of active PG-PG hydrogen bonds involved in the phase transition. Considering all these results relevant for the subcooling and the enthalpy, the uniaxial pressing was chosen as the best processing method for the synthesis of the composites. Moreover, a concentration of only 1 wt.% of additives was selected due to both the good improvement of the subcooling and the minimal impact on the enthalpy of the phase transition.

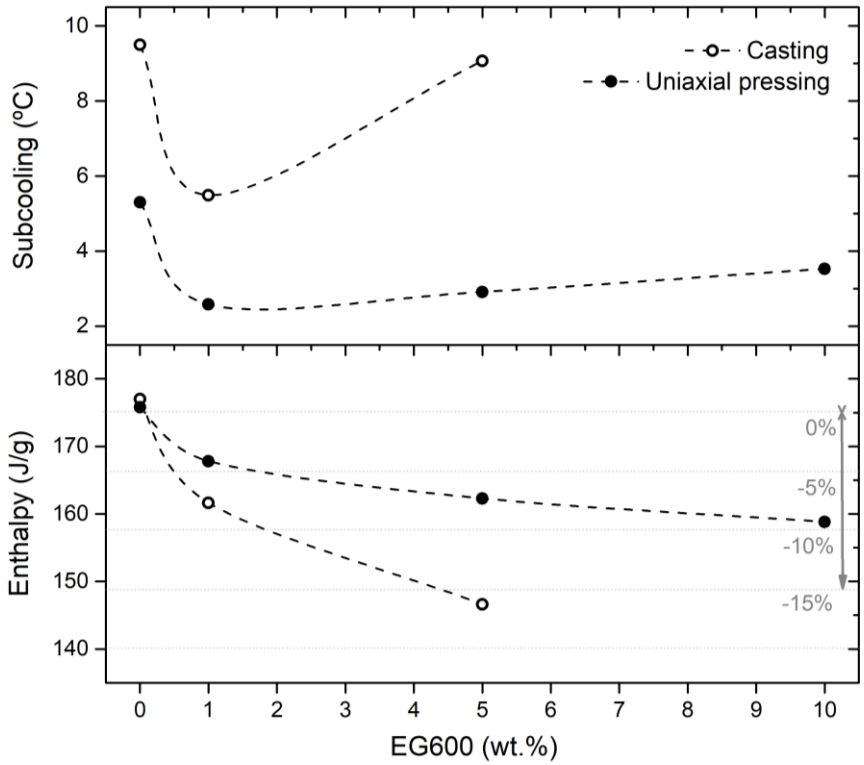

Figure 5.9. Subcooling and enthalpy of transition of pure PG and the EG600 based composites processed by different methods.

The thermal behaviours of the composites of NPG, PG and TRIS were assessed by DSC, and the resulting thermograms are depicted in Figure 5.10, where the onset temperatures are marked with solid circles. The first noticeable behavior found in Figure 5.10 is that the subcooling variations is mostly due to the onset temperature of the transition upon cooling, since the temperature of the transition upon heating is almost constant in all the cases. This is not the case of NPG based composites, in which the differences of the onset temperatures upon heating and cooling are similar. Therefore, as pointed out in section 5.1, the dispersion of particles improves the subcooling by creating new heterogeneous sites in which the mechanism controlled by the phase boundaries takes place. Moreover, the DSC signals of the composites are usually sharper than that of the pure PC, what makes sense since there is a dispersion of a highly thermal conductive particle that enhance the heat transfer, leading to a faster transition.

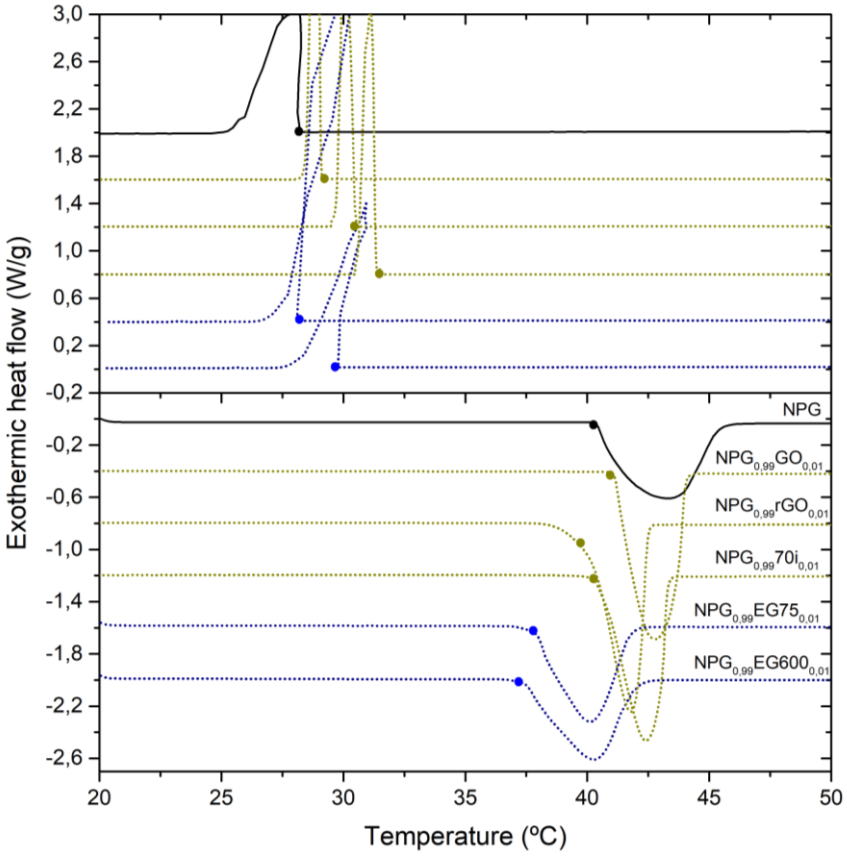

(a)

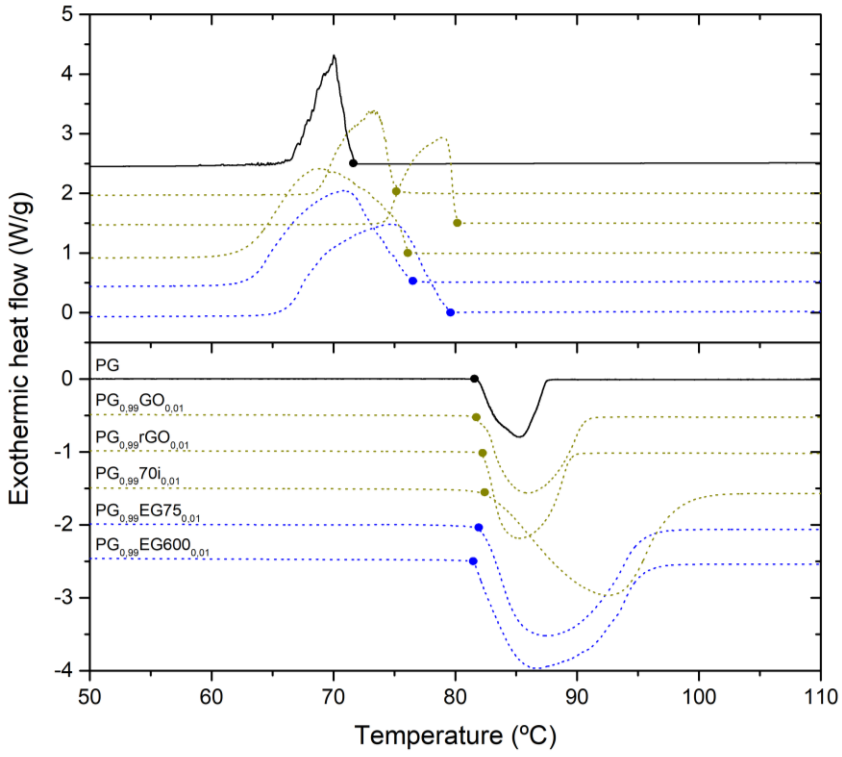

(b)

Figure 5.10. Thermograms of pure and 1 wt.% particles composites of (a) NPG, (b) PG and (c) TRIS.

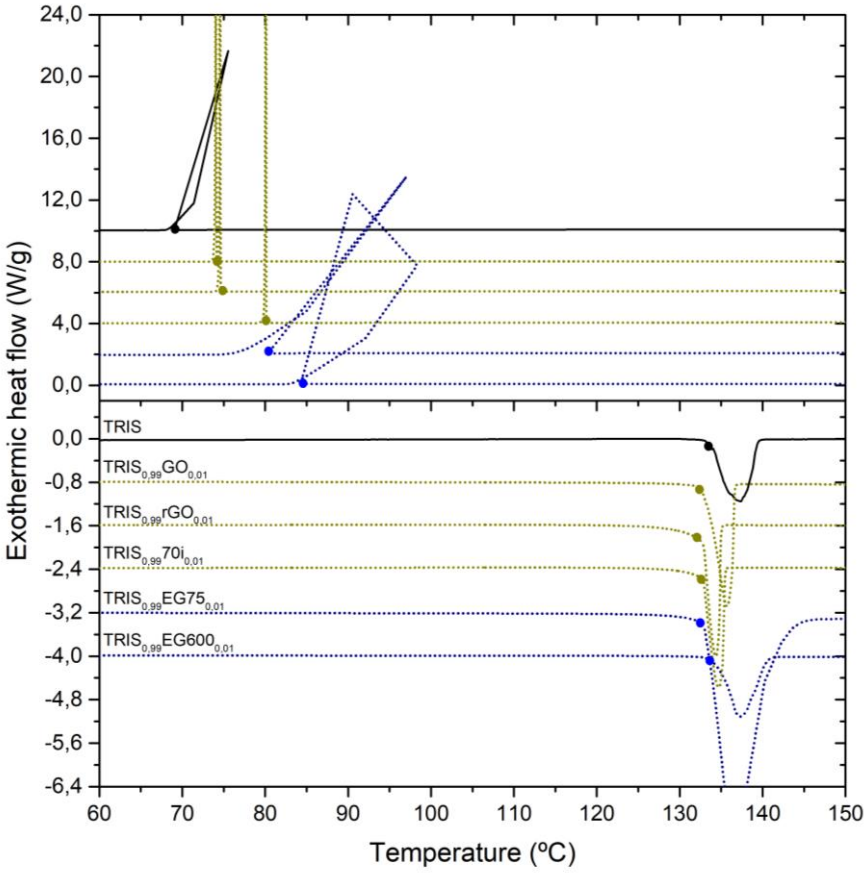

(c)

Figure 5.10. (Continued).

For a further understanding of the relationship between the particle's dispersion and the properties of the composites, the onset temperatures of the solid-solid transitions during heating and cooling are listed in Table 5.3, as well as their difference, i.e., the subcooling degree. Several conclusions can be highlighted. EG600 seems to have the most beneficial effect for improving the subcooling in all the plastic crystals leading to a reduction of up to 62 % in case of PG. As already concluded in Figure 5.10, the onset temperatures upon heating are not affected by the particle's addition, unless for NPG, whose temperature of the crystalline-plastic transition decreases with the addition of EG particles. Regarding the cooling step, the onset temperatures of all the composites are higher than those of the pure polyols, hence supporting a reduction of the subcooling degree. Comparing the different particles, and considering the accuracy given by the DSC (± 1 ºC), it is assumable that just the additives dispersion promotes a decreasing of the subcooling. In addition, only the dispersion of GO led to a similar subcooling to the pure NPG, whereas the dispersion of EG600 led to the best improvement of subcooling for the three tested PCs.

Table 5.3. T_h, T_c and subcooling of pure NPG, PG and TRIS and their composites.

Additive	NPG			PG			TRIS		
	Onset temperatures (ºC)		Subcooling (ºC)	Onset temperatures (ºC)		Subcooling (ºC)	Onset temperatures (ºC)		Subcooling (ºC)
	Heating	Cooling		Heating	Cooling		Heating	Cooling	
n.a.	40.7	28.7	12.0	81.6	72.1	9.5	133.6	70.9	62.7
GO	40.8	29.6	11.2	82.4	74.7	7.7	133.3	75.1	58.2
rGO	39.8	30.5	9.3	82.5	78.0	4.5	133.0	75.6	57.4
70i	40.9	31.3	9.6	82.9	76.2	6.7	133.0	79.9	53.1
EG75	37.9	28.1	9.8	82.4	75.5	6.9	133.2	79.8	53.4
EG600	37.4	29.3	8.1	81.5	77.9	3.6	132.9	85.4	47.5

n.a.: no additive; as received plastic crystal.

In Table 5.4, besides the enthalpy of transition of pure NPG, PG and TRIS, there is a calculation of the expected enthalpy of a composite considering the inert material, listed as n.a. (99 %), Expanded graphite-based composites show a slight decrease of the expected enthalpy. Again, this is explained considering the formation of new particle-PC interactions at expenses of the energetically active PC-PC hydrogen bonds of the phase transitions, contributing to the decrease of the enthalpy of transition. On the other hand, graphene oxide-based composites showed an interesting and surprising increase of the enthalpy of the solid-solid transition. In particular, the addition of only 1 wt.% of GO particles in NPG promotes an enhancement of the enthalpy of transition up to 25% comparing to pure NPG.

Table 5.4. Enthalpies of transition and ratio with respect to pure PC of all the studied composites.

Additive	NPG		PG		TRIS	
	Enthalpy (J/g)	Ratio (%)	Enthalpy (J/g)	Ratio (%)	Enthalpy (J/g)	Ratio (%)
n.a.	122.5	-	176.3	-	275.1	-
n.a. (99%)	121.3	-	174.5	-	272.3	-
GO	147.9	122 %	183.2	105 %	304.1	112 %
rGO	137.2	113 %	179.3	103 %	274.0	101 %
70i	132.5	109 %	170.1	97 %	262.4	96 %
EG75	100.2	83 %	165.5	95 %	272.0	100 %
EG600	106.0	87 %	170.8	98 %	238.0	87 %

n.a.: no additive, pure plastic crystal.

This increasing enthalpy was noticed to follow the trend GO > rGO > 70i. This behavior is clearly linked to the increasing oxygen content of the different graphene particles. These oxidized groups, which can be hydroxyls, carboxylic acids, and epoxy substituents, have hydrogens and/or nucleophilic oxygen atoms enabling the interaction through hydrogen bonds with the polyols. This interaction can lead to a reinforcement of the active PC-PC hydrogen bonds, thus increasing the enthalpy of transition (Figure 5.11a). Indeed, when a new graphene-PC hydrogen bond is formed (Figure 5.11a; 1st), the electronic density of the involved oxygen atom decreases, enlarging the covalent O-H bond (Figure 5.11a; 2nd) that becomes less energetic. Consequently, the PC-PC hydrogen bonds (Figure 5.11a; 3rd) are shortened and hence reinforced due to the higher acidity of the involved hydrogen atom. This scheme is also extensible to more graphene-PC interactions in order to understand how a higher number of oxidated groups can lead to higher enthalpies of transition. Let us consider this time the interaction between $O_{graphene}$-H_{PC}. Following the numeric order, and the equivalent hydrogen bond pairs (4^{th} = 1^{st} and 5^{th} = 2^{nd}), the 3^{rd} hydrogen bond is again reinforced. Therefore, we can assume that the enthalpy increment is due to a hydrogen bond strengthening at higher oxygen content of the graphene particles.

In order to check how different particles' concentration affects the energy involved, the enthalpies for the solid-solid transition of TRIS and different $TRIS_{1-x}GO_x$ ratio upon heating are depicted in Figure 5.11b. GO based composites were chosen since these particles promote the highest enthalpy enhancement, as well as TRIS was selected as the PC of study since it shows the most energetic solid-solid phase transition. Following the same protocol as in Table 5.4, a theoretical enthalpy is also calculated considering the amount of active material in the composite, and it is depicted as a red dashed line in Figure 5.11b. As commented before, the $TRIS_{0.99}GO_{0.01}$ composite shows an increase of the solid-solid enthalpy upon heating up to 304 J/g. However, this behavior is not repeatable for composites with higher concentration of GO (x = 0.025, 0.05 and 0.10), which have lower enthalpy than expected, even much lower with higher amount of additive. Again, this behaviour is probably due to the higher number of interactions between TRIS and the additive at the expense of the active TRIS-TRIS hydrogen bonds involved in the phase transition. That means that there is a twofold phenomena: i) the strengthening of the hydrogen bonds due to the interaction with oxidized particles, and ii) the higher dispersion of particles leading to a higher interaction particle-PC at the expense of numerous active PC-PC interactions. Hence, the reinforcement of the hydrogen bonds is only noticeable at low particles concentration.

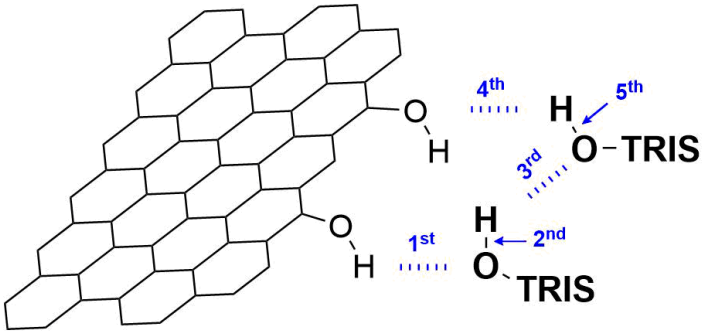

(a)

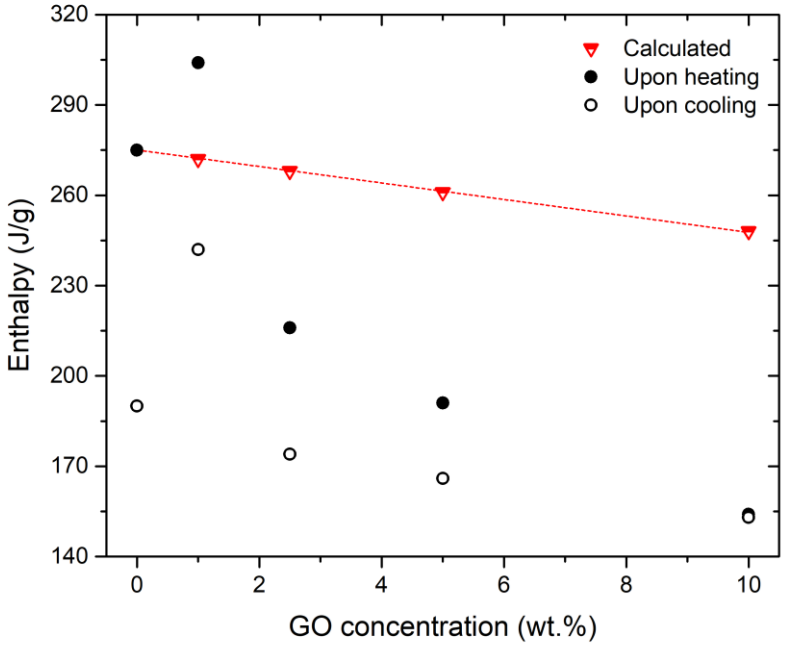

(b)

Figure 5.11. (a) Scheme of the possible reinforcement of the hydrogen bonds of the plastic crystals due to the dispersion of oxidized particles, and (b) plot of the solid-solid transition enthalpies of TRIS at different GO concentration.

5.2.3. Concluding remarks.

The synthesis of new carbon-based composites of NPG, PG and TRIS has been assessed. To this end, two different synthesis methods were tested in order to ensure the best performance as PCM: casting and uniaxial pressing. Using the dispersion of EG600 as a reference, subcooling was notably improved just with the addition of a 1 wt.% of particles and processing the material by uniaxial pressing. In addition, the enthalpy losses were also lower for the composite prepared by uniaxial pressing, since casting composites show a

higher interaction between the PC and the particle, hence decreasing the active hydrogen bonds involved in the phase change. Therefore, uniaxial pressing was the best method in terms of subcooling improvement and enthalpy selected for synthetizing the rest of composites. Moreover, the addition of a higher amount of dopants does not lead to a subcooling improvement, but even to a worsening of it. Regarding the enthalpy, the addition of more amount of inert material leads to less energetic composites, since the amount of active material is lower. Consequently, 1 wt.% of particles were selected as the optimal amount of particles to prepare the composites.

The size and nature of the particles apparently does not affect significantly the subcooling reduction for the same polyol/particles ratio. The particles mostly affect to the onset temperature of the plastic-crystalline transition, as occurs for the reported liquid-solid transitions. Only EG particles led to considerable variation on the onset temperatures of the crystalline-plastic transition of NPG. In all the cases, the variations of temperatures due to the addition of particles were in the sense of improving the subcooling of the solid-solid transitions. Subcooling was reduced a 27%, 43% and 62% in TRIS, NPG and PG; respectively; just by adding 1 wt.% of EG600. Therefore, in principle, EG600 seems to be the best additive to reduce the subcooling.

Surprisingly, the subcooling reduction was accompanied by an enthalpy increase of the solid-solid transition in case of GO and rGO based composites. The addition of these oxidized particles probably reinforces the intermolecular hydrogen bond network, leading to enthalpy increases up to 22% in the case of the $NPG_{0.99}GO_{0.01}$ composite. Homogeneous composites should show a lower enthalpy than the pure polyol, due to the lower amount of active material in the composite, and the reduction of active intermolecular hydrogen bonds in support of new particle-polyalcohol interactions. However, this theory is just a mathematical consideration that does not count with the kind of interaction, as hydrogen bond or Van der Waals forces. Therefore, the enthalpy of the solid-solid transition was increased by a reinforcement of the hydrogen bond network of the PCs thanks to the creation of new particle-PC hydrogen bonds. This phenomenon is not evident at higher concentration of particles, since this reinforcement opposes the reduction of PC-PC active hydrogen bonds at the expense of the new particle-PC interactions. The reinforcement effect is observed in composites with 1 wt.% of particles, which fortunately coincide with the composition providing the best subcooling enhancement.

5.3. Application of pressure.

5.3.1. Antecedents.

Phase transitions are transformations of the intermolecular or interatomic forces of a substance. As such, parameters such as temperature and pressure have a well-known influence on them, since they directly affect the chemical potential, and therefore the equilibrium of a phase transition. Therefore, the application of different pressures can lead to displacements of the phase transition temperature [26]. This is the fundamental of functioning of the heat pumps, for example. The compression of a refrigerant changes the chemical potential and hence displace the temperature of transition of such a liquid [27]. It is worth noting that the higher the compressibility factor of a system, the larger will be the effect of the pressure on the equilibrium. Therefore, in general terms, pressure will affect more at equilibriums in which a gas phase is involved, followed by a liquid, and solid materials will be usually the less affected by the same pressure.

With this regard, the application of pressure could be one of the most efficient approaches in order to displace the temperature of transition of a material and, hopefully, could help to reduce the subcooling. Actually, a recent research about barocaloric materials has been published in Nature regarding one of the plastic Crystals, the NPG [28,29]. The term barocaloric refers to any material whose change in a thermal variable is larger than usual due to the pressure. The plastic crystals possess a compressibility factor much larger than most of the common solids (Figure 5.12a), and this is the reason why pressure differences led to big changes in temperatures. For NPG, the application of 0.5 GPa of isostatic pressure caused an increase of the solid-solid transition temperature of about 35 ºC. This is a huge displacement which is in the order of commercial hydrofluorocarbon refrigerants. This effect is mainly due to the big entropic changes that NPG suffers during the solid-solid phase transition, so that the application of moderate pressures can lead to big changes in temperature (Figure 5.12b). Moreover, there is also a non-linear displacement of the temperature of the solid-solid transition upon cooling, so the subcooling varies from one pressure to another. In the case of NPG, there is a slight reduction of the subcooling of about 3 ºC when applying 0.5 GPa of pressure.

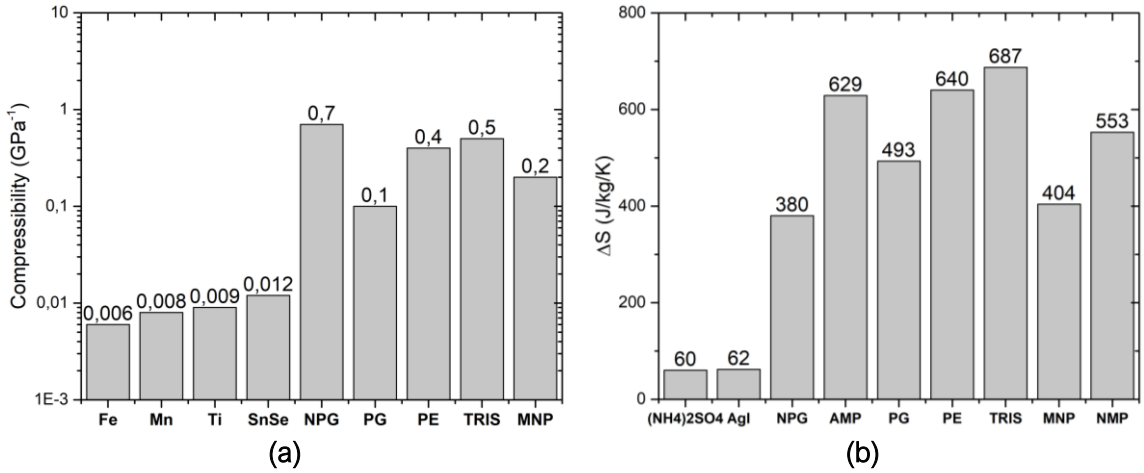

Figure 5.12. (a) Compressibility values of regular solids and plastic crystals and (b) entropy differences of the solid-solid transition of common barocaloric materials [30–34].

Following this approach, PG is selected as barocaloric material of interest in order to check the barocaloric behavior when applying increasing pressures. Transitiometry is the technique in which a pressurized calorimeter is used in order to analyze not only the differences in the transition temperatures at different pressures, but also the variations in enthalpies and volumes during the phase transition. This becomes an useful technique to investigate in depth the solid-solid transition of these materials in order to check different behaviors under pressure and to fully characterize the material in order to use it as, for example, a new generation of solid-state refrigerants.

5.3.2. Results and discussion.

Two PG samples processed by different methods (PG_C and PG_BM) were chosen to check the effect of pressure in the phase transition equilibrium. To this end, isobaric experiments at different pressures (from atmospheric pressure to 350 MPa) have been carried out applying very slow heating and cooling rates (0.2 ºC/min) in order to discard possible thermal gradients inside the samples and/or thermal lags due to poor thermal conductivities of the samples. Figure 5.13a and 5.13b show a phase transition, upon heating and cooling, looks like in a transitiometry measurement, taking PG_BM as an example. During the measurement, it is possible to record simultaneously the four signals: temperature, pressure, volume, and heat flow. In Figure 5.13, it is noticeable how the heating and the cooling ramps are constant with a heating and cooling rate of around 0.2 ºC/min (blue lines). When the endothermic or exothermic phase transition occurs (orange lines in Figures 5.13a and 5.13b, respectively), the typical calorimetric signal is recorded and two main mechanical events are also observed. The volume changes corresponding to the phase transition are

easily recorded both during the heating and the cooling ramp (pink lines), enabling to know what portion of the material is expanding or contracting upon heating and cooling. Moreover, the set pressures of the isobaric experiments are well maintained until the phase transition when a perturbation occurs due to the volume changes during the transition. This is, during expansion of the sample, the pressure is temporary increased until the equipment is able to compensate this perturbation coming back to the set pressure. The same occurs for the opposite scenario, in which the material contracts during the solid-solid phase transition upon cooling and hence the pressure slightly decay until the equipment recovers the desired pressure. These small pressure variations do not influence the measurements being small in comparison to the set pressure, usually less than a 1 %, so that the measurements are reliable.

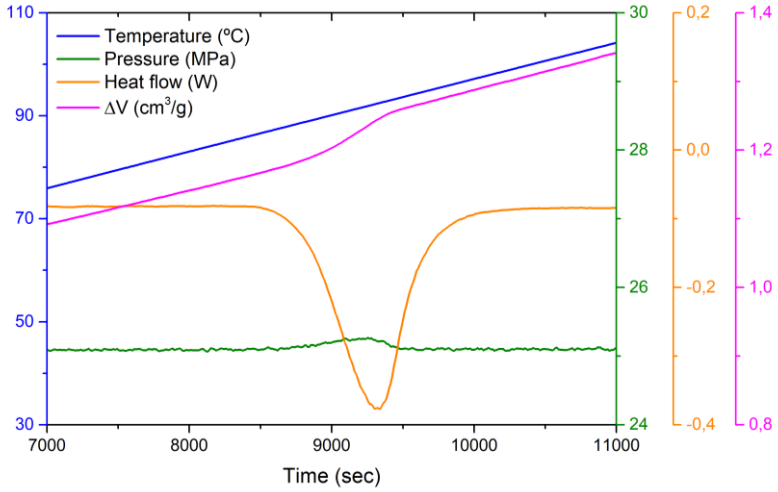

(a)

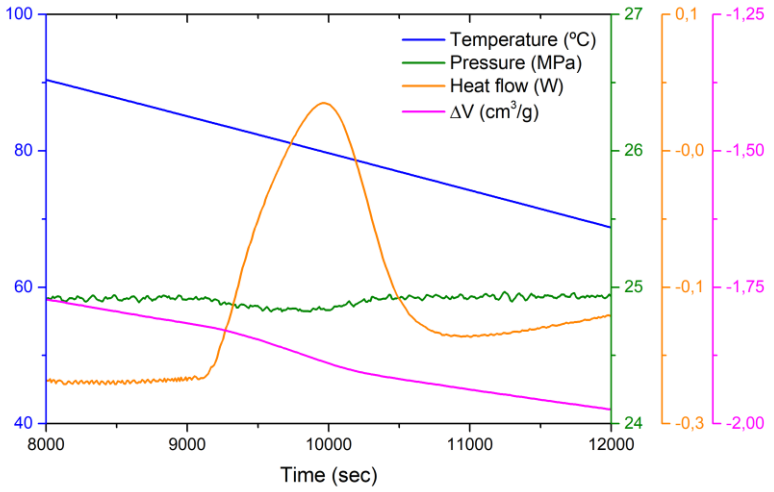

(b)

Figure 5.13. Typical results of phase transitions during isobaric experiments in a transitiometry analysis (a) upon heating and (b) upon cooling. (c) Comparison of the calorimetric signals recorded during all the isobaric experiments at different pressures for PG_BM.

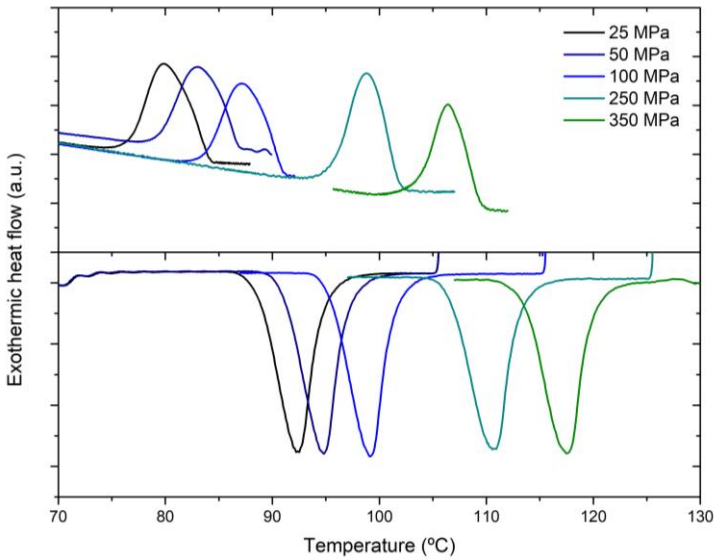

(c)

Figure 5.13. (Continued).

Thanks to the isobaric measurements, it is possible to obtain the onset temperatures and enthalpies of the solid-solid transitions from the calorimetric signal. Figure 5.13c shows how, as expected, there is a displacement of the solid-solid transition when applying pressure following the trend of increasing temperatures at higher applied pressures. This effect is common for both the heating and the cooling ramps.

All the results relevant to PG_BM and PG_C are summarized in Figure 5.14. In there, the subcooling is depicted in the upper part of the image. The values of the subcooling seem to tend to a similar value when applying pressure, no matter the initial subcooling that the material shows due to the processing method. For PG_C with 9.7 ºC of subcooling at atmospheric conditions, the application of pressures leads to a decrease of this value up to 4.9 ºC for the measurement carried out at 50 MPa. Corresponding to a subcooling reduction of 49 %. The increasing of the pressure does not lead to a further improvement, ranging from 5.1 ºC to 6.9 ºC with no trend regarding the pressures. In addition, it is worth taking into account that the measurements performed at the lowest and the highest pressure, 25 MPa and 350 MPa, respectively, were repeated twice, with a dispersion in the results of 0.6 ºC and 0.9 ºC, respectively. Therefore, since the variation in subcooling lay out of these values, the differences of subcooling between 5.1 ºC and 6.9 ºC is due to the sample nature, but there is no a clear trend of how the subcooling can be directly related to the pressure applied. On the other hand, PG_BM shows the opposite effect: an increase of the subcooling when applying

pressure, from 2.9 ºC at atmospheric pressure to 4.1 ºC for 250 MPa. Therefore, it seems that the application of pressure does not improve the subcooling in this case, but it worsens it. Probably, the application of an external pressure reduces the possible motions of the superficial molecules, hence promoting an average value of subcooling no matter the applied pressure. In this case of PG_BM, the subcooling values range from 3.3 ºC to 4.1 ºC, and since the dispersion of the results is ± 0.9 ºC, probably there is a similar subcooling degree for all the pressures. In addition, the average value of subcooling for PG_C and PG_BM is 5.9 ºC and 3.7 ºC, respectively, so taking into account the error of ± 0.9 ºC, the values are still different. Therefore, despite for PG_C and PG_BM there is a decrease and an increase of the subcooling, respectively, PG_BM still maintains a lower subcooling degree than PG_C.

Regarding the enthalpy, both for PG_C and PG_BM the enthalpy is higher for the crystalline-plastic transition than for the plastic-crystalline one. Regarding the former one, the transition is slightly more energetic for PG_C than for PG_BM as pointed out in Chapter 5.1. At higher pressures, the enthalpy of PG_BM seems to increase, probably due to a densification of the material and hence a higher similitude to PG_C. On the other hand, the slight variations with no trend of the enthalpy of transition in PG_C lies within the error bars calculated from the dispersion of the results. Consequently, the pressure seems not to substantially affect the enthalpy of transition.

Finally, the volume differences during the phase transition were recorded as a function of the applied pressure. As pointed out in the dilatometry measurements in Chapter 3, volume changes during the phase transition are lower upon cooling than upon heating, due to the plastic behavior of the plastic phase of most PCs. When applying pressure, there is a clear trend: the higher the applied pressure, the smaller the volume change during the phase transition, just because volume and pressure are inversely related, so that high pressures would hinder big volume changes. Therefore, the application of pressures not only leads to displacements on the temperatures of transition, but also helps to better control the differences on density during the phase transition.

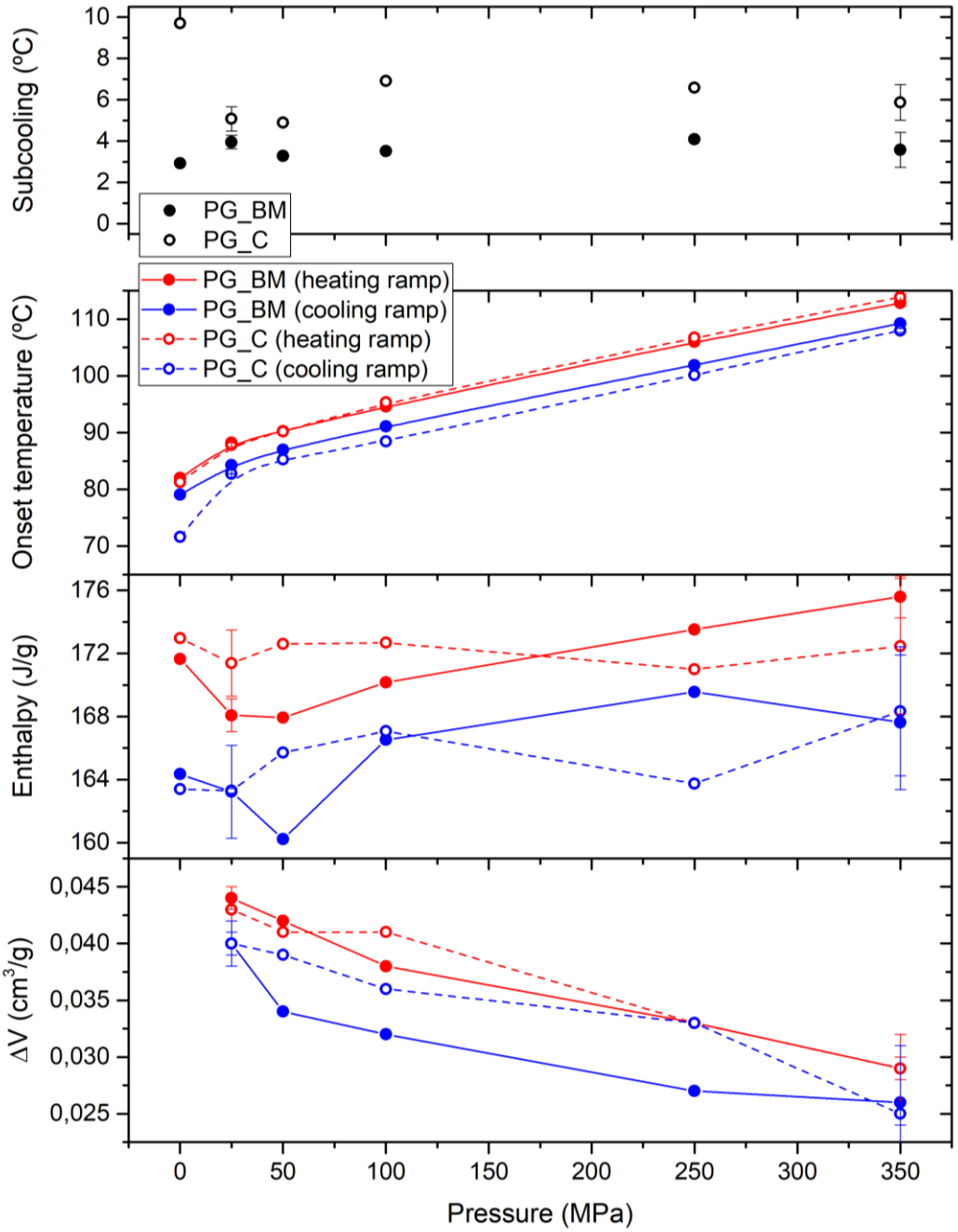

Figure 5.14. Summary of all the results obtained during the isobaric measurements at different pressures and during the heating and cooling ramps of both PG_BM and PG_C.

5.3.3. Concluding remarks.

PG is pointed out as a potential barocaloric PCM whose subcooling is maintained at a certain value. Despite the application of pressure does not improve the subcooling in a substantial way, the temperatures of transition are highly displaced up to about 35 ºC when applying 350 MPa. This is an interesting result since PG can be a potential PCM for use it in

the new generation of solid-state heat pumps. Regarding the enthalpy of transition, the application of pressures does not lead to big differences. However, the changes in density during the phase transition are highly affected by the application of pressure, so that the higher the pressure, the lower the volume variation between both solid phases. Therefore, despite other approaches studied in previous sections seem to be better solutions to mitigate the subcooling phenomenon, the application of pressure can be an efficient a sustainable way to use these materials in a wide range of temperatures for upcoming applications.

References in Chapter 5

[1] A.J. Lopes Jesus, S.C.C. Nunes, M. Ramos Silva, A. Matos Beja, J.S. Redinha, Erythritol: Crystal growth from the melt, Int. J. Pharm. 388 (2010) 129–135. https://doi.org/10.1016/j.ijpharm.2009.12.043.

[2] K.G. Rao, P. Rasoor, G. Anjaneya, J.R. Nataraj, M.R. Srinivas, A review on methods of preventing super cooling in phase change materials (PCMs), in: AIP Conf. Proc., AIP Publishing LLC, 2021: p. 20003. https://doi.org/10.1063/5.0036177.

[3] C.N. Nanev, Theory of nucleation, in: Handb. Cryst. Growth, Elsevier, 2015: pp. 315–358. https://doi.org/10.1016/B978-0-444-56369-9.00007-1.

[4] C.C. Koch, Synthesis of nanostructured materials by mechanical milling: problems and opportunities, Nanostructured Mater. 9 (1997) 13–22. https://doi.org/https://doi.org/10.1016/S0965-9773(97)00014-7.

[5] A.K. Nath, C. Jiten, K.C. Singh, Influence of ball milling parameters on the particle size of barium titanate nanocrystalline powders, Phys. B Condens. Matter. 405 (2010) 430–434. https://doi.org/https://doi.org/10.1016/j.physb.2009.08.299.

[6] K. Du, J. Calautit, Z. Wang, Y. Wu, H. Liu, A review of the applications of phase change materials in cooling, heating and power generation in different temperature ranges, Appl. Energy. 220 (2018) 242–273. https://doi.org/https://doi.org/10.1016/j.apenergy.2018.03.005.

[7] W.D. Callister, D.G. Rethwisch, Materials science and engineering, (2011).

[8] C. Igathinathane, L.O. Pordesimo, E.P. Columbus, W.D. Batchelor, S.R. Methuku, Shape identification and particles size distribution from basic shape parameters using ImageJ, Comput. Electron. Agric. 63 (2008) 168–182. https://doi.org/https://doi.org/10.1016/j.compag.2008.02.007.

[9] A. Mazzoli, O. Favoni, Particle size, size distribution and morphological evaluation of airborne dust particles of diverse woods by Scanning Electron Microscopy and image processing program, Powder Technol. 225 (2012) 65–71. https://doi.org/https://doi.org/10.1016/j.powtec.2012.03.033.

[10] P. Papon, J. Leblond, P.H.E. Meijer, Physics of Phase Transitions, Springer-Verlag Berlin Heidelberg, Germany, 2002.

[11] D.A. Porter, K.E. Easterling, Phase transformations in metals and alloys (revised reprint), CRC press, 2009.

[12] T. Ozawa, Kinetic analysis of derivative curves in thermal analysis, J. Therm. Anal. 2 (1970) 301–324. https://doi.org/10.1007/BF01911411.

[13] J. Šesták, G. Berggren, Study of the kinetics of the mechanism of solid-state reactions at increasing temperatures, Thermochim. Acta. 3 (1971) 1–12. https://doi.org/https://doi.org/10.1016/0040-6031(71)85051-7.

[14] F.J. Gotor, J.M. Criado, J. Malek, N. Koga, Kinetic Analysis of Solid-State Reactions: The Universality of Master Plots for Analyzing Isothermal and Nonisothermal Experiments, J. Phys. Chem. A. 104 (2000) 10777–10782. https://doi.org/10.1021/jp0022205.

[15] K.F. Kelton, A.L. Greer, Heterogeneous nucleation, in: Pergamon Mater. Ser., Elsevier, 2010: pp. 165–226.

[16] G. Wypych, Handbook of nucleating agents, Elsevier, 2021.

[17] P. Jana, E.P. del Barrio, M. Dubois, M. Duquesne, A. Godin, C. Vautrin-Ul, V. Fierro, G. Medjahdi, A. Celzard, Hydrophobised carbon foams for improved long-term seasonal solar thermal energy storage, Sol. Energy Mater. Sol. Cells. 220 (2021) 110849. https://doi.org/10.1016/j.solmat.2020.110849.

[18] S. Salyan, S. Suresh, Study of thermo-physical properties and cycling stability of D-Mannitol-copper oxide nanocomposites as phase change materials, J. Energy Storage. 15 (2018) 245–255. https://doi.org/10.1016/j.est.2017.10.013.

[19] Y. Feng, X. Jin, J.N. Hay, Effect of nucleating agent addition on crystallization of isotactic polypropylene, J. Appl. Polym. Sci. 69 (1998) 2089–2095. https://doi.org/10.1002/(SICI)1097-4628(19980906)69:10<2089::AID-APP20>3.0.CO;2-W.

[20] L.-S. Wong-Pinto, Y. Milian, S. Ushak, Progress on use of nanoparticles in salt hydrates as phase change materials, Renew. Sustain. Energy Rev. 122 (2020) 109727 https://doi.org/10.1016/j.rser.2020.109727.

[21] S. Wu, T. Yan, Z. Kuai, W. Pan, Thermal conductivity enhancement on phase change materials for thermal energy storage: A review, Energy Storage Mater. 25 (2020) 251–295. https://doi.org/10.1016/j.ensm.2019.10.010.

[22] P. Hu, P.P. Zhao, Y. Jin, Z.S. Chen, Experimental study on solid-solid phase change properties of pentaerythritol (PE)/nano-AlN composite for thermal storage, Sol. Energy. 102 (2014) 91–97. https://doi.org/10.1016/j.solener.2014.01.018.

[23] K.P. Venkitaraj, S. Suresh, Effects of Al2O3, CuO and TiO2 nanoparticles son thermal, phase transition and crystallization properties of solid-solid phase change material, Mech. Mater. 128 (2019) 64–88. https://doi.org/10.1016/j.mechmat.2018.10.004.

[24] S. Santos-Moreno, S. Doppiu, G.A. Lopez, N. Marinova, Á. Serrano, E. Silveira, E.P. del Barrio, Study of the phase transitions in the binary system NPG-TRIS for thermal energy storage applications, Materials (Basel). 13 (2020) 1–22. https://doi.org/10.3390/ma13051162.

[25] M. Yuan, C. Xu, T. Wang, T. Zhang, X. Pan, F. Ye, Supercooling suppression and crystallization behaviour of erythritol/expanded graphite as form-stable phase change material, Chem. Eng. J. 413 (2021) 127394. https://doi.org/10.1016/j.cej.2020.127394.

[26] G. Job, R. Rüffler, Physical Chemistry from a Different Angle, Springer Int. Publ. Doi. 10 (2016) 973–978.

[27] W. Grassi, Heat pumps: fundamentals and applications, Springer, 2017.

[28] B. Li, Y. Kawakita, S. Ohira-Kawamura, T. Sugahara, H. Wang, J. Wang, Y. Chen, S.I. Kawaguchi, S. Kawaguchi, K. Ohara, K. Li, D. Yu, R. Mole, T. Hattori, T. Kikuchi, S. ichiro Yano, Z. Zhang, Z. Zhang, W. Ren, S. Lin, O. Sakata, K. Nakajima, Z. Zhang, Colossal barocaloric effects in plastic crystals, Nature. 567 (2019) 506–510. https://doi.org/10.1038/s41586-019-1042-5.

[29] P. Lloveras, A. Aznar, M. Barrio, P. Negrier, C. Popescu, A. Planes, L. Mañosa, E. Stern-Taulats, A. Avramenko, N.D. Mathur, X. Moya, J.L. Tamarit, Colossal barocaloric effects near room temperature in plastic crystals of neopentylglycol, Nat. Commun. 10 (2019) 1–7. https://doi.org/10.1038/s41467-019-09730-9.

[30] J. Font, J. Muntasell, E. Cesari, Plastic crystals: Dilatometric and thermobarometric complementary studies, Mater. Res. Bull. 30 (1995) 839–844. https://doi.org/https://doi.org/10.1016/0025-5408(95)00055-0.

[31] N.T. Trung, L. Zhang, L. Caron, K.H.J. Buschow, E. Brück, Giant magnetocaloric effects by tailoring the phase transitions, Appl. Phys. Lett. 96 (2010) 172504. https://doi.org/10.1063/1.3399773.

[32] J. Cui, Y. Wu, J. Muehlbauer, Y. Hwang, R. Radermacher, S. Fackler, M. Wuttig, I. Takeuchi, Demonstration of high efficiency elastocaloric cooling with large ΔT using NiTi wires, Appl. Phys. Lett. 101 (2012) 73904. https://doi.org/10.1063/1.4746257.

[33] P. Lloveras, E. Stern-Taulats, M. Barrio, J.-L. Tamarit, S. Crossley, W. Li, V. Pomjakushin, A. Planes, L. Mañosa, N.D. Mathur, X. Moya, Giant barocaloric effects at low pressure in ferrielectric ammonium sulphate, Nat. Commun. 6 (2015) 8801. https://doi.org/10.1038/ncomms9801.

[34] D. Bansal, J. Hong, C.W. Li, A.F. May, W. Porter, M.Y. Hu, D.L. Abernathy, O. Delaire, Phonon anharmonicity and negative thermal expansion in SnSe, Phys. Rev. B. 94 (2016) 54307. https://doi.org/10.1103/PhysRevB.94.054307.

Chapter 6

General conclusions and perspectives

General conclusions:

The five reported Plastic Crystals; NPG, AMP, PG, TRIS and PE, are proposed as potential solid-solid PCMs due to the highly energetic transitions they undergo (up to 290 J/g), The phase transition enthalpy increases linearly with increasing number of hydroxyl and/or amine groups in the molecule, due to a higher linking by hydrogen bonds. Moreover, the solid-solid transitions occur at higher temperatures when the number of hydroxyl/amine groups per molecule is higher. The PCs studied are stable upon thermal cycling at temperatures even higher than the corresponding melting points. Other thermophysical properties such as specific heats, densities and thermal conductivities are unusually high compared to other organic PCMs, highlighting them as some of the best candidates within the family of organic PCMs, with phase transitions usually below 300 ºC.

The main drawback of the Plastic Crystals, the subcooling, has been assessed by different techniques in order to understand and mitigate it. The results of the study show that operational parameters such as the sample mass and the heating and cooling rate do not

affect the subcooling degree of this type of molecules, enabling their use in a wide variety of applications which require different operational conditions.

All the Plastic Crystals possess hydroxyl and/or amine groups able to form hydrogen bonds as the strongest intermolecular forces in the solid structure. When comparing the crystalline and the plastic phase involved in the solid-solid transition of plastic crystals, the major structural change is the hydrogen bond arrangement. In addition, in all the PCs crystalline phases the hydroxyl groups are the most rigid part since they take part of the hydrogen bond network. These forces are even stronger for AMP and TRIS, where the hydrogen bonds show an acid/base interaction between the hydroxyl and amine groups, and hence a more ionic character. The plastic phases, on the other hand, are all cubic phases with a high rotational disorder in which the hydrogen bonds are not in a fixed position, but they are exchanging from one molecule to another.

This research evidence that there is a distribution of activation energies of the molecules to perform the solid-solid phase transition, and those that are located at instable sites such as grain boundaries or particle surfaces, are the preferred ones to start the transition. Whereas the hydroxyl groups are the first part of the molecules involved in the phase transition from the crystalline to the plastic phase, the reorganization of the hydrogen bonds required for the opposite transition from the plastic to the crystalline phase upon cooling is hindered due to the high orientational disorder of the hydroxyl and amine groups, probably being the main reason for the subcooling phenomenon. Once the core of the molecule has lost enough motion to reduce the possible molecular conformations, the hydrogen bonds of the crystalline phases are formed again.

Several approaches have been investigated to minimize the subcooling considering the molecules located in active sites, as well as the fast motions of protons located in hydroxyl and amine groups in the plastic phase. This study demonstrated that, the Plastic Crystals with lower particle sizes, and hence a higher surface/bulk ratio, showed a reduced subcooling degree, in agreement with the hypothesis formulated by the insight of this phenomenon by solid-state NMR.

Another approach was investigated concerning the lack of reorganization of the hydrogen bonds of the plastic phases. To solve this drawback, a dispersion of particles in the plastic crystals was performed in order to act as anchor points of such functional groups by synthetizing new carbon-based composites. The new-synthetized carbon-based composites such as the ones with expanded graphite particles improved the subcooling up to 62 % in the

case of PG by adding only 1 wt.% of EG600, hence minimizing the amount of inert material added to the Plastic Crystal. These EG-based composites showed an expected slight decrease in the enthalpy of the solid-solid transition due to the addition of a certain amount of inert material. However, the dispersion of graphene oxide based particles led to an enthalpy enhancement up to 22% for NPG. This is due to the hydrogen bond network strengthening promoted by the creation of new hydrogen bonds between the plastic crystal and the oxidized groups of the graphene oxide. Therefore, the dispersion of a small amount of particles has led to subcooling and enthalpy improvements in terms of a lower thermal hysteresis and a higher energy available, respectively.

Finally, the barocaloric effects present in plastic crystals, particularly in PG, were assessed considering different pressures up to 350 MPa. Controlled heating and cooling ramps were applied in isobaric conditions to PG processed by different methods (casting and ball milling) resulting in a similar subcooling degree which was independent of the initial one promoted by the processing method. Therefore, the subcooling was improved for PG prepared by casting, but it was slightly worsened for the PG prepared by ball milling, reaching similar values of subcooling at pressures higher than 50 MPa. However, it is worth mentioning that both the onset temperatures of the transition upon heating and upon cooling were displaced up to 35 ºC when applying 350 MPa of pressure, hence demonstrating the huge barocaloric behavior of these materials.

Therefore, this work demonstrates how the reduction of the subcooling of the plastic crystals can be assessed by physical processing methods. Moreover, the increase of the enthalpy of transition due to the dispersion of oxidized particles can lead to more energetic materials, and since their transition temperatures can be tailored by the application of pressure, these plastic crystals are pointed out as potential candidates for low-medium temperature applications (lower than 300 ºC), as for example, buildings isolation, district hot water, industrial heat recovery and a new generation of solid-state heat pumps.

Perspectives:

This work summarizes a first attempt to understand the subcooling phenomenon in the solid-solid transitions of potential PCMs as Plastic Crystals are, in order to further mitigate it as much as possible. The early stage in which this research is located, becomes the perfect point to open a wide range of possibilities to investigate such a phenomenon.

Firstly, all the thermophysical properties of plastic crystals can be further improved to state their suitability as PCMs. The dispersion of dopants with different loads of oxidized groups can be carried out in order to check how the enthalpy of transition improves or worsens. Going a step further, such dopants can be highly thermal conductors leading to composites with an enhanced thermal conductivity and/or specific heats.

Regarding the subcooling understanding, a deeper insight is needed adding the use of other techniques. A potential path to arrive to interesting conclusions of the solid-solid phase transitions of plastic crystals would be their study under in-situ X-ray diffraction. This technique would be useful to follow the evolution of the crystal lattices of the materials, so that it would be possible to further characterize the arrangement of molecules and hydrogen bonds during the phase transition. Regarding solid-state NMR, the study can be furtherly continued by performing magic-angle spinning experiments or even by measuring relaxation times of the different atoms involved in the phase transitions. The combination of both techniques could be a strong tandem to obtain valuable information about the motion of protons, confirm some behaviours and reach a deeper understanding of these transitions.

Finally, more approaches can be studied to mitigate subcooling. The tailoring of transition temperatures can be assessed by the creation of binary mixtures of plastic crystals, creating a phase diagram with new transition temperatures. Moreover, despite it could be a more expensive approach, a chemical link between plastic crystals and dopants could be carried out, in order to ensure an anchoring of the hydroxyl and/or amine groups. Moreover, apart from the application of pressure which has been showed in this work, different external stimuli could be also applied to these PCMs in order to see any improvement on the subcooling. The application of a located cold point in the material by a cold finger could lead to a phase transition instigation and propagation which would decrease the subcooling. Therefore, it is considered that there are infinite possibilities to further investigate this phenomenon and the paths to mitigate it. Looking for new alternatives would be an interesting journey for everyone that dives in this recent topic, in which the imagination to test new approaches has no end.

Annex 1: *Supporting information*

Figures:

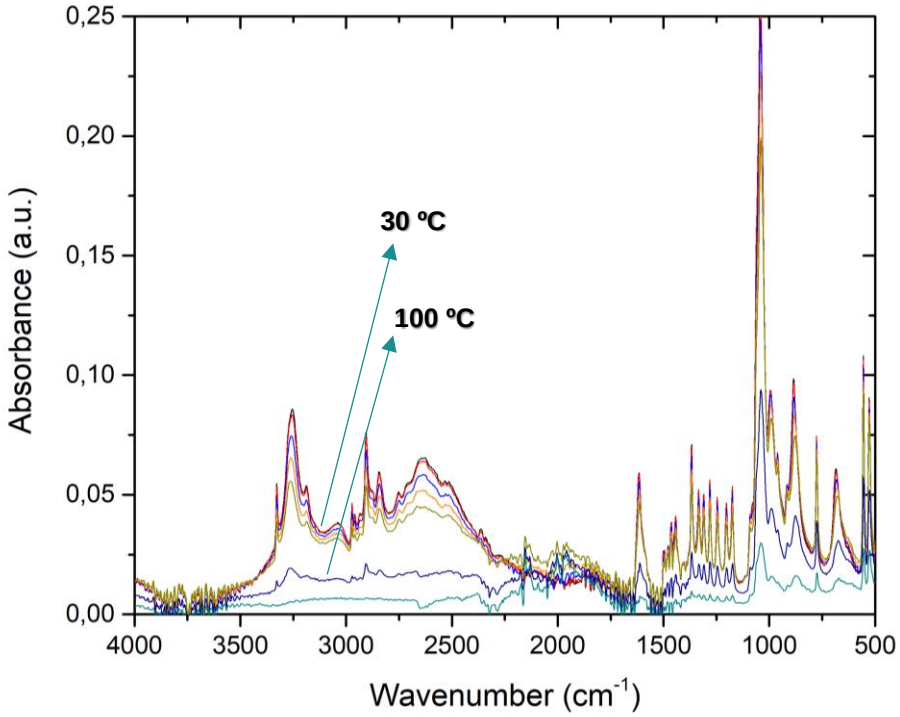

Figure A.1.1. FTIR absorbance spectra of AMP when heating from 30 ºC to 100 ºC.

Tables:

Table A.1.1. Temperatures of transition upon heating and cooling of NPG from DSC measurements at different sample masses and heating/cooling rates.

Mass (mg)	Cycle	Rate (ºC/min)							
		1		5		10		20	
		T_h (ºC)	T_c (ºC)	T_h (ºC)	T_c (ºC)	T_h (ºC)	T_c (ºC)	T_h (ºC)	T_c (ºC)
2.5	1	40.43	31.33	40.88	29.00	40.53	28.62	41.30	27.03
	2	40.39	31.22	40.68	28.82	40.42	28.51	41.46	27.09
	3	40.38	31.13	40.72	28.79	40.34	28.44	41.45	27.19
	4	40.38	30.31	40.72	28.26	40.26	28.70	41.49	26.71
	5	40.38	30.65	40.72	28.72	40.26	28.53	41.45	26.93
	6	40.39	30.17	40.72	28.57	40.19	28.25	41.42	27.08

	7	40.39	31.03	40.76	28.58	40.11	28.32	41.48	27.14
	8	40.40	30.41	40.74	28.42	40.06	28.27	41.44	27.03
	9	40.40	30.34	40.74	28.00	39.97	28.39	41.49	26.74
	10	40.40	30.20	40.73	28.36	39.96	28.14	41.46	26.77
Average		**40.39**	**30.68**	**40.74**	**28.55**	**40.21**	**28.42**	**41.44**	**26.97**
Std. deviation		0.02	0.45	0.05	0.30	0.19	0.18	0.06	0.17
5.0	1	40.31	30.77	40.88	29.32	41.48	28.12	41.52	27.29
	2	40.21	30.97	40.72	29.15	41.25	27.89	41.04	27.26
	3	40.19	30.86	40.73	28.97	40.72	27.94	41.07	27.15
	4	40.15	30.71	40.71	28.95	41.22	27.91	41.23	26.98
	5	40.16	30.71	40.73	29.03	41.21	27.73	41.29	27.13
	6	40.15	30.60	40.73	28.98	41.20	28.09	41.44	26.89
	7	40.14	30.54	40.73	28.82	41.18	27.94	41.41	26.97
	8	40.15	30.47	40.73	28.70	41.20	27.69	41.41	26.92
	9	40.16	30.33	41.21	28.68	41.13	27.54	41.40	26.77
	10	40.18	30.56	40.73	28.69	41.16	27.66	41.43	26.89
Average		**40.18**	**30.65**	**40.79**	**28.93**	**41.18**	**27.85**	**41.32**	**27.03**
Std. deviation		0.05	0.19	0.16	0.21	0.19	0.19	0.16	0.17
10.0	1	40.55	30.81	40.98	29.17	41.35	27.9	41.79	27.41
	2	40.42	30.62	40.72	28.90	41.14	27.91	41.71	27.32
	3	40.38	30.24	40.70	28.76	41.14	27.85	41.64	27.30
	4	40.37	30.74	40.69	28.62	41.13	27.82	41.66	27.30
	5	40.36	30.38	40.69	28.33	41.14	27.83	41.71	27.04
	6	40.35	30.37	40.70	28.51	41.12	27.84	41.71	26.95
	7	40.35	30.54	40.71	28.39	41.11	27.61	41.72	27.06
	8	40.34	30.44	40.70	28.86	41.09	27.83	41.68	26.94
	9	40.34	30.21	40.69	28.36	41.09	27.62	41.74	26.92
	10	40.34	30.41	40.70	28.57	41.07	27.54	41.75	27.06
Average		**40.38**	**30.48**	**40.73**	**28.65**	**41.14**	**27.78**	**41.71**	**27.13**
Std. deviation		0.06	0.20	0.09	0.27	0.08	0.13	0.04	0.18
25.0	1	40.48	31.65	39.54	29.29	40.02	28.26	40.80	26.73
	2	40.38	31.42	39.60	29.25	40.23	28.45	40.90	26.58
	3	40.36	31.44	39.64	28.98	40.29	27.92	40.90	27.41
	4	40.35	31.49	39.65	29.07	40.37	28.40	40.92	26.46
	5	40.33	31.15	39.65	28.72	40.45	27.85	40.98	27.38
	6	40.33	31.20	39.68	29.04	40.51	28.40	41.03	27.25
	7	40.32	31.12	39.70	28.98	40.58	27.78	41.11	27.20
	8	40.32	31.26	39.70	28.84	40.62	27.81	41.16	27.46
	9	40.32	31.27	39.71	28.73	40.68	27.86	41.23	27.32
	10	40.31	31.28	39.75	28.85	40.74	28.58	41.26	27.19

Average	40.35	31.33	39.66	28.98	40.45	28.13	41.03	27.10
Std. deviation	0.05	0.17	0.06	0.20	0.22	0.31	0.16	0.37

Table A.1.2. Temperatures of transition upon heating and cooling of AMP from DSC measurements at different sample masses and heating/cooling rates.

Mass (mg)	Cycle	Rate (ºC/min)			
		1		20	
		T_h (ºC)	T_c (ºC)	T_h (ºC)	T_c (ºC)
2.5	1	-	-	-	-
	2	79.77	-10.14	81.01	26.88
	3	79.77	-9.12	-	
	4	79.75	-7.03	-	
	5	79.75	-10.25	81.08	34.45
	6	79.75	-5.13	81.08	33.71
	7	79.75	-7.33	81.08	32.56
	8	79.72	-5.91	-	
	9	79.72	-1.83	81.11	34.38
	10	79.72	-4.97	-	
Average		79.74	-6.86	81.07	32.40
Std. deviation		0.02	2.75	0.04	3.18
25.0	1	-	-	80.1	
	2	79.67	-16.07	-	14.16
	3	79.66	-15.96	-	15.95
	4	79.64	-14.93	-	15.58
	5	79.62	-13.74	-	16.28
	6	79.6	-13.43	-	17.13
	7	79.59	-12.97	-	16.23
	8	79.58	-11.9	-	17.21
	9	79.57	-12.78	-	15.97
	10	79.56	-11.57	-	16.46
Average		79.61	-13.71	80.10	16.11
Std. deviation		0.04	1.64	0.00	0.90

Table A.1.3. Temperatures of transition upon heating and cooling of PG from DSC measurements at different sample masses and heating/cooling rates.

Mass (mg)	Cycle	Rate (ºC/min)							
		1		5		10		20	
		T_h (ºC)	T_c (ºC)	T_h (ºC)	T_c (ºC)	T_h (ºC)	T_c (ºC)	T_h (ºC)	T_c (ºC)
2.5	1	82.34	72.52	81.73	72.38	80.67	70.83	80.64	68.20
	2	81.66	73.38	80.27	72.85	79.75	69.64	80.69	68.29
	3	81.75	73.38	80.50	71.71	79.98	70.46	81.23	67.85
	4	81.64	72.63	80.80	71.56	80.24	70.72	81.62	67.60
	5	81.63	72.70	80.90	71.08	80.37	70.38	81.87	67.22
	6	81.67	72.61	81.07	71.27	80.53	69.88	82.11	66.60
	7	81.69	71.95	81.12	70.87	80.65	69.59	82.27	66.88
	8	81.70	72.57	81.28	70.91	80.82	69.13	82.42	67.25
	9	81.83	73.36	81.35	71.55	80.86	69.53	82.49	67.24
	10	81.81	72.54	81.48	71.02	80.94	69.43	82.60	67.34
Average		**81.77**	**72.76**	**81.05**	**71.52**	**80.48**	**69.96**	**81.79**	**67.45**
Std. deviation		**0.21**	**0.47**	**0.45**	**0.65**	**0.39**	**0.59**	**0.73**	**0.54**
5.0	1	82.30	76.85	80.51	75.16	80.37	73.71	80.90	67.78
	2	81.81	76.48	80.50	74.88	79.94	73.34	81.47	67.21
	3	81.81	76.53	80.71	74.96	80.23	71.95	81.97	66.76
	4	81.79	77.00	80.81	73.66	80.44	72.98	82.31	66.79
	5	81.82	76.77	80.99	73.90	80.60	72.69	82.52	67.22
	6	81.85	76.77	81.09	73.64	80.72	71.75	82.74	66.94
	7	81.85	76.94	81.22	73.74	80.86	70.55	82.91	67.25
	8	81.90	76.60	81.27	73.55	80.96	70.16	83.06	66.59
	9	81.90	75.61	81.37	73.62	81.12	70.83	83.15	66.19
	10	81.92	76.63	81.50	73.56	81.21	70.40	83.27	66.47
Average		**81.90**	**76.62**	**81.00**	**74.07**	**80.65**	**71.84**	**82.43**	**66.92**
Std. deviation		**0.15**	**0.39**	**0.35**	**0.65**	**0.41**	**1.31**	**0.78**	**0.46**
10.0	1	82.11	76.27	81.21	74.69	81.06	73.66	81.35	67.87
	2	81.84	76.18	80.99	74.74	80.90	73.25	81.47	64.86
	3	81.79	75.41	81.17	74.37	81.13	72.81	81.93	66.79
	4	81.78	75.93	81.30	73.91	81.30	72.49	82.27	65.25
	5	81.80	76.33	81.39	74.45	81.46	72.34	82.50	65.36
	6	81.84	76.01	81.51	73.79	81.59	71.06	82.70	64.41
	7	81.85	76.18	81.54	72.98	81.68	71.10	82.84	64.04
	8	81.89	74.17	81.65	73.22	81.81	70.42	82.99	64.14
	9	81.89	73.29	81.74	73.01	81.89	71.05	83.09	64.04
	10	81.92	72.96	81.77	72.58	81.97	70.83	83.16	64.78
Average		**81.87**	**75.27**	**81.43**	**73.77**	**81.48**	**71.90**	**82.43**	**65.15**

Std. deviation		0.10	1.30	0.26	0.79	0.37	1.14	0.66	1.26
25.0	1	82.66	77.89	82.21	76.20	82.34	74.52	81.21	70.19
	2	82.36	78.01	82.04	75.93	81.90	74.20	80.92	70.12
	3	82.26	78.01	81.98	75.76	81.82	74.10	81.25	69.13
	4	82.22	77.82	81.93	75.68	81.74	73.78	81.56	69.41
	5	82.23	77.77	81.88	75.46	81.73	73.71	81.77	68.95
	6	82.22	77.86	81.85	75.46	81.75	73.55	81.97	68.27
	7	82.24	78.00	81.85	75.55	81.79	73.66	82.12	68.25
	8	82.24	77.78	81.87	75.44	81.83	73.98	82.25	67.28
	9	82.27	77.57	81.88	75.42	81.89	73.64	82.33	67.53
	10	82.28	77.84	81.88	75.48	81.93	73.35	82.43	70.22
Average		**82.30**	**77.86**	**81.94**	**75.64**	**81.87**	**73.85**	**81.78**	**68.94**
Std. deviation		0.13	0.14	0.11	0.26	0.18	0.35	0.53	1.08

Table A.1.4. Temperatures of transition upon heating and cooling of TRIS from DSC measurements at different sample masses and heating/cooling rates.

Mass (mg)	Cycle	Rate (ºC/min)							
		1		5		10		20	
		T_h (ºC)	T_c (ºC)	T_h (ºC)	T_c (ºC)	T_h (ºC)	T_c (ºC)	T_h (ºC)	T_c (ºC)
2.5	1	133.81	70.93	133.39	68.54	134.24	69.86	134.25	66.17
	2	133.74	70.71	133.46	68.42	134.19	70.59	134.07	64.96
	3	133.69	70.20	133.38	70.03	134.17	66.37	134.01	66.50
	4	133.66	68.65	133.31	69.00	134.14	71.37	134.00	65.76
	5	133.64	68.02	133.27	69.35	134.12	65.63	133.96	64.98
	6	133.61	67.92	133.24	70.72	134.08	68.19	133.92	65.22
	7	133.61	64.57	133.20	69.82	134.07	66.53	136.35	66.90
	8	133.57	69.37	133.18	70.49	134.04	63.74	133.92	61.75
	9	133.56	71.11	133.16	70.78	134.01	65.46	133.90	63.98
	10	133.53	62.55	133.15	71.82	134.00	66.62	133.87	63.35
Average		**133.64**	**68.40**	**133.27**	**69.90**	**134.11**	**67.44**	**134.23**	**64.96**
Std. deviation		0.09	2.84	0.11	1.09	0.08	2.48	0.75	1.57
5.0	1	133.98	70.64	133.68	73.30	133.89	60.54	134.54	66.91
	2	133.95	70.80	133.53	69.15	133.59	65.55	134.35	65.62
	3	133.94	70.63	133.59	70.35	133.54	58.61	134.39	65.11
	4	133.93	70.91	133.71	70.50	133.47	64.15	134.39	67.02
	5	133.91	72.35	133.75	70.54	133.45	60.45	134.44	65.83
	6	133.89	72.72	133.74	73.69	133.39	61.48	134.46	66.53
	7	133.87	69.62	133.72	72.09	133.37	61.67	134.54	65.30
	8	133.84	71.70	133.62	72.44	133.34	64.63	134.61	65.50

	9	133.80	68.97	133.65	71.51	133.32	62.05	134.58	64.51
	10	133.75	69.64	133.57	72.32	133.31	59.72	134.64	66.21
Average		**133.89**	**70.80**	**133.66**	**71.59**	**133.47**	**61.89**	**134.49**	**65.85**
Std. deviation		0.07	1.20	0.08	1.44	0.18	2.25	0.10	0.81
10.0	1	133.76	70.69	133.76	68.81	133.15	69.24	133.59	65.80
	2	133.48	70.64	133.46	68.44	133.31	68.39	133.63	63.34
	3	133.45	69.18	133.28	69.04	133.29	69.02	133.61	64.41
	4	133.34	65.54	133.31	75.19	133.27	66.63	133.59	62.94
	5	133.24	69.48	133.35	73.44	133.24	68.17	133.60	61.58
	6	133.27	62.46	133.34	69.34	133.23	71.74	133.59	59.17
	7	133.25	60.36	133.32	67.18	133.21	69.48	133.58	57.99
	8	133.22	58.81	133.31	70.34	133.19	75.02	133.58	61.16
	9	133.22	60.53	133.31	70.81	133.17	66.71	133.56	58.26
	10	133.20	57.81	133.31	66.19	133.15	66.79	133.56	59.57
Average		**133.34**	**64.55**	**133.38**	**69.88**	**133.22**	**69.12**	**133.59**	**61.42**
Std. deviation		0.18	5.14	0.14	2.73	0.06	2.60	0.02	2.68
25.0	1	133.06	70.92	133.60	71.36	133.27	72.10	133.79	72.10
	2	133.20	69.52	133.16	71.46	132.79	67.23	133.76	67.23
	3	134.83	71.46	133.11	70.49	132.85	72.18	133.74	72.18
	4	132.98	68.00	133.15	68.35	132.90	66.45	133.70	66.45
	5	132.91	66.84	133.16	69.54	132.92	67.86	133.74	67.86
	6	132.82	66.14	133.17	68.89	132.91	66.92	133.73	66.92
	7	132.80	65.59	133.18	62.52	132.93	68.00	133.72	68.00
	8	132.78	65.14	133.17	59.82	132.92	68.86	133.78	68.86
	9	132.80	64.10	133.16	57.03	132.91	66.86	133.72	66.86
	10	132.80	60.30	133.16	61.54	132.86	67.55	133.74	67.55
Average		**133.10**	**66.80**	**133.20**	**66.10**	**132.93**	**68.40**	**133.74**	**68.40**
Std. deviation		0.62	3.36	0.14	5.33	0.13	2.08	0.03	2.08

Table A.1.5. Temperatures of transition upon heating and cooling of PE from DSC measurements at different sample masses and heating/cooling rates.

Mass (mg)	Cycle	Rate (ºC/min)							
		1		5		10		20	
		T_h (ºC)	T_c (ºC)	T_h (ºC)	T_c (ºC)	T_h (ºC)	T_c (ºC)	T_h (ºC)	T_c (ºC)
2.5	1	186.07	170.08	185.83	168.97	185.92	169.39	185.60	167.37
	2	185.87	170.95	185.72	167.50	185.72	168.44	185.75	168.42
	3	185.72	171.31	185.64	170.18	185.67	168.44	185.84	168.06
	4	185.52	170.55	185.62	167.84	185.68	168.37	185.90	167.52
	5	185.45	170.54	185.60	169.62	185.70	169.04	185.94	168.08

	6	185.51	172.55	185.65	169.20	185.71	169.52	185.95	167.60
	7	185.54	171.27	185.67	168.79	185.72	168.70	185.93	168.00
	8	185.57	171.47	185.68	169.58	185.69	170.39	185.91	167.94
	9	185.58	171.47	185.68	170.52	185.68	170.80	185.87	167.22
	10	185.63	170.48	185.70	169.89	185.67	170.25	185.85	167.60
Average		**185.65**	**171.07**	**185.68**	**169.21**	**185.72**	**169.33**	**185.85**	**167.78**
Std. deviation		0.19	0.71	0.06	0.97	0.07	0.89	0.11	0.38
5.0	1	186.05	177.01	185.72	170.17	184.20	170.76	186.42	169.87
	2	185.97	177.44	185.78	169.66	184.13	170.52	186.64	168.56
	3	185.92	171.53	185.71	170.18	184.31	168.70	186.84	168.35
	4	185.96	172.04	185.68	170.19	184.41	168.31	186.76	168.57
	5	185.87	172.38	185.65	170.06	184.78	165.85	186.69	167.84
	6	185.78	177.09	185.64	170.33	184.93	165.29	186.57	167.80
	7	185.86	171.13	185.65	169.48	184.91	164.16	186.43	168.00
	8	185.71	176.81	185.61	169.94	184.58	162.90	186.32	167.54
	9	185.84	170.97	185.62	170.65	183.75	162.97	186.24	167.69
	10	185.66	172.53	185.64	170.14	174.61	165.99	186.21	167.48
Average		**185.86**	**173.89**	**185.67**	**170.08**	**183.46**	**166.55**	**186.51**	**168.17**
Std. deviation		0.12	2.80	0.05	0.33	3.13	2.90	0.22	0.72
10.0	1	185.70	171.25	185.31	172.75	185.44	174.65	185.64	170.48
	2	185.59	170.84	185.39	172.70	185.33	171.95	185.58	172.22
	3	185.39	173.26	185.44	172.70	185.32	171.25	185.62	171.20
	4	185.42	171.18	185.47	174.31	185.36	171.16	185.66	170.28
	5	185.40	172.14	185.46	171.23	185.38	171.41	185.69	169.31
	6	185.29	170.83	185.44	172.00	185.42	171.03	185.72	169.06
	7	185.30	172.68	185.41	170.54	185.42	170.51	185.74	169.72
	8	185.33	171.96	185.38	171.86	185.40	170.55	185.77	169.22
	9	185.18	171.37	185.41	171.46	185.46	170.12	185.76	168.15
	10	185.15	170.40	185.46	170.64	185.44	170.74	185.80	169.75
Average		**185.38**	**171.59**	**185.42**	**172.02**	**185.40**	**171.34**	**185.70**	**169.94**
Std. deviation		0.17	0.90	0.05	1.14	0.05	1.28	0.07	1.16
25.0	1	185.91	173.68	185.40	173.71	185.77	172.64	186.12	172.92
	2	186.04	174.15	185.36	174.46	185.30	174.17	185.95	173.02
	3	186.06	174.33	185.40	172.43	185.27	171.98	185.92	172.46
	4	186.11	173.52	185.43	173.12	185.28	173.40	185.88	171.31
	5	186.15	174.36	185.39	173.64	185.27	171.55	185.80	172.13
	6	186.16	173.86	185.36	171.74	185.25	171.47	185.65	172.12
	7	186.20	173.62	185.32	171.91	185.22	172.56	185.56	171.28
	8	186.22	174.91	185.27	172.73	185.20	172.19	185.57	170.88
	9	186.25	175.20	185.24	172.11	185.20	171.14	185.56	171.17

	10	186.27	174.28	185.24	172.72	185.24	172.00	185.52	170.80
Average		**186.14**	**174.19**	**185.34**	**172.86**	**185.30**	**172.31**	**185.75**	**171.81**
Std. deviation		**0.11**	**0.55**	**0.07**	**0.88**	**0.17**	**0.92**	**0.21**	**0.83**

Table A.1.6. Equations of the fitted specific heat values (C_p) of the crystalline and plastic phases of plastic crystals compared to those reported on references.

Compound	Phase	Temperature range (ºC)	Equations	
			This work	Ref. [21]
NPG	Monoclinic	30 - 40	$C_p = 0.0091 \cdot T + 1.3939$	$C_p = 1.168 \cdot T - 162.094$
	FCC	55 - 120	$C_p = 0.0068 \cdot T + 2.1193$	$C_p = 0.466 \cdot T + 110.905$
AMP	Monoclinic	30 - 75	$C_p = 0.0038 \cdot T + 1.2042$	$C_p = 0.993 \cdot T - 130.005$
	BCC	100 - 105	$C_p = 0.0079 \cdot T + 2.0659$	$C_p = 0.580 \cdot T + 119.436$
PG	Tetragonal	30 - 80	$C_p = 0.0134 \cdot T + 0.8594$	$C_p = 0.654 \cdot T + 2.698$
	FCC	100 - 175	$C_p = 0.0038 \cdot T + 2.2041$	$C_p = 0.472 \cdot T + 138.041$
TRIS	Orthorhombic	30 - 130	$C_p = 0.0053 \cdot T + 1.2349$	$C_p = 0.695 \cdot T - 18.355$
	BCC	155 - 165	$C_p = 0.0033 \cdot T + 2.5510$	$C_p = 0.8171 \cdot T + 58.404$
PE	Tetragonal	30 - 175	$C_p = 0.0048 \cdot T + 1.4927$	$C_p = 1.253 \cdot T - 180.015$
	FCC	200 - 210	$C_p = 0.0011 \cdot T + 2.7606$	$C_p = -0.926 \cdot T + 913.335$

Table A.1.7. Density values obtained from dilatometry tests of the plastic crystals at different temperatures upon heating and cooling.

Compound	Heating ramp		Cooling ramp	
	Temperature (ºC)	Density (g/cm³)	Temperature (ºC)	Density (g/cm³)
NPG	30.30	1.02	29.85	1.01
	45.23	1.02	34.47	1.00
	78.05	0.97	38.72	0.98
	83.82	0.96	83.82	0.96
PG	53.13	1.17	51.00	1.11
	84.02	1.17	60.43	1.11
	107.05	1.08	84.56	1.10
	150.51	1.06	150.51	1.06

TRIS	40.92	1.14	37.48	1.15
	127.32	1.13	74.06	1.15
	155.19	1.08	76.86	1.13
	160.09	1.08	160.09	1.08
PE	37.94	1.37	38.36	1.40
	179.72	1.36	155.54	1.38
	216.53	1.25	176.70	1.27
	223.98	1.25	223.98	1.25

Table A.1.8. Different mechanism considered in the masterplot method.

Acronym	Reaction model	Mechanism
F1	Reaction order	Random nucleation followed by an instantaneous nucleus growth
F2		
F3		
P2	Power law	Random nucleation and nucleus growth through different models
P3		
P4		
A2	Avrami-Erofeev	
A3		
A4		
R2	Contracting area	Phase boundary-controlled transformation
R3	Contracting volume	
D1	Diffusion	Penetration of initial phase through a layer of the product phase
D2		
D3		
D4		

Annex 2: *List of figures*

Annex 3: *List of tables*

Annex 4: *List of contributions*

Publications:

◊ **Study of the phase transitions in the binary system NPG-TRIS for Thermal Energy Storage applications**
Sergio Santos-Moreno, Stefania Doppiu, Gabriel Alejandro López, Nevena Marinova, Ángel Serrano, Elena Silveira and Elena Palomo del Barrio

Materials (MDPI) – DOI: 10.3390/ma13051162
Published: March 2020

◊ **Characterization of Fatty Acids as biobased organic materials for Latent Heat Storage**
Marie Duquesne, Clément mailhé, Stefania Doppiu, Jean-Luc Dauvergne, Sergio Santos-Moreno, Alexandre Godin, Guillaume Fleury, Fabien Rouault and Elena Palomo del Barrio.

Materials (MDPI) – DOI:10.3390/ma14164707
Published: August 2021

◊ **NPG-TRIS thermal storage system. Quantification of the limiting processes: Sublimation and water's adsorption**
Noelia de la Pinta, Sergio Santos-Moreno, Stefania Doppiu, Josu Mirena Igartua, Elena Palomo del Barrio and Gabriel Alejandro López

Crystals (MDPI) – DOI:10.3390/cryst11101200
Published: October 2021

◊ **Effect of processing on microstructure and mechanical properties of pentaglycerine based solid-solid phase change materials**
Ángel Serrano, Ignacio Garrido, Sergio Santos-Moreno, Mikel Durán, Jean-Luc Dauvergne, Manuel Carmona and Elena Palomo del Barrio

Journal of Energy Storage (ELSEVIER) – DOI: 10.1016/j.est.2022.105677
Published: September 2022

◊ **Effect of processing on thermal properties of pentaglycerine based solid-solid Phase Change Materials**
Ángel Serrano, Sergio Santos-Moreno, Jean-Luc Dauvergne, Mikel Durán and Elena Palomo del Barrio

Manuscript in preparation

◊ Carbon-based composites of NPG and TRIS as improvement of subcooling phenomenon and enthalpies of transition
Sergio Santos-Moreno, Stefania Doppiu, Nevena Marinova, Elena Silveira, Nerea Uranga, Marta Hernaiz, Gabriel Alejandro López and Elena Palomo del Barrio

Manuscript in preparation

◊ Solid-state NMR characterization of temperature-driven solid-solid phase transition of tris(hydroxymethyl)aminomethane
Sergio Santos-Moreno, Stefania Doppiu, Elena Palomo del Barrio y Juan Miguel López del Amo

Manuscript in preparation

◊ Kinetics of transition in Neopentylglycol by infrared thermography and solid-state NMR
Jean-Luc Dauvergne, Sergio Santos-Moreno, Juan Miguel López del Amo, Artem Nikulin, Stefania Doppiu and Elena Palomo del Barrio.

Manuscript in preparation

Conferences:

◊ *NM4BL: Workshop on New Materials for a Better Life*
NPG/TRIS system and their carbon-based composites as phase change materials for thermal energy storage – Poster presentation

Sergio Santos-Moreno, Stefania Doppiu, Gabriel Alejandro López, Nevena Marinova, Elena Palomo del Barrio and Elena Silveira

◊ *10th GERMN – 9th Ibero American – 7th Iberian NMR Meeting*
Solid state NMR characterization of the solid-state phase transition and subcooling effect in globular polyalcohols – Poster presentation

Sergio Santos-Moreno, Stefania Doppiu, Elena Silveira, Gabriel Alejandro Llópez, Elena Palomo del Barrio and Juan Miguel López del Amo

◊ *ENERSTOCK 2021: 15th International Conference on Energy Storage*
Effect of adding expanded graphite microparticles in organic Plastic Crystals for latent heat storage – Oral presentation

Sergio Santos-Moreno, Stefania Doppiu, Gabriel Alejandro López, Nevena Marinova, Elena Silveira and Elena Palomo del Barrio

◊ *IMPRES 2022: The Sixth International Symposium on Innovative Materials and Processes in Energy Systems*

Solid state NMR characterization of temperature-driven solid-solid phase transition of tris(hydroxymethyl)aminomethane – Oral presentation

Sergio Santos-Moreno, Stefania Doppiu, Gabriel Alejandro López, Elena Palomo del Barrio and Juan Miguel López del Amo